1

Vol. 70

Hemijska industrija

asopis Saveza hemijskih inženjera Srbije

Chemical Industry

1mm

Hemijska industrija

SADRŽAJ/CONTENTS

SADRŽAJ nastavak
CONTENTS continued

GENERALNI POKROVITELJ SAVEZA HEMIJSKIH INŽENJERA SRBIJE

HEMOFARM KONCERN

Aktivnosti Saveza hemijskih inženjera Srbije pomaže:

MINISTARSTVO PROSVETE, NAUKE I TEHNOLOŠKOG RAZVOJA REPUBLIKE SRBIJE

SPONZORI

Tehnološko-metalurški fakultet Univerziteta u Beogradu, Beograd

Prirodno-matematički fakultet Univerziteta u Novom Sadu, Novi Sad

Hemijski fakutet Univerziteta u Beogradu Beograd

Institut za tehnologiju nuklearnih i drugih mineralnih sirovina, Beograd

Institut za opštu i fizičku hemiju, Beograd

Tehnološki fakultet Univerziteta u Novom Sadu, Novi Sad

Hipol a.d., Odžaci

Tehnološki fakultet Univerziteta u Nišu, Leskovac

NU Institut za hemiju, tehnologiju i metalurgiju Univerziteta u Beogradu, Beograd

Fakultet tehničkih nauka, Kosovska Mitrovica

Synthesis of single-walled carbon nanotube networks using monodisperse metallic nanocatalysts encapsulated in reverse micelles

Igor A. Gayduchenko[1], Georgy E. Fedorov[1], Ramil A. Ibragimov[2], Tatiana S. Stepanova[1], Arsen S. Gazaliev[1], Nikolay A. Vysochanskiy[1], Yuri A. Bobrov[3], Anton M. Malovichko[2], Ilya M. Sosnin[4,5], Ivan I. Bobrinetskiy[2]

[1]*National Research Centre "Kurchatov Institute", 123182, Akademika Kurchatova pl., 1, Moscow, Russia*

[2]*Center for probe microscopy and nanotechnology, National Research University of Electronic Technology (MIET), 124498, pass 4806, bld. 5, Moscow, Zelenograd, Russia*

[3]*NT-MDT Co. Building 100, Zelenograd, Moscow 124482, Russia*

[4]*Togliatti State University, 445667, Belorusskaya str, 14, Togliatti, Russia*

[5]*R&D "Nanomet" LCC. 445030, Tsvetnoy Boulevard 3, 48, Samara region, Togliatti, Russia*

Abstract

We report on a method of synthesis of single-walled carbon nanotubes percolated networks on silicon dioxide substrates using monodisperse Co and Ni catalyst. The catalytic nanoparticles were obtained by modified method of reverse micelles of bis-(2-ethylhexyl) sulfosuccinate sodium in isooctane solution that provides the nanoparticle size control in range of 1 to 5 nm. The metallic nanoparticles of Ni and Co were characterized using transmission electron microscopy (TEM) and atomic-force microscopy (AFM). Carbon nanotubes were synthesized by chemical vapor deposition of CH_4/H_2 composition at 1000 $^\circ$C on catalysts pre-deposited on silicon dioxide substrate. Before the temperature treatment during the carbon nanotube synthesis, the most of the catalyst material agglomerates, due to the magnetic forces, while during the nanotube growth disintegrates into the separate nanoparticles with narrow diameter distribution. The formed nanotube networks were characterized using AFM, scanning electron microscopy (SEM) and Raman spectroscopy. We find that the nanotubes are mainly single-walled carbon nanotubes with high structural perfection up to 200 μm long with diameters from 1.3 to 1.7 nm consistent with catalyst nanoparticles diameter distribution and independent of its material.

Keywords: carbon nanotube; nanoparticles, reverse micelle, chemical vapor deposition.

Available online at the Journal website: http://www.ache.org.rs/HI/

The carbon nanotubes (CNTs) are considered to be a promising material to be used for different applications due to their many unique properties. Individual CNTs, as well as arrays of semiconducting CNTs, can be used as basic elements for transistors and logic elements that can be integrated into the systems of information transfer and processing [1,2]. Individual CNTs, as well as CNT films, have bright future for sensor application [3]. CNT films can be used as transparent electrode, *e.g.*, in optoelectronic and photovoltaic devices [4,5]. However, despite the remarkable progress achieved in the laboratories over the past 15 years, the industrial application of nanotubes is restricted by the lack of developed technologies that would allow the control of their properties and methods of proper positioning compatible with large scale production.

There are two techniques most frequently used for deposition of CNTs on a substrate. One employs chemical vapor deposition (CVD) method with the shape and morphology of the synthesized conducting structures being defined by the area where the catalyst was patterned before the synthesis process [6]. Alternative technique involves liquid suspension of preliminary synthesized purified and functionalized nanotubes. This suspension can be ink-printed on a wafer using conventional methods [7]. Importantly the physical and chemical properties of nanotubes can be significantly modified during the last process via incorporation of defects using strong oxidizers [8]. Properties of CVD grown CNTs can be controlled through the catalyst composition [9] and/or synthesis parameters [10].

One of the key parameters is the catalyst particle size that can be controlled by either indirect methods when the catalyst fills in some porous media (ciliates, silicon oxide) [11], or directly when the colloid particles are formed in a solution and stabilized using surfactants [12,13]. Use of the reverse micelles method to grow colloid catalyst particles has several advantages in latter case allowing for an easy control of the particle size in a scalable process compatible with standard lithographic techniques for catalyst patterning [14,15].

In this paper we report on CVD formation of networks of single-walled carbon nanotubes (SWNTs) with a length of about 200 μm using colloid catalyst particles produced with the modified reverse micelles method. Different catalyst types based on cobalt and nickel are studied.

MATERIALS AND METHODS

Synthesis of magnetic nanoparticles in reverse micellar systems

Metal nanoparticles were obtained by the modified reduction method of metal ions to the atomic state with subsequent crystallization [16]. The synthesis was carried out using a reverse micellar systems as the environment and stabilizing shell of obtained nanoparticles. Reverse micellar system was dissolved in a non--polar organic solvent in a sinter of anionic surfactant molecules. Molecules of the reducing agent were located in the core of micelles. Bis-(2-ethylhexyl) sulfosuccinate sodium (Aerosol-OT, AOT, Acros Organics, Belgium) was used as a surfactant, quercetin (CAS No. 849061-97-8) was used as a reduction agent and iso-octane reference (GOST 12433-83, Russia) as a solvent. The Ni^{2+} or Co^{2+} were reduced by quercetin from their 1 M sulphate solutions. The mole ratio of metal ions and molecules of quercetin was 1:1. Before the synthesis, AOT was dissolved in isooctane with a concentration higher than the critical micelle concentration (CMC). As the result, agglomerates of the AOT molecules were formed.

An AOT molecule consists of two parts: the polar head and non-polar hydrocarbon tail [17]. The presence of these two parts accounts for the binary properties of the molecules: the molecule could be dissolved both in polar and non-polar media. Polar head can be dissolved in polar solvents and non-polar tail, respectively, in the non-polar ones. Thus the AOT molecules can be dissolved both in polar and non-polar liquids. If their concentration reaches the CMC values the AOT molecules form agglomerates, *i.e.*, micelles. If AOT is solved in a non-polar liquid, non-polar tails are pointing towards to the solvent, and the polar heads form a cavity which is the core of micelles. The size of this core ranges from 1 to 2 nm. Thus, the reverse micelle can be used as nanoreactor for the reaction of synthesis of a nanocrystal. Micelle limits the size of metal nanoparticles, but is a flexible structure that can be stretched. Therefore, the size of the synthesized nanoparticles can exceed the size of the "empty micelles". Chemical reagents required for the synthesis of nanoparticles are introduced into the micelle during the solubilization process, *i.e.*, when polar substances penetrate into the core of micelles.

In general, the proposed method allows production of highly concentrated solutions of stable metal particles in an organic solvent avoiding both heating to high temperatures and necessity of using oxygen-free atmosphere.

Catalyst deposition and CNT synthesis

The fabricated suspensions of nickel (Ni concentration: 3 mmol/L, AOT: 75 mmol/L) or cobalt (the concentration of Co: 3.6 mmol/L, AOT: 135 mmol/L) nanoparticles in isooctane were further diluted with solvent in a ratio of 1:40. The diluted suspension was then sonicated for 16 h. A droplet of suspension (20 μL) was then dripped onto the chip of oxidized silicon (300 nm of thermally grown SiO_2 on *p*-doped silicon) or quartz with a size of 7×7 mm^2. The catalyst suspension was dried for 40–60 s in the ambient atmosphere, whereupon the catalyst residues were removed under a nitrogen stream.

Carbon nanotubes were synthesized by chemical vapor deposition method. The chips coated with the catalyst were placed in a quartz purge type reactor placed inside a tube furnace and heated up to 1000 °C in an atmosphere of argon during an hour and a half. Then the reactor was blown with H_2 for 10 min at the same temperature, in order to reduce the catalyst. Next, a methane–hydrogen mixture (volume ratio of methane/hydrogen was 3.6:1) at a temperature of 1000 °C was blown through the reactor which gave rise to nanotube growth. Synthesis time was 30 min. The reactor was then cooled down to room temperature under argon.

Characterization methods

Concentration of nanoparticles was measured by spectrophotometer Heliso-α (Thermo electron corporation, UK), size distribution of nanoparticles was characterized using transmission electron microscope (TEM) LEO912 AB OMEGA (Carl Zeiss, Germany) and dynamic light scattering nano-particle size analyzer LB--550 (Horiba, Japan).

Carbon nanotubes grown by CVD method were investigated by scanning electron microscopy (SEM, Helios Nanolab, FEI), and atomic-force microscopy (AFM, Solver-Pro, NT-MDT) using standard silicon cantilevers of NSG30 series in semi-contact mode with f_{res} = 210 kHz. Amount of the structural defects and diameter distribution of carbon nanotubes were characterized using Raman spectroscopy (Centaur HR, Nanoscan Technology).

RESULTS AND DISCUSSION

Nanocatalyst preparation

The process of formation of nanoparticles involved the use of natural reducing agents from the group of flavonoids with chelating effect allowing for robust immobilization of the ion. At the same time flavonoid has high reducing capacity, so the growth of nanoparticles is fast and nanoparticles are additionally stabilized by oxidation products of flavonoids. In the proposed method, the result of a chemical reaction is the growth of catalyst nanoparticles inside of the reverse micelles. The method allows obtaining organic colloidal solution of metal nanoparticles with narrow size distribution with about 85% of nanoparticles having a diameter from 3 to 5 nm. When depositing nickel nanoparticles onto the TEM grid, natural drying of isooctane leads to particles agglomeration (Figure 1a). The cluster size was determined using TEM-images (Figure 1b). Due to magnetic properties of nickel and cobalt nanoparticles micrograph and the corresponding estimate have a margin of error that is significant for nanoscale objects. That in turn leads to an exaggerated spread of particle diameter values.

Atomic-force microscopy of the particles was performed after deposition and drying of catalyst on the silicon oxide plate surface. We found that the sample surface was covered with islands of a uniform thin film into which the fine-grained nanoparticles were embedded (Figure 2a). There were no nanoparticles observed in the areas free from this thin film (Figure 2b). The height of the film (presumably surfactant) is 1.6 to 2 nm, which corresponds to the mono- or bi--layer of the surfactant molecules, sitting vertically on more hydrophobic surface silicone oxide. We also found presence of sparse but large conglomeration with height up to 200–300 nm and lateral size 1–2 μm. We concluded that in general, particles with sized from 6 to 12 nm, were present in agglomerations of 3–5 or more particles. Overall conclusion is that the used method of catalyst deposition allows obtained fine-grained layer of catalyst nanoparticles on the surface (conglomerations do not exceed 3–5 nanoparticles) with narrow distribution of diameters (heights). Minimum height of a single Ni particles is 1–1,5 nm.

(a)

(b)
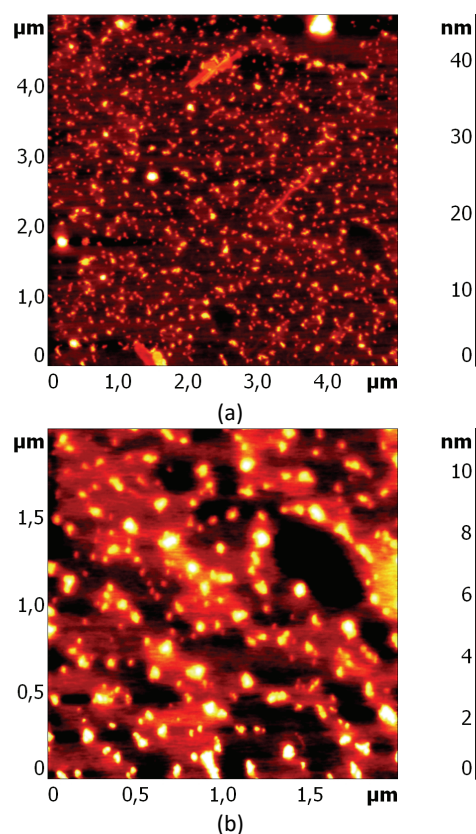
Figure 2. AFM image of nickel nanoparticles deposited from isooctane solution: a - scan size 5x5 microns, b - scan size 2x2 microns.

(a)

(b)

Figure 1. TEM image of nickel nanoparticles deposited from isooctane solution (a) and histogram of cobalt nanoparticles sizes distribution according to TEM (b). Scale bar: 20 nm.

SWNT synthesis is affected significantly by nanoparticles agglomeration and environment [18]. Due to a surplus of the surfactant in the solution, it stays on the chip surface after drying in the form of a surfact-

3

ant/isooctane matrix promoting catalyst particles agglomeration. We note that the agglomeration probability in water solution is higher which may be a reason of lower SWNT yield when catalyst was diluted in water (see below). The influence of surfactant used for nanoparticles formation in reverse micelles is important as well. Micelles determine the nanoparticles shape as well as their surface chemical activity [19].

Investigation of carbon nanotubes grown on the monodisperse catalyst

Topography measurement was carried out by two high-resolution methods: SEM and AFM, which allowed get full picture of surface topography after CVD of carbon nanotubes. In general, nanotubes are relatively uniformly distributed on the surface and have lengths up to 200 μm (Figure 3). In case of cobalt catalyst concentration of shorter nanotubes evaluated visually is higher. Nanotubes with length more than 2 μm have many bends, branching and ring-shaped structures. This can be caused by defect accumulation both in nanotubes and substrate.

AFM image allows us to get more complete information about structure of surface due to visualization of oxidized catalyst particles, which cannot be achieved by standard SEM [20]. Both types of catalyst produce nanotubes of small diameter (height approximately 1.8 nm by AFM data, Figure 4). Dispersion of carbon nanotubes on substrate surface is non-uniform. Nano-sized particles with average diameter (height) of approximately 2 nm might be oxidized catalyst that has not reacted. On average the area of 5 μm×5 μm contains spherical particles with size dispersion from 2.8 to 5.1 nm; the smallest observed size was 1.2 nm, the largest – 6 nm (it might be an agglomeration of several particles). Analysis of AFM images gives the following estimation of catalyst particles sizes and nanotubes diameters, grown on that catalyst:

– particles size: 3.5±0.6 nm (of Ni catalyst) and 3.9±0.8 nm (of Co catalyst) and

– nanotubes diameters 1.8±0.2 nm (for Ni catalyst) and 1.9±0.3 nm (for Co catalyst).

(a)

(b)

(c)

(d)
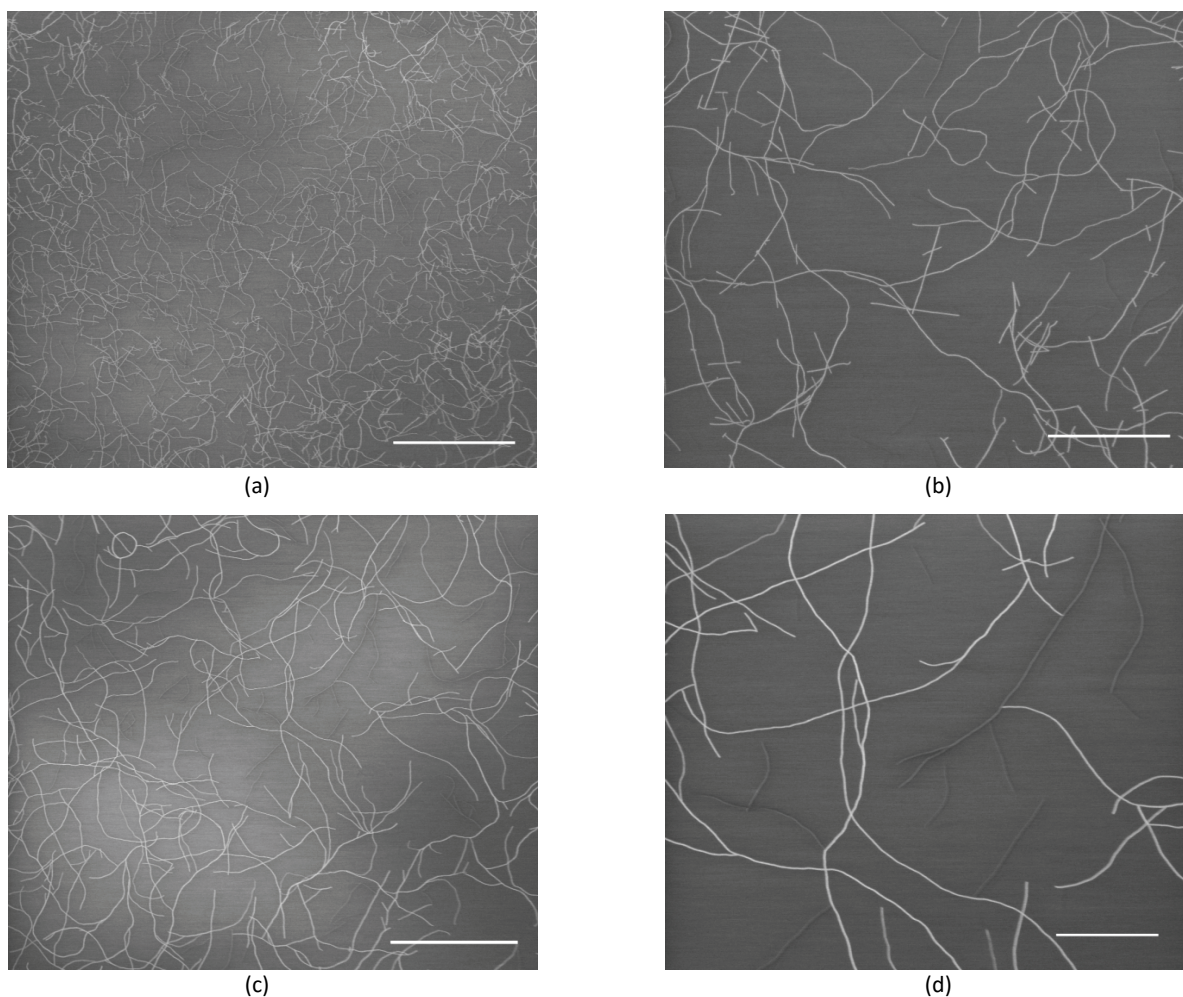
Figure 3. SEM image of the SWNTs formed on the silicon dioxide substrate: a, b – Co catalyst, c, d – Ni catalyst. Scale bar: 20 (a, c) and 5 μm (b, d).

(a)

(b)
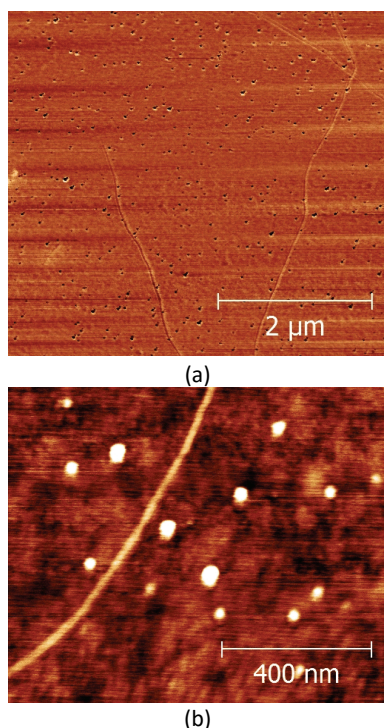
Figure 4. AFM image of wafer surface with grown nanotubes (thread-like structures) and remains of catalyst (dots), obtained by chemical vapor deposition on Ni nanoparticles: a-phase contrast mode, b – zoomed imaged in height mode.

Note that not all nanotubes can be imaged by AFM under normal conditions: small diameter nanotubes can move during scanning or not influence the cantilever oscillations because of adsorbate present on the surface. Moreover, adsorbate presence can significantly distort observed height of nanotubes. Nonetheless, concentration of catalyst nanoparticles can be determined from AFM images, and average concentration of carbon nanotubes can be derived from SEM images with high precision. Effectiveness of growth, determined as ratio of the amount of synthesized SWCNTs to the quantity of the catalyst nanoparticles on the surface, is a value of the order of 1:250, which matches effectiveness of growth on mono-disperse catalyst with methane source [21], but is an order of magnitude less than effectiveness of growth with CO precursor as carbon source [8].

Structural perfection and diameter of SWNTs

Focused laser excitation (focus spot diameter 0,5 µm, wavelength 532 nm, power 35 mW) was used for micro-Raman study of SWNTs synthesized on catalyst with increased density: Ni and Co catalyst deposited on quartz substrate, Figure 5. In main, quite narrow G-band is obtained in areas containing SWNTs. The G-band is associated with C-C stretching in-plain vibrations. We observed G-band shift which we relate to the

(a)

(b)
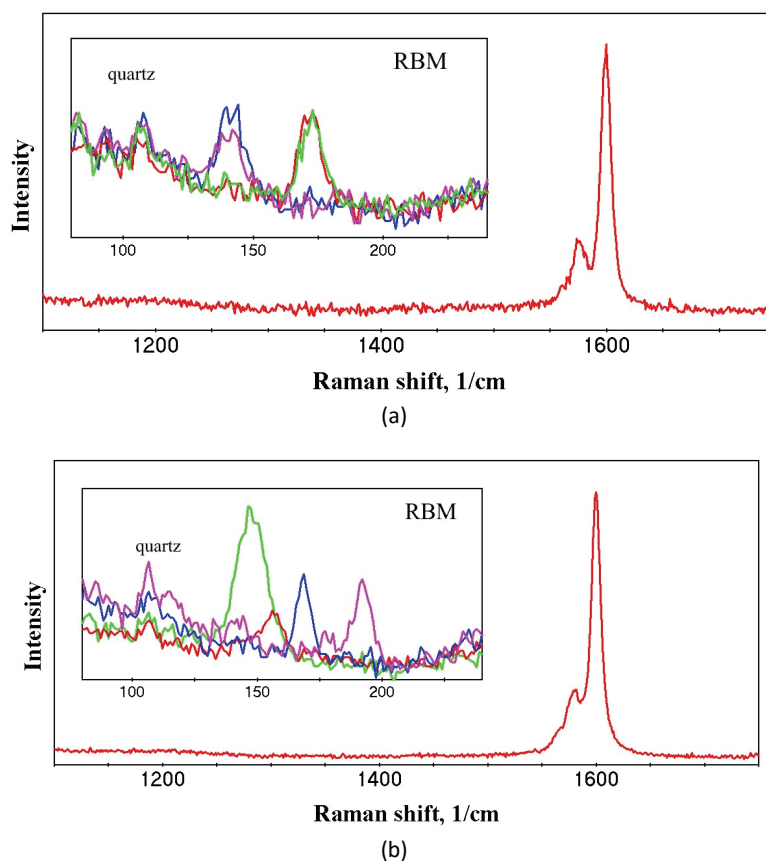
Figure 5. Raman spectra of SWNTs grown with Ni (a) and Co (b) catalyst on quartz substrate (RBM spectra range is given in the insets).

5

variation of the SWNT-substrate interaction force. Nevertheless, no radial breathing mode band (RBM) shift is observed [22]. D-band is not observed even for 100 s of exposition and more, which indicates high crystal perfection of the SWNTs and very small density of dangling bonds [13] (Figure 5). Based on the G-band shape we argue that there are from 1 to 5 SWNTs under laser exposition every single spectra acquisition: G-band peaks are rather narrow, splitting of the G$^+$ and G$^-$ peaks is observed indicating that the nanotubes are single walled. Additionally, based on G$^+$-band and G$^-$ band intensity ratio and general G-peak line shape we deduce that most of the SWNTs are semiconducting ones. The RBM band frequency range is estimated to be from 140 to190 cm^{-1} in case of Co catalyst, while for the Ni catalyst it falls into the 140–170 cm^{-1} range.

Using the simple formula $\omega_{RBM} = C/d_t$ ($C = 248$ cm for an isolated SWNT on Si substrate [23]) we find that the average SWNT diameter equals 1,3–1,7 nm for Co catalyst, and 1,4–1,7 nm for Ni catalyst.

It should be noted that no Raman bands were observed at the surface regions not occupied with SWNTs. This serves as an additional proof that the surfactant together with solvent evaporated during the synthesis, rather than decomposed to carbon phase. Based on the data described above we may conclude that the catalyst material influence on the SWNT quality is insignificant. As was established before SWNT diameter is influenced substantially by the catalyst particle size [24]. Since the particle size was the same in case of Ni- and Co-based catalyst average diameters of SWNTs synthesized in our work did not differ in case of these two catalyst material within the measurement error.

Low synthesis efficiency is related mainly to the use of hydrocarbon precursor, while the catalyst particles size plays the minor role, but still determining the synthesis efficiency via the determination of critical catalyst size of the synthesis termination [21]. Concluding, the method is proposed of rather uniform SWNT lateral arrays synthesis.

CONCLUSION

Ni and Co catalyst monodisperse nanoparticles obtained in the reactor of the reverse micelles were used as a catalyst for CVD growth of lateral arrays of carbon nanotubes from a methane–hydrogen mixture at 1000 °C. As a result predominantly single-walled carbon nanotubes with diameteres 1.3–1.7 nm were obtained. SWNTs length reaches 200 µm, which is great advance in compare to 0,5 µm length SWNTs reported in [21]. The nanotubes have a low number of defects. Growth efficiency is 1:250, which indicates that participation in the process of growth of less than 1% of the catalyst. Increased efficiency may be accomplished by appropriate processing and modification of technology.

REFERENCES

[1] M.M. Shulaker, G. Hills, N. Patil, H.Wei, H.-Y. Chen, H.-S.P. Wong, S. Mitra, Carbon nanotube computer, Nature **501** (2013) 526–530.

[2] D. Sun, M.Y. Timmermans, Y. Tian, A.G. Nasibulin, E.I. Kauppinen, S. Kishimoto, T. Mizutani, Y. Ohno, Flexible high-performance carbon nanotube integrated circuits, Nat. Nanotechnol. **6** (2011) 156–161.

[3] P. Hu, J. Zhang, L. Li, Z. Wang, W. O'Neill, P. Estrela, Carbon nanostructure-based field-effect transistors for label-free chemical/biological sensors, Sensors **10** (2010) 5133–5159.

[4] D. Zhang, K. Ryu, X. Liu, E. Polikarpov, J. Ly, M.E. Tompson, C. Zhou, Transparent, conductive, and flexible carbon nanotube films and their application in organic light-emitting diodes, Nano Lett. **6** (2006) 1880–1886.

[5] T.M. Barnes, X. Wu, J. Zhou, A. Duda, J. van de Lagemaat, T.J. Coutts, C.L. Weeks, D.A. Britz, P. Glatkowski, Single-wall carbon nanotube networks as a transparent back contact in CdTe solar cells, Appl. Phys. Lett. **90** (2007) 243503–243505.

[6] V.K. Sangwan, V.W. Ballarotto, D.R. Hines, M.S. Fuhrer, E.D. Williams, Controlled growth, patterning and placement of carbon nanotube thin films, Solid-State Electron. **54** (2010) 1204–1210.

[7] P.H. Lau, K. Takei, C. Wang, Y. Ju, J. Kim, Z. Yu, T. Takahashi, G.N. Cho, A. Javey, Fully printed, high performance carbon nanotube thin-film transistors on flexible substrates, Nano Lett. **13** (2013) 3864–3869.

[8] B. Zheng, C. Lu, G. Gu, A. Makarovski, G. Finkelstein, J. Liu, Efficient CVD growth of single-walled carbon nanotubes on surfaces using carbon monoxide precursor, Nano Lett. **2** (2002) 895–898.

[9] M.A. Ribas, F. Ding, P.B. Balbuena, B.I. Yakobson, Nanotube nucleation versus carbon-catalyst adhesion–Probed by molecular dynamics simulations, J. Chem. Phys. **131** (2009) 224501–224503.

[10] R. Rao, D. Liptak, T. Cherukuri, B.I. Yakobson, B. Maru-yama, *In situ* evidence for chirality-dependent growth rates of individual carbon nanotubes, Nat. Mat. **11** (2012) 213–216.

[11] G. Lamura, A. Andreone, Y. Yang, P. Barbara, B. Vigolo, C. Hérold, J.-F Marêché, P. Lagrange, M. Cazayous, A Sacuto, M. Passacantando, F. Bussolotti, M. Nardone, High-crystalline single- and double-walled carbon nano-tube mats grown by chemical vapor deposition, J. Phys. Chem., C **111** (2007) 15154–15159.

[12] L. Wei, B. Wang, D. Liu, L.-J. Li, Y. Yang, Y. Chen, In situ formation of cobalt nanoclusters in sol-gel silica films for single-walled carbon nanotube growth, NANO **4** (2009) 99–106.

[13] H. Nishino, S. Yasuda, T. Namai, D.N. Futaba, T. Yamada, M. Yumura, S. Iijima, K. Hata, Water-assisted highly efficient synthesis of single-walled carbon nanotubes forests from colloidal nanoparticle catalysts, J. Phys. Chem., C **111** (2007) 17961–17965.

[14] M. Su, Y. Li, B. Maynor, A. Buldum, J.P. Lu, J. Liu, Lattice-oriented growth of single-walled carbon nanotubes, J. Phys. Chem., B **104** (2000) 6505–6508.

[15] V.B. Golovko, H.W. Li, B. Kleinsorge, S. Hofmann, J. Geng, M. Cantoro, Z. Yang, D.A. Jefferson, B.F.G. Johnson, W.T.S. Huck, J. Robertson, Submicron pattern-ing of Co colloid catalyst for growth of vertically aligned carbon nanotubes, Nanotechnology **16** (2005) 1636––1640.

[16] E.M. Egorova, A.A. Revina. Synthesis of metallic nano-particles in reverse micelles in the presence of quer-cetin, Colloids Surf., A **168** (2000) 87–96.

[17] M. Rao, R.D. Gonzalez, V.T. John, D. Kaplan, J. Akkara, Catalytic and interfacial aspects of enzymatic polymer synthesis in reversed micellar systems, Biotechnol. Bioeng. **41** (1993) 531–540.

[18] A. Magrez, J.W. Seo, R. Smajda, M. Mionić, L. Forró. Catalytic CVD synthesis of carbon nanotubes: towards high yield and low temperature growth, Materials **3** (2010) 4871–4891.

[19] S. Zhang, J. Lee, S. Sun, Controlled Synthesis of Mono-disperse Magnetic Nanoparticles in Solution Phase, The Open Surface Science J. **4** (2012) 26–34.

[20] I.I. Bobrinetskiy, A.S. Seleznev, I.F. Gayduchenko, G.E. Fedorov, A.G. Domantovskiy, M.Yu. Presnyakov, R.Y. Podchernyaeva, G.R. Mikchailova, I. A. Suetina, The interaction between nerve cells and carbon nanotube networks made by CVD process investigation, Biophysics **58** (2013) 409–414.

[21] Y. Li, J. Liu, Y. Wang, Z.L. Wang, Preparation of mono-dispersed Fe−Mo nanoparticles as the catalyst for CVD synthesis of carbon nanotubes, Chem. Mater. **13** (2001) 1008–1014.

[22] L. Ding, W. Zhou, T.P. McNicholas, J. Wang, H. Chu, Y. Li, J. Liu, Direct observation of the strong interaction between carbon nanotubes and quartz substrate, Nano Res. **2** (2009) 903–910.

[23] M.S. Dresselhaus, G. Dresselhaus, R. Saito, A. Jorio, Raman spectroscopy of carbon nanotubes, Phys. Rep. **409** (2005) 47–99.

[24] M. Kumar, Y. Ando, Chemical vapor deposition of car-bon nanotubes: a review on growth mechanism and mass production, J. Nanosci. Nanotechnol. **10** (2010) 3739–3758.

IZVOD

SINTEZA MREŽA JEDNOSLOJNIH UGLJENIČNIH NANOCEVI KORIŠĆENJEM MONODISPERZNIH METALNIH NANOKATALIZATORA OBUHVAĆENIH U REVERZNIM MICELAMA

Igor A. Gayduchenko[1], Georgy E. Fedorov[1], Ramil A. Ibragimov[2], Tatiana S. Stepanova[1], Arsen S. Gazaliev[1], Nikolay A. Vysochanskiy[1], Yuri A. Bobrov[3], Anton M. Malovichko[2], Ilya M. Sosnin[4,5], Ivan I. Bobrinetskiy[2]

[1]*National Research Centre "Kurchatov Institute", 123182, Akademika Kurchatova pl., 1, Moscow, Russia*
[2]*Center for probe microscopy and nanotechnology, National Research University of Electronic Technology (MIET), 124498, pass 4806, bld. 5, Moscow, Zelenograd, Russia*
[3]*NT-MDT Co. Building 100, Zelenograd, Moscow 124482, Russia*
[4]*Togliatti State University, 445667, Belorusskaya str, 14, Togliatti, Russia*
[5]*R&D "Nanomet" LCC. 445030, Tsvetnoy Boulevard 3, 48, Samara region, Togliatti, Russia*

(Naučni rad)

U radu je prikazana metoda sinteze mreža jednoslojnih ugljeničnih nanocevi na silicijum-dioksid podlogama korišćenjem monodisperznih Co i Ni katalizatora. Katalitičke nanočestice su dobijene modifikovanom metodom reversne micele natrijum bis-(2-etilheksil)-sulfosukcinat u izooktan rastvoru, koja obezbeđuje kontrolu veličine nanočestica u rasponu od 1 do 5 nm. Metalne nanočestice Ni i Co su okarakterisane pomoću prenosnog elektronskog mikroskopa (TEM) i mikroskopije atomskih sila (AFM). Ugljenične nanocevi su sintentisane metodom hemijskog taloženja pare CH_4/H_2 na temperaturi od 1000 °C na katalizatorima prethodno deponovanim na silicijum-dioksid podlogama. Pre temperaturnog tretmana tokom sinteze ugljeničnih nanocevi najveći deo materijala katalizatora aglomeriše se usled magnetnih sila, a tokom rasta nanocevi raspada se u odvojene nanočestice uskog prečnika. Formirane mreže nanocevi su okarakterisane pomoću AFM, skenirajuće elektronske mikroskopije (SEM) i Raman spektroskopije. Dobijene su uglavnom jednoslojne ugljenične nanocevi visokog stepena strukturnog savršenstva, dužine do 200 μm, prečnika od 1,3 do 1,7 nm zavisno od raspodele prečnika nanočestica katalizatora i nezavisno od materijala.

Ključne reči: Ugljenične nanocevi • Nanočestice • Reversna micela • Hemijsko taloženje isparenja

Cu(II) immobilization onto a one-step synthesized poly(4-vinylpyridine-*-co*-ethylene glycol dimethacrylate) resin: Kinetics and XPS analysis

Danijela D. Maksin[1], Aleksandra B. Nastasović[2], Tatjana N. Maksin[1], Zvjezdana P. Sandić[1,3], Katja Loos[4], Bojana M. Ekmeščić[2], Antonije E. Onjia[1]

[1]University of Belgrade, Vinča Institute of Nuclear Sciences, Belgrade, Serbia
[2]University of Belgrade, ICTM – Center for Chemistry, Belgrade, Serbia
[3]University of Banja Luka, Faculty of Science, Banja Luka, B&H (Republic of Srpska)
[4]Department of Polymer Chemistry, Zernike Institute for Advances Materials, University of Groningen, Groningen, The Netherlands

Abstract
Synthesis of an unconventional resin based on 4-vinylpyridine (4-VP) and its Cu(II) sorption behavior were studied. Three samples of macroporous crosslinked poly(4-vinylpyridine-*co*--ethylene glycol dimethacrylate) (P4VPE) with different porosity parameters were prepared by suspension copolymerization by varying the *n*-heptane amount in the inert component. The samples were characterized by mercury porosimetry, elemental analysis and X-ray photoelectron spectroscopy (XPS). The sorption of P4VPE for Cu(II) ions, determined under non-competitive conditions, was relatively rapid, *i.e.*, the maximum capacity was reached within 30 min. The maximum experimental sorption capacity for the sample with the highest values of pore diameter and specific pore volume (sample 3, Q_{eq} = 89 mg g^{-1}) was 17.5 times higher than for the sample with the lowest values of pore diameter and specific pore volume (sample 1, Q_{eq} = 5.1 mg g^{-1}). Since the values for pyridine content in all P4VPE samples were almost the same, it was concluded that the porosity parameters have predominant influence on Cu(II) sorption rates on P4VPE. The sorption behavior and the rate-controlling mechanisms were analyzed using six kinetic models (pseudo-first order, pseudo-second order, Elovich, intraparticle diffusion, Bangham and Boyd models). XPS study clarified the nature of the formed P4VPE-Cu(II) species.

Keywords: 4-vinylpyridine, macroporous copolymer, sorption kinetics, XPS.

Available online at the Journal website: http://www.ache.org.rs/HI/

The presence of the weakly basic nitrogen in the ring, combined with good acid and oxidation resistance, as well as their thermostability, render vinylpyridine polymers convenient for flocculation and metal sorption [1]. High internal volume accessible to the constituents of the treated solution that are being removed is a prerequisite for any sorbent material. Surface area, pore size distribution and nature of the pores have a critical influence on the type of sorption process. The existence of active functional groups on the sorbent surface facilitates chemical interactions that typically result in effects that are different from and less reversible than physisorption [2]. Poly(vinylpyridine) copolymers are primarily used in sorption applications after treatment with appropriate reagents to introduce a desired functional moiety in order to target specific sorbate species. For example, quaternized poly(4-vinylpyridine-*co*-divinylbenzene), P4VPD, (Reillex™ HPQ) was used for the recovery of metallic species

(including radioactive metals) like for Hg(II) sorption [3], Cr(VI) removal from aqueous solutions [4], perrhenate sorption from acid solutions [5], uranium sorption from acidic sulfate solutions [6], pertechnetate sorption from nitric acid solutions [7] and separation of plutonium using nitrate anion exchanger [8]. However, additional functionalization of macroporous copolymers is not always recommended. The problems that potentially arise are undesired side reactions leading to ineffective byproducts, unintentional alterations of pore structure as the consequence of chemical modification, low degree of conversion, etc. Structural rigidity and hydrophobicity of P4VPD are undesirable with respect to complexation of metal ions from aqueous solutions [9,10]. These drawbacks could be overcome by using copolymers synthesized with hydrophilic crosslinker, such as ethylene glycol dimethacrylate (EGDMA) or others, like trimethylolpropane trimethacrylate (TRIM) and *N,N*-methylenebisacrylamide (MBA). The study of the sorption abilities of 2-vinylpyridine (2-VP), 4-vinylpyridine (4-VP), or 4-methyl-4'-vinyl-2,2'--bipyridine copolymers synthesized with different dimethacrylate crosslinkers was performed with respect to Cd(II), Co(II), Cu(II), Hg(II) and Ni(II) [10], as well

as on poly(4-vinylpyridine) copolymers crosslinked with oligo(ethylene glycol dimethacrylates) (ethylene glycol dimethacrylate (1EG), triethylene glycol dimethacrylate (3EG) and tetraethylene glycol dimethacrylate (4EG)) used for Co(II), Ni(II), Cu(II) and Hg(II) sorption [9].

To the best of our knowledge, only few papers deal with the application of porous 4VP-based copolymers not further modified to introduce functionalities other than pyridine nitrogen. Porous copolymers of 2-VP and 4-VP crosslinked with divinyl benzene (DVB) were used for Cu(II), Ni(II) and Co(II) sorption [11]. Castro *el al.* used P4VPD as supported Cu(II) polymer catalysts for the catalytic oxidation of phenol at 303 K and atmospheric pressure using air and H_2O_2 as oxidants [12].

In this study, three samples of macroporous crosslinked copolymers of 4-vinylpyridine and ethylene glycol dimethacrylate, P4VPE, with different porosity parameters were tested for Cu(II) sorption from aqueous solutions. Six kinetic models, chemical reaction- and diffusion-based (pseudo-first order (PFO), pseudo-second order (PSO), Elovich, intraparticle diffusion (IPD), Bangham and Boyd model) were used to analyze Cu(II) uptake kinetics in order to define the rate-controlling mechanisms. The nature of interactions between Cu(II) ions and pyridine groups of porous P4VPE was further elucidated by XPS.

EXPERIMENTAL

P4VPE synthesis

4-VP, EGDMA, azo-α,α'-bisisobutyronitrile (AIBN), *n*-heptane, 2-hydroxyethyl cellulose, gelatin and NaCl were purchased from Sigma-Aldrich. All reagents and solvents were used as supplied, except AIBN which was recrystallized from methanol before use.

Three samples of macroporous crosslinked P4VPE were prepared by a radical suspension copolymerization in a 0.5 dm^3 three-necked round bottom flask [13]. The monomer phase (80.9 g) containing monomer mixture (24.2 g of 4-VP and 10.3 g of EGDMA), AIBN as initiator (0.8 g) and inert component (8.1, 24.3 and 40.5 g of *n*-heptane for samples 1–3, respectively) was suspended in the aqueous phase consisting of 237.6 g of water, 0.46 g of gelatin, 0.46 g of 2-hydroxyethyl cellulose and 4.6 g of NaCl. The copolymerization was carried out at 343 K for 8 h with a stirring rate of 200 rpm. After completion of the reaction, the copolymer particles were washed with water and ethanol, kept in ethanol for 12 h and dried in vacuum at 313 K. Synthesized samples were purified by extraction in a Soxhlet apparatus with ethanol. The copolymer particles were dried in vacuum at 343 K and sieved. For further investigations, the fraction with particle size of 150–500 μm was used.

Sample analysis

The pore size distributions of the samples were determined by mercury intrusion porosimetry (high pressure Carlo Erba porosimeter 2000), operating in the interval of 0.1–200 MPa. Sample preparation was performed at room temperature and pressure of 0.5 kPa. Samples were outgassed at 323 K and 1 mPa for 6 h.

The copolymer samples were analyzed for their carbon, hydrogen and nitrogen content using the Vario EL III device (GmbH Hanau Instruments, Germany). Elemental composition was calculated from multiple determinations of elemental analysis within ±0.2% agreement.

The Cu(II) concentrations were determined by flame atomic absorption spectrometry (FAAS, SpektrAA Varian Instruments). Standard statistical methods were used to determine the mean values and standard deviations for each set of data.

X-ray photoelectron spectroscopy (XPS) was performed with a Surface Science Instruments SSX-100 photoelectron spectrometer with a monochromatic Al Kα X-ray source ($h\nu$ = 1486.6 eV; 1 eV = 1.6022×10^{-19} J). Measurements were carried out at the photoelectron take-off angle of 35° with respect to the sample surface. The resolution of the survey scans was set to 4, and the acquisition of C 1s signal was done at the constant pass energy of 50 eV. All spectra were the averaged results of four measurements. Data analysis was performed with the software package Winspec 2.09. To compensate for the surface charging effect, all the binding energies were referred to the neutral C 1s peak of 284.6 eV. The elemental compositions were calculated with the following relative sensitivity factors: O 1s: 2.49; N 1s: 1.68; C 1s: 1; Si 2s: 1.03; Si 2p: 0.90.

Batch metal-uptake experiments

The sorption of Cu(II) ions from $CuCl_2$ aqueous solutions (initial concentration of 0.05 M) was investigated in batch experiments under non-competitive conditions, at 298 K. P4VPE (2.0 g) was soaked in 5 cm^3 of buffer solution (NaOAc/HOAc, pH 5.5) for 1h. After that, the copolymer was contacted with 72.5 cm^3 of $CuCl_2$ solution (0.05 M) and 72.5 cm^3 of buffer solution. At the appropriate time intervals, the samples were filtered, washed subsequently with water and ethanol, and dried. The remaining solutions were kept for Cu(II) analysis. The reproducibility of the sorption experiments results was verified in triplicate. Standard statistical methods were used to determine the mean values and standard deviations for each set of data and relative standard deviations did not exceed 5.0%. The amount of Cu(II) ions sorbed onto unit mass of macroporous copolymer beads was calculated by using the following expression:

$$Q_t = \frac{(C_i - C_t)V}{m} \tag{1}$$

RESULTS AND DISCUSSION

Samples characterization

Porosity, such an essential characteristic of macroporous copolymers, can be controlled by the type and the amount of the inert component (porogen) and the type and the amount of crosslinking monomer in the reaction mixture [14]. The generally accepted opinion among the leading experts in the field of polymer science is that the difference in the solubility parameters of polymer and inert component, *i.e.*, $|\delta_P - \delta_S|$, can be used as an indication of the inert component impact on the porous structure of copolymers [15]. The solubility parameter, δ_P, for P4VPE (calculated according to the Van Krevelen equation) is 23.6 (J cm^{-3})$^{1/2}$ [16]. The literature value of solubility parameter, δ_S, for *n*-heptane is 15.1 (J cm^{-3})$^{1/2}$ [17]. Thus, based on the difference in the solubility parameters, *n*-heptane is frequently used as the inert component, *i.e.*, porogen for the synthesis of vinylpyridine macroporous copolymers (as non-solvent) [18–20]. Additionally, the literature data confirm that the pore volume of P4VPD can be increased by adding a non-solvent component in the inert component and/or by increasing the inert component content [21].

The values of porosity parameters (V_S and $d_{V/2}$) of P4VPE were calculated from the cumulative pore volume distribution curves while specific surface was calculated on the basis of the cylindrical pore model as described in literature [22,23]. The relevant P4VPE porosity parameters were previously published and collected in Table 1 [13].

Table 1. Porosity parameters of the synthesized P4VPE samples [13]

Sample	V_S / cm^3 g^{-1}	S_{Hg} / m^2 g^{-1}	$d_{V/2}$ / nm
1	0.20	4.2	830
2	0.74	7.3	1800
3	1.15	8.8	2400

The pyridine content of P4VPE samples calculated from the elemental analysis of nitrogen for samples 1––3 was 5.36, 5.24 and 5.19 mmol g^{-1}, respectively. The theoretical pyridine content of P4VPE samples calculated on the basis of the feed composition, *i.e.*, 4-VP content in the monomer mixture, was 5.45 mmol g^{-1}. The pyridine content calculated from the elemental analysis data is somewhat lower than the theoretical. Although the elemental analysis data for the samples is in fair agreement with the theoretical values, the minor

discrepancies can be ascribed to the loss of 4-vinyl-pyridine due to its solubility in the aqueous phase [24].

Sorption kinetics

From the perspective of potential applications, one of the key properties of the chelating polymers is the rate at which metal sorption attains equilibrium. Rapid sorption of metal ions is advantageous, providing a short residence time required for the completion of the actual process. The previously published results [13] demonstrated the increase of Cu(II) amount sorbed by P4VPE with time, reaching almost 90% of the maximum capacity already after 30 min. The excellent achieved sorption half-time values were comparable with the literature data (3, 5 and 6 min for samples 1–3, respectively). Sugii *et al.* found the $t_{1/2}$ values for Cu(II) and Ni(II) sorption on P4VPD to be 3 and 5 min, respectively [11]. Also, they found higher Cu(II) sorption rates for P4VPE than for P4VPD in the acetate buffer [9]. The $t_{1/2}$ values for Hg(II) sorption on P4VPD quaternized with 2-chloroacetamide were 4 and 14 min from diluted mercury acetate and mercury chloride solutions, respectively [3].

The amount of Cu(II) ions sorbed at equilibrium for sample 3 (Q_{eq} = 1.40 mmol g^{-1}, 89 mg g^{-1}), *i.e.*, the sample with the highest values of pore diameter and specific pore volume was 17.5 times higher than for sample 1 (Q_{eq} = 0.08 mmol g^{-1}, 5.1 mg g^{-1}) and 2 times higher than for sample 2 (Q_{eq} = 0.69 mmol g^{-1}, 44 mg g^{-1}). As the pyridine content in all P4VPE samples is roughly the same, it can be deduced that the porosity parameters of the copolymer samples used in the sorption experiments had the predominant influence on the Cu(II) uptake behavior. The pH value of 5.5 was selected as the optimum, being as close to neutral as possible, but at the same time taking into consideration that at pH values higher than 6 significant hydrolysis of Cu(II) occurs at high concentrations which are the order of magnitude higher than the ones used in this study [25].

Kinetic modeling

The migration rates of metal ions from the bulk solution to the sorbent surface and the accumulation on this surface govern the kinetics of sorption process and thus its efficiency [2]. The analysis of kinetics offers an insight into the possible mechanisms of sorption and reaction pathways. Sorption mechanisms are dependent on sorbate–sorbent interactions and system conditions, making it impossible to classify sorption mechanisms by solute type [26]. A logical classification based on kinetic models was introduced and generally accepted.

Previously published studies indicate that there are four consecutive phases in the sorption of sorbate by a porous sorbent: bulk diffusion, film or boundary layer

diffusion, intraparticle diffusion and finally solute sorption by complexation or physicochemical sorption or ion exchange [26,27]. The overall sorption rate may be principally controlled by any of these steps or a combined effect of a few steps is also probable. The most extensively used kinetic models are those that presume that the final step constitutes the major contribution to the process kinetics [28,29]. This step is referred to as the "surface reaction", not necessarily meaning that the actual chemical reaction occurs on the sorbent surface involving the formation of chemical bonds. These kinetic models are known as surface reaction-based models and they do not take into consideration the possible influence of diffusion in sorption processes. However, if diffusion driven kinetics are presumed, in diffusion-based modeling the typical assumption is that bulk diffusion and solute sorption onto the surface of the sorbent are instantaneous and, therefore, not rate determining. Consequently, the rate-controlling parameter may be distributed between film diffusion and intraparticle diffusion. With the intention of analyzing the controlling mechanism of Cu(II) sorption process by P4VPE, several equations (PFO, PSO, Elovich, IPD, Bangham and Boyd models) were tested against the experimental data.

Surface reaction-based kinetic modeling

A variety of kinetic models have based their description of the reaction order of sorption systems on solution concentration. Alternatively, reaction orders based on the capacity of the sorbent have also been successfully introduced [30]. In all probability, the earliest known and one of the most extensively used kinetic equations so far for the sorption of a solute from a liquid solution is the Lagergren's equation or the PFO equation [31]:

$$\log\left(Q_{eq} - Q_t\right) = \log Q_{eq} - \frac{k_1 t}{2.303}$$ (2)

A plot of $\log\left(Q_{eq} - Q_t\right)$ *vs. t* should give a straight line to confirm the applicability of this kinetic model. If the process is strictly first-order, $\log Q_{eq}$ should be equal to the intercept of the plot $\log\left(Q_{eq} - Q_t\right)$ *vs. t*.

The PSO rate expression is employed to describe chemisorption involving valence forces through either sharing or exchange of electrons between the sorbent and sorbate as covalent forces, and ion exchange [32]. The PSO equation is applied in the given form [30]:

$$\frac{t}{Q_t} = \frac{1}{k_2 Q_{eq}^2} + \frac{1}{Q_{eq}} t$$ (3)

A plot of t/Q_t *vs. t* should give a linear relationship for the second-order kinetics. Additionally, the initial sorption rate can be determined using the equation [30]:

$$h = k_2 Q_{eq}^2$$ (4)

The extensively used PSO equation, sometimes denoted as Ho's, has the following advantages according to its author: It does not have the problem of assigning the effective sorption capacity, and the PSO rate constant and the initial sorption rate all can be calculated from the equation without having prior knowledge of any of the parameters [30]. An additional advantage of the PSO equation for estimating the Q_{eq} values is its reduced sensitivity to the influence of random experimental errors [2]. This equation deserves particular attention as it predicts the behavior over the whole range of studies and is in agreement with chemisorption being the rate controlling step [32]. The relevant parameters calculated from the values of the intercepts and slopes of the corresponding plots for the PFO and the PSO equations are given in Table 2. Plots $\log\left(Q_{eq} - Q_t\right)$ vs. *t* (PFO) and t/Q_t vs. *t* (PSO) for Cu(II) sorption by P4VPE are shown in Figure 1.

Table 2. Kinetic parameters for Cu(II) uptake using P4VPE samples as sorbent

Parameter	Sorbent		
	1	2	3
Q_{eq} / mmol g^{-1}	0.08	0.69	1.40
Pseudo-first order			
k_1 / min^{-1}	0.049	0.065	0.064
Q_{eq}^{calc} / mmol g^{-1}	0.04	0.45	0.89
R^2	0.864	0.946	0.870
Pseudo-second order			
k_2 / g mmol^{-1} min^{-1}	3.97	0.31	0.14
h / mmol g^{-1} min^{-1}	0.03	0.16	0.31
Q_{eq}^{calc} / mmol g^{-1}	0.082	0.73	1.48
R	0.999	0.999	0.999
Elovich			
a_e / mmol g^{-1} min^{-1}	0.31	0.60	0.96
b_e / g mmol^{-1}	95.2	8.16	3.82
R^2	0.962	0.952	0.944
Intraparticle			
k_{id} / mmol g^{-1} min$^{-0.5}$	0.003	0.047	0.13
C_{id} / mmol g^{-1}	0.05	0.39	0.62
R^2	0.987	0.985	0.995
Bangham			
$k_b \times 10^3$ / g^{-1}	0.07	0.43	0.79
α	0.219	0.356	0.477
R^2	0.784	0.804	0.849

The theoretical Q_{eq} values estimated from the first-order kinetic model were not in compliance with the experimental Q_{eq}, and the observed coefficients of determination were rather low. Accordingly, the PFO model is not valid for Cu(II) sorption on P4VPE. On the
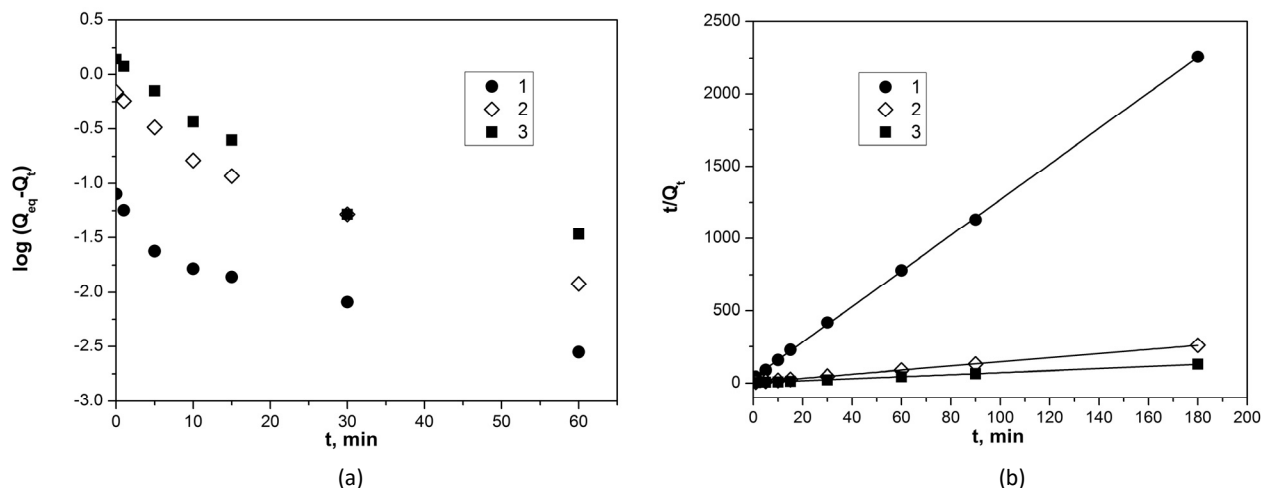
Figure 1. Pseudo-first (a) and pseudo-second order kinetics (b) of Cu(II) uptake by P4VPE samples (sample 1 – black circles, sample 2 – white rhombs, sample 3 – black squares).

other hand, the theoretical Q_{eq} values calculated from the PSO model were found to be in close agreement with the experimental Q_{eq} values with coefficients of determination higher than 0.99. Such R^2 values verify that the sorption data are well represented by PSO kinetics for the whole sorption period and, in consequence, maintain the premises of the model [30].

The initial sorption rate is the highest for the sample with the highest specific pore volume and pore diameter (sample 3), reflecting the greatest availability of sorption centers in this sample and thus the most pronounced affinity of sample 3 for Cu(II) ions. The superior fit of the PSO rate expression to the experimental data indicates that the sorption process is surface reaction-controlled through chemisorption by sharing or exchange of electrons between P4VPE and Cu(II) as covalent forces and/or through ion exchange [30]. In the past decade, the PSO kinetic model has been widely applied to the pollutants sorption from aqueous solutions [30].

The Elovich equation, also successfully employed to describe second-order kinetics is based on the supposition that the actual sorbent surface is energetically heterogeneous and that neither desorption nor interactions between the sorbed species could considerably influence the sorption kinetics at low surface coverage [33]. This equation does not propose any definite mechanism for sorbate-sorbent reaction, but it has been broadly used in sorption kinetics to describe chemisorption through mechanisms which are chemical reactions by nature [34]. The complexity of the original Elovich equation encouraged the habitual use of its simplified linear form [33]:

$$Q_t = \frac{\ln a_e b_e}{b_e} + \frac{1}{b_e}\ln t \qquad (5)$$

The Elovich coefficients a_e and b_e can be calculated from the plots of Q_t *vs.* $\ln t$ (Figure 2). The relevant kinetic parameters for surface reaction-based kinetic models, as well as coefficients of determination were listed in Table 2.
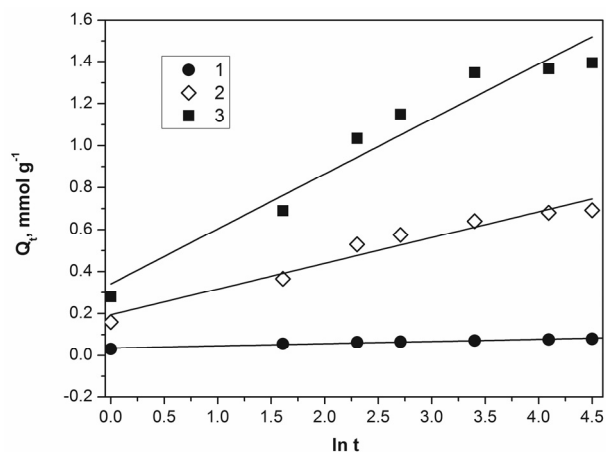
Figure 2. Elovich plots for Cu(II) sorption on PVPE samples (sample 1 – black circles, sample 2 – white rhombs, sample 3 – black squares).

The non-physical behaviour of Eq. (5) for longer sorption times is easily noticeable, *i.e.*, $q(t\rightarrow\infty) = \infty$ [28]. Theoretical interpretations of this equation suggest that the underlying reason for such behavior is that the rate of simultaneously occurring desorption is neglected. Consequently, the applicability of the Elovich equation is in practice restricted to the initial times of sorption process, when the system is relatively far from equilibrium [28]. Yet, recent studies demonstrate very similar behavior of the Elovich and the PSO equations under the assumption that the system is not close to equilibrium [28]. Rudzinski and Plazinski have quantitatively proved that in spite of their different mathe-

matical form, both the PSO and the Elovich equations display basically identical behaviour when taking into account the values of fractional surface coverages lower than about 0.7 [29].

Diffusion-based kinetic modeling

Generally, metal sorption by porous sorbents is a multi-step process involving transport of the solute molecules from the aqueous phase to the surface of the solid particulates followed by diffusion into the interior of the pores [26,27]. Thus, diffusional mass transport models, such as film diffusion and intra-particle diffusion, warrant further consideration. Their role is very significant especially in processes where ion exchange and ionic bonding are not as dominant as in chemisorption processes [32].

Since the PFO, the PSO and Elovich kinetic models cannot identify this influence of diffusion on sorption, the Weber and Morris equation was used for calculation of the rate constants of the IPD model [35]. This model presumes that film or boundary layer diffusion is negligible, and that IPD is the only rate-controlling step. The rate of IPD can be calculated according to the equation [36]:

$$Q_t = C_{id} + k_{id} t^{0.5} \tag{6}$$

where C_{id} is the intercept which is proportional to the boundary layer thickness [37]. The values of C_{id} and k_{id} are tabulated in Table 2. The k_{id} value was estimated from the slope of the linear portion of the plot Q_t *vs.* $t^{0.5}$ displayed in Figure 3. If the Q_t *vs.* $t^{0.5}$ plot is linear over the whole time range and if the line passes through the origin, IPD is the only rate-controlling step [38]. If not, it is indicative of involvement of some other mechanisms.

Figure 3. Plots based on intraparticle diffusion model for Cu(II) uptake using P4VPE as sorbent (sample 1 – black circles, sample 2 – white rhombs, sample 3 – black squares).

The plots Q_t *vs.* $t^{1/2}$ presented in Figure 3 for Cu(II) sorption on P4VPE did not pass through the origin suggesting that even though the sorption process included

IPD, it was not the only rate-controlling step [38]. The positive value of intercept is indicative of some degree of boundary layer control. Its contribution increases with the increase of k_{id}, *i.e.*, as the surface area and pore diameter become larger. The multilinear shape of Q_t *vs.* $t^{1/2}$ relationships indicates that more than one process governs Cu(II) sorption on P4VPE, too. The first sharper portion (Figure 3) can be regarded as external surface sorption or faster sorption stage, succeeded by gradual sorption where IPD is rate controlling. After that, in the final equilibrium stage IPD slows down due to the low sorbate concentration in solution. Kumar et al. observed the similar behavior for Cr(III) removal by using an amine-based polymer, aniline-formaldehyde condensate (AFC) coated on silica gel [39]. When all other conditions are the same (size of sorbate mole-cule, sorbate concentration and its affinity towards the sorbent, the diffusion coefficient of the sorbate in the bulk, the degree of mixing), the rate of uptake is limited by the sorbent pore size distribution [38]. In this case, it is apparent from Table 2 that the increase in specific pore volume and pore diameter is crucial for the obs-erved trend in the k_{id} values. IPD is facilitated by the presence of macroporosity.

It is also noticeable that the dependence of the amount of Cu sorbed on the square-root of time has a concave character for all three samples (Figure 3). The model analysis by Plazinski *et al.* has demonstrated that such curve shape may be attributable to a combined effect of the rate of surface reaction and that of the solute transport from the bulk to the surface [28], in support of the conclusions arrived at in the case of this sorbate-sorbent system examined in this paper.

Kinetic data were further analyzed using Bangham's equation in order to confirm that pore diffusion is one of the rate-controlling steps in this sorption system. This equation is commonly expressed as [40]:

$$\log\log\left[\frac{C_i}{C_i - C_s Q_t}\right] = \log\left[\frac{k_b C_s}{2.303V}\right] + \alpha \log t \tag{7}$$

k_b and α are calculated from the intercept and the slope of the straight line plots of log log $[C_i/(C_i−C_sQ_t)]$ *vs.* log t. If this expression is an adequate illustration of experimental data, than the sorption kinetics is limited by pore diffusion [41].

The Bangham plot for P4VPE samples is shown in Figure 4. Bangham´s kinetic parameters were calcul-ated and tabulated in Table 2.

Bangham's plot should be linear if intraparticle dif-fusion is the only rate controlling step [42]. Non-line-arity of the Bangham plots as well as the significant intercept values obtained from the intraparticle dif-fusion model indicated that both film diffusion as well as pore diffusion were rate-limiting [43]. The correl-ation coefficients given by the Bangham's equation

verified that the model did not entirely fit the experimental data for Cu(II) sorption on P4VPE.
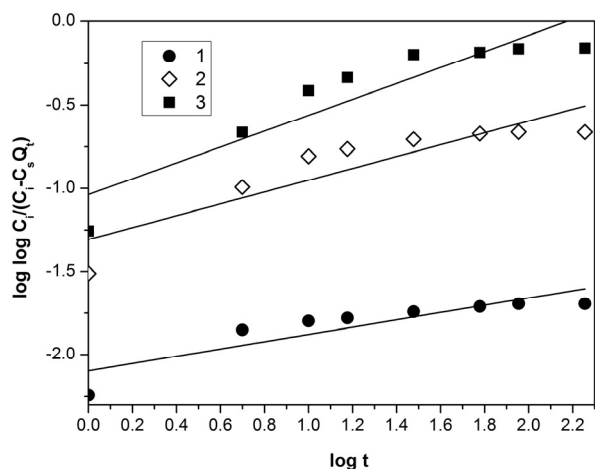
Figure 4. Plot of Bangham's equation for Cu(II) sorption using P4VPE as sorbent (sample 1 – black circles, sample 2 – white rhombs, sample 3 – black squares).

The contribution of boundary layer or film diffusion implied by the non-zero values of the intraparticle plot intercept is often ascertained using the model given by Boyd [36]:

$$F = 1 - \frac{6}{\pi^2} \sum_{n=1}^{\infty} \frac{1}{n^2} \exp\left(-\frac{n^2 \pi^2 D_i t}{r^2} \right) \qquad (8)$$

$$F = 1 - \frac{6}{\pi^2} \sum_{n=1}^{\infty} \frac{1}{n^2} \exp\left(-n^2 B t \right) \qquad (9)$$

where *F* is obtained from the expression:

$$F = \frac{Q_t}{Q_{eq}} \qquad (10)$$

And

$$B = \frac{D_i \pi^2}{r^2} \qquad (11)$$

The approximations for *Bt* proposed by Reichenberg [44] are as follows:

$$F \text{ values} < 0.85, \ Bt = \left(\pi^{\frac{1}{2}} - \left(\pi - \frac{\pi^2 F}{3} \right)^{\frac{1}{2}} \right)^2 \qquad (12)$$

$$F \text{ values} > 0.85, \ Bt = -0.4997 - \ln(1-F) \qquad (13)$$

Thus, the value of *Bt* can be computed for each value of *F*, and then plotted against time. The linearity of these so-called Boyd plots (Figure 5) was examined to distinguish between sorption controlled by film dif-

fusion and particle diffusion [24]. If the plot is in the form of straight line passing through the origin, this indicates that sorption processes are governed by particle-diffusion mechanisms. If not, they are controlled by film diffusion [45]. From Figure 5, it was observed that the plots were neither linear nor passed through the origin indicating the strong influence of film diffusion during the sorption of Cu(II) on P4VPE, as well.
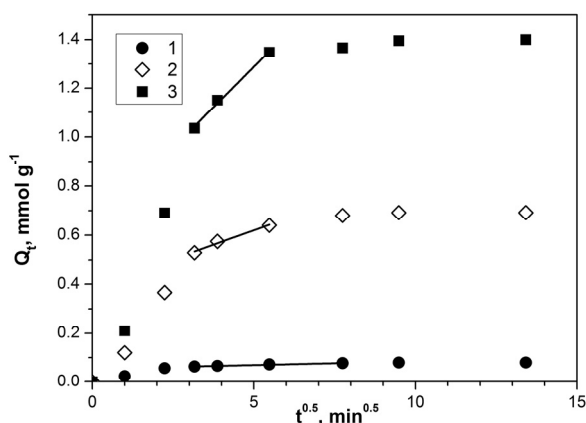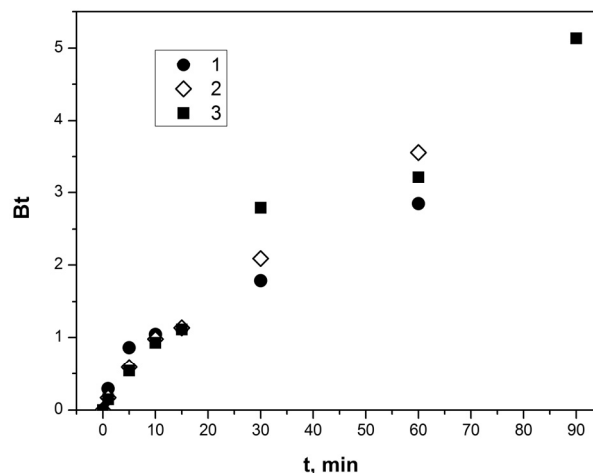

Figure 5. Plots based on Boyd's model for Cu(II) sorption using P4VPE as sorbent (sample 1 – black circles, sample 2 – white rhombs, sample 3 – black squares).

The strong external resistance only during the initial stages of sorption (0–10 min) as seen in Figures 3 and 5 may be mainly due to the absence of mixing and high affinity of the sorbate for the sorbent [46]. Thus, the intraparticle diffusion limits the overall rate of sorption since the investigated systems have high concentration of sorbate and relatively large sorbent particle size of as well as high porosity.

XPS analysis

Positively charged Cu(II) cations form coordination complexes with the nitrogen atom of the pyridine group due to the strong affinity of pyridyl group to metals and its ability to undergo hydrogen bonding, as was established in some previously published studies of P4VPD [12].

XPS measurements were carried out for two P4VPE samples loaded with Cu(II) (Figure 6). Because of the low Q_{eq} value, the results for Sample 1 were omitted from XPS analysis.

Spectral deconvolution of the N 1s XPS spectra of sample 2 (Figure 6a) revealed three distinguishable peaks. The first one at the lowest binding energy of 398.8 eV could be ascribed to the pyridine nitrogen, N(1), [47,48], while the second component at 400.1 eV, N(2), and the third component at 401.6 eV, N(3), were assigned to the pyridine nitrogen interacting with the copper cations and protonated N atoms of P4VPE, res-
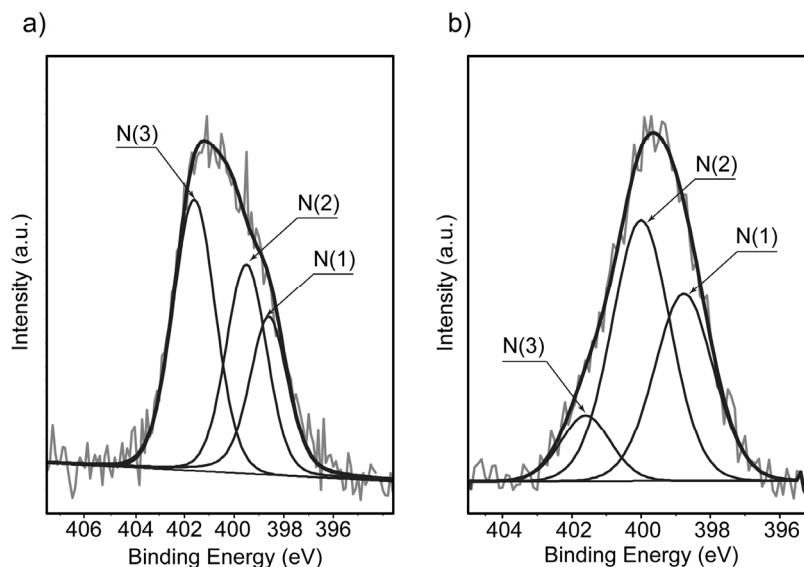
Figure 6. N 1s XPS spectra of P4VPE sample 2 (a) and sample 3 (b) loaded with Cu(II) at pH 5.5 (N(1) = –N, N(2) = –N· · ·Cu^{2+}, N(3) = –NH$^+$).

pectively. Pardey *et al*. reported the N 1s spectrum for poly(4-vinylpyridine), P4VP with a symmetric peak at 399.0 eV and the N 1s spectrum of the fresh and used CuCl$_2$/P4VPD (with 2% of DVB) catalyst with broader and more asymmetric peaks, which could be deconvoluted into two peaks, at 399.0 and 400.3 eV. The peak at 400.3 eV indicated that a fraction of pyridine nitrogen interacts with copper cations [47]. Liu *et al*. observed the peak at 398.6 eV for the pyridine nitrogen in poly(EGDMA-*co*-4VP), PE4VP, and the peak at 400.7 eV for nitrogen atoms in the poly(EGDMA-*co*-4VP) supported-Au nanocolloid [49].

The N 1s peak for Sample 3 was also resolved into three components, *i.e.*, the neutral pyridine nitrogen peak at 398.8 eV, N(1), the peak for pyridine nitrogen of 4PVPE interacting with the copper cations at 400.1 eV, N(2) [48] and the peak for the protonated nitrogen atoms at 401.6 eV, N(3). With the copper ions sorbed on the P4VPE, the N 1s XPS spectra in Figure 6a and b show the component of N(2) peak at 400.1 eV, which can be attributed to the nitrogen atoms in the pyridine groups coordinated with copper ions [50]. The nitrogen atoms share a lone pair of electrons with the electron-withdrawing copper ions to form surface complexes. Consequently, the electron density of the nitrogen atoms in the amine groups is reduced and the N 1s binding energy increased (observed at a higher eV value than neutral pyridine N 1s). It can therefore be concluded that the sorption mechanism is based on the formation of metal complexes by the copper ions with the nitrogen atoms in the neutral pyridine groups. In other words, N· · ·Cu^{2+} complexes were formed on the surfaces of P4VPE. The relative peak ratios of N(1), N(2) and N(3) have been calculated from the areas under

each peak in the spectra of Figures 6a and 6b and the results are given in Table 3.

Table 3. Positions and content of N 1s peaks of P4VPE samples 2 and 3 loaded with Cu(II)

Data/Sample	Groups and atoms		
	N(1)	N(2)	N(3)
Position, eV	398.8	400.1	401.6
	Content, %		
2	24.5	36.2	39.2
3	35.3	53.3	11.4

Due to the enhanced Cu(II) uptake of sample 3 (Q_{eq} = 1.40 mmol g^{-1}) in comparison to sample 2 (Q_{eq} = = 0.69 mmol g^{-1}), N(3)/N(2) ratio is larger than for sample 3.

CONCLUSION

Three samples of macroporous crosslinked poly(4-vinylpyridine-*co*-ethylene glycol dimethacrylate) (P4VPE) with different porosity parameters were prepared by suspension copolymerization by varying the *n*-heptane amount in the inert component and used as Cu(II) sorbents from aqueous solutions. The samples were characterized by mercury porosimetry, elemental analysis and x-ray photoelectron spectroscopy (XPS). It was established that the porosity parameters of P4VPE have strong influence on the Cu(II) sorption rate. Sorption behavior of Cu(II) on P4VPE and the rate-controlling mechanisms were analyzed using six kinetic models (PFO, PSO, Elovich, IPD, Bangham and Boyd models). XPS study clarified the nature of the formed P4VPE-Cu(II) species.

List of symbols

a_e Initial sorption rate from Elovich model ($\text{mmol g}^{-1}\,\text{min}^{-1}$)

α Constant calculated from slope of the Bangham's straight line

B Time constant (Boyd's model) (min^{-1})

b_e Parameter related to the extent of surface coverage and activation energy for chemisorption from Elovich model (g mmol^{-1})

C_e Equilibrium metal ions concentration in solution (mmol dm^{-3})

C_i Initial metal ions concentration (mmol dm^{-3})

C_{id} Constant in IPD model (mmol g^{-1})

C_s Dosage of sorbent (Boyd's model) (g dm^{-3})

C_t Concentration of Cu(II) ions after sorption time t (mmol dm^{-3})

δ_P Solubility parameters of polymer and inert component ($\text{J cm}^{-3})^{1/2}$

δ_S Solubility parameters of polymer and inert component ($\text{J cm}^{-3})^{1/2}$

D_i Effective diffusion coefficient of the metal ions in the sorbent phase ($\text{cm}^2\,\text{min}^{-1}$)

$d_{V/2}$ Pore diameter which corresponds to half of pore volume (nm)

F Fractional attainment of equilibrium at time t (Boyd's model) (min)

h Initial sorption rate from PSO model ($\text{mmol g}^{-1}\,\text{min}^{-1}$)

k_1 PFO rate constant (min^{-1})

k_2 PSO rate constant ($\text{g mmol}^{-1}\,\text{min}^{-1}$)

k_b Constant calculated from the intercept (Bangham's model) (g^{-1})

k_{id} IPD rate constant ($\text{mmol g}^{-1}\,\text{min}^{-0.5}$)

m Mass of the copolymer beads used for the experiment (g)

n Integer that defines the infinite series solution (Boyd's model)

PFO   Pseudo-first kinetic model (PFO)

P4VPE   Poly(4-vinylpyridine-*co*-ethylene glycol dimethacrylate)

PSO   Pseudo-second-order (PSO) kinetic model

Q_{eq} Amount of sorbed metal ions at equilibrium (mmol g^{-1})

Q_e^{cal} Amount of sorbed metal ions at equilibrium calculated from PSO (mmol g^{-1})

Q_{max} Maximum sorption capacity (mmol g^{-1})

Q_t Amount of metal ions sorbed by the sorbent at time t (mmol g^{-1})

r Radius of the copolymer bead assumed to be spherical (cm)

R^2 Determination coefficient

S_{Hg} Specific surface area ($\text{m}^2\,\text{g}^{-1}$)

$t_{1/2}$ Sorption half-time; *i.e.*, time required to reach 50% of the total sorption capacity (min)

V Volume of the aqueous phase (dm^3)

V_s Specific pore volume ($\text{cm}^3\,\text{g}^{-1}$)

REFERENCES

[1] H.F. Mark, J.I. Kroschwitz, in: Encyclopedia of Polymer Science and Engineering, Wiley New York, 1989, pp 567–587.

[2] S.S. Gupta, K.G. Bhattacharyya, Kinetics of adsorption of metal ions on inorganic materials: a review, Adv. Colloid. Interface Sci. **162** (2011) 39–58.

[3] H.B. Sonmez, N. Bicak, Quaternization of poly(4-vinyl pyridine) beads with 2-chloroacetamide for selective mercury extraction, React. Funct. Polym. **51** (2002) 55––60.

[4] V. Neagu, S. Mikhalovsky, Removal of hexavalent chromium by new quaternized crosslinked poly(4-vinyl-pyridines), J. Hazard. Mater. **183** (2010) 533–540.

[5] D. Jermakowicz-Bartkowiak, B.N. Kolarz, Poly(4-vinyl-pyridine) resins towards perrhenate sorption and desorption, React. Funct. Polym. **71** (2011) 95–103.

[6] M. Chanda, G.L. Rempel, Uranium sorption behavior of a macroporous, quaternized poly(4-vinylpyridine) resin in sulfuric acid medium, React. Funct. Polym. **18** (1992) 141–154.

[7] K.R. Ashley, J.R. Ball, A.B. Pinkerton, K.D. Abney, C. Norman, Sorption behavior of pertechnetate on Reillex™ - HPQ anion exchange resin from nitric acid solution, Solvent Extr. Ion Exch. **12** (1994) 239–259.

[8] F.S. Marsh, Reillex™ - HPQ: A new, macroporous poly-vinylpyridine resin for separating plutonium using nitrate anion exchange, Solvent Extr. Ion Exch. **7** (1989) 889–908.

[9] A. Sugii, N. Ogawa, K. Harada, K. Nishimura, Metal Sorption of Macroreticular Poly(4-vinylpyridine) Resins Cross-Linked with Oligo(ethylene glycol dimethacrylates), Anal. Sci. **4** (1988) 399–402.

[10] G.G. Talanova, L. Zhong, R.A. Bartsch, New chelating polymers for heavy metal ion sorption, J. Appl. Polym. Sci. **74** (1999) 849–856.

[11] A. Sugii, N. Ogawa, Y. Iinuma, H. Yamamura, Selective metal sorption on cross-linked poly(vinylpyridine) resins, Talanta **28** (1981) 551–556.

[12] I.U. Castro, F. Stüber, A. Fabregat, J. Font, A. Fortuny, C. Bengoa, Supported Cu(II) polymer catalysts for aqueous phenol oxidation**,** J. Hazard. Mater. **163** (2009) 809–815.

[13] A. Nastasović, D. Đorđević, D. Jakovljević, T. Novaković, Z. Vuković, S. Jovanović, Heavy Metal Ions Removal with

Macroporous Poly(4-vinylpyridine-ethylene Glycol Dimethacrylate), in: R.K. Bregg (Ed.), Leading Edge Polymer Research, Nova Science publishers, New York 2006, pp. 213–234.

[14] F. Švec, Interaction of Reactive Sizes of Macroporous Copolymers Glycidyl Methacrylate-Ethylene Dimethacrylate, Angew. Makromol. Chem. **144** (1986) 39–49.

[15] O. Okay, Macroporous copolymer networks, Progr. Polym. Sci. **25** (2000) 711–779.

[16] D.W. van Krevelen, Properties of Polymers, Elsevier, New York, 1990.

[17] H. Burell, Solubility Parameter Values, in: J. Brandrup, E.H. Immergut (eds.), Polymer Handbook, John Wiley, New York, 1975, p. IV 337.

[18] L.C. Santa Maria, A.P. Aguiar, M.R.M.P. Aguiar, A.C. Jandrey, P.I.C. Guimaraes, L.G. Nascimento, Microscopic analysis of porosity of 2-vinylpyridine copolymer networks: 1. Influence of diluent, Mater. Lett. **58** (2004) 563–568.

[19] F.M.B. Coutinho, C.T. Lima Luz, The influence of diluents on the formation of porous structure in ion exchanger resins based on 2-vinylpyridine and divinylbenzene, Eur. Polym. J. **29** (1993) 1119–1123.

[20] C.T. Lima Luz, F.M.B. Coutinho, The influence of the diluent system on the porous structure formation of copolymers based on 2-vinylpyridine and divinylbenzene-diluent system: I. *n*-Heptane/diethylphthalate, Eur. Polym. J. **36** (2000) 547–553.

[21] M.A. Malik, E. Ur-Rehman, R. Naheed, N.M. Alam, Pore volume determination by density of porous copolymer beads in dry state, React. Funct. Polym. **50** (2002) 125––130.

[22] S. Jovanović, A. Nastasović, N. Jovanović, K. Jeremić, Z. Savić, The influence of inert component composition on the porous structure of glycidyl-methacrylate /ethylene glycol dimetacrylate copolymers, Angew. Makromol. Chem. **219** (1994) 161–168.

[23] P.A. Webb, C. Orr, Analytical Methods in Fine Particle Technology, Micromeritics Instrument Corporation, Norcross, GA, 1997, p. 185.

[24] N. Hird, M.G.J.T. Morrison, D.C. Sherrington, J.C. Trillow, Tailoring of 4-vinylpyridine-based resins for hydrolytic degradation and solubilisation, Tetrahedron **55** (1999) 9585–9594.

[25] R. Djeribi, O. Hamdaoui, Sorption of copper(II) from aqueous solutions by cedar sawdust and crushed brick, Desalination **225** (2008) 95–112.

[26] Y.S. Ho, J.C.Y. Ng, G. McKay, Kinetics of pollutant sorption by biosorbents: review, Sep. Purif. Methods **29** (2000) 189–232.

[27] C.Y. Kuo, C.H. Wu, J.Y. Wu, Adsorption of direct dyes from aqueous solutions by carbon nanotubes: Determination of equilibrium, kinetics and thermodynamics parameters, J. Colloid Interface Sci. **327** (2008) 308–315.

[28] W. Plazinski, W. Rudzinski, A. Plazinska, Theoretical models of sorption kinetics including a surface reaction mechanism: a review, Adv. Colloid Interface Sci. **152** (2009) 2–13.

[29] W. Rudzinski, W, Plazinski, On the applicability of the pseudo-second order equation to represent the kinetics of adsorption at solid/solution interfaces: a theoretical analysis based on the statistical rate theory, Adsorption **15** (2009) 181–192.

[30] Y.S. Ho, Review of second-order models for adsorption systems, J. Hazard. Mater. **B136** (2006) 681–689.

[31] S. Lagergren, About the theory of so-called adsorption of soluble substances, K. Sven. Vetenskapsakad. Handl. **24** (1898) 1–39.

[32] Y.S. Ho, G. McKay, A comparison of chemisorption kinetic models applied to pollutant removal on various sorbents, Process Saf. Environ. Prot. (Trans. Ichem. E Part B) **76** (1998) 332–340.

[33] D.L. Sparks, Kinetics of Soil Chemical Processes, Academic Press Inc., New York, 1989.

[34] F.C. Wu, R.L. Tseng, R.S. Juang, Characteristics of Elovich equation used for the analysis of adsorption kinetics in dye chitosan systems, Chem. Eng. J. **150** (2009) 366––373.

[35] W.J. Weber, J.C. Morris, Kinetics of adsorption on carbon from solution, J. Sanit. Eng. Div. AM. Soc. Civ. Eng. **89** (1963) 31–60.

[36] G.E. Boyd, A.W. Adamson, L.S. Myers, The exchange adsorption of ions from aqueous solutions by organic zeolites, II: kinetics, J. Am. Chem. Soc. **69** (1947) 2836––2842.

[37] A.M. Donia, A.A. Atia, W.A. Al-Amrani, A.M. El-Nahas, Effect of structural properties of acid dyes on their adsorption behaviour from aqueous solutions by amine modified silica, J. Hazard. Mater. **161** (2009) 1544–1550.

[38] A.S. Özcan, A Özcan, Adsorption of acid dyes from aqueous solutions onto acid-activated bentonite, J. Colloid Interface Sci. **276** (2004) 39–46.

[39] P.A. Kumar, M. Ray, S. Chakraborty, Adsorption behaviour of trivalent chromium on amine-based polymer aniline formaldehyde condensate, Chem. Eng. J. **149** (2009) 340–347.

[40] A. Bhatnagar, A.K. Jain, A comparative adsorption study with different industrial wastes as adsorbents for the removal of cationic dyes from water, J. Colloid Interface Sci. **281** (2005) 49–55.

[41] E. Tutem, R. Apak, C.F. Unal, Adsorptive removal of chlorophenols from water by bituminous shale, Water. Res. **32** (1998) 2315–2324.

[42] I.D. Mall, V.C. Sivastava, N.K. Agarwal, Removal of Orange-G and methyl violet dyes by adsorption on to bagasse fly ash – kinetic study and equilibrium isotherm analyses, Dyes Pigments **69** (2006) 210–223.

[43] M.A. Malana, R.B. Qureshi, M.N. Ashiq, Adsorption studies of arsenic on nano aluminium doped manganese copper ferrite polymer (MA, VA, AA) composite: Kinetics and mechanism, Chem. Eng. J. **172** (2011) 721–727.

[44] D. Reichenberg, Properties of Ion-Exchange Resins in Relation to their Structure. III. Kinetics of Exchange, J. Am. Chem. Soc. **75** (1953) 589–597.

[45] D. Mohan, K.P. Singh, Single- and multi-component adsorption of cadmium and zinc using activated carbon

derived from bagasse—an agricultural waste, Water. Res. **36** (2002) 2304–2318.

[46] V. Vadivelan, K.V. Kumar, Equilibrium, kinetics, mechanism, and process design for the sorption of methylene blue onto rice husk, J. Colloid Interface Sci. **286** (2005) 90–100.

[47] A.J. Pardey, A.D. Rojas, J.E. Yánez, P. Betancourt, C. Scott, C. Chinea, C. Urbina, D. Moronta, C. Longo, Spectroscopic characterization of coordination complexes based on dichlorocopper(II) and poly(4-vinylpyridine): Application in catalysis, Polyhedron **24** (2005) 511–519.

[48] N. Graf, E. Yegen, T. Gross, A. Lippitz, W. Weigel, S. Krakert, A. Terfort, W.E.S. Unger, XPS and NEXAFS studies of aliphatic and aromatic amine species on functionalized surfaces, Surf. Sci. **603** (2009) 2849–2860.

[49] W. Liu, X. Yang, L. Xie, Size-controlled gold nanocolloids on polymer microsphere-stabilizer *via* interaction between functional groups and gold nanocolloids, J. Colloid Interface Sci. **313** (2007) 494–502.

[50] C. Liu, R. Bai, L. Hong, Diethylenetriamine-grafted poly-(glycidyl methacrylate) adsorbent for effective copper ion adsorption, J. Colloid Interface Sci. **303** (2006) 99–108.

IZVOD

IMOBILIZACIJA Cu(II) POMOĆU JEDNOSTEPENO SINTETISANOG POLI(4-VINILPIRIDIN-*CO*-ETILEN--GLIKOLDIMETAKRILATA): ANALIZA KINETIKE SORPCIJE I XPS KARAKTERIZACIJA PRODUKATA

Danijela D. Maksin[1], Aleksandra B. Nastasović[2], Tatjana N. Maksin[1], Zvjezdana P. Sandić[1,3], Katja Loos[4], Bojana M. Ekmeščić[2], Antonije E. Onjia[1]

[1]*Univerzitet u Beogradu, Institut za nuklearne nauke "Vinča", Beograd, Srbija*

[2]*Univerzitet u Beogradu, IHTM – Centar za hemiju, Beograd, Srbija*

[3]*Univerzitet u Banja Luci, Prirodno–matematički fakultet, Banja Luka, BiH (Republika Srpska)*

[4]*Department of Polymer Chemistry, Zernike Institute for Advances Materials, University of Groningen, Groningen, The Netherlands*

(Naučni rad)

U okviru ovog rada sintetizovan je kopolimer na bazi 4-vinilpiridina i ispitana mogućnost njegovog korišćenja za sorpciju Cu(II). Tri umrežena makroporozna uzorka poli(4-vinilpiridin-co-etilenglikoldimetakrilata) (P4VPE) sa različitim parametrima porozne strukture sintetizovani su suspenzionom kopolimerizacijom. Parametri porozne strukture su podešavani variranjem udela *n*-heptana u inertnoj komponenti. Uzorci su okarakterisani živinom porozimetrijom, elementarnom analizom i rendgenskom fotoelektronskom spektroskopijom (XPS). Zapažene su relativno velike brzine sorpcije Cu(II) jona na uzorcima P4VPE pri nekompetitivnim uslovima, odnosno, vrednost maksimalnog kapaciteta se dostiže za 30 min. Maksimalni kapacitet sorpcije za uzorak sa najvećom vrednošću prečnika pora i specifične zapremine pora (uzorak 3, Q_{eq} = 89 mg g^{-1}) je 17,5 puta veći od kapaciteta za uzorak sa najmanjom vrednošću prečnika pora i specifične zapremine pora (uzorak 1, Q_{eq} = 5,1 mg g^{-1}). Budući da je sadržaj piridinskih grupa skoro isti u svim uzorcima P4VPE, zaključeno je da na brzinu sorpcije Cu(II) jona odlučujući uticaj imaju parametri porozne strukture uzoraka. Kinetika sorpcije je analizirana pomoću šest kinetičkih modela (pseudo-prvog, pseudo-drugog reda, Elovičevog, unutarčestične difuzije, Bangamovog i Bojdovog modela) da bi se odredilo koji model najbolje opisuje sorpciju Cu(II) jona pomoću P4VPE. Priroda interakcija P4VPE–Cu(II) vrsta nastalih sorpcijom razjašnjena je metodom fotoelektronske spektroskopije x-zracima.

Optimization of ammonia removal by natural zeolite from aqueous solution using response surface methodology

Zahra Beagom Mokhtari-Hosseini[1], Ehsan Kazemian[2], Reza Tayebee[3], Toktam Shenavaei-Zare[1]

[1]Chemical Engineering Group, Faculty of Petroleum and Petrochemical Engineering, Hakim Sabzevari University, Sabzevar, Iran
[2]Faculty of Engineering, Islamic Azad University Shahrood Branch, Shahrood, Iran
[3]Chemistry Group, Faculty of Science, Hakim Sabzevari University, Sabzevar, Iran

Abstract
Ammonium removal from aqueous solution was investigated using natural zeolite. Operating variables were optimized by statistical design for this process. Eight variables including pH, contact time, dose and size of adsorbent, initial ammonia concentration, temperature, agitation and concentration of other adsorbate were screened by Plackett–Burman design. The results indicated that particle size, contact time, dose of zeolite and initial ammonia concentration are effective on removal efficiency with p-value < 0.02. Optimizations of three important factors were conducted by response surface method. The optimal condition of ammonia removal in terms of removal efficiency was found to be at 0.18––0.4 mm particle size, 4 min contact time and 111 g L^{-1} dose of zeolite. The removal efficiency was found to be 98.25% at optimal condition. The maximum adsorption capacity of ammonium was 1.276 mg g^{-1} that was obtained at 0.18–0.4 mm zeolite size, 60 min contact time and 20 g L^{-1} zeolite dosage. The Langmuir and Freundlich isotherms adequately described the adsorption of ammonium ions by HCl-modified natural zeolite.

Keywords: ammonia removal, natural zeolite, Plackett–Burman design, Box–Behnken design, response surface method (RSM).

Available online at the Journal website: http://www.ache.org.rs/HI/

Ammonia is one of the major pollutants in the environment which exists in a considerable quantity in sewages of industries such as petrochemicals. The removal of ammonia from wastewater and sewages is necessary because the existence of ammonium ion in water causes some problems, such as reducing the concentration of dissolved oxygen in water, accelerating the growth of algae and finally coating the surface of water resources which leads to changes in the taste and color of water [1]. Various biological, physical and chemical treatment methods have been used to remove ammonia from aqueous solution [2–11]. One of the proposed methods for ammonia removal from industrial wastewater is the use of low-cost adsorbents such as agriculture wastes [12] and silicate minerals like zeolite [13–17]. This method seems to be a good option for ammonium treatment due to high efficiency in removing ammonia, simplicity and low costs. Zeolites are alumino-silicate minerals with water, containing alkali and alkaline earth metals. Zeolites are commonly used in scientific and industrial fields because of their structural characteristics and chemical composition [18,19].

Optimization of physicochemical parameters of process is one method for increasing process yield and reducing process cost. To reduce the number of experiments, in regard to the large number of variables, statistical design of experiments have been used in many studies [20–23].

Some of batch adsorption parameters are pH, temperature, particle size and dose of adsorbent and initial concentration of adsorbate. Several studies have been conducted about removing ammonium from wastewater using zeolites. In some studies effective variables on adsorption process were considered and some important variables were recognized [14–17]. However in these studies, the statistical designs of experiments were not employed for optimization of the ammonia adsorption from aqueous solution.

In the present study, an Iranian natural zeolite which was extracted from Sabzevar region, for the first time, was used as adsorbent. In this work, the statistical design of experiments was applied for optimization of ammonia adsorption from aqueous solution. For this purpose, important process parameters were first screened and selected on the basis of the Plackett––Burman design (PBD). Subsequently, the significant variables were optimized by Response surface method (RSM) using Box–Behnken design (BBD).

Correspondence: Z.B. Mokhtari-Hosseini, Chemical Engineering Group, Faculty of Petroleum and Petrochemical Engineering, Hakim Sabzevari University, P.O. Box 9617976-487, Sabzevar, Iran.
E-mail: z.mokhtari@hsu.ac.ir; zb_mokhtari@yahoo.com

MATERIALS AND METHODS

Preparation and modification of zeolite

The natural zeolite was obtained from Sabzevar town, North East of Iran. The samples were grounded and sieved based on the U.S. standard mesh. After washing with distilled water and drying, zeolites were stored in the desiccators for the next stages. The prepared zeolites were modified using phosphoric, nitric, sulfuric and hydrochloric acids, separately, according to the following condition: 10 g zeolites were added into 250 mL acid solution (1 M) and shaken for 6 h at 60 °C and 150 rpm. The solid phase was separated by filter paper and was rinsed in hot distilled water, and then in cold distilled water until pH was adjusted to 7. Then, zeolites were dried for 24 h at 100 °C and kept in the desiccator to prevent moisture adsorption.

Adsorption

The ammonia solution was prepared by dissolving an accurately weighed sample of ammonium chloride (NH_4Cl) in deionized water. Batch adsorption experiments were carried out by shaking a series of bottles containing determined amounts of adsorbent and adsorbate solution at desired condition.

In the first stage the adsorption of acid-modified zeolite and unmodified zeolite was examined at similar conditions of 1.0–1.7mm zeolite size, 50 g/L dose of the zeolite, 3 h contact time, 25 °C temperature, 200 rpm agitation, 25.6 mg/L initial ammonium concentration and pH 7.

In screening and optimization stage, adsorption condition was set according to experimental design and pH was adjusted by 0.1 M HCl or 0.1 M NaOH. After adsorption process, the adsorbent particles were separated from the suspensions by filtration through 0.43 µm filter paper and the residual concentration of ammonia was determined. In order to reduce the experimental errors, all experiments were conducted three times and the mean experimental data was reported.

To investigate the adsorption isotherms the series of NH_4^+ solutions with different initial ammonia concentration (C_0) (10–120 mg/L) were kept in contact with 20 g/L zeolite (0.6–0.85mm) at 35 °C and 50 rpm until arriving to equilibrium concentration. Then, the equilibrium adsorption capacity (q_e) was determined and agreement of obtained data with three isotherm models, Linear, Langmuar and Frendlich were studied.

Statistical experimental design

Review of published reports [14–17] showed that pH, contact time, dose and size of adsorbent, initial ammonia concentration, temperature, agitation and concentration of other adsorbate, may be effective on adsorption process. Ca^{2+} was studied as another adsorbate. Plackett–Burman design was used to screen these variables. Selected levels of variables are shown in Table 1.

Table 1. Selected levels of variables for PBD of ammonia removal from aqueous solution by HCl-modified natural zeolite

Variable		Coded value	
		(+1)	(−1)
d	Particle size, mm	1.7–3.35	Below 0.075
pH	pH	9	4
t	Contact time, min	180	10
m	Dose of zeolite, g/L	200	4
C_0	Initial ammonia concentration, mg/L	25.6	2.56
θ	Temperature, °C	45	25
S	Agitation, rpm	200	50
C_{Ca}	Concentration of other cation, mEq/L	5	0

After the identification of important variables, Box––Behnken design was used for optimization of process variables which were found to be important for ammonium adsorption while other factors were kept at a constant level. Selected levels of variables have been shown in Table 2. The results of the experimental designs were analyzed and interpreted using Minitab 16 statistical software.

Table 2. Selected levels of variables for BBD of ammonia removal from aqueous solution by HCl-modified natural zeolite

Variable		Coded value		
		+1	0	−1
d	Particles size, mm	1–1.4	0.6–0.85	0.18–0.3
t	Contact time, min	60	32	4
m	Dose of zeolite, g/L	160	90	20

Analysis techniques

The quantitative determination of major elements contained in the zeolite sample was carried out using the wavelength dispersive X-ray fluorescence (XRF) technique (model CE3021 made by CECIL Instruments, USA). The mineralogical composition of the natural adsorbent was determined by using Philips X'pert Modular Powder diffractometer (MPD). The concentration of ammonia in solution was measured using Phenat method [24].

RESULTS AND DISCUSSION

Identification of zeolite

Table 3 presents the elemental composition of the Sabzevar zeolite using XRF. According to these results

the mass ratio of SiO_2/Al_2O_3 is equal to 6.55. Loss on ignition (L.O.I.) is the percentage of volatile components, mainly crystal bound water and organic carbon (as CO_2), driven off from a sample when heated at 1000 °C. Table 3 indicated 15.62% of zeolite is volatile components.

the results of experiments are shown in Table 5. Table 6 displays the analysis results of the PBD using minitab16 software.

The statistically significant effect of each variable was screened by probability test and variables with a confidence interval greater than 98% (*p*-value < 0.02)

Table 3. Determined composition of zeolite sample using XRF

Component	SiO_2	Al_2O_3	Na_2O	MgO	CaO	K_2O	TiO_2	MnO	P_2O_5	Fe_2O_3	SO_3	LOI
Perception	62.68	9.57	2.43	0.77	5.51	1.76	0.17	0.09	0.03	0.041	0.00	15.62

The mineralogical composition of the natural adsorbent was determined by using Philips MPD; the results obtained were as follows: 76% clinoptilolite, 24% calcite.

Acid-modification

The removal of ammonia from aqueous solution using different acid-modified zeolite was determined and compared with unmodified zeolite (Table 4). According to Table 4, modification of zeolite significantly increased removal efficiency. When natural zeolites were modified with acid, aluminum ions were replaced by hydronium ions. Due to the replacement of protons with small radius (H_3O^+) by cations of larger radius (Al^{3+}), Si/Al ratio and pore size of zeolites increased. Among acid-modified zeolite, HCl-modified zeolite and H_3PO_4-modified zeolite had the highest adsorption amounts. HCl-modified zeolite was selected for further study.

Screening of variables

Eight variables pH, contact time, dose and size of adsorbent, initial adsorbate concentration, temperature, agitation and the presence of other adsorbate (Ca^{2+}) were evaluated using twelve matrix of PBD and

were considered as a significant variable. According to Table 6, in terms of removal efficiency particle size, contact time, zeolite dosage and initial ammonium concentration are significant. Table 6, also, indicates that particle size, pH, contact time and presence of Ca^{2+} have negative effect on removal efficiency and other variables have positive effect. High negative effect of contact time shows that continuous process could obtain high removal efficiency. The results of the study are consistent with study of Huang et al. [15].

Table 4. The comparison of the removal ammonia by different acid-modified zeolite

Zeolite	Removal efficiency, %
Unmodified zeolite	29.59
HCl-modified zeolite	97.87
H_3PO_4-modified zeolite	97.51
HNO_3-modified zeolite	95.66
H_2SO_4-modified zeolite	92.78

In terms of adsorption capacity, only two variables, the initial ammonia concentration (C_0) and dose of zeolite (m) in studied range are significant with con-

Table 5. Plackett–Burman design matrix and corresponding results for ammonia removal from aqueous solution by HCl-modified natural zeolite

Trail	Coded factor[a]								Removal efficiency %	Adsorption capacity
	d	pH	t	m	C_0	θ	S	C_{Ca}		
1	1	−1	1	−1	−1	−1	1	1	23.83±0.39	0.1525±0.0025
2	1	1	−1	1	−1	−1	−1	1	66.99±1.76	0.0086±0.0002
3	−1	1	1	−1	1	−1	−1	−1	72.38±1.17	4.6325±0.0750
4	1	−1	1	1	−1	1	−1	−1	80.47±0.39	0.0103±0.0000
5	1	1	−1	1	1	−1	1	−1	95.25±0.06	0.1219±0.0001
6	1	1	1	−1	1	1	−1	1	48.42±1.04	3.0987±0.0662
7	−1	1	1	1	−1	1	1	−1	80.08±2.73	0.0102±0.0003
8	−1	−1	1	1	1	−1	1	1	97.89±0.04	0.1253±0.0000
9	−1	−1	−1	1	1	1	−1	1	97.71±0.14	0.1251±0.0002
10	1	−1	−1	−1	1	1	1	−1	97.95±0.02	6.2688±0.0012
11	−1	1	−1	−1	−1	1	1	1	97.05±0.49	0.6211±0.0031
12	−1	−1	−1	−1	−1	−1	−1	−1	75.39±0.78	0.4825±0.0050

[a]Factors refer to those in Table 1

Table 6. Analysis of PBD results for ammonia removal from aqueous solution by HCl-modified natural zeolite

Variable	Removal efficiency, %			Adsorption capacity, mg/g		
	Effect	*t*-value	*p*-value	Effect	*t*-value	*p*-value
Particles size (*d*)	−17.93	−3.85	0.002	0.611	1.28	0.220
pH	−2.18	−0.47	0.647	0.221	0.46	0.650
Contact time (*t*)	−21.21	−4.55	0.000	0.067	0.14	0.890
Dose of zeolite (*m*)	17.23	3.70	0.002	−2.476	−5.18	0.000
Initial ammonia concentration (C_0)	14.30	3.07	0.008	2.181	4.57	0.000
Temperature (θ)	11.66	2.50	0.024	0.768	1.61	0.128
Agitation (*S*)	8.45	1.81	0.090	−0.176	−0.37	0.717
Concentration of Ca (C_{Ca})	−11.60	−2.49	0.025	−1.232	−2.58	0.021

fidence interval greater than 98%. According to Table 6, dose of zeolite, agitation and presence of Ca^{2+} have negative effect on adsorption capacity and effects of other variables are positive. Du et al. studied the same variables for ammonia removal and found that all of these variables affect the adsorption process [14].

Optimization of effective variables

The most important parameters which affect the efficiency of ammonia removal are particles size *(d)*, contact time (*t*) and dose of zeolite (*m*) and initial ammonium concentration (C_0). Further study was conducted with initial constant ammonium concentration because it is constant in actual process. Then, the other three variables were optimized in initial concentration 25.6 mg L^{-1} at 30 °C and 50 rpm without the presence of Ca^{2+} and adjusting pH. RSM was employed to investigate the combined effect of these factors to reveal the optimum conditions for ammonia removal and to build models. BBD was applied to evaluate the interactive effects of adsorption variables and optimize the ammonia removal process. The range and levels of variables are coded according to Eq. (1) and summarized in Table 2.

$$x = \frac{X - X_0}{\Delta X} \qquad (1)$$

where *x* and *X* are the coded and the real values of variables. X_0 and ΔX are the center point of *X* and the step change in *X*, respectively. The results of experiments were measured according to BBD of three independent variables and were reported in Table 7. The results were analyzed using minitab16 software. The experimental results of removal efficiency (%) and adsorption capacity were fitted with a second order polynomial equation.

The fitted equations (in terms of coded values) for removal efficiency (Y_1) and adsorption capacity (Y_2) were as follows:

$$Y_1 = 65.895 + 5.602m + 0.884t - 5.387d - 1.199m^2 + 3.855t^2 + 22.618d^2 - 0.559mt + 5.450md + 1.031td \qquad (2)$$

$$Y_2 = 0.1874 - 0.3961m + 0.0220t - 0.0544d + 0.3046m^2 - 0.0328t^2 + 0.1082d^2 - 0.0500mt + 0.1006md + 0.0029td \qquad (3)$$

The coefficients of the regression model (Eqs. (2) and (3)) that appear as one constant, three linear, three quadratic and three interaction terms are listed in Table 8.

Table 7. Box–Behnken design matrix and corresponding results for ammonia removal from aqueous solution by HCl-modified natural zeolite

Trail	Coded factors[a]			Removal efficiency, %	Adsorption capacity
	m	*t*	*d*		
1	−1	−1	0	53.65±0.41	0.6867±0.0052
2	1	−1	0	67.02±0.44	0.1072±0.0007
3	−1	1	0	71.20±0.49	0.9113±0.0063
4	1	1	0	82.34±0.86	0.1317±0.0014
5	−1	0	−1	98.64±0.12	1.2626±0.0016
6	1	0	−1	97.89±0.30	0.1566±0.0005
7	−1	0	1	65.84±0.37	0.8427±0.0047
8	1	0	1	86.88±0.57	0.1390±0.0009
9	0	−1	−1	99.67±0.08	0.2835±0.0002
10	0	1	−1	84.71±0.47	0.2410±0.0013
11	0	−1	1	97.96±0.05	0.2786±0.0001
12	0	1	1	87.13±0.42	0.2478±0.0012
13	0	0	0	65.70±0.09	0.1869±0.0002
14	0	0	0	65.89±0.01	0.1874±0.0000
15	0	0	0	66.10±0.07	0.1880±0.0002

[a]Factors refer to those in Table 1

The significance of each coefficient was determined by p-values. The *p*-values imply that the first order main effects of particles size and zeolite dosage and second order main effects of particles size are significant in terms of the removal efficiency. Therefore,

Table 8. Analysis of BBD results for ammonia removal from aqueous solution by HCl-modified natural zeolite

Term	Removal efficiency (%)			Adsorption capacity		
	Coefficient	*t*-value	*p*-value	Coefficient	*t*-value	*p*-value
Constant	65.895	19.538	0.000	0.1874	5.801	0.000
Dose of zeolite (*m*)	5.602	2.712	0.013	−0.3961	−20.018	0.000
Contact time (*t*)	0.884	0.428	0.673	0.0220	1.111	0.280
Particle size (*d*)	−5.387	−2.608	0.017	−0.0544	−2.751	0.012
m^2	−1.199	−0.394	0.697	0.3047	10.460	0.000
t^2	3.855	1.268	0.219	−0.0328	−1.128	0.273
d^2	22.618	7.440	0.000	0.1081	3.713	0.001
mt	−0.559	−0.191	0.850	−0.0500	−1.788	0.089
md	5.450	1.866	0.077	0.1006	3.594	0.002
td	1.031	0.353	0.728	0.0029	0.105	0.918

they can act as limiting adsorption. There is not any significant interaction for removal efficiency. In terms of adsorption capacity, the main effects of zeolite dosage and particles size, quadratic variables zeolite dosage and particles size and interaction between zeolite dosage and particles size are effective on process.

Coefficients of correlation were determined by the analysis of variance using Minitab16 software. R^2 = = 78.92 for removal efficiency shows there are relatively good agreement between the experimental results and the predicted results by the model and for adsorption capacity the R^2 = 96.48 indicates a very good agreement of model prediction data with experimental data.

The 2D contour plots are the graphical representations of the regression equation and are plotted to understand response variation with variation of two variables, while the other independent variable is constant. Moreover, the 2D cotour plots indicate the interaction of these variables and locate the optimum level of each variable for maximum response. Figures 1 and 2 indicate contour plots for removal efficiency and adsorption capacity, respectively.

According to Figure 1a and c, at low levels of particles size, removal efficiency is relatively independent of zeolite dosage and contact time, but at high levels of particles size, the removal efficiency is dependent on zeolite dosage (increasing of removal efficiency with increasing of dose of zeolite) and the response is independent of contact time. This shows that zeolite dosage and particles size have interaction in removal efficiency (Figure 1c). Figure 1a shows there is not any interaction between particles size and contact time and in constant contact time at low levels and high levels of zeolite dose, removal efficiency is higher than middle levels.

Contour plot of adsorption capacity versus contact time and particle size at optimal value of dose of zeolite shows adsorption capacity rises with increasing par-

ticles size and reducing contact time and maximum adsorption capacity exists at maximum contact time and minimum particle size (Figure 2a). Figure 2b indicates reducing particle size and zeolite dosage increases adsorption capacity. According to Figure 2c, in constant dose of zeolite, adsorption capacity relatively doesn't vary with variation of contact time.

The optimum condition for maximum response was obtained using Minitab16 software. In the studied range of variables, the optimum condition for removal efficiency were $d = -1$, $t = -1$ and $m = 0.3$ means 0.18––0.4 mm particle size, 4 min contact time and 111 g/L dose of zeolite. Under this condition, predicted removal efficiency by software was 98.19% and for the experimental study it was 98.25% for removal efficiency which indicates consistent results and proves the validity of the model. The optimum condition for adsorption capacity, in the studied range of variables, were $d = -1$, $t = 1$ and $m = -1$; in terms of coded value or the 0.18–0.4 mm size of zeolite, 60 min contact time and 20 g/L zeolite dosage in terms of actual value. Predicted adsorption capacity by software at optimum condition was 1.2 mg NH_3/g zeolite. Experimental adsorption capacity in this condition yielded 1.276 that is very close to predicted value and validates the model.

Adsorption isotherms

Fitting of adsorption isotherm equations to experimental data is often an important aspect of data analysis. In this study, three typical isotherms Linear, Langmuir and Freundlich models were used for fitting the adsorption experimental data. Table 9 indicates equilibrium concentration and adsorption in different initial ammonia concentration. Experimental data of Table 9 were fitted with three isotherm model, linear, Langmuir and Freundlich.

Parameters of these models can be determined by linear regression of the experimental data. The model parameters and correlation coefficients (R^2) are summarized in Table 10. Higher values of R^2 (0.9886) for
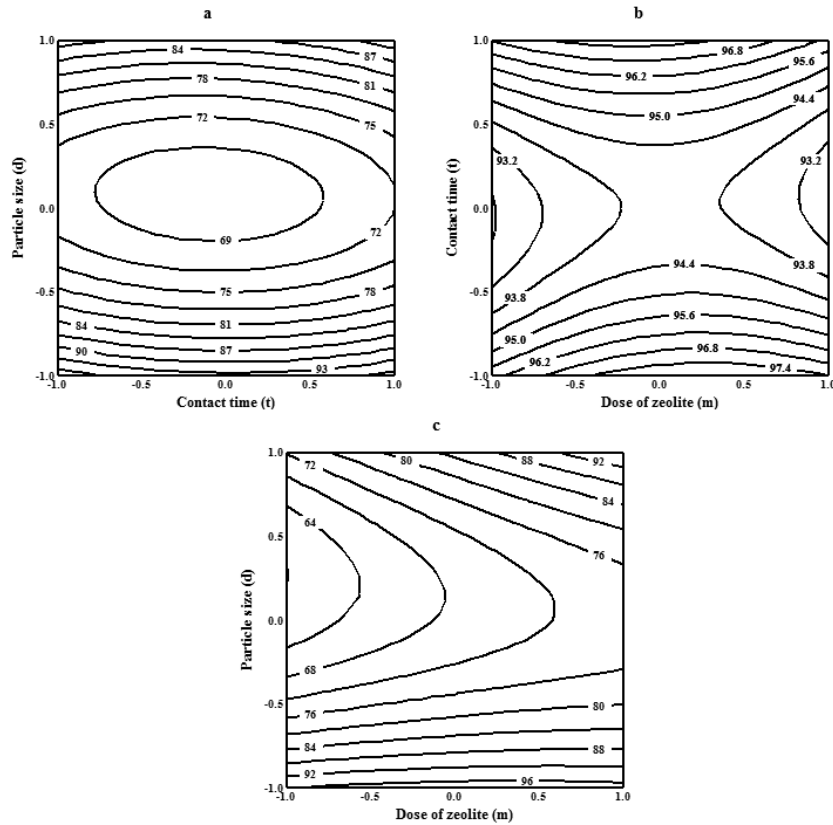
Figure 1. Contour plots of removal efficiency (a) vs particle size and contact time, (b) vs particle size and adsorbent amount and (c) vs adsorbent amount and contact time at optimal levels of other components (d, t and m are coded variables).

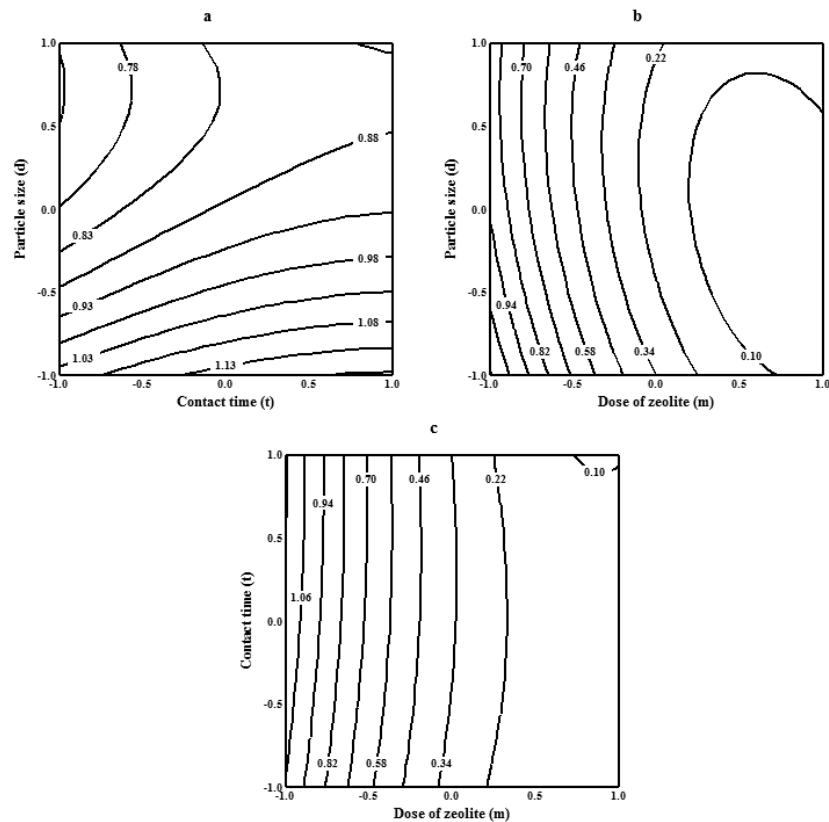*Figure 2. Contour plots of adsorption capacity (a) vs particle size and contact time, (b) vs particle size and dose of zeolite and (c) vs dose of zeolite and contact time at optimal levels of other components (d, t and m are coded variables).*

Table 9. Variation of equilibrium concentration and adsorption versus different initial ammonia concentration for ammonia adsorption from aqueous solution by HCl-modified natural zeolite

C_0 / mg L^{-1}	C_e / mg L^{-1}	q_e / mg NH$_3$ (g zeolite)$^{-1}$
10.000	0.135	0.493
20.000	0.300	0.985
40.000	0.480	1.976
80.000	3.263	3.837
100.000	6.045	4.698
120.000	9.334	5.533

Table 10. Model parameters and correlation coefficients (R^2) of Linear, Langmuir and Freundlich isotherms for ammonia adsorption from aqueous solution by HCl-modified natural zeolite

Isotherm model	Equation	Model parameters		R^2
Linear	$q_e = aC_e + b$	a / L g^{-1}	0.5185	0.8925
		b / mg g^{-1}	1.2304	
Langmuir	$q_e = \dfrac{q_m b C_e}{1 + b C_e}$	q_m / mg g^{-1}	6.2189	0.9886
		b / L mg^{-1}	0.6429	
Freundlich	$q_e = k_f C_e^{\frac{1}{n}}$	k_f / L g^{-1}	1.9102	0.9378
		n	1.8815	

Langmuir isotherm indicate better fitness of Langmuir isotherm to the experimental data.

CONCLUSION

Process variables of ammonia removal from aqueous solution using HCl-modified natural zeolite were optimized by statistical design. Screening of variables by PBD indicated four factors particle size, contact time, dose of zeolite and initial ammonia concentration are effective on removal efficiency. Three important factors were optimized by RSM. Quadratic models, counter plots and optimum conditions were obtained for this design using Minitab 16 software. It was observed that decrease in particle size and increase in adsorbent dose and contact time increased removal of ammonia by zeolite. Also, it was found that reduction in particle size and dosage of adsorbent and increase in contact time increased adsorption capacity of ammonium by zeolite. In optimum condition of 0.18–0.4 mm particle size, 4 min contact time and 111 g L^{-1} dose of zeolite, 98.25% of ammonium was removed. The Langmuir and Freundlich isotherm models were used to investigate the adsorption equilibrium of HCl-modified natural zeolite for ammonium adsorption. Adsorbent showed that it fits better to Langmuir isotherm which suggests that adsorption is homogeneous in nature. Ammonia removal from aqueous solution using HCl--modified natural zeolite is an inexpensive, effective and suitable process.

REFERENCES

[1] H. Shan, J.P. Obbard, Ammonia removal from freshwater using nitrifying bacteria enriched from a seawater aquaculture pond, Biotechnol. Lett. **25** (2003) 1469–1471.

[2] S.N. Ashrafizadeh, Z. Khorasani, Ammonia removal from aqueous solutions using hollow-fiber membrane contactors, Chem. Eng. J. **162** (2010) 242–249.

[3] F. Nosratinia, M. Ghadiri, H. Ghahremani, Mathematical modeling and numerical simulation of ammonia removal from wastewaters using membrane contactors, J. Ind. Eng. Chem. **20** (2014) 2958–2963.

[4] L. Yang, X. Wang, T.L. Funk, Strong influence of medium pH condition on gas-phase biofilter ammonia removal, nitrous oxide generation and microbial, Bioresource Technol. **152** (2014) 74–79.

[5] D. Qu, D. Sun, H. Wang, Y. Yun, Experimental study of ammonia removal from water by modified direct contact membrane distillation, Desalination **326** (2013) 135–140.

[6] A. Serna-Maza, S. Heaven, C.J. Banks, Ammonia removal in food waste anaerobic digestion using a side-stream stripping, Bioresource Technol. **152** (2014) 307–315.

[7] M. Chen, W. Wang, Y. Feng, X. Zhu, H. Zhou, Z. Tan, X. Li, Impact resistance of different factors on ammonia removal by heterotrophic nitrification–aerobic denitrification bacterium Aeromonas sp. HN-02, Bioresource Technol. **167** (2014) 456–461.

[8] M. Yang, P. Sun, R. Wang, J. Han, J. Wang, Y. Song, J. Cai, X. Tang, Simulation and optimization of ammonia removal at low temperature for a double channel oxidation ditch based on fully coupled activated sludge model

(FCASM): A full-scale study, Bioresource Technol. **143** (2013) 538–548.

[9] M. Han, Z. Zhao, W. Gao, F. Cui, Study on the factors affecting simultaneous removal of ammonia and manganese by pilot-scale biological aerated filter (BAF) for drinking water pre-treatment, Bioresource Technol. **145** (2013) 17–24.

[10] Y. Gendel, O. Lahav, A novel approach for ammonia removal from fresh-water recirculated aquaculture systems, comprising ion exchange and electrochemical regeneration, Aquacult. Eng. **52** (2013) 27–38.

[11] M. Li, C. Feng, Z. Zhang, X. Liu, W. Ma, Q. Xue, N.Sugiura, Optimization of electrochemical ammonia removal using Box–Behnken, Electroanal. Chem. **657** (2011) 66––73.

[12] H. Liu, Y. Dong, Y. Liu, H. Wang, Screening of novel low-cost adsorbents from agricultural residues to remove ammonia nitrogen from aqueous solution, J. Hazard. Mater. **178** (2010) 1132–1136.

[13] H. Huang, D. Xiao, R. Pang, C. Han, L. Ding, Simultaneous removal of nutrients from simulated swine wastewater by adsorption of modified zeolite combined with struvite crystallization, Chem. Eng. J. **256** (2014) 431–438.

[14] Q. Du, S. Liu, Z. Cao, Y. Wang, Ammonia removal from aqueous solution using natural Chinese clinoptilolite, Sep. Purif. Technol. **44** (2005) 229–234.

[15] H. Huang, X. Xiao, B. Yan, L. Lyang, Ammonia removal from aqueous solution by using natural Chinese (chende) zeolite as adsorbent, J. Hazard. Mater. **175** (2010) 247–252.

[16] L. Lei, X. Li, X. Zhang, Ammonia removal from aqueous using microwave-treated natural Chinese zeolite, Sep. Purif. Technol. **58** (2008) 359–366.

[17] R. Malekian, J. Abedi-Koupai, S. Eslamian, F. Mousavi, K.C. Abbaspour, M. Afyuni, Ion-exchange process for ammonium removal and release using natural Iranian zeolite, Appl. Clay Sci. **51** (2011) 323–329**.**

[18] N.A.S. Ramli, N.A.S. Amin, Fe/HY zeolite as an effective catalyst for levulinic acid production from glucose: Characterization and catalytic performance, Appl. Catal., B **163** (2015) 487–491.

[19] E. Mahmoud, R.F. Lobo, Recent advances in zeolite science based on advance characterization techniques, Micropor. Mesopor. Mat. **189** (2014) 97–106.

[20] C. Hana, H. Pua, H. Li, L. Denga, S. Huanga, S. Heb, Y. Luo, The optimization of As(V) removal over mesoporous alumina by using response surface methodology and adsorption mechanism, J. Hazard. Mater. **254**–**255** (2013) 301–309.

[21] Z.B. Mokhtari-Hosseini, E. Vasheghani-Farahani, A. Heidarzadeh-Vazifekhoran, S.A. Shojaosadati, R. Karimzadeh, K. Khosravi Darani, Statistical media optimization for growth and PHB production from methanol by a methylotrophic bacterium, Bioresource Technol. **100** (2009) 2436–2443.

[22] Y. Liu, J. Wang, Y. Zheng, A. Wang, Adsorption of methylene blue by kapok fiber treated by sodium chlorite optimized with response surface methodology, Chem. Eng. J. **184** (2012) 248–255.

[23] N. Sivarajasekar, R. Baskar, Adsorption of basic red 9 on activated waste *Gossypium hirsutum* seeds: Process modeling, analysis and optimization using statistical design, J. Ind. Eng. Chem. **20** (2014) 2699–2709.

[24] G. Park, H. Oh, S. Ahn, Improvement of the ammonia analysis by the Phenate method in water and wastewater, Bull. J. Korean Chem. Soc. **30** (2009) 2032–2037.

IZVOD

OPTIMIZACIJA UKLANJANJA AMONIJAKA IZ VODENOG RASTVORA PRIRODNIM ZEOLITOM KORIŠĆENJEM METODE POVRŠINSKOG ODZIVA

Zahra Beagom Mokhtari-Hosseini[1], Ehsan Kazemiyan[2], Reza Tayebee[3], Toktam Shenavaei-Zare[1]

[1]Chemical Engineering Group, Faculty of Petroleum and Petrochemical Engineering, Hakim Sabzevari University, Sabzevar, Iran
[2]Faculty of Engineering, Islamic Azad University Shahrood Branch, Shahrood, Iran
[3]Chemistry Group, Faculty of Science, Hakim Sabzevari University, Sabzevar, Iran

(Naučni rad)

U radu je ispitivano uklanjanje azota iz vodenog rastvora korišćenjem prirodnog zeolita. Operativne promenljive (ili uslovi u sistemu) su optimizovane primenom statističke analize. Praćeno je i analizirano, Planet–Burkman metodom, osam parametara: pH, vreme kontakta, doza i veličina adsorbenta, početna koncentracija amonijaka, temperatura, mešanje i koncentracija drugih adsorbata. Rezultati su pokazali da vreme kontakta, doziranje zeolita i početna koncentracija amonijaka utiču na efikasnost uklanjanja amonijaka sa *p*-vrednošću <0.02. Optimizacija tri važna parametra izvršena je metodom površinskog odziva. U pogledu efikasnosti uklanjanja azota postavljeni su optimalni uslovi: veličina čestica 0,18–0,4 mm, vreme kontakta 4 min, doziranje zeolita 111 g L^{-1}. Utvrđeno je da je efikasnost uklanjanja azota 98,25% od optimalne vrednosti. Maksimalni adsorpcioni kapacitet amonijaka bio je 1,276 mg g^{-1} dobijen na zeolitu veličine 0,18–0,4 mm, sa vremenom kontakta 60 min i doziranjem zeolita od 20 g L^{-1}. Adsorpcija amonijum jona na prirodnom zeolitu modifikovanom hlorovoroničnom kiselinom opisana je Langmuiri Freundlich izotermama.

Uticaj termičkih tretmana na sintezu akrilamida i njegova kvantifikacija metodom gasne hromatografije sa azot–fosfornim detektorom

Veselin M. Delević[1], Refik M. Zejnilović[2], Biljana S. Jančić-Stojanović[3], Milica D. Zrnić Ćirić[4], Brižita I. Đorđević[4], Ivan M. Stanković[4]

[1]Institut za javno zdravlje, Podgorica, Crna Gora
[2]Farmaceutski fakultet, Podgorica, Crna Gora
[3]Katedra za analitiku lekova, Farmaceutski fakultet, Univerzitet u Beogradu, Srbija
[4]Katedra za bromatologiju, Farmaceutski fakultet, Univerzitet u Beogradu, Srbija

Izvod

U radu je ispitivan uticaj termičkih tretmana (kuvanje, pečenje i prženje) na sadržaj akrilamida u krompiru i izvršena je kvantifikacija njegovog sadržaja pomoću gasne hromatografije sa azot–fosfornim detektorom (GC-NPD). Priprema uzoraka je vršena primenom sledećih termičkih tretmana: kuvanjem u vodi 30 min na 110 °C, pečenjem u rerni 30 min na 200 °C i prženjem u ulju 5, 10 i 15 min na 250 °C. Kvantifikaciji akrilamida predhodile su: homogenizacija uzorka, ekstrakcija i uparavanje ekstrakta. Kalibraciona kriva konstruisana je u opsegu koncentracija 0–10 mg/kg a dobijena je vrednost $R^2 > 0,99$. Određene su limit detekcije (*LOD*) i limit kvantifikacije (*LOQ*) i dobijene su sledeće vrednosti 0,26 mg/kg za *LOD* i 0,40 mg/kg za *LOQ*. Recovery vrednosti u opsegu od 102 do 110% potvrdile su tačnost metode. Predložena gasno-hromatografska metoda je jednostavna, pouzdana i precizna za određivanje akrilamida u uzorcima termički tretiranih namirnica. Dobijeni rezultati pokazuju da je sadržaj akrilamida u krompiru koji je termički tretiran kuvanjem bio manji od limita detekcije, dok se u krompiru pripremljenom pečenjem ili prženjem kretao u opsegu od 0,6 do 2,7 mg/kg. Upoređivanjem sadržaja akrilamida u krompiru nađeno je da termički tretman ima veliki uticaj na sintezu akrilamida pa bi bilo poželjno razviti postupak za dobijanje pomfrita i čipsa sa niskim ili bez sadržaja akrilamida sa teksturom privlačnom za konzumaciju.

Ključne reči: akrilamid, termički tretman, hrana, GC-NPD.

Dostupno na Internetu sa adrese časopisa: http://www.ache.org.rs/HI/

Termički tretman predstavlja najuobičajeniji način obrade namirnica radi dužeg čuvanja namirnica i pretvaranja u jestivi oblik. Pored pozitivnih efekata termičkog tretmana dolazi i do nepoželjnih interakcija nutrimenata pri čemu mogu nastati i toksična jedinjenja u koje spada i akrilamid.

Akrilamid ($CH_2=CH–CONH_2$, 2-propenamid), jedinjenje sa molekulskom masom 71,02, stabilan na sobnoj temperaturi, svrstan je od strane međunarodne Agencije za istraživanje kancera (eng. International Agency for Research on Cancer, IRAC) u grupu 2A – verovatno kancerogen za ljude. Akrilamid je privukao veliku pažnju posle objavljivanja od strane švedskih institucija za bezbednost namirnica i Univerziteta u Stokholmu da je njegovo prisustvo utvrđeno u širokom spektru termički tretiranih namirnica [1,2]. Danas je pokrenuto nekoliko naučnih inicijativa da bi se u potpunosti razumjela njegova hemija i toksikologija, fokusirajući se prvenstveno na njegove mehanizme formiranja i mo-

guće posledice po ljude. Ispitivanja na životinjama su pokazala da visoke doze akrilamida (>203 μg/kg) imaju nepoželjne efekte na razvojne funkcije u neonatalnom periodu kod glodara. Kod glodara je primećena nervna degeneracija, zatim nedostatak intestinalnih enzima, kao i abnormalna spermatogeneza, itd. S druge strane, epidemiološke studije za različite vrste raka nijesu pokazale vezu između ishranom unešenog akrilamida i pojave kancera [3,4]. Međutim, došlo se do zaključka da standardne epidemiološke studije imaju nisku statističku validnost kako bi se utvrdila povezanost pojave raka sa izloženošću akrilamidu [5]. Imajući ovo u vidu zajednička stručna komisija FAO/WHO za aditive (eng. Joint FAO/WHO Expert Committee on Food Additives, JECFA) istakla je važnost dobijanja što više validnih podataka o sadržaju akrilamida u namirnicama koje se konzumiraju u zemljama u razvoju kao vredan instrument u obavljanju procene unosa akrilamida, u cilju redukovanja unosa akrilamida u opštoj populaciji [6].

Naša tradicionalna ishrana bazirana je na namirnicama bogatim ugljenim hidratima (pečeni i prženi krompir, pekarski proizvodi i dr.), koje se podvrgavaju termičkom tretmanu na visokim temperaturama. Ovakav način ishrane može predstavljati rizik u smislu unosa većih količina akrilamida [6].

Cilj ovog istraživanja je da utvrdi uticaj termičkog tretmana na stvaranje akrilamida u izabranim uzorcima krompira koji su pripremljeni termičkim tretmanom: kuvanjem, pečenjem i prženjem primenom novorazvijene metode gasne hromatografije sa azot–fosfornim detektorom (eng. Gas Chromatography-Nitrogen Phosphorus Detector – GC-NPD).

U dostupnoj literaturi prikazane su analitičke metode bazirane na HPLC ili GC za određivanje akrilamida u termički tretiranim namirnicama, vodi, biološkom materijalu kao i u namirnicama koje nisu termički tretirane [7–9]. U preglednom radu [10] publikovanom 2012. godine navedene su do tada publikovane elektroforetske metode, zatim GC metode i HPLC metode sa različitim tipovima detekcije. U radu se navode i različiti postupci pripreme uzoraka kao što su ekstrakcija sa *n*-propanolom [11], ekstrakcija sa *n*-heksanom i vodenim rastvorom natrijum-hlorida [12], ekstrakcija na čvrstoj fazi (eng. Solid Phase Exstaction – SPE) [13,14], ekstrakcija sa metanolom, prečišćavanje sa rastvorom CAREZ I i II [15], itd. Uzorci u kojima je određivan sadržaj akrilamida bile su različito termički tretirane namirnice, čipsevi, pomfrit, kafa i surogati kafe, kao i druge. Analizom do sada publikovanih radova zaključeno je da se za detekciju akrilamida zahtevaju veoma skupi i složeni detektori pri čemu se najčešće zahteva spregnuta masena detekcija. Kako ove metode nisu ekonomski opravdane zbog visoke cene instrumenata javila se potreba da se razvije pouzdana, osetljiva, brza i ekonomična metoda koja može da zameni masenu spektrometriju. Pored toga, poželjno je da priprema uzorka kao nephodan korak pre svake instrumentalne metode, bude tako razvijena da se uz minimalan utrošak resursa i vremena dobije uzorak odgovarajuće čistoće.

U ovom istraživanju prikazana je primena GC metode sa NPD detektorom u određivanju sadržaja akrilamida. Kako do sada ima mali broj publikovanih radova [16] u kojima je opisana primena GC-NPD metode za određivanje akrilamida u termički tretiranim uzorcima krompira, zaključeno je da će se ovim istraživanjem dati značajan naučni doprinos u analitici akrilamida. Predloženu metodu karakteriše jednostavnost pripreme uzorka i izvođenja hromatografske analize uz zadržavanje odgovarajućih karakteristika u pogledu osetljivosti i tačnosti.

EKSPERIMENTALNI DEO

Aparatura i reagensi

Za određivanje sadržaja akrilamida korišćen je gasni hromatograf Agilent 6890A opremljen sa azot–fosfornim detektorom i kapilarnom kolonom DB-WAX (0,32 mm i.d.×30 m×0,25 μm debljina filma, J&W Scientific, Folsom, CA, USA). Obrada podataka i kontrola GC sistema vršena je pomoću softvera Agilent Technologies 6890N Gas Chromatography chemstation softver (Hew-

lett-Packard, Palo Alto, CA, USA). Kao standard korišćen je rastvor akrilamida (čistoća > 99,8%) proizvođača Sigma-Aldrich (St. Louis , MO, USA). Organski rastvarači (etil-acetat, metanol, aceton i metilen-hlorid) takođe su od proizvođača Sigma-Aldrich (St. Louis, MO, USA).

Priprema rastvora

Osnovni rastvor standarda akrilamida koncentracije 1 mg/mL (1000 mg/dm^3) pripremljen je rastvaranjem u etil-acetatu.

Radni rastvor pripremljen je rastvaranjem osnovnog rastvora standarda u opsegu koncentracija od 0 do 10 mg/dm^3 u etil-acetatu. Svi rastvori standarda čuvani su na temperaturi od 4 °C do ispitivanja, a pre ispitivanja temperirani su do sobne temperature.

Priprema uzoraka

Po šest uzoraka krompira pripremljeni su za konzumiranje primenom tri različita termička tretmana:

– Kuvanjem u vodi na temperaturi do 110 °C u trajanju od 5, 10 i 15 min.

– Pečenjem u rerni na temperaturi od 200 °C u trajanju od 5, 10 i 15 min.

– Prženjem u fritezi na temperaturi ulja od 250 °C u trajanju od 5, 10 i 15 min.

Postupak pripreme uzoraka

Izmeri se 20 g dobro homogenizovanog uzorka i ostavi da bubri upijajući 200 mL dejonizovane vode (70±1 °C) u trajanju od 60 min. Smeša se ponovo homogenizuje i dobijeni supernatant odvoji i profiltrira kroz stakleni filter pora 0,45 μm (Witeg Labortechnik GmbH, Germany). Dobijeni filtrat zasiti se kristalnim NaCl i u smešu doda 100 mL etil-acetata. Nastala suspenzija se meša 1 sat. Dobijeni rastvor prenese se u levak za odvajanje zapremine od 500 mL i izdvoji se etil-acetatni sloj. Zaostala voda odvoji se filtriranjem kroz filter papir sa anhidrovanim natrijum-sulfatom. Filtrat se upari na zapreminu manju od 10 mL zagrevanjem na 60 °C pomoću rotacionog vakuum uparivača (Rotavapor R-124; Buchi, Swicerland), i dopuni do 10 mL etil-acetatom. Jedan mikrolitar finalnog ekstrakta se injektuje u prethodno pripremljen hromatografski sistem.

Postupak GC-NPD analize

Nakon stabilizovanja GC-NPD sistema uradi se kalibracija. Svi potrebni parametri (vremenske funkcije, izbor metode izračunavanja, atenuacije i dr.) unesu se softverskom metodom koja omogućava praćenje razdvajanja akrilamida. Hromatografski uslovi su navedeni u tabeli 1.

Statistička analiza

Za statističku obradu podataka korišćeni su programi Microsoft Office Excel i Statistica. Primenjene su regresiona i korelaciona analiza.

Tabela 1. Hromatografski uslovi
Table 1. Chromatographic conditions

Mobilna faza	He, 99,999% (27 ml/min)
Temperaturni program	50–180 °C (20 °C /min); 8 min
Temperatura injektora	250 °C, splitless mode
Temperatura detektora	280 °C

REZULTATI I DISKUSIJA

Za određivanje sadržaja akrilamida u termički treti-ranim uzorcima primenjena je GC-NPD metoda. Kao što je navedeno u uvodu, cilj je bio da se razvije metoda koja će biti brža i ekonomičnija od uobičajenih metoda koje podrazumevaju masenu detekciju a da se sa druge strane zadrži odgovarajuća osetljivost metode. Stoga, preliminarna faza istraživanja je podrazumevala pode-šavanje optimalnih uslova GC-NPD metode a nakon tog procesa, dalje je vršena validacija metode.

Validacija metode

Pod optimalnim hromatografskim uslovima injek-tovan je rastvor standarda akrilamida i rastvor uzorka krompira. Dobijeni hromatogrami prikazani su na slici 1 i pokazuju da nema interferencija uzorka sa pikom akrilamida.

Dalje, urađena je verifikacija vrednosti *LOD* i *LOQ*. Za verifikaciju *LOD* i *LOQ* pripremljen je radni standard (veštački uzorak) koji sadrži 0,2 mg/kg akrilamida. Do-bijeni rezultati prikazani su u Tabeli 2.

Tabela 2. Verifikacija granice detekcije i granice kvantifikacije; radni rastvor akrilamida koncentracije 0,2 mg/kg
Table 2. Verification of limits of detection and limit of quantification

Parametar	Vrednost
Koncentracija, mg/kg	0,20
	0,18
	0,23
	0,22
	0,19
	0,20
X sr	0,203
RSD	0,018

Vrednosti *LOD* i *LOQ* izračunate su primenom for-mula (1) i (2):

$$LOD = X\text{sr} + 3SD = 0{,}203 \text{ mg/kg} + 3{\times}0{,}018 \text{ mg/kg} = 0{,}26 \text{ mg/kg} \tag{1}$$

$$LOQ = X\text{sr} + 10SD = 0{,}203 \text{ mg/kg} + 10{\times}0{,}018 \text{ mg/kg} = 0{,}40 \text{ mg/kg} \tag{2}$$

U narednoj fazi urađena je procena linearnosti metode. Zavisnost površine hromatografskog pika i koncentracije akrilamida ispitana je regresionom anali-zom i dobijena je linearna kalibraciona kriva sa koefi-cjentom determinacije $R^2 > 0{,}99$. Kalibracija je vršena u opsegu koncentracija 0–10 mg/kg (0, 1, 2, 5 i 10 mg/kg)
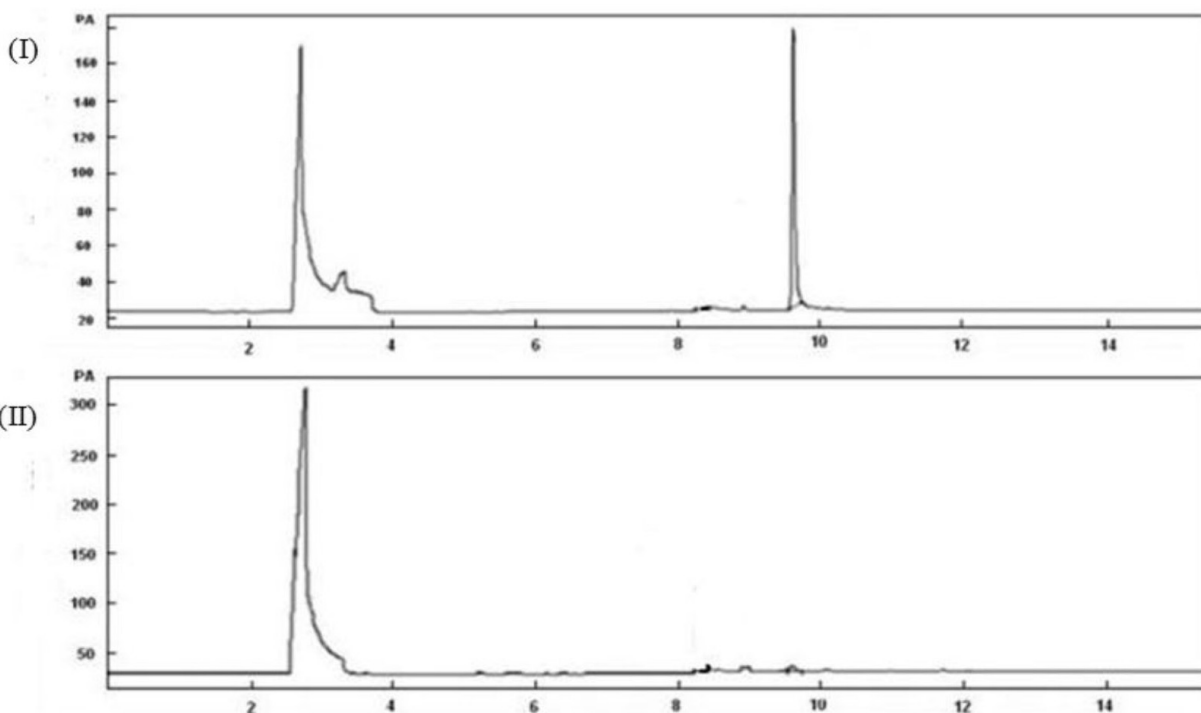
Slika 1. Hromatogram standarda akrilamida 10 mg/dm³ (I) i hromatogram akrilamida 1,4 mg/dm³ detektovan u uzorku krompira.
Figure 1. The chromatogram standard acrylamide 10 mg / dm³ (I) and a chromatogram of acrylamide 1,4 mg/dm³ is detected in a sample of potatoes.

i dobijena je jednačina prave: $y = 0,801x + 0,45$. Na slici 2 prikazana je dobijena kalibraciona kriva.

Tačnost metode procenjena je na taj način što je uzorak krompira koji je sadržao 1,4 mg/kg akrilamida opterećen sa po 1,0; 2,0 i 5,0 mg/kg akrilamida i dobijene vrednosti su prikazane u tabeli 3. Vrednosti dobijene iz šest paralelno urađenih ekstrakcije kvantitativno su obrađene GC-NPD postupkom.

Tabela 3. Recovery vrednost za akrilamid u opterećenim uzorcima krompira
Table 3. Recovery value for acrylamide spiked in potato

Početna konc. AA mg/kg	Dodata količna AA mg/kg	Dobijena konc. AA mg/kg	Očekivana konc. AA mg/kg	Tačnost %
1,40	1,0	2,64	2,40	110,0
1,33		2,58	2,33	110,7
1,45		2,68	2,45	109,3
1,37		2,60	2,37	109,7
1,39		2,50	2,39	110,8
1,44		2,68	2,44	109,8
Csr = 1,40				110,0
1,40	2,0	3,48	3,40	102,3
1,33		3,39	3,33	101,8
1,45		3,54	3,45	102,6
1,37		3,42	3,37	101,5
1,9		3,47	3,39	102,3
1,44		3,53	3,44	102,6
Csr = 1,40				102,2
1,40	5,0	6,55	6,40	102,3
1,33		6,45	6,33	101,8
1,45		6,61	6,45	102,4
1,37		6,52	6,37	102,3
1,39		6,50	6,39	101,7
1,44		6,55	6,44	101,7
Csr = 1,40				102,0

Vrednosti za Recovery dobijene za tri nivoa koncentracija potvrđuju da je metoda tačna.

Dobijeni rezultati za ispitane parametre validacije potvrđuju pouzdanost metode pa je validirana GC-NPD metoda primenjena za određivanja sadržaja akrilamida u krompiru nakon kuvanja, pečenja i prženja na različitim temperaturama i vremenskim intervalima. U tabeli 4 prikazani su dobijeni rezultati.

Visoka temperatura i duže vreme prženja pogoduju sintezi veće količine akrilamida.

Generalno, na temperaturi od 250 °C za 5 min pri pripremanju pomfrita dolazi do sinteze akrilamida u koncentraciji od 1,6 mg/kg dok se za 15 min zagrevanja na istoj temperaturi sintetiše akrilamid u koncentraciji od od 2,7 mg/kg. Smanjenjem temperature prženja sa 250 na 180–200 °C smanjen je sadržaj akrilamida ali

pomfrit je bio manje hrskav i mnogo manje privlačan za konzumaciju. U ovom radu uzorci krompira nakon termičkih tretmana su pripremani tečno–tečnom ekstrakcijom, i dobijene su zadovoljavajuće *Recovery* vrednosti [17–19]. Akrilamid je identifikovan na osnovu retencionog vremena (9,68 min), čime je postignuta neophodna specifičnost metode, a linearnost je dobijena u opsegu 0,25–10 mg/kg. Pri hromatografskoj analizi uzoraka krompira pripremljenih procedurom ekstrakcije navedenom u ovom radu nije primećeno prisustvo dodatnih pikova koji bi mogli da potiču od interferirajućih supstancija, što ukazuje na selektivnost primenjenog postupka. Osnovne prednosti predložene metode, u odnosu na metode opisane u literaturi, su jednostavnost pripreme uzoraka i izvođenja hromatografske procedure i ekonomičnost. Predložena metoda, takođe, ima zadovoljavajuće karakteristike u pogledu osetljivosti i tačnosti. Do sada sadržaj akrilamida u namirnicama po našim zakonskim propisima nije limitiran niti je limitiran u Evropskoj uniji. Evropska komisija je izdala preporuku broj 2007/331/ES kojom podstiču države članice da prate sadržaj akrilamida u hrani kako bi se dobilo što više relevantnih podataka za procenu rizika unosa akrilamida putem namirnicama.
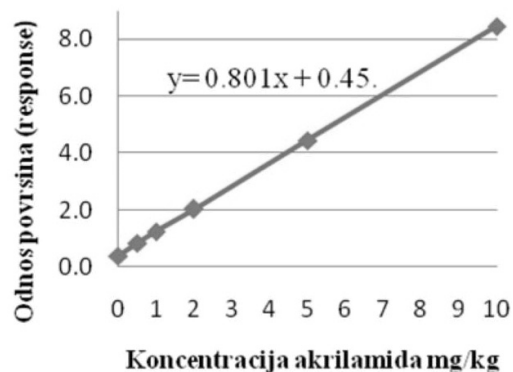
Slika 2. Standardna kriva za akrilamid u opsegu koncentracija od 0 do 10 mg/kg
Figure 2. Standard curve for the acrylamide concentration in the range 0 to 10 mg/kg

Tabela 4. Sadržaj akrilamida u krompiru nakon termičkog tretmana
Table 4. The content of acrylamide in potato after thermal treatment

Tretman	Termički tretman, min		
	5	10	15
Kuvanje u vodi na 110 °C	< LOD	< LOD	< LOD
Pečenje u rerni na 200 °C	0,6	1,4	1,9
Prženje u ulju na 250 °C	1,6	2,4	2,7

ZAKLJUČAK

U ovom radu predložena je GC-NPD metoda za određivanje sadržaja akrilamida u termički tretiranim

uzorcima krompira. Opisana metoda je tačna, jedno-stavna i ekonomična, pa je zbog toga veoma pogodna za praktičnu primenu. Pored toga, predstavlja i zna-čajan naučni doprinos analitici akrilamida jer je do sada publikovan veoma mali broj radova u kojima je opisana primena NPD detektora za određivanje akrilamida. Na kraju, na osnovu analize rezultata uzoraka može se zaključiti da je poželjno razviti postupak za dobijanje pomfrita sa niskim ili čak bez sadržaja akrilamida sa teksturom privlačnom za konzumaciju.

LITERATURA

[1]   IARC.Monographs on the evalution of carcinogen risk to humans [serial on the Internet]. 2011 (http://monographs.iarc.fr).

[2]   Swedish National Food Administration (SNFA). Infor-mation about acrylamide in food Uppsala [serial on the Internet] (http://www.slv.se).

[3]   H.Mojska, I.Gielecinska, L.Zsponar, M.Oltarzewski, Estimation of the dietary acrylamide exposure of the Polish population, Food. Chem. Toxicol. **48** (2010) 2090––2096.

[4]   Food Standards Agency. Stady of acrylamide in food [serial on the Internet], 2010 (http://www.food.gov.uk).

[5]   Scientific Committee on food. Opinon of the SCF on new findings regarding the presence of acrylamide in food [serial on the Internet]. 2010 (http://www.europa.eu).

[6]   FAO/WHO (Food and Agricultural Organisation/World HealthOrganization).Summary and conclusions report of the seventy-second meeting of the Joint FAO/WHO Expert Committee on Food Additives (JECFA) 1-16, 2010 (http://www.fao.org).

[7]   N.Marchettini, S. Focardi, M. Guarnieri, C. Guerranti, G.Perra, Determination of acrylamide in local and com-mercial cultivar of potatoes from biological farm, Food. Chem. **136** (2013) 1426–1428.
       C. Laurence, E. Sune, Analytical methods used to measure acrylamide concentrations in Foods, J. AOAC Int. **88** (2005) 274–284.

[8]   Y.Zhang, G. Zhang, Occurrence and analytical methods of acrylamide in heat-treated foods review and recent developments, J. Chromatogr., A **1075** (2005) 1–21.

[9]   S.E. Kepekci Tekkeli, C. Onal, A. Onal, A Review of cur-rent methods for the determination of acrylamide in food products, Food. Anal. Methods. **5** (2012) 29–39.

[10] L. Dunovska, T. Cajka, J. Hajslova, K. Holadova, Direct determination of acrylamide in food by gas chromato-graphy-high-resolution time-of-flight mass spectro-metry, Anal. Chim. Acta **578** (2006) 234–240.

[11] Y. Zhang, Y. Dong, Y. Ren, Y. Zhang, Rapid determination of acrylamide contaminant in conventional fried foods by gas chromatography with electron capture detector, J. Chromatogr., A **1116** (2006) 209–216.

[12] C.M. Soares, R.C. Alves, S.Casal, M.B. Oliveira, J.O. Fer-nandes, Development and validation of a matrix solid-phase dispersion method to determine acrylamide in coffee and coffee substitutes, J. Food. Sci. **75** (2010) 57––63.

[13] E.K. Paleologos, M.G.Kontominas, Determination of acrylamide and methacrylamide by normal phase high performance liquid chromatography and UV detection, J. Chromatogr., A **1077** (2005) 128–135.

[14] V. Gokmen, H.Z. Senyuva, J. Acar, K. Sarioglu, Deter-mination of acrylamide in potato chips and crisps by high-performance liquid chromatography, J. Chro-matogr., A **1088** (2005) 193–199.

[15] S.H. Kim, J.H. Hwang, K.G. Lee, Analysis of acrylamide using gas chromatography – nitrogen phosphorus det-ector (GC-NPD), Food. Sci. Biotechnol. **20** (2011) 835––839.

[16] Scientific Committee on food. Opinion of the SCF on new findings regarding the presence of acrylamide in food [serial on the Internet], 2010 (http://www.europa.eu).

[17] W. Bremser, The fitness for purpose of analytical method: A laboratory guide to method validation and related topic. EURACHEM Guide 1s English edition. [serial on the Internet], 2010 (http://www.eurachem.ul.pt).

[18] International Conference on Harmonization, Q2B: Vali-dation of Analytical Procedures: Methodology; Avail-ability, Federal Register **62** (1997) 27463–27467.

SUMMARY

THE EFFECT OF HEAT TREATMENTS ON THE SYNTHESIS OF ACRYLAMIDE AND ITS QUANTIFICATION BY GAS CHROMATOGRAPHY WITH A NITROGEN–PHOSPHORUS DETETECTOR

Veselin M. Delević[1], Refik M. Zejnilović[2], Biljana S. Jančić-Stojanović[3], Milica D. Zrnić Ćirić[4], Brižita I. Đorđević[4], Ivan M. Stanković[4]

[1]Institute of Public Health, Podgorica, Montenegro
[2]Faculty of Pharmacy, Podgorica, Montenegro
[3]Department of of Drug Analysis, Faculty of Pharmacy, University of Belgrade, Belgrade, Serbia
[4]Department of Bromatology, Faculty of Pharmacy, University of Belgrade, Belgrade, Serbia

(Scientific paper)

In this paper, the influence of thermal treatment (cooking, baking and frying) on the content of acrylamide in potato was followed by gas chromatography with nitrogen–phosphorus detector (GC-NPD). Sample preparation was performed in the conventional manner, applying heat treatment as follows: in boiling water at 110 °C for 30 min, by baking in an oven for 30 minu at 220 °C, and frying in oil for 15 min at 250 °C. Quantification of acrylamide is preceded by homogenization of the sample, extraction, and evaporation of the extract. The calibration is performed in the concentration range 0–10 mg/kg and obtained value for R^2 was higher than 0.99. Limit of detection and limit of quantification were determined and obtained values were 0.26 and 0.41 mg/kg, respectively. Recovery values were ranged from 102 to 110% and confirmed that metod is accurate. The proposed GC-NPD method is simple, reliable and accurate for determination of the content of acrylamide in food samples. Obtained results show that the content of acrylamide in potato prepared by heat-cooking was below *LOD*, while for samples treated by baking or frying were in range from 0.6 to 2.7 mg/kg. By comparing the content of acrylamide in potato we concluded that heat treatment has a major impact on the synthesis of acrylamide and it would be desirable to develop a process for the preparation of French fries and potato chips with low or no acrylamide content with textured attractive for consumation.

The quality analyses of olive cake fuel pellets – Mathematical approach

Tea I. Brlek[1], Lato L. Pezo[2], Neven M. Voća[3], Đuro M. Vukmirović[1], Radmilo R. Čolović[1], Darko E. Kiš[4], Jovana S. Brkljača[1]

[1]*Institute of Food technology Novi Sad, University of Novi Sad, Novi Sad, Serbia*
[2]*Institute of General and Physical Chemistry, University of Belgrade, Beograd, Serbia*
[3]*Faculty of Agriculture, University of Zagreb, Zagreb, Croatia*
[4]*Faculty of Agriculture, University of Osijek, Osijek, Croatia*

Abstract
This article investigates the effect of processing parameters (conditioning temperature and binder content), on final quality of produced agro-pellets for heat energy generation, obtained from four different olive cultivars using different technological parameters. Technological, physical and chemical properties of pellets (carbon, hydrogen, nitrogen and sulphur content, particle density, abrasion length, moisture, ash content, higher and lower heating values, fixed carbon and volatile matter content) have been determined to assess their quality. The performance of Artificial Neural Network (ANN) was compared with the performance of second order polynomial (SOP) model, as well as with the obtained experimental data in order to develop rapid and accurate mathematical model for prediction of final quality parameters of agro-pellets. SOP model showed high coefficients of determination (r^2), between 0.692 and 0.955, while ANN model showed high prediction accuracy with r^2 between 0.544 and 0.994.

Keywords: olive cake, olive cultivar, agro-pellets, pelleting, mathematical model.

Available online at the Journal website: http://www.ache.org.rs/HI/

Due to global reduction in fossil energy sources, investigations have turned to renewable sources. Among renewable energy sources, biomass particularly stands out because it can be used to cover a variety of energy needs and it can also be stored, unlike other renewable energy sources [1]. The use of biomass as an energy source also enables closing of the carbon cycle, which is not the case when fossil fuels are used [2].

Widely available biomass is agricultural waste. In order to meet the world's trends in waste utilization and valorisation, olive oil mill waste, *i.e.*, olive cake, has been used in this research as an potential energy source (prepared as agro-pellets). Due to the initiatives and stimulants from the Croatian government the olive oil production has been increasing in the last ten years. Therefore, the quantities of olive cake have also risen. Croatia currently produces about 38,000 t of olives per year, with the average yield of 2.2 t/ha which results with approximately 16,000 t of fresh olive cake [3]. That is a large quantity considering the narrow coastal area of Croatia where olives are grown. This kind of waste has a negative influence on the environment due to its chemical composition and therefore cannot be disposed to the conventional landfill. One of the solutions for olive cake disposal is production of fuel pellets. Pelletized material is much easier to manipulate and store, moreover it has higher density and better heating value/volume ratio [4].

Results of quality analyses of olive cake pellets obtained in a previous investigation were used in this paper [5]. Improved mathematical approach of the previously obtained results was applied in order to more accurately analyse the quality of the produced agro fuel pellets in order to optimize the pelleting process. The goal is to obtain high quality fuel pellets which are in line with European standards for fuel pellets and are produced with no unnecessary costs.

Response surface methodology (RSM) is used as an effective tool for optimizing a variety of processes [6––8]. The main advantage of RSM is reduced number of experimental runs that provide sufficient information for statistically valid results. The RSM equations describe effects of the test variables on the observed responses, determine test variables interrelationships and represent the combined effect of all test variables in the observed responses, enabling the experimenter to make efficient exploration of the process.

Nonlinear models are found to be more suitable for real process simulation. Response Surface Methodology (RSM) and Artificial Neural Network (ANN) models have gained momentum for modelling and control of processes [9,10].

ANN models are recognized as a good modelling tool since they provide the empirical solution to the problems from a set of experimental data, and are capable of handling complex systems with nonlinear-

Correspondence: L.L. Pezo, University of Belgrade, Studentski trg 12/V, 11000 Beograd, Serbia.
E-mail: latopezo@yahoo.co.uk

ities and interactions between decision variables [11]. The specific objective of this study was to investigate the effect of olive cultivar, conditioning temperature and binder content on technological, physical and chemical properties of pellets (carbon, hydrogen, nitrogen and sulphur content, particle density, abrasion length, moisture, ash content, higher and lower heating values, fixed carbon and volatile matter content). The performance of ANN was compared with SOPs, as well as to experimental data in order to develop rapid and accurate prediction models.

The current study intends to investigate the effects of conditioning temperature and added binder content on the final quality of agro-pellets produced from four different olive cultivars using different technological treatments. Also, this investigation is focused on finding the appropriate mathematical models for carbon, hydrogen, nitrogen and sulphur content, particle density, abrasion and length, and also moisture and ash content, higher and lower heating value (HHV and LHV), fixed carbon and volatile matter content, regarding observed process parameters: conditioning treatment and added binder content.

MATERIALS AND METHODS

Raw-material

Pellets from four different olive cake cultivars were used in this research; Istarska Bjelica, Buža, Leccino and Pendolino. Olive cake was obtained from an olive oil mill in Istria, Croatia. Parameters which were varied during preparation of olive cake for pelleting were steam conditioning treatment (unconditioned and conditioned at 50 and 80 °C) and amount of added binder (no binder and 1 and 2% of added binder). The treatments resulted in nine combinations for each of four cultivars used, making a total of 36 combinations for pelleting, which are presented in Table 1. Detailed description of the preparation of the material and the process of pelleting of the olive cake is given in a previous paper [5].

Table 1. Experimental design for each olive cultivar

Design No.	Conditioning	Binder
1	No conditioning	No binder
2		1% binder
3		2% binder
4	Conditioned at 50 °C	No binder
5		1% binder
6		2% binder
7	Conditioned at 80 °C	No binder
8		1% binder
9		2% binder

Analyses of the pellets

Proximate analyse that were done on the samples were: moisture content [12], ash content [13], fixed carbon (calculated by difference between 100 and the sum of volatile matter, ash and moisture) and volatile mater [14]. Samples were analysed for ultimate composition: content of C, H, N [15] and S [16], HHV and LHV [17].

Physical characteristics determined in this study were abrasion, density and length of pellets. Abrasion was determined with abrasion test device "Pfost" (Bühler, Switzerland). Density was analysed using the hydrostatic method on the analytical balance, with ethanol as a medium for wetting. Length of the pellets was measured by calliper. Detailed description of the performed measurements is given in our previous work [5].

Mathematical modelling

Descriptive statistical analyses for all the obtained results have been expressed as the mean ± standard deviation (*SD*). Furthermore, the evaluation of one-way ANOVA and PCA analyses of the obtained results has been performed using StatSoft Statistica 10.0® software. Collected data have been subjected to one-way analysis of variance (ANOVA) for the comparison of means, and significant differences are calculated according to post-hoc Tukey's HSD ("honestly significant differences") test at $p < 0.05$ significant level, 95% confidence limit. All data are reported as means ± standard deviations.

Response surface methodology

The experimental data used for the study of experimental results were obtained using a $4{\times}3^2$ full factorial experimental design (3 levels–2 parameters), with 9 runs (4 blocks, for each of four different cultivars), according to Response surface methodology [18]. It was used to design the final product quality, considering two factors: conditioning temperature and added binder content.

The following second order polynomial (SOP) model was fitted to the experimental data. Thirteen models of the following form were developed to relate thirteen responses (*Y*) and two process variables (*X*), for each of four different olive cultivars:

$$Y_k^l = \beta_{k0}^l + \sum_{i=1}^{2} \beta_{ki}^l X_i + \sum_{i=1}^{2} \beta_{kii}^l X_i^2 + \beta_{k12}^l X_1 X_2,$$

$$k \in [1,13], l \in [1,4] \tag{1}$$

where: β_{k0}^l, β_{ki}^l, β_{kii}^l, β_{k12}^l are constant regression coefficients; Y_k^l, either C, H, N or S content, particle density, abrasion and length, moisture and ash content, HHV, LHV, fixed carbon or volatile matter content; X_1 – conditioning temperature; X_2 – binder content.

Artificial neural network (ANN)

The database for ANN was randomly divided to: training data (60%), cross-validation (20%) and testing data (20%). The cross-validation data set was used to test the performance of the network, while training was in progress as an indicator of the level of generalization and the time at which the network has begun to over-train. Testing data set was used to examine the network generalization capability. To improve the behaviour of the ANN, both input and output data were normalized. In order to obtain good network behaviour, it is necessary to make a trial and error procedure and also to choose the number of hidden layers, and the number of neurons in hidden layer(s). A multi-layer perceptron models (MLP) consisted of three layers (input, hidden and output). Such a model has been proven as a quite capable of approximating non-linear functions [19] giving the reason for choosing it in this study. In this work the number of hidden neurons for optimal network was ten. Broyden–Fletcher–Goldfarb–Shanno (BFGS) algorithm was used for ANN modelling.

After defining the architecture of ANN, the training step was initiated. The training process was repeated several times in order to get the best performance of the ANN, due to a high degree of variability of parameters. It was accepted that the successful training was achieved when learning and cross-validation curves approached zero. Testing was carried out with the best weights stored during the training step. Coefficient of determination (r^2) and sum of squares (SOS) were used as parameters to check the performance (*i.e.*, the accuracy) of the obtained ANNs. After the best behaved ANN was chosen, the model was implemented using an algebraic system of equations to predict carbon, hydrogen, nitrogen and sulphur content, particle density, abrasion and length, and also moisture and ash content, higher and lower heating value (HHV and LHV), fixed carbon and volatile matter content.

Sensitivity analysis

Sensitivity analysis is a sophisticated technique which is necessary to use for studying the effects of observed input variables and also the uncertainties in obtained models and general network behaviour. Neural networks were tested using sensitivity analysis, to determine whether and under what circumstances obtained models might result in an ill-conditioned system [20]. On the basis of developed ANN models, sensitivity analysis was performed in order to more precisely define the influence of processing variables on the observed outputs. The infinitesimal amount (+0.0001%) has been added to each input variable, in 10 equally spaced individual points encompassed by the minimum and maximum of the train data. These signals were normally distributed with a constant intensity and frequency. It was used to test the model sensitivity and measurement errors.

Normal standard score

Normal scores have been calculated for each assay, and were used for complex comparison of observed samples, regarding their technological, physical and chemical properties. The ranking procedure between different samples has been performed based upon the ratio of raw data and extreme values for each applied assay [5,21,22], according to these equations:

$$\bar{x}_i = 1 - \frac{\max_i x_i - x_i}{\max_i x_i - \min_i x_i}, \quad \forall i$$

in case of "the higher, the better" criteria, or

$$\bar{x}_i = \frac{\max_i x_i - x_i}{\max_i x_i - \min_i x_i}, \quad \forall i$$

in case of "the lower, the better" criteria, where x_i represents the raw data.

Unlike others variables, normalized scores for moisture and length have been evaluated according to optimal values, using trapezoidal function, as follows:

$$A(x,a,m,n,b) = \begin{cases} a \leq x < m, & \dfrac{x-a}{m-a} \\ m \leq x < n, & 1 \\ n \leq x < b, & 1 - \dfrac{x-n}{b-n} \end{cases} \quad (2)$$

where x is whether moisture and length parameter, and the values of a, b, m and n are function parameters. Interval [a,b] represents the range in which measured values occur in the experiment (minimum and maximum values), while range [m,n] is the proposed optimal values range for response variables, chosen for technological reasons. An optimization with procedure was performed using MicroSoft Excel 2007 to determine the workable optimum conditions for agro-pellets production.

RESULTS AND DISCUSSION

The agro-pellets production was studied in terms of common technological, physical and chemical parameters, *i.e.*, C, H, N and S content, particle density, abrasion and length, moisture and ash content, HHV, LHV, fixed carbon and volatile matter content.

Each of the process variables has been coded, as shown in Table 2, and these codes are used for easier representation of experimental data.

Table 2. Codes

Code	1	2	3	4
Cultivar name	Istarska Bjelica	Buža	Leccino	Pendolino
Temperature, °C	0	50	80	–
Binder content, %	0	1	2	–

Response surface methodology

Ultimate analysis

Chemical characteristics (C, H, N and S content) of four different cultivars (Bjelica, Buža, Leccino and Pendolino) of olive cake are presented in Table 3. Tukey's HSD test showed significant differences for most cases.

The analysis of variance (ANOVA) exhibits the significant independent variables as well as interactions of

Table 3. Ultimate analysis and physical properties of oil cake; the results are presented as mean±SD; different letter within the same row indicate significant differences (p < 0.05), according to Tukey's test. Polarity: + = the higher the better criteria, − = the lower the better criteria, C – cultivar type, T – temperature, B – binder content code

Run No.	C	T °C	B %	Ultimate analysis (Content, %)				Physical properties		
				C	H	N	S	Particle density g/cm^3	Abrasion	Length mm
1	1	1	1	54.37±0.16^{abc}	7.41±0.05^{bcd}	0.69±0.01^{a}	0.07±0.00^{d}	1.24±0.00^{efghijk}	15.92±0.01^{z}	11.24±0.04^{f}
2	1	1	2	54.62±0.08^{ab}	7.33±0.06^{bcd}	0.69±0.00^{ab}	0.07±0.00^{d}	1.23±0.01^{cdefghi}	15.92±0.04^{z}	11.16±0.06^{f}
3	1	1	3	53.53±0.42^{a}	7.37±0.05^{bcd}	0.70±0.00^{bcd}	0.07±0.00^{bcd}	1.26±0.01^{klmnop}	10.37±0.05^{r}	9.98±0.07^{e}
4	1	2	1	54.63±0.18^{abc}	7.34±0.02^{ab}	0.70±0.00^{ab}	0.07±0.00^{cd}	1.25±0.01^{efghijkl}	9.47±0.05^{q}	12.27±0.04^{hi}
5	1	2	2	54.52±0.27^{abc}	7.28±0.02^{ab}	0.71±0.01^{abc}	0.07±0.00^{bcd}	1.26±0.01^{ghijklmn}	9.22±0.02^{p}	12.71±0.04^{lm}
6	1	2	3	53.70±0.25^{a}	7.26±0.03^{a}	0.72±0.01^{d}	0.07±0.00^{abc}	1.27±0.01^{lmnopq}	8.97±0.02^{o}	11.84±0.06^{g}
7	1	3	1	54.67±0.24^{abc}	7.43±0.06^{cde}	0.69±0.00^{ab}	0.07±0.00^{abc}	1.20±0.00^{ab}	5.33±0.02^{hi}	12.42±0.11^{ijk}
8	1	3	2	54.31±0.35^{abc}	7.39±0.06^{abc}	0.70±0.00^{abc}	0.07±0.00^{ab}	1.22±0.01^{abc}	5.37±0.01^{ghi}	13.17±0.11^{p}
9	1	3	3	53.61±0.11^{a}	7.35±0.06^{abc}	0.72±0.00^{cd}	0.07±0.00^{a}	1.23±0.01^{cdefgh}	5.25±0.03^{fgh}	12.63±0.07^{klm}
10	2	1	1	56.60±0.47^{jklm}	8.07±0.03^{klmn}	1.03±0.00^{ijkl}	0.08±0.00^{mnopq}	1.25±0.01^{lmnopq}	15.22±0.09^{y}	7.18±0.01^{b}
11	2	1	2	57.06±0.02^{m}	8.09±0.01^{klmn}	1.06±0.01^{opq}	0.08±0.00^{r}	1.27±0.01^{nopqr}	14.20±0.12^{x}	6.43±0.02^{a}
12	2	1	3	56.83±0.41^{ijklm}	8.16±0.04^{no}	1.07±0.00^{pq}	0.08±0.00^{ijk}	1.29±0.01^{qrs}	13.90±0.10^{w}	6.45±0.04^{a}
13	2	2	1	56.72±0.38^{jklm}	8.18±0.03^{no}	1.04±0.01^{ghij}	0.08±0.00^{ef}	1.26±0.01^{jklmno}	7.97±0.04^{n}	13.11±0.11^{o}
14	2	2	2	57.68±0.27^{lm}	8.19±0.07^{no}	1.06±0.01^{mnop}	0.08±0.00^{lmn}	1.28±0.00^{opqr}	7.14±0.04^{m}	13.08±0.10^{op}
15	2	2	3	57.38±0.31^{jklm}	8.21±0.03^{lmno}	1.06±0.00^{lmnop}	0.08±0.00^{ghij}	1.30±0.01^{rs}	6.89±0.04^{l}	12.48±0.06^{hij}
16	2	3	1	56.85±0.13^{ghijkl}	8.19±0.07^{mno}	1.07±0.00^{lmnop}	0.08±0.00^{e}	1.21±0.01^{a}	6.71±0.05^{k}	12.58±0.06^{ijk}
17	2	3	2	57.08±0.44^{jklm}	8.15±0.07^{lmno}	1.07±0.01^{q}	0.08±0.00^{opqr}	1.23±0.00^{bcde}	5.47±0.03^{ij}	12.29±0.02^{h}
18	2	3	3	57.29±0.18^{klm}	8.08±0.05^{klm}	1.06±0.01^{opq}	0.08±0.00^{nopqr}	1.25±0.01^{fghijklm}	4.51±0.04^{d}	12.66±0.11^{lm}
19	3	1	1	56.36±0.13^{efghij}	7.63±0.02^{efg}	1.06±0.00^{mnop}	0.08±0.00^{kl}	1.26±0.00^{hijklmno}	11.26±0.06^{t}	7.24±0.06^{b}
20	3	1	2	55.87±0.20^{defghi}	7.63±0.04^{efg}	1.02±0.01^{fgh}	0.08±0.00^{fgh}	1.25±0.01^{hijklmno}	11.16±0.05^{t}	8.03±0.04^{d}
21	3	1	3	55.81±0.25^{efghij}	7.72±0.08^{ghi}	1.04±0.00^{ghijk}	0.08±0.00^{qr}	1.29±0.01^{pqrs}	10.42±0.09^{s}	8.20±0.06^{d}
22	3	2	1	56.40±0.31^{hijklm}	7.50±0.06^{def}	1.05±0.01^{jklmn}	0.08±0.00^{ghij}	1.27±0.01^{nopqr}	5.57±0.02^{j}	12.35±0.06^{ijk}
23	3	2	2	55.90±0.06^{efghij}	7.69±0.01^{efg}	1.01±0.00^{f}	0.08±0.00^{fgh}	1.27±0.01^{klmnop}	5.62±0.04^{j}	12.98±0.10^{o}
24	3	2	3	56.06±0.28^{efghij}	7.84±0.04^{ij}	1.03±0.01^{ghijk}	0.08±0.00^{pqr}	1.30±0.01^{s}	4.93±0.01^{e}	12.54±0.03^{jkl}
25	3	3	1	55.44±0.02^{cdefg}	7.70±0.04^{ghi}	1.05±0.01^{jklm}	0.08±0.00^{lmnop}	1.23±0.01^{defghi}	5.28±0.03^{ghi}	12.74±0.08^{lm}
26	3	3	2	54.87±0.39^{bcdef}	7.95±0.04^{jk}	1.02±0.01^{fghi}	0.08±0.00^{klm}	1.22±0.00^{abcd}	5.13±0.03^{f}	12.42±0.05^{ijk}
27	3	3	3	55.41±0.59^{bcde}	8.20±0.04^{no}	1.06±0.00^{nop}	0.09±0.00^{s}	1.26±0.01^{mnopqr}	4.24±0.01^{c}	12.74±0.04^{lm}
28	4	1	1	54.26±0.49^{abc}	7.37±0.04^{bcd}	0.89±0.00^{e}	0.07±0.00^{a}	1.23±0.01^{bcde}	13.47±0.13^{v}	7.13±0.01^{b}
29	4	1	2	55.77±0.16^{defghi}	7.68±0.06^{gh}	1.02±0.00^{fg}	0.08±0.00^{fghi}	1.23±0.01^{defghij}	12.79±0.06^{u}	7.48±0.04^{c}
30	4	1	3	56.12±0.37^{defghi}	7.74±0.03^{ghi}	1.04±0.01^{ghijk}	0.08±0.00^{opqr}	1.26±0.01^{mnopqr}	9.40±0.04^{pq}	8.15±0.03^{d}
31	4	2	1	56.06±0.26^{fghijk}	7.53±0.03^{def}	1.05±0.01^{klmno}	0.08±0.00^{hij}	1.26±0.01^{jklmnop}	5.20±0.00^{fg}	12.04±0.01^{g}
32	4	2	2	55.94±0.38^{defgh}	7.63±0.01^{fg}	1.01±0.00^{fgh}	0.08±0.00^{efg}	1.24±0.01^{efghijk}	5.15±0.04^{f}	13.15±0.09^{op}
33	4	2	3	56.10±0.09^{efghij}	7.84±0.04^{hij}	1.04±0.01^{hijk}	0.08±0.00^{nopqr}	1.29±0.01^{rs}	4.49±0.01^{d}	12.45±0.11^{ijk}
34	4	3	1	55.54±0.19^{cdefgh}	7.72±0.05^{fg}	1.05±0.01^{jklmn}	0.08±0.00^{lmno}	1.23±0.01^{bcdefg}	4.42±0.02^{d}	12.76±0.06^{mn}
35	4	3	2	55.37±0.08^{abcd}	8.02±0.07^{jkl}	1.03±0.01^{ghij}	0.08±0.00^{jkl}	1.22±0.00^{bcdef}	3.68±0.02^{b}	13.00±0.07^{no}
36	4	3	3	55.54±0.25^{cdef}	8.22±0.02^{o}	1.06±0.01^{mnop}	0.09±0.00^{s}	1.26±0.01^{mnopqr}	3.43±0.02^{a}	13.17±0.05^{p}
Polarity				+	+	−	−	+	−	Opt. <30 mm

these variables. In this article, ANOVA was conducted by StatSoft Statistica, ver. 10, to show the significant effects of independent variables to the responses, and to show which of responses were significantly affected by the varying treatment combinations.

The analysis revealed that the linear terms contributed substantially in all cases to generate a significant SOP model. The SOP models for all variables were found to be statistically significant and the response surfaces were fitted to these models.

The most influential variable for SOP model calculation was found to be the type of olive cultivar. Non-linear terms of SOP models have been found most influential for C and H content, while linear terms have been most important for N and S content calculation. The influences of temperature and binder content are also observed, but far less important than the cultivar type.

Nitrogen content is mostly affected by cultivar type, but the effects of conditioning temperature and binder content have also been observed. Sulphur content is mostly affected by cultivar type, but the influence of linear and quadratic terms of conditioning temperature and binder content have been also noticed on $p < 0.05$ statistically significant level.

Nitrogen and sulphur content should be especially monitored while these elements can be the most harmful for the environment due to emission of polluting gasses during combustion. Therefore it is desirable that their content is as low as possible. N content was in range from 0.69 to 1.07 (Table 3), which is slightly lower than in literature data [23] and the minimum content has been observed in pellets produced from Istarska Bjelica cultivar. According to European standards for fuel pellet quality the highest allowed concentration of nitrogen is 1.0% [24], therefore it is evident that these pellets are mostly in acceptable range. It is known that wood, as a raw material for the production of pellets, has a lower proportion of nitrogen than agricultural biomass [25]. Johansson *et al.* [26] found only 0.08% of nitrogen in wood pellets. Coal on the other hand has about 1% nitrogen [27], which is very similar to the values obtained for olive cake pellets. Therefore olive cake pellets will cause equal nitrogen oxides emissions as coal.

Produced pellets contained approximately 0.07–0.08% of sulphur (Table 3), which is consistent with data in the literature [23] and the highest allowed content by EU standards is 0.04 [24]. Minimum sulphur content has been observed in pellets made of Istarska Bjelica cultivar. Produced pellets exceed the proscribed boundaries, but according to [28], there are pellets that are allowed 0.08% S. Very small amounts of S can be found in wood and wood pellets [26,29], while on the other hand coal has much higher contents of S: 2–3%

[27,30]. Therefore biomass produces significantly less sulphur oxides during combustion.

Carbon content is affected by both quadratic and linear term in SOP model (statistically significant at $p < 0.05$ level), while the influence of binder content has been found to be insignificant. Besides cultivar type, the most influential terms in SOP model of hydrogen content are linear terms of conditioning temperature and binder content ($p < 0.05$), and also the nonlinear terms. As presented in Table 3, carbon content varied in the range from 53.53 to 57.68% which is consistent with the literature, while hydrogen was also in common values: 7.26–8.22 [3,23]. Slightly lower contents of carbon and hydrogen have been noticed in pellets made of Istarska Bjelica cultivar, compared to other cultivars. Carbon and hydrogen are not limiting factors, thus their amount is not proscribed by standards. Moreover, it is desirable that material has higher content of C and H, while it contributes to higher heating energy.

Physical properties

Physical properties (particle density, abrasion and length) are also presented in Table 3. Statistically significant differences have been found in most cases, mostly influenced by process temperature ($p < 0.05$). Binder content has been found as most influential variable for particle density calculation, while both linear and quadratic terms of conditioning temperature have been found statistically significant at $p < 0.05$ level. Cultivar type showed minor impact on particle density, but still statistically significant. Particle density of all samples was above 1.12 g/cm^3 which is the value proscribed by several EU standards [28]. The density of the pellets treated with the same conditioning treatment increased with the addition of binder, as shown in Table 3. Both abrasion and length calculation are most influenced by conditioning temperature, while cultivar type terms have been found statistically significant.

Abrasion of the pellets varied from 3.43 to 15.92%. The highest allowed level of abrasion in fuel pellets is 10.0% according to literature [28]; therefore most of the produced pellets fall into this range. Conditioning treatment and addition of binder decreases abrasion of all samples, because conditioning increases moisture content of the material as well as exposes it to elevated temperatures which facilitate particle binding [32,33].

Proximate analysis

The results of proximate analysis (moisture and ash content, HHV, LHV, fixed carbon and volatile matter content) of oil cake is presented in Table 4, and the ANOVA calculation of these parameters is presented in Table 5. Statistically significant differences of samples have been found in most cases, according to Tukey's HSD test, for various observed assays. Conditioning

Table 4. Proximate analysis of oil cake; the results are presented as mean±SD; different letter within the same row indicate significant differences (p < 0.05), according to Tukey's test. Polarity: + = the higher the better criteria, − = the lower the better criteria

Run No.	Moisture, %	Ash	*HHV* / MJ kg^{-1}	*LHV* / MJ kg^{-1}	Fixed carbon, %	Volatile matter, %
1	7.18±0.01^{bc}	1.92±0.01^{gh}	22.33±0.06^{abc}	20.84±0.22^{ab}	16.43±0.06^{gh}	80.82±0.3^{gh}
2	7.02±0.05^{b}	1.93±0.01^{h}	22.41±0.08^{abc}	20.86±0.14^{ab}	16.13±0.12^{fg}	80.65±0.46^{efgh}
3	7.09±0.04^{bc}	1.95±0.01^{gh}	22.44±0.16^{abc}	20.81±0.07^{ab}	17.68±0.05^{mn}	78.71±0.39^{bcdef}
4	9.34±0.05^{f}	1.94±0.01^{gh}	22.41±0.11^{abc}	20.88±0.13^{ab}	16.28±0.13^{gh}	80.69±0.40^{efgh}
5	9.34±0.03^{f}	1.92±0.01^{h}	22.30±0.07^{ab}	20.81±0.15^{ab}	15.90±0.05^{f}	80.53±0.38^{fgh}
6	9.31±0.09^{f}	1.93±0.02^{gh}	22.39±0.15^{abc}	20.67±0.07^{ab}	17.21±0.08^{l}	79.48±0.53^{cdefgh}
7	12.42±0.11^{i}	1.90±0.00^{gh}	22.36±0.21^{abc}	20.72±0.06^{ab}	16.06±0.00^{fg}	80.77±0.31^{efgh}
8	12.60±0.10^{i}	1.90±0.01^{efg}	22.41±0.04^{abc}	20.85±0.06^{ab}	15.40±0.08^{e}	81.43±0.71^{h}
9	12.40±0.09^{i}	1.89±0.01^{fgh}	22.44±0.14^{a}	20.75±0.08^{ab}	16.41±0.03^{ghi}	80.14±0.40^{cdefgh}
10	6.15±0.03^{a}	1.56±0.01^{a}	22.62±0.14^{abc}	20.92±0.03^{ab}	16.37±0.14^{ghi}	80.55±0.21^{h}
11	6.17±0.03^{a}	1.56±0.00^{a}	22.51±0.15^{abc}	20.93±0.19^{ab}	16.65±0.13^{ijk}	80.26±0.64^{defgh}
12	6.16±0.02^{a}	1.56±0.01^{a}	22.49±0.10^{abc}	20.73±0.20^{ab}	17.54±0.08^{lm}	79.49±0.47^{bcde}
13	9.30±0.05^{f}	1.56±0.01^{a}	22.76±0.18^{abc}	20.98±0.01^{ab}	16.93±0.09^{jk}	79.35±0.20^{cdefgh}
14	9.37±0.09^{f}	1.55±0.01^{a}	22.59±0.11^{abc}	20.94±0.12^{ab}	16.87±0.03^{jk}	80.18±0.29^{cdefgh}
15	9.30±0.02^{f}	1.56±0.01^{a}	22.57±0.17^{abc}	20.81±0.08^{ab}	17.56±0.15^{lm}	78.85±0.42^{cdef}
16	11.16±0.11^{g}	1.56±0.01^{a}	22.73±0.06^{bc}	20.79±0.07^{ab}	16.90±0.02^{k}	79.39±0.23^{cdefgh}
17	11.18±0.06^{g}	1.54±0.00^{a}	22.64±0.07^{abc}	20.91±0.16^{ab}	16.55±0.11^{hij}	79.68±0.61^{cdefg}
18	11.09±0.03^{g}	1.56±0.01^{a}	22.66±0.04^{abc}	20.90±0.12^{ab}	16.86±0.07^{k}	79.41±0.78^{bc}
19	7.22±0.06^{bc}	1.87±0.01^{de}	22.63±0.17^{abc}	20.88±0.15^{ab}	12.97±0.04^{d}	83.96±0.39^{i}
20	7.21±0.06^{c}	1.86±0.02^{de}	22.46±0.05^{abc}	20.85±0.01^{ab}	18.89±0.08^{o}	77.88±0.02^{ab}
21	7.16±0.06^{bc}	1.83±0.02^{bc}	22.55±0.07^{abc}	21.02±0.14^{ab}	19.04±0.15^{p}	77.32±0.46^{a}
22	8.94±0.07^{e}	1.86±0.01^{d}	22.53±0.16^{bc}	20.94±0.04^{b}	5.45±0.03^{a}	92.33±0.18^{j}
23	8.80±0.08^{e}	1.87±0.01^{def}	22.57±0.14^{abc}	20.97±0.18^{ab}	11.54±0.08^{b}	84.90±0.50^{i}
24	8.86±0.06^{e}	1.85±0.01^{bcd}	22.48±0.02^{abc}	20.73±0.11^{ab}	12.26±0.08^{c}	84.47±0.12^{i}
25	10.96±0.08^{g}	1.84±0.01^{bcd}	22.52±0.10^{abc}	20.85±0.12^{ab}	11.38±0.08^{b}	85.15±0.41^{i}
26	10.96±0.04^{g}	1.85±0.01^{d}	22.57±0.07^{abc}	20.74±0.19^{ab}	17.88±0.00^{n}	78.65±0.27^{bc}
27	11.00±0.05^{g}	1.85±0.02^{bcd}	22.35±0.17^{abc}	20.79±0.05^{ab}	19.02±0.15^{op}	77.32±0.71^{a}
28	7.08±0.05^{bc}	1.85±0.00^{bcd}	22.46±0.11^{abc}	20.88±0.16^{b}	16.34±0.00^{ghi}	80.53±0.09^{efgh}
29	7.10±0.07^{b}	1.86±0.01^{de}	22.60±0.02^{c}	20.86±0.17^{ab}	18.69±0.10^{o}	80.62±0.28^{gh}
30	7.03±0.02^{b}	1.84±0.01^{b}	22.56±0.15^{abc}	20.89±0.09^{ab}	19.14±0.10^{p}	81.16±0.46^{h}
31	8.19±0.02^{d}	1.86±0.01^{de}	22.52±0.06^{abc}	20.93±0.12^{ab}	5.43±0.04^{a}	80.23±0.44^{fgh}
32	8.17±0.04^{d}	1.86±0.01^{def}	22.73±0.03^{bc}	20.95±0.03^{ab}	11.55±0.02^{b}	81.36±0.58^{h}
33	8.18±0.06^{d}	1.85±0.01^{d}	22.56±0.18^{abc}	20.87±0.12^{ab}	12.15±0.09^{c}	80.96±0.15^{efgh}
34	12.04±0.09^{h}	1.84±0.01^{bcd}	22.52±0.14^{abc}	20.86±0.09^{ab}	11.37±0.10^{b}	78.58±0.74^{bc}
35	11.98±0.06^{h}	1.85±0.02^{cd}	22.39±0.13^{abc}	20.85±0.07^{ab}	18.00±0.14^{n}	79.14±0.58^{bcd}
36	11.93±0.02^{h}	1.85±0.02^{bcd}	22.49±0.10^{abc}	20.67±0.12^{a}	18.94±0.10^{op}	80.18±0.69^{cdefgh}
Polarity	0pt. <10%	−	+	+	+	+

treatment has been the most important variable for moisture content and fixed carbon.

Ash content and *HHV* were mostly impacted by cultivar type, while *LHV* was mostly influenced by conditioning and binder content. ANOVA calculation showed complex influence of linear and nonlinear terms for variables: fixed carbon and volatile matter. Recommended moisture content is up to 10%, which was the case for all pellets except the ones made from material conditioned at 80 °C. Ash content varied in range 1.54–1.95%, which is in boundaries proscribed by EU standards [28], where the highest allowed value is 6.0% of ash. Lower ash content increases heating value and improves combustion properties. *LHV* proscribed by EU standards advises values in range: from >16.0 to >18 MJ/kg. All of the samples had *LHV* higher than 20 MJ/kg and thus meet the proscribed norms.

Also shown in Table 5 is the residual variance where the lack of fit variation represents other contributions except for the higher order terms. A significant lack of

Table 5. ANOVA table (sum of squares for each assay); *: significant at p < 0.05 level, **: significant at p < 0.10 level, 95% confidence limit, error terms have been found statistically insignificant, C – cultivar, T – temperature, B – binder. dF – degrees of freedom

Parameter	dF	Particle density	Abrasion	Length	Moisture	Ash	Carbon	H	N	S	*HHV*	*LHV*	Fixed carbon	Volatile matter
C	1	0.00*	135.22*	7.37*	2.99*	0.01*	8.21*	0.93*	1.16*	0.00*	0.18*	0.01**	83.86*	8.38**
C^2	1	0.01*	0.17	10.85*	4.62*	0.87	59.67*	4.12*	0.94*	0.00*	0.09*	0.00	0.07	20.76*
T	1	0.01*	1132.59*	363.28*	404.35*	0.00	1.20*	0.46*	0.01**	0.00*	0.06*	0.10*	16.03**	1.99
T^2	1	0.01*	109.95*	106.29*	2.10*	0.00	2.80*	0.14**	0.00	0.00*	0.00	0.00	286.33*	97.48*
B	1	0.02*	44.91*	0.01	0.02	0.00	0.01	0.42*	0.01**	0.00*	0.17*	0.06*	220.98*	94.37*
B^2	1	0.00*	3.32	1.36	0.00	0.00	0.24	0.00	0.00	0.00	0.00	0.02**	19.05**	6.99**
$C{\times}T$	1	0.00*	5.79*	18.97*	1.42*	0.00	0.34	0.42*	0.01**	0.00*	0.01**	0.06*	4.14	3.08**
$C{\times}B$	1	0.00	0.26	4.13*	0.00	0.00	0.86**	0.69*	0.00	0.00*	0.01**	0.04*	98.21*	1.23
$T{\times}B$	1	0.00	9.87*	0.16	0.00	0.00	0.12	0.01	0.00	0.00	0.01**	0.00	3.25	0.14
Error	98	0.01	108.28	57.27	19.60	1.23	48.43	3.61	0.26	0.00	0.74	0.58	498.23	4.18
r^2		0.841	0.930	0.899	0.955	0.719	0.753	0.765	0.892	0.845	0.736	0.697	0.774	0.692

fit generally shows that the model failed to represent the data in the experimental domain at which points were not included in the regression [34]. All SOP models had insignificant lack of fit tests, which means that all the models represented the data satisfactorily.

The coefficient of determination, r^2, is defined as the ratio of the explained variation to the total variation and is explained by its magnitude [18]. It is also the proportion of the variability in the response variable, which is accounted for by the regression analysis. A high r^2 is indicative that the variation was accounted and that the data fitted satisfactorily to the proposed model (SOP in this case).

The r^2 values for C (0.753), H (0.765), N (0.892) and S content (0.845), particle density (0.841), abrasion (0.930) and length (0.899), moisture and ash content (0.955 and 0.719), *HHV*, *LHV*, fixed carbon and volatile matter content (0.736, 0.697, 0.774 and 0.692, respectively) were satisfactory and show the good fitting of the model to experimental results. Table 6 shows the regression coefficients for the response SOP models of C, H, N and S content, particle density, abrasion and length, moisture and ash content, *HHV*, *LHV*, fixed carbon and volatile matter content used by Eq. (1) for predicting the values.

Artificial neural network

All variables considered in the RSM, were also used for the ANN modelling. Determination of the appropriate number of hidden layers and number of hidden neurons in each layer is one of the most critical tasks in ANN design. The number of neurons in a hidden layer depends on the complexity of the relationship between inputs and outputs. As this relationship becomes more complex, more neurons should be added [35].

The optimum number of hidden neurons was chosen upon minimizing the difference between predicted ANN values and desired outputs, using SOS during testing as performance indicator. Used multi-layer perceptron models (MLPs) were marked according to StatSoft Statistica's notation. MLP was followed by number of inputs, number of neurons in the hidden layer, and the number of outputs. According to ANNs summary, it was noticed that the optimal number of neurons in the hidden layer for responses prediction was 9 (network MLP 3-9-13), when obtaining high values of r^2 (0.914, 0.890 and 0.825 for training, testing and validation period, respectively) and low values of *SOS* (0.059, 0.084 and 0.108 for training, testing and validation period, respectively). The used activation functions were: hyperbolic tangent for hidden layer and logistic, for output layer; used training algorithm was BFGS 149. Performances of the optimal ANN, regarding r^2 between experimental measurements and predicted results are presented on Table 6.

Optimal network, used for prediction of response variables was able to predict reasonably well the output for a broad range of the process variables. The predicted values were very close to the experimental (target) values in most cases, in terms of r^2 value for both SOP and ANN models.

Table 6. Performance of the optimal ANN

Cycle	Particle density	Abr.	Length	Moisture	Ash	Carbon	H	N	S	HHV	LHV	Fixed carbon	Volatile matter
Train.	0.941	0.981	0.980	0.983	0.994	0.951	0.965	0.997	0.960	0.672	0.544	0.967	0.914
Test.	0.934	0.980	0.985	0.981	0.988	0.932	0.981	0.997	0.968	0.504	0.431	0.962	0.883
Valid.	0.953	0.949	0.959	0.973	0.989	0.907	0.977	0.997	0.965	0.247	0.118	0.929	0.828

It can be seen that the r^2 value for ANN model is greater than this associated with the SOP model (except those for *HHV* and *LHV* calculation). Generally, ANN model is more complex (186 weights-biases for calculation) than SOP, and it has performed better fitting of experimental data due to the high *nonlinearity* of the developed system [36,37].

The mean and the standard deviation of residuals has also been analysed. The mean and standard deviation (*SD*) of residuals is presented in Table 7. These results showed a good approximation to a normal distribution around zero with a probability of 95% (2*SD*), which means a good generalization ability of ANN model for the range of observed experimental values (Figure 1).

Sensitivity analysis

In order to or assess the effect of changes in the outputs due to the changes in the inputs, a sensitivity analysis was performed (Figure 2). The greater effect observed in the output implies that greater sensitivity is presented with respect to the input [38]. Sensitivity analysis has been performed to test an infinitesimal change in an input value in 10 equally spaced individual points, ranged by the minimum and maximum of the observed assay, in order to explore the changes in observed outputs. It is also used to test the model sensitivity and measurement errors.

The influence of the input over the output variables, *i.e.*, calculated changes of output variables for infinitesimal changes in input variables, is shown in Figure 3. Obtained values corresponded to level of experimental errors, and also showed the influence of cultivar type, temperature and binder content on response variables.

According to Figure 3, particle density is mostly influenced by cultivar type, showing higher values for Leccino and Pendolino, then for Istarska Bjelica and Buža. Temperature becomes more influential at the

Table 7. Mean and standard deviation of the residuals for the optimal ANN

Deviation	Particle density	Abr.	Length	Moisture	Ash	Carbon	H	N	S	HHV	LHV	Fixed carbon	Volatile matter
Mean	0.001	0.125	−0.081	0.022	−0.002	0.068	−0.002	0.001	0.000	0.015	−0.009	−0.036	0.158
SD	0.009	0.859	0.483	0.400	0.018	0.381	0.078	0.012	0.002	0.125	0.120	0.991	1.238

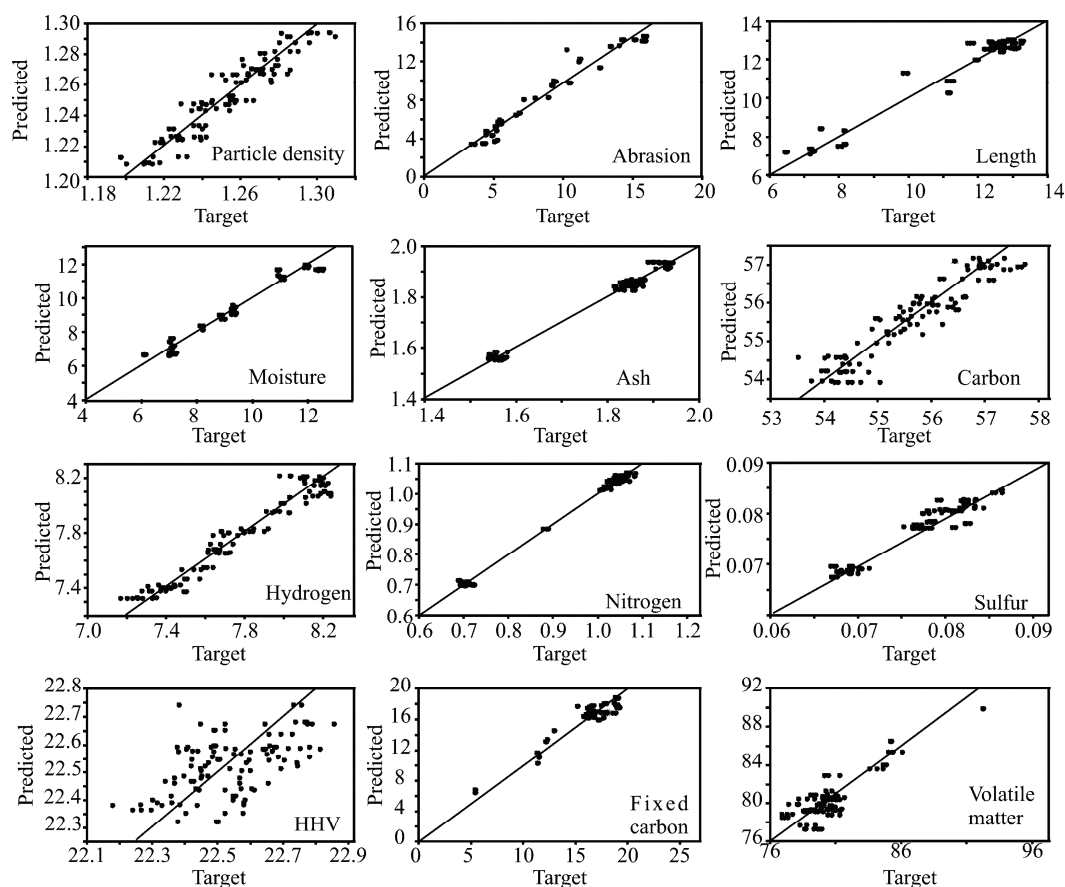*Figure 1. Comparison of experimentally obtained results with ANN predicted values of carbon, hydrogen, nitrogen and sulphur content, particle density, abrasion and length, and also moisture and ash content, higher heating value, fixed carbon and volatile matter content.*
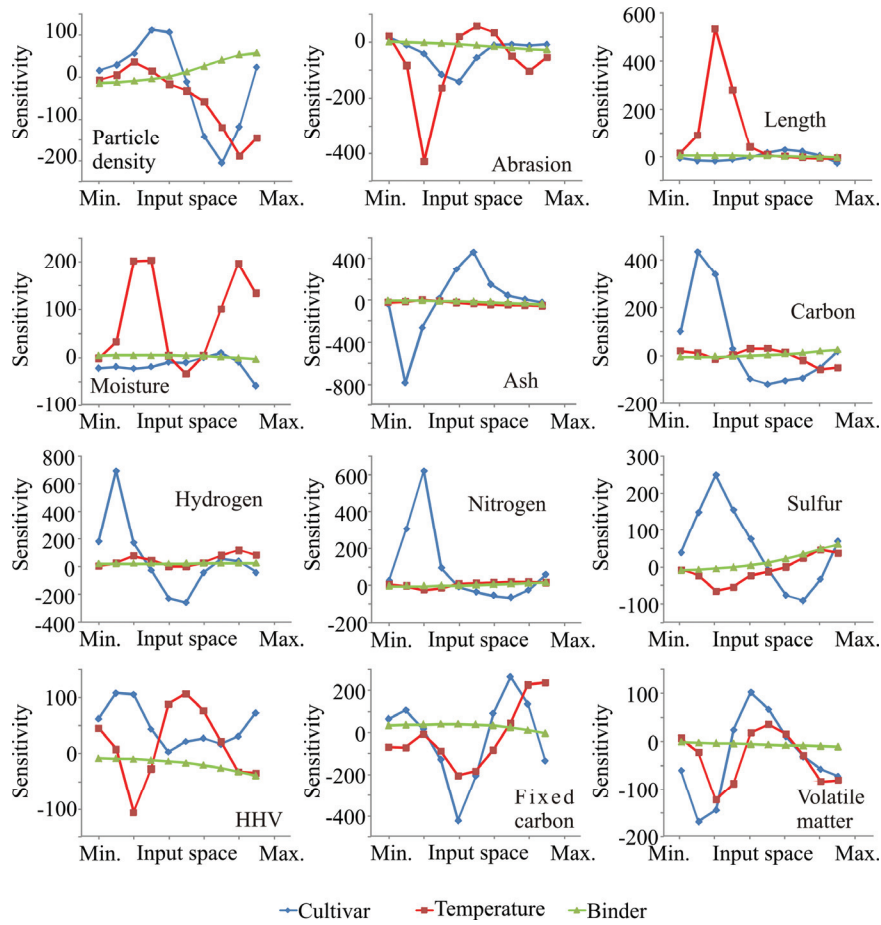
Figure 2. Sensitivity analysis – the influence of the input over the output variables.
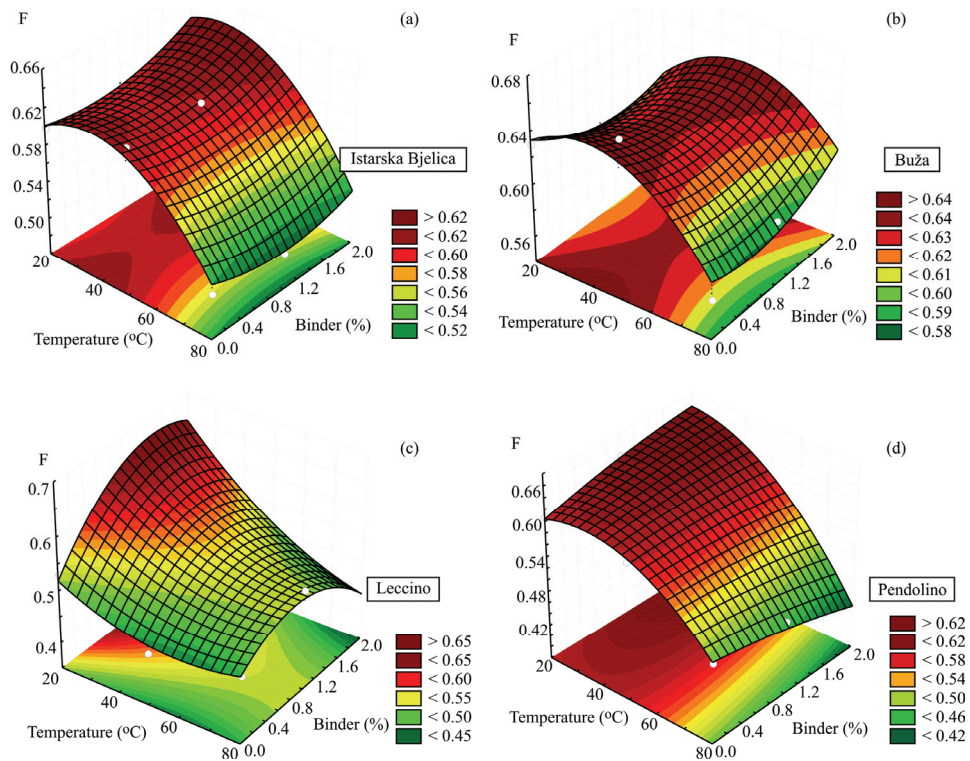

Figure 3. Optimization function (F) for oil cake pellets.

maximum of input space, decreasing the particle density, while binder content slightly increases this parameter at the maximum of input space.

Temperature of the treatment seems to be the most influential variable for abrasion and the length of pellets, especially for temperatures close to minimum of input space (abrasion is decreased, while the length is being increased for small changes in temperature). Istarska Bjelica and 'Buža showed tendency for being more abrasive. The olive cultivar type is the most important for prediction of ash content, as well as C, H, N and S content, as expected. HHV, fixed carbon and volatile matter are also mostly influenced by cultivar type, but the final value of these responses could be increased if conditioned at higher temperatures. All of these findings are in accordance with ANOVA analysis, as well as with experimental measurements.

Normal standard score optimization of the thirteen response variables was accomplished in order to find the processing variables (conditioning temperature and binder content), that give optimal values of response variables. Trapezoidal membership function was used as optimization method, according to Eq. (2), in which [*a*,*b*] covered the complete interval (minimum and maximums), where obtained values for separately tested samples were found during the experiment, and [*m*,*n*] represented the optimal values for observed product group (written in Tables 3 and 4). The "higher the better" or the "lower the better" criteria have been used according to the sign in "Polarity" raw in Tables 3 and 4, while moisture and length parameters have been represented by their optimal values.

The objective function (*F*) is the mathematical function whose maximum would be determined, by summing the FSE results for of the thirteen models, according to Eq. (1). Each response variable (C, H, N and S content, particle density, abrasion and length, and also moisture and ash content, *HHV*, *LHV*, fixed carbon and volatile matter content) has equal weight, when calculating the function *F*.

The maximum of function *F* represents the optimal parameters for processing parameters, and also the optimum for response variables. The three-dimensional graphs for four different olive cultivars, were obtained using objective function to determine optimum production conditions, regarding production parameters (conditioning temperature and binder content), Fig. 1. If the value of membership trapezoidal function is close to 1, it shows the tendency of tested processing parameters of being optimal. Three-dimensional plots were drawn for calculated FSE data visualization (white coloured points) and for the purpose of observation. F functions were plotted using RSM procedure, and the obtained coefficients of determinations in ANOVA analysis, regarding the accuracy of fitting, were: 0.883 (for

Istarska Bjelica), 0.865 (for Buža), 0.956 (for Leccino) and 0.973 (for Pendolino).

FSE analysis showed that the best results were obtained with conditioning treatment at 50 °C and without binder addition for cultivar Buža (maximum *F* = = 0.66), Fig. 1b. Istarska.Bjelica (Fig. 1a), also had satisfactory results, with largest *F* = .64, for lower temperature regime (closer to 40 °C), and increased binder content (approx. 2%). Other two cultivars (Pendolino (Fig. 1d) and Leccino (Fig. 1c)) had somewhat lower results with maximum *F* value of 0.63, with no conditioning and with binder content of 2%.

Generally the analysed agro-pellets had good quality for energy utilization and almost all characteristics were within the limits of EU standards. Although these standards are primary intended to regulate characteristic of pellets made from wood and wood residues, the produced olive cake pellets were almost as good.

CONCLUSION

Investigation concerning the utilization of olive cake cultivars Istarska Bjelica, Buža, Leccino and Pendolino for production of fuel agro-pellets, suggested following conclusions.

The applied response surface methodology of data gave accurate results concerning pellet quality. The obtained models presented good fitting to experimental results and had presented them satisfactory.

Olive cultivar was the variable which had had significant influence on all the measured parameters, especially on the ultimate analyses results. Physical characteristics were also significantly affected by conditioning temperature and binder content. ANOVA calculation of proximate analyses showed complex influence of linear and nonlinear terms and the parameters were influenced by all variables.

The obtained results point out that olive pellets from cultivar Buža, presented the best quality when processed at 50 °C, without addition of binder (optimizing function gained its maximum value of 0.66). However, this analysis also showed that agro-pellets made from unconditioned material, with 2% addition of binder gave very good results (optimizing function gained values ranging from 0.63–0.64), except for Buža cultivar.

Olive cake pellets present a good quality fuel. Most of the produced pellets were in boundaries proscribed by EU standards for fuel pellets. Some of the cultivars had higher levels of nitrogen and all had elevated sulphur, which are limiting factors. These higher levels cause high nitrogen and sulphur oxides emissions during combustion which are environmental pollutants. The resolution of that problem could be in combination of olive cake and for example wood in pellet production, which can lead to decrease of N and S content.

Conditioning treatment at 80 °C caused excessive rise of the moisture of the material, which consequently caused poorer quality of pellets, affecting mostly abrasion. SOP and ANN-based models were developed for prediction of C, H, N and S content, particle density, abrasion and length, and also moisture and ash content, *HHV*, *LHV*, fixed carbon and volatile matter content for a wide range of input variables. Both models are easy to implement and could be effectively used for predictive purposes, modelling and optimization. As compared to RSM, ANN model yielded a better fit of experimental data. Taking into account that a considerable amount and wide variety of data were used in the present work to obtain the ANN model, and considering that the model turned out to yield a sufficiently good representation of the experimental results, it can be expected that it will be useful in practice.

Aknowledgement

REFERENCES

[1] C. Gokcol, B. Dursun, B. Alboyaci, E. Sunan, Importance of biomass energy as alternative toother sources in Turkey, Energ. Policy **37** (2009) 424–431.

[2] M.F. Demirbaş, M. Balat, H. Balat, Potential contribution of biomass to the sustainable energy development, Energy Convers. Manage. **50** (2009) 1746–1760.

[3] Croatian bureau of statistics, Statistički ljetopis Republike Hrvatske (Statistical yearbook), CROSTAT, RH, 2011.

[4] G. DiGiacomo, L. Taglieri, Renewable energy benefits with conversion of woody residues to pellets, Energy **34** (2009) 724–731.

[5] T. Brlek, L. Pezo, N. Voća, T. Krička, Đ. Vukmirović, R. Čolović, M. Bodroža-Solarov, Chemometric approach for assessing the quality of olive cake pellets, Fuel Process. Technol. **16** (2013) 250–256.

[6] A. Dean, D. Voss, Design and Analysis of Experiments, Springer-Verlag, New York, 1999.

[7] S.E. Maxwell, H.D. Delaney, Designing Experiments and Analyzing Data (2nd ed.), Lawrence Erlbaum Associates, Mahwah, NJ, 2004.

[8] T.P. Ryan, Modern Experimental Design, Wiley, Hoboken, NJ, 2007.

[9] K.L. Priddy, P.E. Keller, Artificial Neural Networks: An Introduction, Spie Press Book, Belingham, 2005.

[10] A.I. Khuri, S. Mukhopadhyay, Response surface methodology. WIREs Comp. Stat. **2** (2010) 128–149.

[11] J.S. Almeida, Predictive non-linear modelling of complex data by artificial neural networks,. Curr. Opin. Biotech. **13** (2002) 72–76.

[12] NREL/TP-510-42621, Determination of Total Solids in Biomass and Total dissolved Solids in liquid Process Samples, 2008.

[13] NREL/TP-510-42622, Determination of ash in biomass, 2005.

[14] CEN/TS 15148, Solid Biofuels—Method for the Determination of the Content of Volatile Matter, European Committee for Standardization, 2005.

[15] [CEN/TS 15104, Solid Biofuels—Determination of Total Content of Carbon, Hydrogen and Nitrogen—Instrumental Methods, European Committee for Standardization, 2005.

[16] CEN/TS 15289, Solid Biofuels—Determination of Total Content of Sulphur and Chlorine, European Committee for Standardization, 2006.

[17] CEN/TS 14918, Solid Biofuels—Method for the Determination of Calorific Value, European Committee for Standardization, 2005.

[18] P.S. Madamba, The Response Surface Methodology: An Application to Optimize Dehydration Operations of Selected Agricultural Crops, Lebensm.-Wiss. Technol. **35** (2002) 584–592.

[19] X. Hu, Q. Weng, Estimating impervious surfaces from medium spatial resolution imagery using the self-organizing map and multi-layer perceptron neural networks, Remote Sens. Environ. **113** (2009) 2089–2102.

[20] B.J. Taylor, Methods and procedures for the verification and validation of artificial neural networks, Springer Science+Business Media, New York, 2006.

[21] S.C. Sharma, Applied multivariate techniques, John Wiley & Sons Inc., New York, 1996.

[22] J.H. Zar, Biostatistical analysis, 3rd ed., Prentice Hall Inc, Upper Saddle River, New York, 1996.

[23] T. Miranda, S. Román, J.I. Arranz, S. Rojas , J.F. González, I. Montero, Emissions from thermal degradation of pellets with different contents of olive waste and forest residues, Fuel Process. Technol. **91** (2010) 1459–1463.

[24] European Pellet Council. Handbook for the Certification of Wood Pellets for Heating, Purposes, version 2.0, April 2013, En 14961 – 2.

[25] S.V. Vassilev, D. Baxter, L.K. Andersen, C.G. Vassileva, An overview of the chemical composition of biomass, Fuel **89** (2010) 913–933.

[26] L.S. Johansson, B. Leckner, L. Gustavsson, D. Cooper, C. Tullin, A. Potter, Emission characteristics of modern and old-type residential boilers fired with wood logs and wood pellets. Atmos. Environ. **38** (2004) 4183–4195.

[27] S. Bilgen, K. Kaygusuz. The calculation of the chemical exergies of coal-based fuels by using the higher heating values, Appl. Energ. **85** (2008) 776–785.

[28] A. García-Maraver, V. Popov, M. Zamorano, A review of European standards for pellet quality, Renew. Energ. **36** (2011) 3537–3540.

[29] V.K. Verma, S. Bram, F. Delattin, P. Laha, I. Vandendael, A. Hubin, J. De Ruyck, Agro-pellets for domestic heating boilers: Standard laboratory and real life performance, Appl. Energy **90** (2012) 17–23.

[30] A.T. Atimtay, M. Varol, Investigation of co-combustion of coal and olive cake in a bubbling fluidized bed with secondary air injection, Fuel **88** (2009) 1000–1008.

[31] M. Varol, A.T. Atimtay, Combustion of olive cake and coal in a bubbling fluidized bed with secondary air injection, Fuel **86** (2007) 1430–1438.

[32] N. Kaliyan, R.V. Morey, Factors affecting strength and durability of densified biomass products, Biomass Bioenerg. **33** (2009) 337–359.

[33] R. Samuelsson, S.H. Larsson, M. Thyrel, T.A, Lestander. Moisture content and storage time influence the binding mechanisms in biofuel wood pellets, Appl. Energy **99** (2012) 109–115.

[34] D.C. Montgomery, Design and Analysis of Experiments. 2nd ed., John Wiley and Sons, New York, 1984.

[35] B.L. Ćurčić, L.L. Pezo, V.S. Filipović, M.R. Nićetin, V. Knežević, Osmotic Treatment of Fish in Two Different Solutions-Artificial Neural Network Model, J. Food Process. Pres. (2014), DOI: 10.1111/jfpp.12275.

[36] S. Karlović, T. Bosiljkov, M. Brnčić, D. Jezek, B. Tripalo, F. Dujmić, I. Dzineva and A. Skupnjak, Comparison of artificial neural network and mathematical models for drying of apple slices pretreated with high intensity ultrasound, Bulg. J. Agric. Sci. **19** (2013) 1372–1377.

[37] P.B. Chattopadhyaya, R. Rangarajana, Application of ANN in sketching spatial nonlinearity of unconfined aquifer in agricultural basin, Agr. Water Manage. **133** (2014) 81–91.

[38] L. Pezo, B. Ćurčić, V. Filipovič, M. Nićetin, G. Koprivica, N. Mišljenović, Lj. Lević, Artificial neural network model of pork meat cubes osmotic dehydration, Hem. Ind. **67** (2013) 465–475.

IZVOD

ANALIZA KVALITETA AGRO-PELETA DOBIJENIH OD POGAČE MASLINE – MATEMATIČKI PRISTUP

Tea I. Brlek[1], Lato L. Pezo[2], Neven M. Voća[3], Đuro M. Vukmirović[1], Radmilo R. Čolović[1], Darko E. Kiš[4], Jovana S. Brkljača[1]

[1]*Institut za prehrambene tehnologije u Novom Sadu, Univerzitet u Novom Sadu, Novi Sad, Srbija*
[2]*Institut za opštu i fizičku hemiju, Univerzitet u Beogradu, Beograd, Srbija*
[3]*Faculty of Agriculture, University of Zagreb, Zagreb, Croatia*
[4]*Faculty of Agriculture, University of Osijek, Osijek, Croatia*

(Naučni rad)

U ovom članku su ispitivani uticaja procesnih parametara (temperature kondicioniranja i sadržaj veziva), na kvalitet konačnog proizvoda, agro- peleta, koje se koriste za oslobađanje toplotne energije, dobijene od četiri različite vrste maslina, iskazan preko različitih tehnoloških parametara. Tehnološke, fizičke i hemijske osobine peleta (sadržaj ugljenika, vodonika , azota i sadržaj sumpora, zatim gustina čestica, dužine, habanje, vlage, sadržaja pepela, gornje i donje toplotne moći, sadržaj fiksnog ugljenika i sadržaj lako zapaljivih materija) su određeni da bi se izvršila procena njihovog kvaliteta. U radu je izvršeno poređenje performansi neuronske mreže (engl. Artificial Neural Network – ANN) sa razvijenim matematičkim modelom u obliku polinoma drugog reda (engl. Second Order Polynomial – SOP), kao i sa vrednostima dobijenim eksperimentalnim merenjima, u cilju dobijanja dovoljno tačnog i adekvatnog matematičkog modela za predviđanje parametara kvaliteta agro-peleta. SOP model je pokazao dobru tačnost, iskazanu visokim koeficijentima determinacije (r^2) ,koji su bili između 0,692 i 0,955, dok je ANN model pokazao visok stepen poklapanja sa eksperimentalnim merenjima, sa r^2 vrednostima između 0,544 i 0,994 .

Ključne reči: Pogača masline • Sorte masline • Agro-pelete • Peletiziranje • Matematički model

Encapsulation of *α*-lipoic acid into chitosan and alginate/gelatin hydrogel microparticles and its *in vitro* antioxidant activity

Bojana B. Vidović[1], Nikola Z. Milašinović[2,3], Jelena M. Kotur-Stevuljević[1], Sanda P. Dilber[1], Melina T. Kalagasidis Krušić[4], Brižita I. Đorđević[1], Zorica D. Knežević-Jugović[4]

[1]University of Belgrade, Faculty of Pharmacy, Belgrade, Serbia
[2]Academy of Criminalistic and Police Studies, Belgrade, Serbia
[3]University of Belgrade, Innovation Center of the Faculty of Technology and Metallurgy, Belgrade, Serbia
[4]University of Belgrade, Faculty of Technology and Metallurgy, Belgrade, Serbia

Abstract

Alpha-lipoic acid is an organosulphur compound well-known for its therapeutic potential and antioxidant properties. However, the effective use of *α*-lipoic acid depends on biological plasma half-life and its preserving stability, which could be improved by encapsulation. In this study, *α*-lipoic acid was incorporated into chitosan microparticles obtained by reverse emulsion crosslinking technique, as well as into microparticles of alginate/gelatin crosslinked with zinc ions. Encapsulation of *α*-lipoic acid in both cases was carried out by swelling of synthesized dried microparticles by their dipping in a solution of the active substance under strictly controlled conditions. Encapsulation efficiency of *α*-lipoic acid obtained in this study was up to 53.9%. The structural interaction of *α*-lipoic acid with the carriers was revealed by Fourier transform infrared spectroscopy. *In vitro* released studies showed that controlled release of α-lipoic acid was achieved through its encapsulation into chitosan microparticles. The results of *in vitro* antioxidative activity assays of released *α*-lipoic acid indicated that antioxidant activity was preserved at a satisfactory level. These obtained results suggested that chitosan microparticles could be suitable for modeling the controlled release of *α*-lipoic acid.

Keywords: alpha-lipoic acid, microparticles, chitosan, sodium alginate/gelatin, antioxidant activity.

Available online at the Journal website: http://www.ache.org.rs/HI/

Alpha-lipoic acid (LA), also known as 1,2-dithiolane-3-pentanoic acid ($C_8H_{14}O_2S_2$) is a yellow solid organosulphur compound [1]. Having an asymmetric carbon atom, LA exists as two enantiomers: the R-(+)-LA and S-(−)-LA. Only the R-isomer is endogenously synthesized and is an essential cofactor for mitochondrial enzyme complexes that catalyze reaction responsible for oxidative glucose metabolism and cellular energy production. Synthetic racemic LA, a 50/50 mixture of R-and S-enantiomers, has been extensively used as a therapeutic agent in the treatment of diabetic neuropathy and as an antioxidant supplement in European countries and the United States [2].

Exogenously supplied LA is readily absorbed, transported to tissues and rapidly taken up by cells. Within the cells LA is reduced to dihydrolipoic acid (DHLA), then rapidly removed from cells and metabolized. Several lines of evidence indicated that both LA and its reduced form, DHLA, exerted potent antioxidant activities, both *in vitro* and *in vivo*. In addition to direct free radicals scavenging and metal chelating properties, LA/DHLA redox couple appears to be able to regenerate other endogenous antioxidants such as vitamins C and E, and glutathione, as well as to modulate the redox signaling pathways [3–5]. There is evidence that administration of LA might have a beneficial role in a variety of oxidative stress conditions such as ischemia--reperfusion injury, type 2 diabetes and associated complications, neurological disorders, ischemia-reperfusion injury [1].

Human pharmacokinetic studies have found that oral administrated LA is characterized by rapid absorption within 1 h, short plasma half-lives, extensive hepatic metabolism and low and varying bioavailability [6]. The short half-live of LA (about 30 min) may inhibit effective use [7]. On the other hand, LA is unstable under light and heat and gradually decomposes at room temperature. Temperatures greater than its melting point (59–62 °C) cause immediate polymerization and render it unusable, as polymerized LA is insoluble in almost all solvents [8]. Furthermore, the decomposition of LA is accompanied by an unpleasant odor due to the sulphur content [9].

In the past several years, a forms of stabilized and controlled released LA were designed with the assumption that the efficacy of LA could be improved by slowing the absorption and keeping blood levels of LA above baseline for longer periods after ingestion [10]. However, the efficacy and safety from sustained-release dosage of *α*-lipoic acid forms have not been clear.

Active substances such as minerals, vitamins, proteins, enzymes, peptides, probiotics, phenolic compounds, etc., are widely used in the food, pharmaceutical and cosmetic industry nowadays [11]. These substances are very sensitive to extreme temperatures, presence of oxygen, microorganisms and moisture that often come in contact with, thereby losing their activity, both during storage and application conditions. Therefore, in the last few decades, a great attention has been put to mode the administration of active substances which should also provide the maintenance of their activities and their optimum (concentration) effect in specific parts of the body.

One of the most common ways to overcome these problems is the encapsulation of these substances into various carriers. Encapsulation can mask the unpleasant taste or smell, but also provides control of the release of the active substance. The main goal of encapsulation is to protect the substance from adverse conditions (light, moisture and oxygen) thereby contributing to the increase of the shelf life and, at the same time, controlling the release and increasing the *in vivo* half-life of encapsulated product [12]. In addition to the choice of the appropriate method of encapsulation, it is also important to choose the appropriate carrier. The ideal matrix for encapsulation must not have the degradation effect to the active substance, and at the same time it should be non-toxic and relatively easy to synthesize. Nowadays, various systems for encapsulation of active substances, most often consisting of carbohydrates, proteins, natural or synthetic polymers (chemically or physically crosslinked) are used among which hydrogels have become very popular as carriers in the various industry fields [13].

The aim of this study was to investigate the possibility of encapsulation of LA into chitosan and alginate/gelatin microparticles and to investigate its release as this has not been studied extensively [10,14,15], as well as to investigate the antioxidant activity of released LA compared to the activity of free LA and its active metabolite DHLA. First part of the study was the attempt to encapsulate LA into chitosan microparticles obtained by reverse emulsion crosslinking technique, as well as into microparticles of alginate/gelatin (of various gelatin content) crosslinked using zinc ions. The synthesized microparticles were characterized by FT-IR and SEM analyses. Further on, the release of LA in pH simulated GI tract conditions

were monitored followed by the experiment regarding *in vitro* antioxidant capacity of released LA expressed as Trolox equivalent antioxidant capacity (*TEAC*) and ferric reducing/antioxidant power (*FRAP*). The samples of plasma from healthy subjects were used for *in vitro* determination of antioxidant activities of released LA from selected investigated samples.

MATERIALS AND METHODS

Materials

Chitosan (Ch), sodium alginate (A) and gelatin (G) used for microparticles preparation were obtained from Sigma, Japan, while itaconic acid (2-methylidene-butanedioic acid) was purchased from Sigma–Aldrich, Germany. Glutaraldehyde (GA, pentane-1,5-dial), paraffin oil (light liquid paraffin) and zinc chloride were obtained from Centrohem, Serbia. Tween 80 (polyoxyethylene (20) sorbitan monooleate) used as an emulsifier was obtained from Riedel-de Haën, Germany. *α*-Lipoic acid (LA) (purity > 98%) was obtained from "Ivančić i sinovi" Belgrade, Serbia. Distilled water was used for the preparation of buffer solutions of pH 2.20±0.01 (KCl/HCl, Merck) and pH 6.80±0.01 (Na$_2$HPO$_4$/ /NaH$_2$PO$_4$, Lach-Ner). Folin–Ciocalteu reagent, ABTS (2,2'-azinobis (3-ethylbenzothiazoline-6-sulfonic acid diammonium salt), potassium persulphate, TPTZ (2,4,6--Tris(2-pyridyl)-*s*-triazine), chloramine T trihydrate and peroxidase type I from horseradish were purchased from Sigma-Aldrich, Germany. Malonaldehyde bis(dimethyl acetal), Trolox ((±)-6-hydroxy-2,5,7,8-tetramethylchromane-2-carboxylic acid) and TMB powder (3,3',5,5'-tetramethylbenzidine) were purchased from Acros Organics. 2-Thiobarbituric acid, trichloracetic acid, dimethylsulfoxide (DMSO) and hydrogen peroxide were purchased from Merck, Germany. All other chemicals and reagents used were of analytical reagents grade quality and obtained from standard commercial suppliers. Dihydrolipoic acid (DHLA) was prepared by treating LA with NaBH$_4$ using a method described in a previous report [16]. Purity was confirmed by NMR, comparing with literature data.

Preparation of chitosan and alginate/gelatin microparticles

Chitosan microparticles, with 1.5% (*w/V*) of chitosan content crosslinked with glutaraldehyde of various contents (0.1–0.4 vol.%) were prepared as previously described [17]. The ratio of oil-to-water phases in all emulsion preparations was 1:5 with the addition of 2.0 vol.% Tween 80 (1 cm^3) as an emulsifier. Hydrogels of Na-alginate and gelatin (various ratios) in the form of microparticles were synthesized, as well, using Zn^{2+} as the crosslinking agent, while keeping the concentration of crosslinking agent constant. Namely, Na-alginate was

added to 14 cm^3 of distilled water and allowed to dissolve using magnetic stirring at 500 rpm at 50 °C. After on, gelatin was added to the solution to reach the total mass of the reactants of 0.8000 g. Then the stirring speed was reduced to 100 rpm in order to remove air bubbles. For the synthesis of microparticles Syringe pump (New Era Pump Systems Inc., model NE-1000) was used. The mixture of 10 cm^3 was added drop wised at the rate of 75 µL/min to 100 cm^3 0.1 M ZnCl$_2$ solution. During the instillation immediate formation of hydrogel microparticles was evident. Hydrogel microparticles were left for 24 h in a solution of zinc chloride in order to achieve complete crosslinking. After that, a solution of zinc chloride has been removed, and the hydrogel particles were washed with water three times and maintained in 100 cm^3 of water for 24 h in order to remove unreacted substances. Then the synthesized microparticles were immersed in acetone for 30 min, knowing that acetone would ease the drying process not allowing the coalescence of microparticles. The particles were then removed from acetone solution and allowed to dry to constant weight. The compositions of all investigated samples are given in Table 1.

Table 1. The composition of the synthesized hydrogel microparticles

Sample	Content, wt.%			Crosslinking agent concentration, mol/dm^3
	Ch	A	G	
S1	2.0	–	–	0.08
S2	0.5			0.02
S3	1.0			0.04
S4	–	100	–	0.10
S5		66.7	33.3	
S6		50.0	50.0	
S7		33.3	66.7	

Fourier transform infrared spectroscopy

A Bomem MB 100 FT-IR spectrophotometer was used to record infrared spectra of the microparticles, applying the KBr disc method. Sample/KBr (ratio 1/50) was mixed and grounded and then compressed into a pellet under an 11 tones weight, for one minute, using Grase by Specac, model 15.011. FT-IR spectra were obtained in the wavenumber range 4000–400 cm^{-1}, at 25 °C and at 4 cm^{-1} spectral resolution.

Swelling degree studies

In order to simulate the gastrointestinal (GI) tract temperature and pH conditions as well as the average time spent in GI tract, the swelling studies were carried out at 37 °C, by immersing the microparticles for 2 h in a buffer solution of pH value of 2.20±0.01 and subsequently in a buffer solution of pH 6.80±0.01 for the next 22 h. After immersion, microparticles' weight was

measured in pre-determined time intervals. The degree of swelling was calculated according to the following equation:

$$q = w_t/w_0 \tag{1}$$

where w_t corresponds to the weight of swollen microparticles at time t and w_0 to the weight of dried microparticles. The swelling process was monitored gravimetrically.

Scanning electron microscopy

The surface morphology of microparticles was evaluated using scanning electron microscopy (Tescan Mira3 XMU, Cranberry Twp, PA, USA). Prior to SEM analysis samples were coated with gold/platinum alloy (15/85) under vacuum conditions, using Polaron SC502 vacuum sputter coater. Samples were analyzed in two different forms: dry microparticles and rehydrated microparticles.

Determination of encapsulation efficiency of *α*-lipoic acid

Alpha-lipoic acid was encapsulated by immersing ready-made hydrogels into solution of *α*-lipoic acid that consists of 1 g of active substance dissolved into 75 cm^3 mixture of ethanol and 2 vol.% acetic acid solution (ratio 1:2). The pH of the obtained solution was 2.70 offering the good environment for LA encapsulation. The LA encapsulation efficiency was determined spectrophotometrically. Encapsulation efficiency was calculated as the ratio of the actual loading, (Total LA content)$_e$, of the hydrogel particles with *α*-lipoic acid and the theoretical loading, (Total LA content)$_i$, using the following equation:

$$EE(\%) = (\text{Total LA content})_e/(\text{Total LA content})_i \tag{2}$$

(Total LA content)$_e$ was calculated as the difference between the total amount of LA in the initial solution used for encapsulation and the free amount of LA left in the solution after encapsulation process).

Calibration curve of LA

A calibration curve is required for the determination of encapsulation efficiency and release rates of the microparticles. A known concentration of LA in buffers of pH values of 2.20 and 6.80 were scanned in the range of 200–500 nm by using UV/Vis spectrophotometer. Prominent peaks at 329 and 332 nm were noticed. The concentration of LA was obtained from the calibration curve prepared by measuring the absorbance (329 and 332 nm) of different concentrations of LA.

***In vitro* antioxidant activity of the released LA**

The anti-oxidant capacity of released LA following *in vitro* digestion was examined by FRAP and ABTS assays.

The ferric reducing/antioxidant power (FRAP) assay was carried out according to the method described by Benzie and Strain [18]. The working FRAP reagent was prepared by mixing 300 mmol/L acetic buffer (pH 3.60), 10 mmol/L TPTZ in 40 mmol/L HCl and 20 mmol/L $FeCl_3 \cdot 6H_2O$ in a ratio of 10:1:1. Then 200 µl of sample from release test medium was added to 3.80 cm^3 of FRAP reagent. After 4 min of reaction, the absorbance at 593 nm was read. The FRAP values were expressed, taking into account a standard curve of $FeSO_4 \cdot 7H_2O$ and the results are expressed as µmol $Fe(II)/g_{particles}$. All measurements were performed in triplicate.

Determination of antioxidant activity using the ABTS method was performed according to the method described by Re *et al.* [19]. The free radical-cation $ABTS^{\bullet+}$ was generated by the oxidation reaction of the ABTS with potassium persulphate in the dark condition for 12–16 h at room temperature. After 24 h, the absorbance was adjusted with PBS pH 7.4 up to 0.70 units, at 732 nm. For the evaluation, 20 µL of the sample was added to 1880 µL of the $ABTS^{\bullet+}$ and the absorbance readings were taken after exactly 6 min. The results were expressed as *TEAC* (trolox equivalent antioxidant capacity) by the construction of a standard curve, using several concentrations of the Trolox antioxidant. All measurements were performed in triplicate.

Evaluation of antioxidant activity of LA in human plasma

After night-time fasting, blood samples from healthy, non-smoking volunteers were collected into EDTA-containing sample tubes according to the ethical review board approved protocols. The plasma was pooled and used for all subsequent analysis. Tested solutions of native LA, its active metabolite (DHLA) and released LA from chitosan microparticles were added to the samples of plasma (0.7 cm^3) and incubated for 1 at 24 h at 37 °C. The control plasma samples (without tested solutions) were prepared. To evaluate the antioxidant activity of the test solutions against copper induced oxidative stress, plasma samples were also incubated with copper sulphate (2 mmol/L) plus tested compounds and released LA added in combination. Incubation of plasma samples was stopped by cooling the samples in an ice-bath.

The levels of lipid peroxidation products in plasma were assayed in plasma according to Girroti *et al*. [20]. This assay is based on the formation of a complex between thiobarbituric acid and malondialdehyde, an end product of lipid peroxidation, which absorbs at 535 nm. Total anti-oxidant capacity (*TAC*) was measured in plasma according to Erel's method [21]. This assay is based on the bleaching of the characteristic color of a stable 2,2'-azinobis-(3-ethylbenzothiazoline-6-sulfonic acid) radical cation ($ABTS^{\bullet+}$) by antioxidants present in plasma. The TAC value of the samples tested is exp-

ressed as µmol Trolox equivalent/L. Prooxidant–antioxidant balance (*PAB*) was measured according to the previously published method [22], slightly modified in our laboratory. The assay is based on 3,3',5,5'-tetramethylbenzidine and its cation, used as a redox indicator participating in two simultaneous reactions. The standard solutions were prepared by mixing varying proportions of (0–100%) of 250 µmol/L hydrogen peroxide with 10 mmol/L uric acid. *PAB* is expressed in arbitrary HK units, which represent the percentage of hydrogen peroxide in the standard solution.

Statistical analysis

All the values were expressed as mean ± *SD*. The data were analyzed with the one-way repeated measures analysis of variances using SPSS version 18 (Chicago, IL, USA).

RESULTS AND DISCUSSION

FT-IR analyses

FT-IR spectra of pure chitosan microparticles were discussed in our earlier paper [17]. FT-IR spectra of the samples S4–S7 and pure gelatin are shown in Figure 1.

From Figure 1 in the spectrum of gelatin the following characteristic bands occur: 3425 cm^{-1} (NH stretching vibrations), 1641 cm^{-1} (amide I band which comes mainly from the C=O stretching vibration) and 1562 cm^{-1} (amide II band that comes from NH deformation vibration in the plane coupled with CN stretching vibration). Amide III band at 1300 cm^{-1} comes from the CN stretching vibration coupled with NH deformation vibration) [23,24]. In the FT-IR spectrum of the sample S4 the most important are the following bands: 3436 cm^{-1} (OH stretching vibration), 1625 cm^{-1} (COO asymmetrical stretching vibration) and 1420 cm^{-1} (COO symmetrical stretching vibration) [24]. In the spectrum of the hydrogels containing gelatin, the absorption bands corresponding to the OH stretching vibration of alginate (about 3430 cm^{-1}) is shifted towards lower wave numbers as the content of gelatin within the samples increases. This is due to the formation of hydrogen bonding between gelatin and alginate. Also, COO asymmetric stretching vibration of alginate at 1625 cm^{-1} is coupled with the C=O stretching vibration of gelatin, which caused displacement of the band corresponding to this vibration to higher wavenumbers as the gelatin content increases. At the same time, there was a shift of the absorption bands corresponding to the COO symmetric vibrations towards lower wave numbers. All the above mentioned shows the existence of intermolecular interactions between alginate and gelatin, caused by the formation of hydrogen bonding between the $-COO^-$, $-OH$, $-C=O$ and $-NH_2$ groups of the alginate, and gelatin [23].
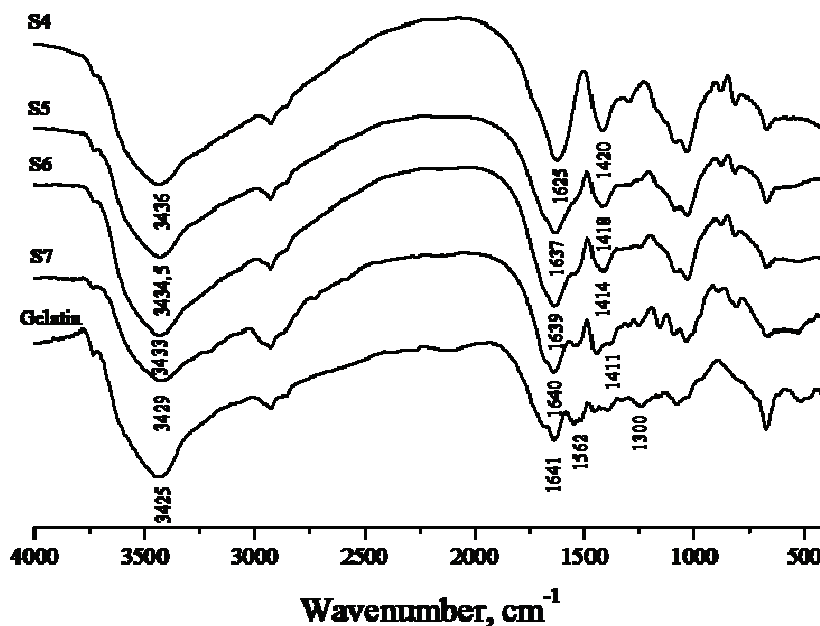
Figure 1. FT-IR spectra of alginate/gelatin samples (S4–S7) and pure gelatin.

FT-IR spectra of selected microparticles after encapsulation of α-lipoic acid were given in Figure 2.

The spectra of encapsulated LA were analyzed in two major regions; 3600–2800 cm^{-1} and 1800–445 cm^{-1}. The characteristic high-intensity bands for –CH$_2$ stretching of LA are evident around 2933 cm^{-1}). Other characteristic bands of LA at 1717 cm^{-1} (C=O stretching), already reported in the literature [25] were assumed to be shifted upon LA encapsulation within alginate/gelatin and chitosan carriers. Namely, (C=O) has been shifted from 1717 to 1720 or 1713 cm^{-1}, respectively. The shift to lower wavenumbers can be attributed to the interruption of strong hydrogen bonding in LA upon encapsulation with alginate/gelatin carrier, showing relatively weak affinity for this matrice. However, shifting to somewhat higher wavenumbers after encapsulation of LA into chitosan matrices suggests that there is interaction between LA and chitosan carrier implying
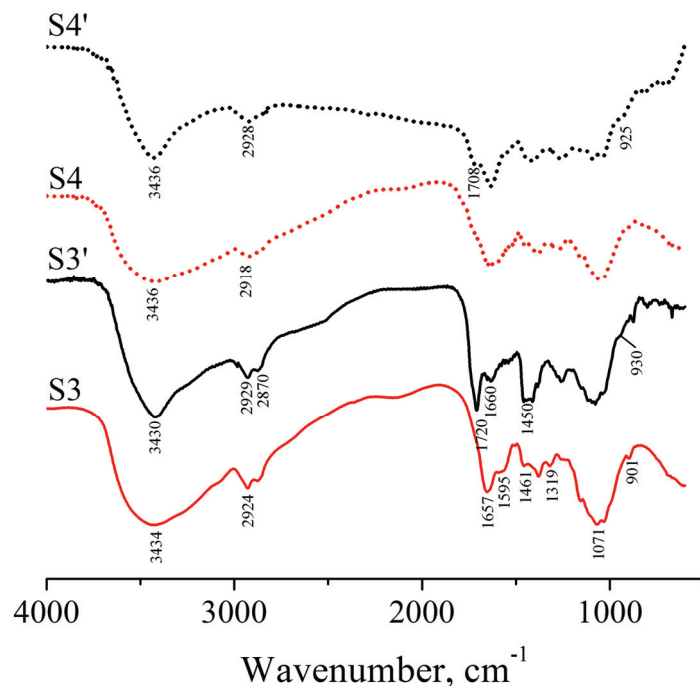

Figure 2. FT-IR spectra of chitosan microparticles without (S3) and with (S3') encapsulated α-lipoic acid; alginate/gelatin microparticles without (S4) and with (S4') encapsulated α-lipoic acid.

that carbonyl property of LA bounded to the chitosan support gets stronger than that of free LA. The bands at 930 and 925 cm^{-1} belong to O–H vibrations of LA. A small shoulder peak at 1660 cm^{-1} appears in the spectrum of the LA encapsulated chitosan sample due to the overlapping of the carboxylic acid group in LA with the amide group in chitosan [14].

The swelling kinetics

Figure 3 shows dynamic swelling behavior of all samples in simulated gastric fluid of pH 2.20±0.01 for 2 h and in intestinal fluid of pH 6.8±0.01 up to 24 h. In an acidic environment, the swelling rate increased since the chitosan amino groups were protonated (NH$_3^+$) and the positive charges induce repulsive forces between polymer chains [26]. As expected, the swelling rate was lower as the concentration of glutaraldehyde in chitosan microparticles was higher (less free amino groups available for protonation offer lower swellability of chitosan microparticles) in acidic medium. After being transferred to the medium of pH 6.80±0.01 chitosan microparticles shrunk, due to the hydrogen bonds tendency to associate by changing –NH$_3^+$ into –NH$_2$ groups, and after on the swelling of microparticles remained constant. This implies that swollen chitosan microparticles remained stable and can be used for delivery of low molecular weight molecules such as LA.
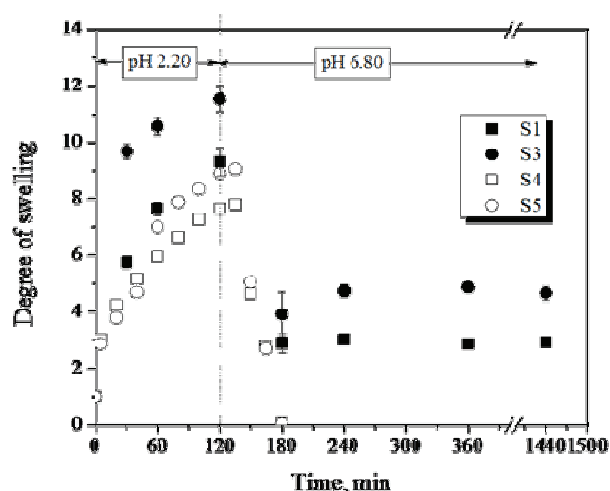

Figure 3. The swelling kinetics of chitosan microparticles (S1 and S3) and the effect of gelatin on the degree of swelling of alginate/gelatin microparticles (S4 and S5) in pH 2.20±0.01 and 6.8±0.01 at 37 ℃.

Alginate is a natural polymer having carboxyl groups with pK_a values of 3.38–3.65. This means that the carboxyl groups of the alginate are ionized at pH values higher than the pK_a value, while at the pH below this value they appear in their non-ionized form. On the other hand, gelatin represents an amphiphilic component that is ionized at all pH values, except at its isoelectric point (4.8–5.5). Based on this, one would exp-

ect that the synthesized hydrogels showed significant swelling at higher pH values.

At pH 2.20±0.01 carboxyl groups of the alginate are in non-ionized form so that there is no electrostatic repulsion between the functional groups, and the degree of swelling of all the samples is minute. It can be observed that the smallest equilibrium degree of swelling has sample S4, while with increasing the gelatin content in the sample increases and the equilibrium degree of swelling. This can be explained by the fact that at this pH gelatin is below its isoelectric point and positively charged when it comes to the electrostatic repulsion between molecules of gelatin which causes an increase in hydrophilicity of the network and increases the volume of the hydrogel. Also, with the increase of gelatin concentration the possibility of aggregation within the hydrogel reduces since part of the functional groups of alginate are already used for the formation of hydrogen bonds with gelatin, which enhances the swelling of hydrogels.

At pH 6.80±0.01, which is higher than the pK_a value of an alginate, carboxyl groups exist in their ionized form (–COO$^-$). When the sample of pure alginate, S4 is placed in a phosphate buffer of pH 6.80±0.01, it comes to the exchange of Na$^+$ present in the buffer solution with the Zn^{2+} bonded to the –COO$^-$ group in polymannuronic segments. The electrostatic repulsion between –COO$^-$ groups appears thereby increasing the hydrophilicity of the polymer chain and the swelling of the hydrogel. In the further process of swelling, there is an exchange of the Na$^+$ with Zn^{2+} bound to –COO$^-$ groups in polyguluronic segments. As these Zn^{2+} are responsible for crosslinking of Na-alginate and hydrogel formation, the established ionic interactions are broken, the physical crosslinking disappears and the sample transforms from the gel into solution.

In other samples it was found that there is no complete "dissolution" after 24 h. It can be seen that there has been a loss of mass in samples S5 (and S6, data not shown), indicating that some ionic interactions have been terminated to some extent due to exchange of sodium and zinc ions. Also, when increasing the content of gelatin the weight loss of the investigated microparticles is slower, increasing the stability of the gels. It is assumed that gelatin hinders the zinc ion exchange with Na$^+$, and microparticles dissolution. With the increase of gelatin content in the samples a slight increase in the equilibrium degree of swelling is achieved. This pH values, besides the ionization of the carboxyl groups of the alginate, allows negative charging of gelatin molecules, leading to additional electrostatic repulsion and microparticles volume increase.

SEM analysis

SEM analysis was performed in order to collect information about morphology of chitosan and algi-

nate/gelatin microparticles. The surface morphology is an important characteristic when particles come in contact with fluid, solid or gaseous environment and together with its internal structure, will influence its suitability for a targeted use [17].

Micrographs (Figure 4) reveal the surface of microparticles of the investigated oven-dried chitosan microparticles (Figure 4a), while Figure 4b shows the alginate/gelatin sample without encapsulated α-lipoic acid swollen to equilibrium in ethanol/acetic acid mixture at 25 °C. In order to investigate the inner structure of S4 (Figure 4c), microparticles were freeze-dried, immersed in liquid nitrogen and cut.

SEM analysis confirmed that the test particles have a porous surface and structure. As known that the appearance of the particles depends on the temperature of the medium in which the particles swell, the increase in temperature leads to a partial termination of the physical connection to the gelatin molecule due to the uncoiling of the triple helix, which reduces cross-linking gelation.

Antioxidant capacity

The encapsulation efficiency of α-lipoic acid into ready-made hydrogel microparticles was in the range between 11.6 (S2) and 53.9% (S3). Modeling of controlled release of active substances at different sites in the gastrointestinal (GI) tract is preferred approach for preventing its degradation, as well as to obtain the desired serum levels over the extended period of time [27]. Moreover, antioxidant capacity will depend on the release of LA *via* swelling and/or degradation of chitosan microparticles. In order to explore whether the encapsulation influences the antioxidant capacity of LA, ferric reducing/antioxidant power (*FRAP*) assay and ABTS radical cation discoloration assay were performed. *In vitro* release of LA and its antioxidant capacity was evaluated in simulated gastric fluid (pH 2.20) and simulated intestinal fluid (pH 6.80), separately. The amount of released LA was determined spectrophotometrically at 329 nm (pH 2.20) and 332 nm (pH 6.80). The obtained results are presented in Figure 5.

The results show sustained release of LA from chitosan microparticles (sample S3). The amount of LA rel-
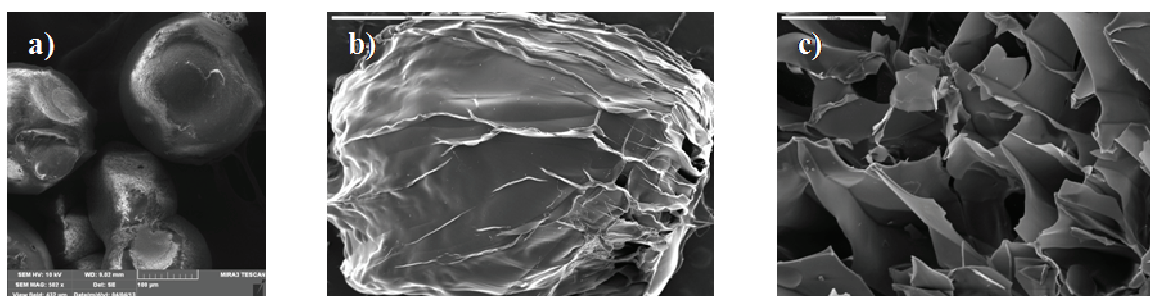
Figure 4. SEM micrographs of microparticles without encapsulated α-lipoic acid of: a) oven-dried chitosan microparticles (S3), b) whole alginate/gelatin microparticles (S4) upon reaching equilibrium degree of swelling in ethanol/acetic acid mixture at 25 °C and c) cross-section of the alginate/gelatin (S4) microparticles.
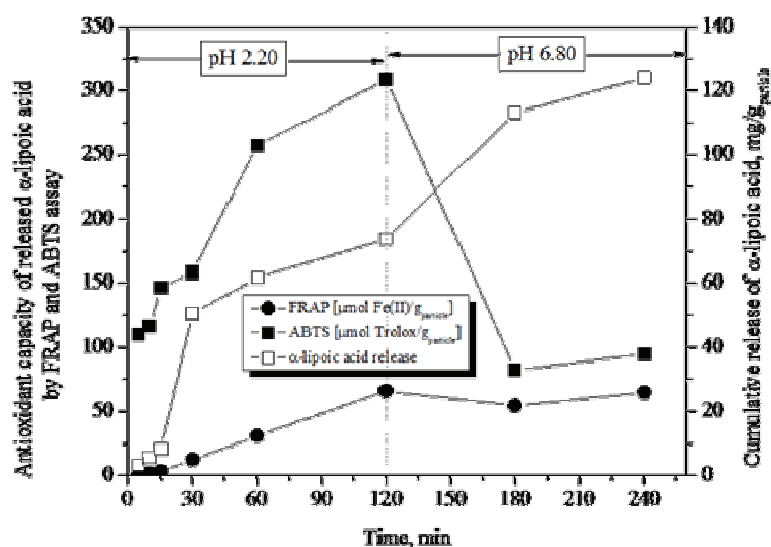
Figure 5. Antioxidant capacity of released α-lipoic acid by FRAP and ABTS assays and cumulative release of LA in simulated conditions of gastrointestinal tract (n = 3).

eased from the carrier was about 11.5 and 13.7% after 60 and 120 min, respectively. Changing the dissolution medium from pH 2.2 to pH 6.8 did not result in disintegration of the LA chitosan microparticles in contrast to alginate/gelatin hydrogel microparticles (release data not shown), and controlled release of LA was achieved. After 240 min, approximately 25% of the LA was released after simulated dissolution test at pH 6.80. The rate of release of LA from chitosan microparticles associated with observed changes in the antioxidant capacity measured by FRAP and ABTS assay.

Plasma lipid peroxidation was significantly increased in $CuSO_4$ treated plasma samples. This increment was abolished at least in part with LA and especially with DHLA preparation. This difference between LA and DHLA is more evident after 24 h of incubation. The same pattern of influence was clear from prooxidative–antioxidative balance, a parameter which showed the superiority of DHLA in antioxidative protection. At

the same time, antioxidative plasma capability measured through the TAC level was abrogated upon Cu^{2+} influence and revitalized through the antioxidative LA and DHLA protection, which is the highest in the case of reduced LA formulation (DHLA).

In this study, we assessed the effect of released LA from chitosan microparticles, native LA and its reduced metabolite (DHLA) on the modification of oxidative/ /antioxidative balance induced by $CuSO_4$ *in vitro* by measuring the plasma level of lipid peroxidation, the prooxidant-antioxidant balance levels, as well as the total antioxidant capacity (Figure 6). In agreement with previous reports, we confirmed that incubation with the copper increased the oxidation of plasma phospholipids [28] that resulted in an elevation of levels of lipid peroxidation and depletion of vitamin E and other antioxidants in plasma [29]. The obtained results showed that the increase of lipid peroxidation is significantly lower in plasma supplemented with LAs and
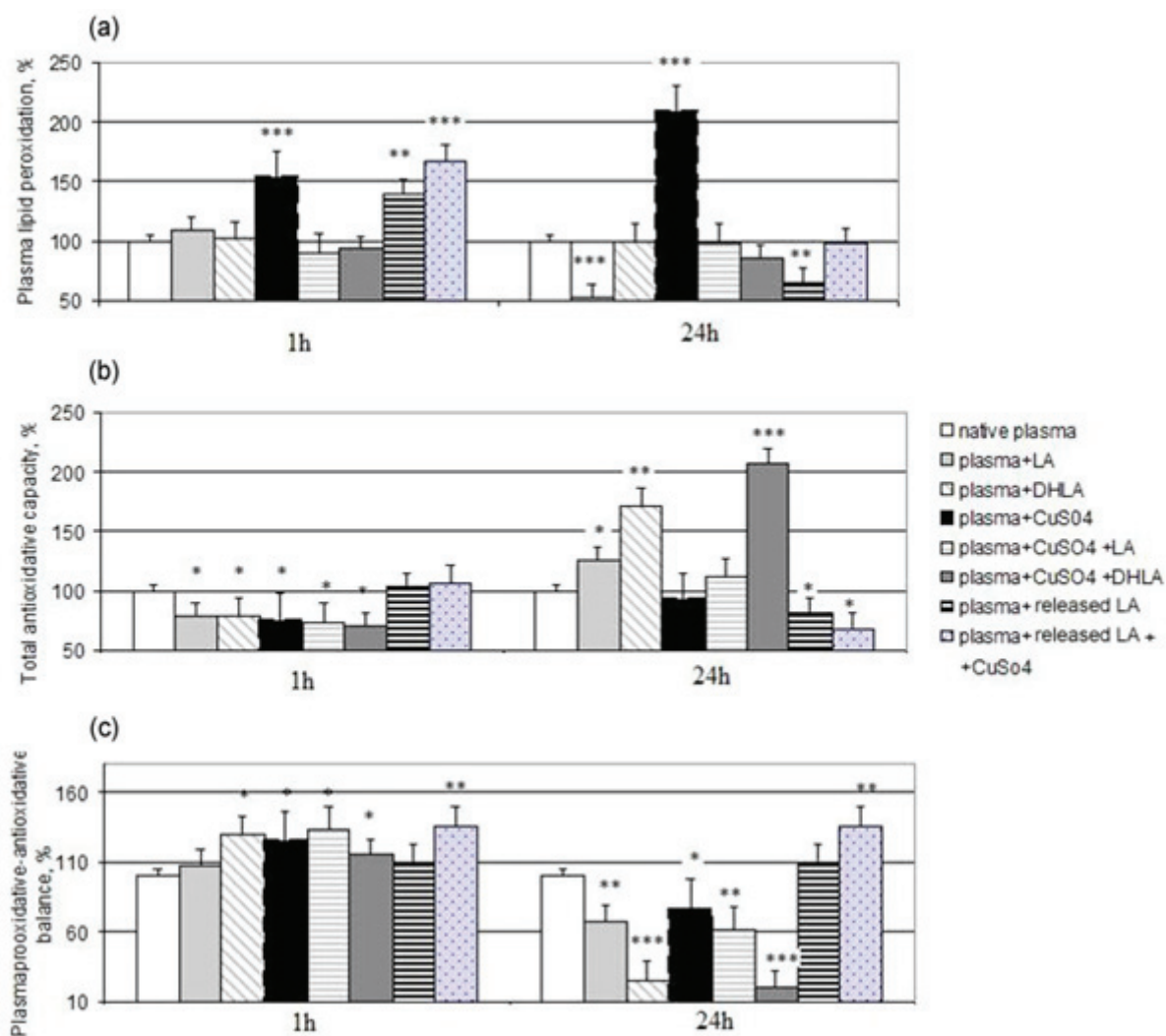

Figure 6. The effect of LA, DHLA and LA released from chitosan microparticles on plasma lipid peroxidation level (a), total antioxidative capacity (TAC) (b) and prooxidative-antioxidative balance (PAB) (c) in human plasma treated with $CuSO_4$ as oxidative reactions catalyst (***p < 0.001, **p < 0.01, *p < 0.05 vs. native plasma according to repeated measures ANOVA test).

DHLA in the presence of cupric ion, indicating antioxidant properties of LA. This effect is more evident after 24 h incubation of plasma samples. The same pattern of influence was noticed from prooxidant-antioxidant balance. At the same time, antioxidative plasma capability measured through the TAC level was abrogated upon Cu^{2+} influence and revitalized through the antioxidative LA and DHLA protection.

CONCLUSIONS

In conclusion, this study showed the alginate/gelatin hydrogel microparticles are unable to release LA in a controlled manner. However, the presented results indicated the potential benefit of using chitosan microparticles for controlled release of LA and sufficient antioxidative protection during the prolonged period of time.

Acknowledgement

REFERENCES

[1] L. Packer, E.H. Witt, H.J. Tritschler, Alpha-lipoic acid as a biological antioxidant, Free Radic. Biol. Med. **19** (1995) 227–250.

[2] K.P. Shay, R.F. Moreau, E.J. Smith, A.R. Smith, T.M. Hagen, Alpha-lipoic acid as a dietary supplement: molecular mechanisms and therapeutic potential, Biochim. Biophys. Acta. **1790** (2009) 1149–1160.

[3] G.P. Biewenga, G.R. Haenen, A. Bast, The pharmacology of the antioxidant lipoic acid, Gen. Pharmacol. **29** (1997) 315–331.

[4] A. Bast, G.R. Haenen, Lipoic acid: a multifunctional antioxidant. BioFactors **17** (2003) 207–213.

[5] A. Bilska, L. Włodek, Lipoic acid - the drug of the future? Pharmacol. Rep. **57** (2005) 570–577.

[6] J. Teichert, R. Preiss, in M.S.Patel, L.Packer (Eds.), Lipoic acid: energy production, antioxidant activity and health effects, Taylor & Francis Group, Boca Raton, FL, 2008, pp. 271–291.

[7] J. Teichert, J. Kern, H.J. Tritschler, H. Ulrich, R. Preiss. Investigations on the pharmacokinetics of alpha-lipoic acid in healthy volunteers, Int. J. Clin. Pharmacol. Therapeut. **36** (1998) 625–628.

[8] A.F. Wagner, E. Walton, G.E. Boxer, M.P. Pruss, F.W. Holly, K. Folkers, Properties and derivatives of *α*-lipoic acid, J. Am. Chem. Soc. **78** (1956) 5079–5081.

[9] K. Kofuji, M. Nakamura, T. Isobe, Y. Murata, S. Kawashima, Stabilization of α-lipoic acid by complex formation with chitosan, Food. Chem. **109** (2008) 167–171.

[10] A. Bernkop-Schnürch, H. Schuhbauer, A.E. Clausen, R. Hanel, Development of a sustained release dosage form for alpha-lipoic acid, I. Design and in vitro evaluation, Drug. Dev. Ind. Pharm. **30** (2004) 27–34.

[11] M.R. Corbo, A. Bevilacqua, L. Petruzzi, F.P. Casanova, M. Sinigaglia, Functional Beverages: The Emerging Side of Functional Foods, Compr. Rev. Food Sci. F. **13** (2014) 1192–1206.

[12] P. Gao, X. Nie, M. Zou, Y. Shi, G. Cheng, Recent advances in materials for extended-release antibiotic delivery system, J. Antibiot. **64** (2011) 625–634

[13] N. Kashyap, N. Kumar, M.N. Kumar, Hydrogels for pharmaceutical and biomedical applications, Crit. Rev. Ther. Drug Carrier Syst. **22** (2005) 107–149.

[14] R. Weerakody, P. Fagan, S.L. Kosaraju, Chitosan microspheres for encapsulation of *α*-lipoic acid, Int. J. Pharm. **357** (2008) 213–218.

[15] K. Kofuji, T. Isobe, Y. Murata, Controlled release of alpha-lipoic acid through incorporation into natural polysaccharide-based gel beads, Food Chem. **115** (2009) 483–487.

[16] H.T. Uyeda, I.L. Medintz, J.K. Jaiswal, S.M. Simon, H. Mattoussi, Synthesis of compact multidentate ligands to prepare stable hydrophilic quantum dot fluorophores, J. Am. Chem. Soc. **127** (2005) 3870–3878.

[17] K.T. Trifković, N.Z. Milašinović, V.B. Djordjević, M.T. Kalagasidis Krušić, Z.D. Knežević-Jugović, V.A. Nedović, B.M. Bugarski, Chitosan microbeads for encapsulation of thyme (*Thymus serpyllum* L.) polyphenols, Carbohydr. Pol. **111** (2014) 901–907.

[18] I.F. Benzie, J.J. Strain, The ferric reducing ability of plasma (FRAP) as a measure of "antioxidant power": the FRAP assay, Anal. Biochem. **239** (1996) 70–76.

[19] R. Re, N. Pellegrini, A. Proteggente, A. Pannala, M. Yang, C. Rice-Evans, Antioxidant activity applying an improved ABTS radical cation decolourization assay, Free. Radic. Biol. Med. **26** (1999) 1231–1237.

[20] M.J. Girotti, N. Khan, B.A. McLellan, Early measurement of systemic lipid peroxidation products in plasma of major blunt trauma patients, J. Trauma. **31** (1991) 32––35.

[21] O. Erel, A novel automated direct measurement method for total antioxidant capacity using a new generation, more stable ABTS radical cation, Clin. Biochem. **37** (2004) 277–285.

[22] D.H. Alamdari, K. Paletas, T. Pegiou, M. Sarigianni, C. Befani, G. Koliakos, A novel assay for the evaluation of the prooxidant-antioxidant balance, before and after antioxidant vitamin administration in type II diabetes patients, Clin. Biochem. **40** (2007) 248–254.

[23] L. Fan, Y. Du, R. Huang, Q. Wang, X. Wang, L. Zhang, Preparation and characterization of alginate/gelatin blend fibers, J. Appl. Polym. Sci. **96** (2005) 1625–1629.

[24] S.M. Milosavljević, Strukturne instrumentalne metode, Hemijski fakultet, Beograd, 1994.

[25] M.A. Moyano, A.M. Broussalis, A.I. Segall, Thermal analysis of lipoic acid and evaluation of the compatibility with excipients. J. Therm. Anal. Calorim. **99** (2010) 631––637.

[26] S.J. Kim, S.R. Shin, Y.M. Lee, S.I. Kim, Swelling Characterizations of Chitosan and Polyacrylonitrile Semi-Interpenetrating Polymer Network Hydrogels, J. Appl. Polym. Sci. **87** (2003) 2011–2015.

[27] F. Becerra-Bracamontes, J.C. Sanchez-Diaz, A. Gonzalez-Alvarez, P. Ortega-Gudiňo, E. Michel-Valdivia, A. Martinez-Ruvalcaba, Design of a drug delivery system based on poly(acrylamide-co-acrylic acid)/chitosan nanostructured hydrogels, J. Appl. Polym. Sci. **106** (2007) 3939––3944.

[28] A.Dasgupta, T. Zdunek, *In vitro* lipid peroxidation of human serum catalyzed by cupric ion: antioxidant rather than prooxidant role of ascorbate, Life Sci. **50** (1992) 875–882.

[29] D. Steinberg, J.L. Witztum, Is the oxidative modification hypothesis relevant to humanatherosclerosis? Do the antioxidant trials conducted to date refute the hypothesis? Circulation **105** (2002) 2107–2111.

IZVOD

INKAPSULACIJA α-LIPONSKE KISELINE U HITOZANSKE MIKROČESTICE I MIKROČESTICE ALGINATA I ŽELATINA I *IN VITRO* ANTIOKSIDATIVNA AKTIVNOST

Bojana B. Vidović[1], Nikola Z. Milašinović[2,3], Jelena M. Kotur-Stevuljević[1], Sanda P. Dilber[1], Melina T. Kalagasidis Krušić[4], Brižita I. Đorđević[4], Zorica D. Knežević-Jugović[4]

[1]*Univerzitet u Beogradu, Farmaceutski fakultet, Vojvode Stepe 450, Beograd, Srbija*
[2]*Kriminalističko–policijska akademija, Cara Dušana 196, 11080 Beograd, Srbija*
[3]*Univerzitet u Beogradu, Inovacioni centar Tehnološko–metalurškog fakulteta, Karnegijeva 4, Beograd, Srbija*
[4]*Univerzitet u Beogradu, Tehnološko–metalurški fakultet, Karnegijeva 4, Beograd, Srbija*

(Naučni rad)

Alfa-liponska kiselina je organosumporno jedinjenje koje ima poznati terapeutski potencijal i izražena antioksidativna svojstva. Relativno kratko poluvreme eliminacije i hemijska stabilnost α-liponske kiseline prema faktorima iz spoljašnje sredine mogu se modifikovati njenom inkapsulacijom na čvrste nosače. Alfa-liponska kiselina iz egzogenih izvora se brzo apsorbuje, distribuira do tkiva, odnosno ćelija u kojima se redukuje u dihidroliponsku kiselinu, a potom brzo uklanja iz ćelija i eliminiše. Prema rezultatima *in vitro* i *in vivo* istraživanja α-liponska kiselina kao i njen redukovani oblik, dihidrolipoinska kiselina, imaju izražena antioksidantivna svojstva. U ovom radu izvršena je inkapsulacija α-liponske kiseline u hitozanske mikročestice dobijene reverznom emulzionom tehnikom. Takođe, ispitana je i mogućnost inkapsulacije α-liponske kiseline u mikročestice alginata i želatina koje su umrežene jonima dvovalentnog cinka. Inkapsulacija α-liponske kiseline u oba nosača izvršena je metodom bubrenja, odnosno potapanjem sintetisanih suvih čestica nosača u rastvor α-liponske kiseline pod strogo kontrolisanim uslovima. Interakcija α-liponske kiseline sa nosačima potvrđena je primenom infracrvene spektroskopije sa Furijerovim transformacijama. Nakon inkapsulacije α-liponske kiseline u ispitivane nosače *in vitro* studijom otpuštanja u simuliranim uslovima gastrointestinalnog trakta potvrđeno je kontrolisano otpuštanje α-liponske kiseline iz hitozanskih mikročestica. Efikasnost inkapsulacije α-liponske kiseline iznosila je do 53,9%. U *in vitro* eksperimentima pokazan je zadovoljavajući nivo antioksidativne aktivnosti otpuštene α-liponske kiseline iz hitozanskih mikročestica. Ovi rezultati ukazuju da hitozanske mikročestice mogu biti pogodni nosači za kontrolisano otpuštanje α-liponske kiseline.

Ključne reči: Alfa-liponska kiselina • Mikročestice • Hitozan • Natrijum-alginat//želatin • Antioksidativna aktivnost

Uporedni prikaz nutritivne vrednosti hladno presovanih ulja semena tikve (*Cucurbita pepo* L.) različitog porekla

Biljana B. Rabrenović[1], Vesna B. Vujasinović[2], Miroslav M. Novaković[3], Selma Č. Čorbo[4], Zorica N. Basić[5]

[1]*Poljoprivredni fakultet, Univerzitet u Beogradu, Zemun, Srbija*
[2]*Visoka škola za menadžment i poslovne komunikacije, Sremski Karlovci, Srbija*
[3]*Institut za hemiju, tehnologiju i metalurgiju, Univerzitet u Beogradu, Beograd, Srbija*
[4]*Poljoprivredno–prehrambeni fakultet, Univerzitet u Sarajevu, Sarajevo, Bosna i Hercegovina*
[5]*Vojnomedicinska akademija, Beograd, Srbija*

Izvod

U radu je ispitana nutritivna vrednost, na bazi sadržaj najznačajnijih bioaktivnih komponenata, sedam uzoraka hladno presovanog tikvinog ulja različitog porekla. Četiri uzorka ulja su proizvedena hladnim presovanjem semena tri domaće i jedne austrijske sorte uljane tikve, a tri uzorka hladno presovanog ulja su bila dobijena iz semena nepoznatog porekla i uzeta slobodnim izborom na tržištu. Kao pokazatelji nutritivne vrednosti određeni su sastav i sadržaj masnih kiselina, tokoferola i sterola. U sastavu masnih kiselina dominantne su bile oleinska (34,2±0,09–43,9±0,04%) i linolna masna kiselina (30,8±0,09–46,9±0,015%). Ovim istraživanjima je potvrđeno da je u tikvinom ulju dominantan $\beta+\gamma$-tokoferol, čiji se sadržaj kretao od 34,65±0,03 do 44,59±0,69 mg/100 g. Određen je sastav i sadržaj Δ^7 fitosterola, posebno specifičnih za ulje tikve. Detektovano je pet Δ^7 sterola: spinasterol, $\Delta^{7,22,25}$-stigmastatrienol, $\Delta^{7,25}$-stigmastadienol, Δ^7-stigmasterol i Δ^7-avenasterol. Dominantan po sadržaju je bio $\Delta^{7,22}$-stigmastadienol ili spinasterol sa 39,98–50,31% od ukupnog sadržaja sterola.

Ključne reči: hladno presovano tikvino ulje, nutritivna vrednost, masne kiseline, tokoferoli, steroli*.*

Dostupno na Internetu sa adrese časopisa: http://www.ache.org.rs/HI/

Danas se na tržištu u Srbiji mogu naći hladno presovana ulja poreklom iz različitih sirovina od različitih proizvodjača. Potreba za funkcionalnim proizvodima uticala je i na proizvodjače hladno presovanih ulja da svoj asortiman razvijaju u pravcu proizvodnje ulja sa povoljnim nutritivnim sastavom. S obzirom da u Srbiji postoji duga tradicija uzgajanja tikve (*Cucurbita pepo* L.), ona se nametnula kao izvor sirovine – semenki, iz kojih se hladnim presovanjem dobija visoko kvalitetno i nutritivno vredno ulje. Obična tikva, *Cucurbita pepo* L.*,* u filogenetskom sistemu biljaka spada u familiju Cucurbitaceae [1,2]. Za razliku od stočne tikve, uljana tikva se prvenstveno gaji radi semena koje je bogato uljem, a meso ploda je sporedni proizvod. Naziv „uljana bundeva" je pogrešan jer se ne radi o bundevi (*Cucurbita maxima)* već o običnoj tikvi *(Cucurbita pepo)*. Uljana tikva je dobila naziv po semenu koje je bogato uljem. Na osnovu izgleda semena razlikuju se dve forme uljane tikve: uljana tikva sa ljuskom, čije je seme obloženo čvrstom semenjačom (ljuskom) bele ili žućkaste boje i uljana tikva golica koja se prepoznaje po „golom" semenu, bez čvrste semenjače. Golosemena tikva se prvi put pojavila na prostorima današnje Austrije, u Štajerskoj, osamdesetih godina XIX veka, kao prirodna mutacija. I danas se tradicionalno najviše gaji u Austriji i zemljama u okruženju, Sloveniji, Madjarskoj, Nemačkoj i Hrvatskoj. Zbog popularnosti tikvinog semena i posebno ulja u ovom regionu, pojava golosemene forme je odmah prepoznata kao prednost koja je omogućavala lakše i efikasnije izdvajanje ulja. U suštini, ova prirodna mutacija je pretvorila tikvu u uljaricu. Prva sorta uljane tikve golice, „869 Feldkürbis" se pojavila u katalogu semena iz 1915 godine [3]. Prema podacima iz 2006. godine, *Cucurbita pepo* convar. citrullinina var. styriaca*,* se u Austriji uzgajala na 18.151 ha, sa prosečnim prinosom semena od 0,61 t/ha. Ova sorta tikve danas se gaji širom sveta, uključujući i Kanadu [4]. Kod nas se gaji u severnom delu Srbije (Vojvodini) [5], a u poslednje vreme počinje njeno gajenje u Bosni i Hercegovini [6], Ukrajini i Rusiji. U domaćem sortimentu postoji uljana tikva sa ljuskom Olivija, dok uljane tikve golice čine registrovane sorte Olinka, Olea i Olimax, nastale u Institutu za ratarstvo i povrtarstvo u Novom Sadu. Poznate su i inostrane sorte od kojih se posebno ističu austrijske selekcije, pre svega Gleisdorfer Ölkürbis.

Većina semenki tikvi koje se proizvode i prodaju na našem tržištu nemaju u deklaraciji poreklo sirovine, u smislu sorte i osnovnih sortnih karakteristika, što može da bude pokazatelj kvaliteta semena iz koga se pravil-

nom preradom može dobiti nutritivno vredno ulje. Međutim, proizvodjači hladno presovanog ulja se, tokom otkupa i prerade semenki tikve, ne vode činjenicom koju sortu ili hibrid, određenih parametara kvaliteta, će preraditi već uglavnom po kojoj ceni ih mogu otkupiti.

S obzirom na to da se golosemene sorte mogu uz mnogo manje tehnoloških operacija i uz uštedu u energiji preraditi do finalnog proizvoda – hladno presovanog ulja, sasvim je opravdano što proizvodjači teže preradi ove vrste semena, iako sorte sa ljuskom (čvrstom semenjačom), gde ljuska služi kao prirodna zaštita semenki, mogu duže vreme biti skladištene bez gubitka na kvalitetu, što se odražava i na kvalitet dobijenog ulja.

Cilj ovoga rada je bio da se sagleda uticaj određene sorte na nutritivni kvalitet hladno presovanog ulja semena tikvi dobijenih iz sortimenta Instituta za ratarstvo i povrtarstvo u Novom Sadu u poređenju sa uljem sa tržišta koje je dobijeno iz golica nepoznatog porekla. Kao pokazatelji nutritivne vrednosti odredjeni su sastav i sadržaj masnih kiselina, tokoferola, a poseban osvrt je dat na sastav i sadržaj fitosterola, kao specifičnih komponenti tikvinog ulja.

MATERIJAL I METODE

Materijal

U okviru ovog rada ispitano je ukupno 7 uzoraka hladno presovanog ulja semena uljanih tikvi. Četiri uzorka semena, koja su preradjena u hladno presovano ulje, je nabavljeno od Instituta za ratarstvo i povrtarstvo (Novi Sad, Srbija), od toga 3 uzorka su bile domaće slobodnooplodne sorte ili eksperimentalni hibridi, 1 uzorak je bio poreklom iz Austrije (Saatzucht Gleisdorf GmbH, Gleisdorf, Austria), dok su 3 komercijalna uzorka hladno presovanog ulja bila nabavljena slučajnim izborom na tržištu.

Svi uzorci semena uljane tikve golice su bili celog jezgra, bez vidljivih oštećenja i osušeni do ravnotežne skladišne vlage, a uzorak semena sa ljuskom je ručno oljušten, neposredno pre presovanja semena. Seme je

čuvano u zatvorenim plastičnim kesama pri temperaturi od 4 °C, u mraku, do momenta izdvajanja ulja. U tabeli 1 je data karakterizacija uzoraka semena uljane tikve i hladno presovanog ulja sa tržišta.

Izdvajanje ulja

Za izdvajanje ulja iz uzoraka semena tikve primenjen je postupak hladnog presovanja. U ovom radu korišćena je pužna presa kompanije „Kern Kraft" (Nemačka) kapaciteta 40 kg semena na sat, snage 4,0 kW, dimenzija 480 mm×480 mm×620 mm, namenjena za ceđenje semena repice, suncokreta, soje, lana, tikve, konoplje, grožđa, šipurka, susama, kikirikija i drugih sirovina. Izdvojeno ulje je, nakon 24 h sedimentacije, dekantovanjem odvojeno od taloga i do momenta analize čuvano u tamno zelenoj staklenoj ambalaži koja je bila zatvorena metalnim navojnim zatvaračem. Boce su čuvane u frižideru na temperaturi od 4 °C do momenta analize koja je obavljena u naredne dve nedelje.

Metode

Sastav i sadržaj masnih kiselina

Masne kiseline tikvinog ulja prevedene su u metilestre postupkom transmetilacije. Zatim su metil-estri podvrgnuti gasno-hromatografskoj analizi radi identifikacije pojedinačnih masnih kiselina i određivanja njihovog relativnog odnosa. Dobijanje metil-estara masnih kiselina izvedeno je u skladu sa metodom (ISO 5509:2000, Animal and vegetable fats and oils — Preparation of methyl esters of fatty acids). Princip metode je transesterifikacija triacilglicerola metanolnim rastvorom KOH. Heksanski rastvor metil-estara masnih kiselina (test rastvor) korišćen je dalje u gasno-hromatografskoj analizi.

Ispitivanje sastava masnih kiselina vršeno je na gasnom hromatografu Varian, model 1400, sa plameno jonizujućim detektorom (FID). Korišćene su metalne kolone dimenzija 300 cm×0,32 cm pakovane sa LAC-3R-728 (20%; Cambridge Ind. Co., Cambridge, UK) na Chromosorb W/AW (80–100 mesh; Merck, Darmstadt, Germany). Kao gas nosač je služio azot protoka 24 mL/min. Temperatura kolone je bila 175 °C, a tempera-

Tabela 1. Karakterizacija uzoraka tikvinog semena i ulja sa tržišta
Table 1. Characterization of pumpkin seed samples and oils from the market

Naziv-oznaka uzorka	Sorta/hibrid	Vrsta semena	Zemlja porekla
Olinka	Slobodnooplodna sorta	Golica	Srbija
SB	Slobodnooplodna sorta	Golica	Srbija
Gleisdorfer Diamant	F1 hibrid	Golica	Austrija
Olivija	Slobodnooplodna sorta	Seme sa ljuskom	Srbija
Hladno presovano ulje semena tikve sa tržišta			
1 - Tikvino ulje	–	Golica	Srbija
2 - Tikvino ulje	–	Golica	Srbija
3 - Štajersko tikvino ulje	–	Golica	Slovenija

tura injektorskog bloka i FID detektora 200 °C. Analiza je rađena u „splitless mode". Injektirano je u gasni hromatograf po 1 μl referentnog rastvora i test rastvora. Kao referentni rastvor korišćena je komercijalna smeša metilestara masnih kiselina (37 Component FAME Mix, 47885-U, Supelco, razblaženo 10× u n-heksanu). Pri navedenim uslovima određivanja nisu korišćeni korekcioni faktori za preračunavanje, jer je analizom standardnog referentnog rastvora utvrđeno da dobijeni površinski udeli odgovaraju masenim udelima.

Sadržaj i sastav tokoferola

Sadržaj i sastav tokoferola određen je HPLC metodom. Uzorci su pripremani na sledeći način: u odmerenu zapreminu uzorka ulja (0,5 mL) dodavano je 20 mL 95% etanola i 3 mL vodenog rastvora KOH. Ovako pripremljen rastvor zagrevan je 30 min na $t = 60$ °C uz povratni hladnjak i mešanje. Kada je saponifikacija bila završena, rastvor je ohlađen i prenesen u normalni sud od 50 mL, koji je dopunjen 95% etanolom. Alikvot je odmeravan u epruvetu sa šlifovanim zatvaračem i dodavane su jednake zapremine heksana i vode. Sve je promešano na vibracionom mešaču u trajanju od 3 min. Heksanski sloj je zatim odvojen i uz dodatak 0,5 mL KH_2PO_4 promešan još 30 s na vibracionom mešaču. Odmerena zapremina heksanskog rastvora uparavana je do suva u struji azota i nakon toga rekonstituisana u metanolu. Posle filtriranja kroz membranski špric-filter (Cronus Syringe Filter Nylon 25 mm, 0,45 μm, Cronus, UK), 10 μl ovog rastvor injektirano je u HPLC sistem. Razdvajanje je izvedeno na HPLC sistemu Waters M600E, izokratsko eluiranje, uz protok mobilne faze 1,0 mL/min i 95% MeOH koji je korišćen kao mobilna faza, uz Rheodyne 7125 injektor, na analitičkoj koloni Nucleosil 50-5 C18. Spektrofotometrijska detekcija analita je izvedena na fluoroscentnom detektoru RF/535 (Shimadzu, Japan) na talasnim dužinama 295 nm za ekscitaciju i 330 nm za emisiju. U analizi su korišćene standardne supstance tokoferola proizvođača Sigma Co (Supelko, USA), od kojih su pripremani rastvori za ispitivanje limita detekcije i limita kvantifikacije (serija rastvora od 0,01 do 0,5 μg/mL), kao i rastvori za kalibracionu krivu (1,0, 2,5, 5,0, 10,0 i 20,0 μg/mL). Određeni su: limit detekcije i limit kvantifikacije, koji iznose 0,03 μg/mL za β, γ i δ, odnosno 0,05 μg/mL za α tokoferol, specifičnost metode, zbog moguće interferencije, linearnost (odnosa površine pika i koncentracije) za standardne rastvore tokoferola u rasponu od 1,0 μg/mL do 20 μg/mL. Kalibracione krive su dobijene kao rezultat četiri injiciranja za svaki koncentracioni nivo i određeni su koeficijenti korelacije: $r = 0,99937$ za α-tokoferol, $r = 0,9991$ za $\beta+\gamma$-tokoferol, odnosno $r = 0,99924$ za δ-tokoferol, preciznost za koncentraciju od 5,0 μg/mL ($RSD = 1,43$, 2,11, odnosno 0,78%), kao i analitički prinos (recovery) metode (98,4% za α-tokoferol, 97,2% za $\beta+\gamma$-tokoferol, odnosno 97,5% za δ-to-

koferol). Obrada podataka je obavljena pomoću Clarity chromatography station for Windows.

Sadržaj i sastav sterola

Sastav i sadržaj sterola odeđen je metodom koju je opisao Verleyen [7].

Odmeravano je po 4,5 g uzorka ulja i dodavano je 7,5 mL rastvora internog standarda (0,15% rastvor holesterola u metilen-hloridu). Zatim je metilen-hlorid uparavan do suva na rotacionom vakuum uparivaču pri 40 °C. U uparene uzorke dodavano je 20 mL 6 M NaOH i 30 mL etanola (u kome je bilo 5% etra). Saponifikacija je obavljena na vodenom kupatilu pri temperaturi između 85 i 90 °C u trajanju od 90 min. Nakon saponifikacije dodavano je 30 mL destilovane vode i nesaponifikovani deo je ekstrahovan sa 45 mL petroletra uz snažno mućkanje, a potom sa 45 mL dietiletra. Ovi ekstrakti su bili spojeni i potom ispirani dva puta sa po 20 mL 0,5 M KOH i 2–3 puta sa po 20 mL 5% NaCl do neutralne reakcije koja se proverava lakmus papirom. Zatim je ekstrakt osušen dodavanjem Na_2SO_4, filtriran kroz filter hartiju, a potom uparavan na rotacionom vakuum uparivaču pri 40 °C. Dobijenom ekstraktu je dodavana smeša 1,5 mL suvog piridina, 0,2 mL heksametildisilazana i 0,1 mL trimetilsilana. Derivatizovan uzorak je potom bio prebačen u vial i spreman za analizu koja je morala biti obavljena u narednih 6 sati. Svaki uzorak je injektiran po tri puta.

GC i GC/MS analize su urađene na instrumentu Agilent 7890AG C sa 5975C (inertni XL EI/CI) MSD i FID detektorima povezanim dvosmernim razdeljivačem (spliterom) kapilarnom protočnom tehnologijom sa pomoćnim gasom. Kolona korišćena za razdvajanje bila je HP-5MS kapilarna kolona (30 m×0.25 mm×0.25 μm). Početna temperatura GC instrumenta od 60 °C je podizana brzinom od 3 °C/min do 300 °C, a potom održavana 10 min na 300 °C. Kao noseći gas je korišćen helijum sa konstantnim protokom od 1,5 mL/min na 60 °C. Injekciona zapremina bila je 1 μl. Uzorak je analiziran u "splitless mode". Temperatura inleta GC instrumenta bila je 250 °C, a temperatura FID detektora bila je 300 °C. MS podaci su dobijeni u EI modu, sa opsegom m/z vrednosti od 30–550. Temperatura izvora bila je 230 °C, a temperatura kvadrupola 150 °C. Maseni detektor je uključen 3 min po injektovanju. Identifikacija je potvrđena metodom zaključavanja retencionih vremena (RTL) i njihovim poređenjem sa Adams bazom podataka.

Statistička analiza podataka

Eksperimentalne vrednosti su izražene kao srednja vrednost tri pojedinačna određivanja. Za analizu varijanse (ANOVA) korišćen je program Statistica 7.0 (StatSoft, USA). Razlika između srednjih vrednosti, na nivou 5% statističke značajnosti ($p < 0,05$), određivana je korišćenjem Dankan testa.

REZULTATI I DISKUSIJA

Sastav i sadržaj masnih kiselina tikvinog ulja

Masne kiseline molekula triacilglicerola su reaktivni deo molekula masti i određuju njena fizička i hemijska svojstva. U tabeli 2 dat je prikaz sastava masnih kiselina ispitivanih uzoraka tikvinog ulja.

Prema sastavu masnih kiselina ulje semena uljane tikve pripada grupi ulja oleinsko-linolnog tipa. Kao što se vidi iz tabele 2 sadržaj ove dve dominantne masne kiseline se kretao od 34,2±0,09 do 43,9±0,04% za olein-sku masnu kiselinu i 30,8±0,09 do 46,9±0,015% za li-nolnu masnu kiselinu. Značajne po sadržaju su bile i dve zasićene masne kiseline. palmitinska (9,9±0,13– –15,3±0,30%) i stearinska (4,1±0,04–9,3±0,02%). U tra-govima su identifikovane miristinska (C14:0), palmito-oleinska (C16:1), alfa-linolenska (C18:3), arahinska (C20:0) i behenska (C22:0) kiselina. Dobijeni podaci su u saglasnosti sa sa literaturnim podacima [8–13]. Rezul-tati ovih istraživanja ukazuju na to da poreklo semena odnosno ulja je imalo uticaja na sadržaj pojedinih mas-nih kiselina. Kod svih uzoraka ulja dobijenih iz semena poznatog porekla bila je dominantna mononezasićena oleinska masna kiselina. Relativan sadržaj oleinske ma-sne kiseline je bio u negativnoj korelaciji sa relativnim sadržajem linolne masne kiseline ($r = -0,83$), koja je bila dominantna kod svih uzoraka ulja sa tržišta.

S obzirom na to da je sastav masnih kiselina veoma značajan pokazatelj nutritivne vrednosti biljnih ulja, ali i njihove oksidativne stabilnosti, veoma je važan i uku-pan sadržaj zasićenih (SFA), mononezasićenih (MUFA) i polinezasićenih (PUFA) masnih kiselina. Posmatrano sa stanovišta oksidativne stabilnosti ulja poželjan je viši sadržaj SFA, ali sa nutritivnog stanovišta, u cilju pre-vencije kardiovaskularnih obolenja, ulja sa višim sadr-žajem MUFA imaju prednost. Iz tabele 2 može se pri-metiti da je sadržaj MUFA bio značajno viši kod uzoraka ulja poreklom iz semena uljanih tikvi poznatog porekla u odnosu na uzorke sa tržišta.

Odnosu zasićenih i nezasićenih masnih kiselina jesti-vih ulja u savremenoj ishrani se, takođe, poklanja velika pažnja. Zbog visoko aterogenog potencijala zasićenih masnih kiselina [14] preporučuje se da njihov odnos bude ispod 1 [15]. Na osnovu podataka iz tabele 2 se može zaključiti da je odnos zasićenih i nezasićenih mas-nih kiselina svih uzoraka daleko ispod 1, što takođe daje pozitivan doprinos nutritivnoj vrednosti tikvinog ulja.

Sastav i sadržaj tokoferola tikvinog ulja

Tokoferoli su veoma važne neglicericidne kompo-nente biljnih ulja i ukupan sadržaj ovih prirodnih anti-oksidanasa, kao i prisustvo određenih njihovih izomera, zavisi od mnogo činilaca (sortnih karakteristika semena, vrste ulja, klimatskih uslova, postupaka izdvajanja ulja, metode određivanja tokoferola, itd.).

Sastav i sadržaj tokoferola u ispitivanim uljima pri-kazan je u tabeli 3.

Ovim istraživanjem je potvrđeno da je u tikvinom ulju dominantan β+γ-tokoferol. Naime, β-tokoferol je bio prisutan u zanemarljivo maloj količini i bilo ga je vrlo teško razdvojiti od γ-tokoferola, zato je dat ukupan sadržaj ova dva izomera tokoferola. Kao što se vidi iz tabele 3 sadržaj β+γ-tokoferola se kretao od 34,65±0,03 do 44,59±0,69 mg/100 g, odnosno, procentualno je bio

Tabela 2. Sastav i sadržaj (%, sr. vrednost±SD, n = 3) masnih kiselina uzoraka hladno presovanih ulja semena tikve
Table 2. Composition and content (%,sr. vrednost±SD, n = 3) of fatty acids in cold-pressed pumpkin seed oils

Masna kiselina (mas.%)[A]	Ulje semena uljane tikve golice			Ulje semena uljane tikve sa ljuskom	Hladno presovana ulja semena tikve sa tržišta		
	Olinka	SB	Gleisdorfer Diamant	Olivija	1	2	3
C14:0	nd	0,1±0,03	0,2±0,00	nd	nd	nd	0,1±0,00
C16:0	12,9±0,09[a]	11,6±0,06[b]	15,3±0,30[c]	11,9±0,12[d]	10,9±0,10[e]	9,9±0,13[f]	11,5±0,08 [g]
C16:1	nd	nd	0,2±0,13	nd	nd	nd	0,1±0,09
C18:0	6,2±0,05[a]	5,1±0,01[b]	9,3±0,02[c]	6,5±0,10[d]	4,1±0,04[e]	5,0±0,06[f]	5,1±0,04f[g]
C18:1	43,9±0,04[a]	42,9±0,02[b]	43,5±0,03[c]	42,3±0,05[d]	34,2±0,09 [e]	38,9±0,04 [f]	39,9±0,03 [g]
C18:2	36,7±0,06[a]	40,2±0,20[b]	30,8±0,09[c]	39,0±0,12[d]	46,9±0,30[e]	41,7±0,15[f]	43,4±0,08[g]
C18:3	0,1±0,02[a]	0,1±0,01[a]	0,1±0,00[ba]	0,2±0,04[cb]	1,2±0,06[d]	1,1±0,08[e]	0,1±0,00[f]
C20:0	nd	nd	0,2±0,02	0,1±0,00	nd	nd	0,2±0,1
C22:0	nd	nd	0,5±0,05	nd	nd	nd	0,3±0,03
SFA	19,1±0,14	16,8±0,10	25,5±0,59	18,5±0,22	15,0±0,46	14,9±0,58	17,2±0,15
MUFA	43,9±0,78	42,9±0,67	43,7±0,71	42,3±0,70	34,2±0,09	38,9±0,04	40,0±0,98
PUFA	36,8±0,79	40,3±0,88	30,9±0,60	39,2±0,69	48,1±0,04	42,8±0,68	43,5±0,40
$\frac{SFA}{MUFA+PUFA}$	0,24	0,20	0,34	0,22	0,18	0,18	0,21

[A]Različita mala slova po redovima ukazuju na postojanje statistički značajne razlike u sadržaju dominantnih masnih kiselina između uzoraka ulja ($p < 0,05$); nd – nije detektovano; SFA – zasićene masne kiseline; MUFA – mononezasićene masne kiseline; PUFA – polinezasićene masne kiseline

Tabela 3. Sastav i sadržaj (mg/100g, sr. vrednost±SD, n=3) tokoferola u ispitivanim uzorcima hladno presovanog tikvinog ulja
Table 3. Tocopherol composition and content (mg/100g, mean±SD, n=3) in cold-pressed pumpkin seed oil

Oznaka uzorka	α-Tokoferol	$\beta+\gamma$-Tokoferol	δ-Tokoferol	Ukupni tokoferoli
Ulje semena uljane tikve golice				
Olinka	5,39±0,05[a]	44,59±0,69[a]	2,99±0,12[a]	52,97±4,12[a]
SB	4,57±0,05[b]	40,09±0,89[b]	4,26±0,07[b]	48,92± 6,17[b]
Gleisdorfer Diamant	2,98±0,08[c]	34,65±1,90[c]	10,54±0,20[c]	48,17±6,98[c]
Prosečan udeo (% u ukupnom sadržaju)	8,57	79,35	13,31	–
Ulje semena uljane tikve sa ljuskom				
Olivija	4,60±0,11[d]	46,99±0,94[d]	5,55±0,05[d]	57,14± 5,32[d]
Udeo (% u ukupnom sadržaju)	8,05	82,24	9,71	–
Hladno presovana ulja semena tikve sa tržišta				
1	4,24±0,06[e]	42,38±1,11[e]	6,36±0,19[e]	52,98±3,12[e]
2	4,48±0,09[f]	37,29±0,79[f]	7,95±0,11[f]	49,72±14,17[f]
3	3,6±0,08[g]	42,12±1,67[g]	3,08±0,09[g]	48,86±5,83[g]
Prosečan udeo (% u ukupnom sadržaju)	8,17	80,40	11,43	–

[A]Različita mala slova u kolonama ukazuju na postojanje statistički značajnih razlika u sadržaju pojedinih izomera tokoferola u ispitivanim uzorcima ulja ($p < 0,05$)

zastupljen u ukupnom sadržaju tokoferola sa 79,35––82,24%. Najviši sadržaj je zabeležen kod ulja poreklom iz semenki uljanih tikvi iz domaćeg sortimenta, Olinke (44,59±0,69 mg/100 g) i Olivije (46,99±0,94 mg/100 g). Sadržaj α-tokoferola se kretao od 2,98±0,25 do 5,39±0,05 mg/100 g, odnosno, procentualno je bio zastupljen sa 5,48–8,57%. Posebno je interesantan sadržaj δ-tokoferola, izomera koji, pored γ-tokoferola, najviše doprinosi oksidativnoj stabilnosti, pri čemu se po visokom sadržaju izdvojio uzorak ulja poreklom iz semenki austrijskog hibrida, Gleisdorfer Diamant (10,54±0,20 mg/100 g).

Sastav i sadržaj sterola tikvinog ulja

Za većinu biljnih ulja karakteristični su Δ^5 steroli, dok su Δ^7 steroli karakteristični za samo nekoliko biljnih familija, među kojima je i Cucurbitaceae [16]. Upravo prisustvo ove grupe sterola u tikvinom ulju, bez obzira da li se radi o golosemenim sortama ili sortama sa ljuskom, omogućava da se utvrdi da li je skupoceno tikvino ulje falsifikovano nekim jeftinijim uljem, kao što je suncokretovo ili ulje semena repice. Naime, intezivna tamno-zelena boja i karakterističan miris veoma otežavaju potrošačima da detektuju prisustvo druge vrste ulja, čak i kada su zastupljeni u većoj količini [16–19]. Nažalost, analitika detekcije i određivanja Δ^7 sterola je veoma složena, s obzirom na to da ne postoje komercijalni standardi Δ^7 sterola i potrebna je kolona velike polarnosti da bi se dobilo dobro razdvajanje pojedinačnih sterola iz ove grupe. U okviru ovih istraživanja, korišćenjem kapilarne kolone HP-5MS gasnog hromatografa razdvojeno je pet Δ^7 sterola, a identifikacija je obavljena delom preko retencionih vremena iz Adams

baze gasnog hromatografa, delom na osnovu masenih spektara i literaturnih podataka [16,20–24].

Kao što se vidi iz tabele 4 i u ispitivanim uzorcima ulja dominantni su Δ^7 steroli. Profil sterola odnosno hromatogrami svih uzorka su pokazali identičan raspored sterola, a dominantan po sadržaju je bio $\Delta^{7,22}$ stigmastadienol ili spinasterol sa 39,98–50,31% od ukupnog sadržaja sterola. Sledeći po sadržaju je $\Delta^{7,22,25}$-stigmastatrienol, čiji se udeo u ukupnom sadržaju sterola kreće od 20,23 do 30,89%. Zatim sledi Δ^7-stigmasterol, sa 10,47–19,48%, potom $\Delta^{7,25}$-stigmastadienol, čiji je udeo u ukupnom sadržaju 5,70–10,76%. Najmanju površinu pika, a samim tim i najnižu procentualnu zastupljenost, kod gotovo svih uzoraka, imao je Δ^7-avenasterol sa 1,50–13.42%. Izvesna odstupanja postoje kod uzorka broj 2 sa tržišta, kod koga je sadržaj $\Delta^{7,25}$-stigmastadienola bio najniži.

Posebno je važno što je i u uzorcima sa tržišta utvrđeno da su prisutni samo Δ^7-steroli, jer to ukazuje da ispitivana ulja nisu falsifikovana nekim drugim, jeftinijim uljem.

U literaturi ne postoje podaci o sadržaju sterola u hladno presovanom tikvinom ulju, kao ni njihov sastav, tako da se postojeći rezultati mogu uporediti samo sa rezultatima za devičanska tikvina ulja ili eventualno druga hladno presovana ulja.

Sastav sterola devičanskog tikvinog ulja je isti kao kod hladno presovanih ulja, ali je udeo pojedinih sterola u ukupnom sadržaju različit. Nakić i sar. [24] navode da su po sadržaju odnosno procentualnom udelu u ukupnom sadržaju sterola, spinasterol, $\Delta^{7,22,25}$-stigmastatrienol i $\Delta^{7,25}$-stigmastadienol slični i taj udeo se redom kretao 19,88–26,81%; 24,03–26,24%; 21,36––22,68%. Najmanji udeo u ukupnom sadržaju sterola u

Tabela 4. Sastav i sadržaj (% od ukupnog sadržaja sterola) pojedinačnih sterola hladno presovanog ulja semena uljane tikve
Table 4. Composition and content of sterols (wt.% of total sterols, mean±SD, n = 3) in cold-pressed pumpkin seed oils

Oznaka uzorka[A]	Spinasterol	$\Delta^{7,22,25}$- stigmastatrienol	$\Delta^{7,25}$-stigmastadienol	Δ^7-stigmasterol	Δ^7-avenasterol
		Ulje semena uljane tikve golice			
Olinka	42,15±2,14[a]	30,89±1,14[a]	6,40±0,24[a]	17,91±0,68[a]	2,65±0,16[a]
SB	49,73±1,42[b]	28,34±0,99[b]	8,05±0,10[b]	10,47±0,60[b]	3,42±0,20[b]
Gleisdorfer Diamant	42,33±2,05[c,a]	26,93±1,78[c]	7,25±0,25[c]	18,87±0,41[c]	4,61±0,17[cb]
		Ulje semena uljane tikve sa ljuskom			
Olivija	50,31±3,32[d]	24,81±0,49[d]	5,94±0,17[d]	17,42±0,20[d]	1,50±0,11[d]
		Hladno presovana ulja semena tikve sa tržišta			
1	40,15±4,34[e]	26,60±1,21[e]	5,70±0,22[e]	14,23±0,55[e]	7,02±0,56[e]
2	39,98±3,22[f]	23,48±0,89[f]	3,64±0,40[f]	19,48±0,76[f]	13,42±0,78[f]
3	42,03±7,11[g]	27,38±3,28[g]	10,76±0,88[g]	10,88±1,16[g]	8,95±0,99[g]

[A]Različita mala slova po kolonama ukazuju na postojanje statistički značajne razlike u sadržaju pojedinih sterola između uzoraka ulja ($p < 0,05$)

uzorcima koje su ispitivali Nakić i sar. [24] imao je Δ^7-stigmasterol, 1,46–1,99%, za razliku od uzoraka ispitivanih u ovom radu gde je Δ^7-avenasterol bio procentualno najmanje zastupljen.

Szterk i sar. [25] navode ukupan sadržaj sterola od 349 mg/100 g u devičanskom tikvinom ulju, sa dominantnim spinasterolom (53,85%), $\Delta^{7,25}$-stigmastadienol (21,23%) i Δ^7-avenasterolom (20,17%), dok je $\Delta^{7,22,25}$-stigmastatrienol bio zastupljen sa svega 4,78%.

ZAKLJUČAK

Rezultati ovih istraživanja su pokazali da sadržaj pojedinih bioaktivnih komponenti statistički značajno varira u ispitivanim uzorcima ulja, a što se može dovesti pre svega u vezu sa sortnim karakteristikama.

Kada je u pitanju sastav masnih kiselina uzorci ulja dobijeni iz sorti razvijenih u Institutu za ratarstvo i povrtarstvo u Novom Sadu, kao dominantnu su imali mononezasićenu oleinsku masnu kiselinu, koja je sa stanovišta nutritivne vrednosti ulja najpoželjnija a doprinosi i oksidativnoj stabilnosti ulja, za razliku od uzoraka iz semenki nepoznatog porekla koji su imali dominantnu linolnu masnu kiselinu, koja i pored toga što je esencijalna masna kiselina, doprinosi oksidativnoj nestabilnosti ulja.

U pogledu sadržaja tokoferola takođe postoji statistički značajna razlika između ispitivanih uzoraka, a posebno u sadržaju dominantnih $\beta+\gamma$-tokoferola, međutim, njihov udeo u sadržaju ukupnih tokoferola kod svih uzoraka je bio izuzetno visok, kretao se oko 80%.

U sastavu ispitanih uzoraka ulja detektovano je pet Δ^7-sterola: spinasterol, $\Delta^{7,22,25}$- stigmastatrienol, $\Delta^{7,25}$-stigmastadienol, Δ^7-stigmasterol i Δ^7-avenasterol. Dominantan po sadržaju je bio $\Delta^{,22}$-stigmastadienol ili spinasterol sa 39,98–50,31% od ukupnog sadržaja sterola.

LITERATURA

[1] T.W. Whitaker, G.N. Davis, Cucurbits botany, cultivation and untilization, Interscience Publishers, New York, 1962.

[2] K. Mägdefrau, F. Ehrendorfer, Udžbenik botanike za više škole, III dopunjeno izdanje, Školska knjiga, Zagreb, 1988.

[3] H. Teppner, Cucurbita pepo L. (Cucurbitaceae)—history, seed, coat types, thin coated seeds and their genetics. Phyton-Int. J. Exp. Bot. **40** (2000) 1–42.

[4] G.O. Fruhwirth, A. Hermetter, Production technology and characteristics of Styrian pumpkin seed oil, Eur. J. Lipid. Sci. Tech. **110** (2008) 637–644.

[5] J. Berenji, Uljana tikva i njena proizvodnja. Institut za ratarstvo i povrtarstvo, Novi Sad, 2010, str. 14,15.

[6] S. Čorbo, S. Škaljić, H. Bijelić, Karakteristike uzgoja i kvalitet ulja tikve golive (*Cucurbita pepo*), 48. Savetovanje industrije ulja: Proizvodnja i prerada uljarica, Zbornik radova, , Herceg Novi, 2007, str. 129–134.

[7] T. Verleyen, Stability of minor components during vegetable oil refining, PhD Thesis, Ghent University, 2002.

[8] W. Schuster, W. Zipse, R. Marquard, The Influence of Genotype and Growing Location on several Substances of Seeds of the pumpkin (*Cucurbita pepo* L.), Eur. J. Lipid. Sci. Tech. **85** (1983) 56–64.

[9] C. Wentzel, Recent Studies on the Fatty Acid Composition of Styrian Pumpkin Seed Oils, Ernährung/Nutrition **11** (1987) 752–755.

[10] O. Radočaj, E. Dimić, Physico-chemical and nutritive characteristics of selected cold-pressed oils found in the European market, Rivista Ital. Sost. Grasse **90** (2013) 219–228.

[11] G.O. Fruhwirth, T. Wenzl, R. El-Toukhy, F.S. Wagner, A. Hermetter, Fluorescence screening of antioxidant capa-

city in pumpkin seed oils and other natural oils, Eur. J. Lipid. Sci. Tech. **105** (2003) 266–274.

[12] V. Vukša, E. Dimić, V. Dimić, Characteristics of cold pressed pumpkin seed oil, 9th Symposium: Vitamine und Zusatzstoffe in der Ernährung von Mensch und Tier, Proceedings, Jena/Thüringen, 2003, pp. 493–496.

[13] V. Vujasinović, S. Đilas, E. Dimić, R. Romanić, A. Takači, Shelf life of cold pressed pumpkin (*Cucurbita pepo* L.) seed oil obtained with a screw press, J. Am. Oil. Chem. Soc. **87** (2010a) 1497–1505.

[14] L. Lepšanović, Lj. Lepšanović, Klinička lipidologija, Savremena administracija, Beograd, 2000.

[15] V. Vujasinović, Uticaj termičke obrade na nutritivnu vrednost i oksidativnu stabilnost ulja semena uljane tikve golice *Cucurbita pepo* L., Doktorska disertacija, Univerzitet u Novom Sadu, Tehnološki fakultet, Novi Sad, 2011.

[16] P. Breinhölder, L. Mosca, W. Lindner, Concept of sequential analysis of free and conjugated phytosterols in different plant matrices, J. Chromatogr., B **777** (2002) 67–82.

[17] V.K. Garg, W.R. Nes, Occurrence of delta-5-sterols in plants producing predominantly delta7-sterols: Studies on the sterol compositions of six Cucurbitaceae seeds. Phytochemistry **25** (1986) 2591–2598.

[18] M.H. Gordonand, L.A.D. Miller, Development of the sterylester analysis for the detection of admixtures of vegetable oils, J. Am. Oil. Chem. Soc. **74** (1997) 505–510.

[19] T. Mandl, G. Reich, W. Lindner, Detection of adulteration of pumpkin seed oil by analysis of content and composition of specific Δ^7-phytosterols, Eur. Food Res. Technol. **209** (1999) 400–406.

[20] T. Akihisa, W.C.M.C. Kokke, T. Tamura, Naturally occurring sterols in physiology and biochemistry of sterols, edited by G.W. Patterson and W.D. Nes, American Oil Chemists' Society Press, Champaign, IL, 1992, pp. 172––178.

[21] A. Kamal-Eldin, L.A. Appelqvist, G. Yousif, G.M. Iskander, Seed lipids of Sesamum indicum and related wild species in Sudan. The sterols, J. Sci. Food Agr. **59** (1992) 327–334.

[22] T. Wentzel, E. Prettner, K. Schweiger, F. S. Wagner, An improved method to discover adulteration of Styrian pumpkin seed oil, J. Biochem. Bioph. Meth. **53** (2002) 193–202.

[23] R.A. Moreau, B.D. Whitaker, K.B. Hicks, Phytosterols, phytostanols, and their conjugates in foods: structural diversity, quantitative analysis, and health-promoting uses, Prog. Lipid Res. **41**(2002) 457–500.

[24] S. Nakić-Nedjeral, D. Rade, D. Skevin, D. Strucelj, Z. Mokrovcak, M. Bartolic, Chemical characteristics of oils from naked and husk seeds of *Cucurbita pepo* L., Eur. J. Lipid. Sci. Tech. **108** (2006) 936–943.

[25] A. Szterk, M. Roszko, E. Sosinska, D. Derewiaka and P. P. Lewicki, Chemical Composition and Oxidative Stability of Selected Plant Oils, J. Am. Oil. Chem. Soc. **87** (2010) 637–645.

SUMMARY

COMPARATIVE REVIEW OF THE NUTRITIONAL VALUE OF COLD-PRESSED PUMPKIN (*Cucurbita pepo* L.) SEED OIL OF DIFFERENT ORIGINS

Biljana B. Rabrenović[1], Vesna B. Vujasinović[2], Miroslav M. Novaković[3], Selma Čorbo[4], Zorica N. Basić[5]

[1]*Faculty of Agriculture, University of Belgrade, Nemanjina 6, 11080 Zemun, Serbia*
[2]*College of Professional Studies in Management and business Communication, Mitropolita Stratimirovica 110, 21205 Sremski Karlovci, Serbia*
[3]*Institute of Chemistry, Technology and Metallurgy, University of Belgrade, 11001 Belgrade, Serbia*
[4]*Faculty of Agriculture and Food Sciences, Zmaja od Bosne br. 8, 71000 Sarajevo, Bosnia and Herzegovina*
[5]*Military Medical Academy, Institute of Hygiene, Crnotravska 17, 11000 Belgrade, Serbia*

(Scientific paper)

The objective of this study was to investigate the nutritional value of seven samples of cold pressed pumpkin oil of different origins and influence of seed origin on the content of the most important bioactive components. Four samples of a pumpkin oil is obtained by cold pressing of the seeds of domestic and Austrian varieties, and three samples of cold pressed oils were obtained from the seeds of unknown origin, taken by free choice in the market. As indicators of the nutritional values are determined by the composition and content of fatty acids, tocopherols and sterols. In the composition of the fatty acid were oleic dominant (34.2±0.09–43.9±0.04%) and linolenic fatty acid (30.8±0.09–46.9±0.015%). This study confirmed that the oil pumpkin dominant $\beta+\gamma$-tocopherol, whose contents ranged from 34.65±0.03 to 44.59±0.69 mg/100 g. We determine the composition and content of Δ^7-phytosterols, especially for specific oil pumpkins. It was detected five Δ^7-sterols: spinasterol, $\Delta^{7,22,25}$-stigmastatrienol, $\Delta^{7,25}$-stigmastadienol, Δ^7-stigmasterol and Δ^7-avenasterol. Dominant content was $\Delta^{7,22}$-stigmastadienol or spinasterol with 39.98 to 50.31% of the total content of sterols.

Keywords: Cold-pressed pumpkin oil • Nutritive value • Fatty acids • Tocopherols • Sterols

Influence of grinding method and grinding intensity of corn on mill energy consumption and pellet quality

Djuro M. Vukmirović[1], Jovanka D. Lević[1], Aleksandar Z. Fišteš[2], Radmilo R. Čolović[1], Tea I. Brlek[1], Dušica S. Čolović[1], Olivera M. Đuragić[1]

[1]University of Novi Sad, Institute of Food Technology in Novi Sad, Novi Sad, Serbia
[2]University of Novi Sad, Faculty of Technology, Novi Sad, Serbia

Abstract

In recent years there is an emerging trend of coarse grinding of cereals in production of poultry feed due to the positive influence of coarse particles on poultry digestive system. Influence of grinding method (hammer mill *vs.* roller mill) and grinding intensity of corn (coarseness of grinding) on mill specific energy consumption and pellet quality was investigated. By decreasing grinding intensity of corn (coarser grinding), specific energy consumption of both hammer mill and roller mill was significantly decreased ($p < 0.05$). When comparing similar grinding intensities on hammer mill and roller mill (similar geometric mean diameter or similar particle size distribution), specific energy consumption was higher for the hammer mill. Pellet quality decreased with coarser grinding on hammer mill but, however, this effect was not observed for the roller mill. Generally, pellet quality was better when roller mill was used. It can be concluded that significant energy savings could be achieved by coarser grinding of corn before pelleting and by using roller mill instead of hammer mill. From the aspect of pellet quality, if coarser grinding is applied it is better to use roller mill, concerning that more uniform particle size distribution of corn ground on roller mill probably results in more uniform particle size distribution in pellets and this provides better pellet quality.

Keywords: grinding, energy consumption, pellet quality, poultry, corn.

Available online at the Journal website: http://www.ache.org.rs/HI/

Dominating principle in poultry breeding is to use complete mixtures (diets) in pelleted form [1] because it has been shown that pelleting (compared to using diets in mash form) increases feed intake [2], reduces feed wastage [3], prevents birds from selecting larger particles [4], prevents segregation of diet components [5], etc. The first step in production of pelleted poultry feed is grinding of diet ingredients. Grinding is most commonly done by hammer mills while roller mills are not widely used in animal feed production even though they grind with lower energy consumption [6], give less dust during grinding and are less noisy [7]. Hammer mills (HM) produce some large and many small particles, and roller mills (RM) produce more uniform particle size distribution (PSD) [6,8]. Higher cost for purchase and maintenance are the major disadvantage of roller mills [7].

Although fine grinding was considered as a key for achieving proper feed utilization in poultry digestive system [9], there is a lot of literature that emphasizes the importance of coarse particles in poultry diets [1]. Coarse particles stimulate development of gizzard, and well developed gizzard improves energy utilization and nutrient digestibility [10] and decreases pH value of digested material [11] lowering the risk of coccidiosis [12] and feed-borne pathogens [2]. Thus, coarser grinding of cereals, as the main component of poultry diets, should be applied. Additionally, coarser grinding will save energy and time in the grinding process.

On the other hand, it is well known that pelleting reduces size of micro-particles that constitute the pellets [4], but it is expected that coarser grinding before pelleting will increase the share of coarse particles in pellets to a certain extent which will enhance gizzard development. Problem with coarse grinding of cereals is the influence on pellet quality. Physical quality of pellets is important from the aspect of transport and handling, where certain resistance to abrasion is required, but also from the aspect of nutritional quality, *i.e.*, higher feed intake and, perhaps, improved nutritional value of good quality pellets [13–15]. Even though dominating belief is that pellet quality decreases with coarser grinding [16], Reece *et al.* [17] determined that coarseness of grinding has no effect on pellet quality. Thus, results about influence of grinding intensity on pellet quality are contradictory.

The aim of this research was to determine the influence of mill type (hammer mill vs. roller mill, *i.e.*, wide *vs.* narrow distribution of particle size) and

coarseness of grinding on mill energy consumption and pellet quality.

MATERIAL AND METHODS

Experiments were conducted at pilot-plant facility of Institute of Food Technology (University of Novi Sad, Serbia). Dent corn obtained from local company (Agrobačka a.d., Bačka Topola, Serbia) was ground using hammer mill (ABC Engineering, Pančevo, Serbia) and roller mill (ROSKAMP TP650-9, California pellet mill, USA). Hammer mill had 16 hammers arranged in four rows and it was driven by 2.2 kW motor with rotational speed of hammers of 2880 rpm. By using hammer mill equipped with sieve openings diameter of 3, 6 and 9 mm, three different coarseness of corn were obtained: fine (treatment HM-F), medium (HM-M) and coarse (HM-C), respectively. Roller mill had three pairs of rollers with 1.8–5.5 corrugations per cm and differential speed of 1:1.5 for each pair of rollers. The upper pair was driven by a 5.5 kW motor and two lower pairs by an 11 kW motor. Gap between two higher pairs of rollers was fixed at 4.4 and 2.6 mm for all grinding treatments while gap between lower pair of rollers was set to 1.4, 2.0 and 2.6 mm for obtaining three different coarseness, *i.e.* medium (RM-M), coarse (RM-C) and very coarse (RM-VC), respectively.

Specific energy consumption (kWh/t) of hammer mill and roller mill was measured according to equation (1) described by Payne *et al.* [18]:

$$\text{Specific energy consumption} = \frac{\sqrt{3}\left(I - I_0\right)U\cos\varphi}{1000}\frac{1}{Q} \quad (1)$$

In Eq. (1), I (A) and I_0 (A) are average hammer mill or roller mill motor amperage with and without material, respectively, U (V) is the voltage, $\cos\varphi$ is the power factor (ratio between the actual load power and the apparent load power drawn by an electrical load) and Q (kg/h) is the throughput of material.

Moisture content of ground corn was adjusted to 16% by the addition of water in the double shaft pedal mixer (SLHSJ0.2 Muyang, China) and corn was pelleted using flat pellet press (14-175, Amandus Kahl, Germany) with 6 mm diameter of die openings and 24 mm thickness, while throughput of material was 20 kg/h.

PSD of ground corn was determined according to ISO 1591-1 1988 (E) using sieve shaker (Endecotts, UK) with the following size of sieve openings: 5600, 4000, 3150, 2000, 1600, 1000, 630, 250 and 125 µm. Geometric mean diameter (*GMD*) and geometric standard deviation (*GSD*) were determined according to A.S.A.E. standard [19] using the Eqs. (2)–(4):

$$GMD = \log_{-1}\frac{\sum_{i=1}^{n} W_i\log d_i'}{\sum_{i=1}^{n} W_i} \quad (2)$$

$$d_i' = \sqrt{d_i + d_{i+1}} \quad (3)$$

$$GSD = \log_{-1}\frac{\sum_{i=1}^{n} (\log d_i' - \log GMD)}{\sum_{i=1}^{n} W_i} \quad (4)$$

where d_i (µm) is the size of sieve openings of ith sieve and W_i (g) is the mass on i^{th} sieve.

Pellet quality was measured using Holmen pellet tester (NHP 100, Norfolk, UK) and expressed as pellet durability index (*PDI*) which is calculated as the ratio of mass of pellets after the test and the mass of pellets before the analyses. Duration of treatment was 30 s and pellets were sieved before and after the treatment using a sieve with 4.8 mm size of sieve openings (sieve opening diameter = 0.8×pellet diameter).

One-way analysis of variance (ANOVA), applying Tukey HSD test, was used for comparison of sample means to analyze variations of the results (statistical software Statistica 12). Differences between the means with probability $p < 0.05$ were accepted as statistically significant.

RESULTS AND DISCUSSION

In production of pelleted poultry diets, cereals, as the main components, are usually finely ground using 3 to 4.5 mm hammer mill sieve openings diameter [9]. Thus, HM-F treatment represented grinding that is usually performed in practice. In other treatments of this study, coarseness of grinding was increased, with extreme coarseness for RM-VC treatment. Obtained *GMD*s and *GSD*s for different grinding treatments of corn are presented in Table 1. As it can be seen, wide range of GMDs was achieved, and *GSD*s were different for different mill type (hammer *vs.* roller mill), while for grinding treatments within the same mill, values were similar. According to A.S.A.E. [19], when *GSD* is equal to 1 all particles are exactly the same, and *GSD* around 3 or more indicates a lot of variation in particle size. This implies that for roller mill produced more uniform PSDs.

For RM-M and RM-C grinding treatments the distance between lower pair of rollers was selected in order to reflect 6 and 9 mm hammer mill grinding, *i.e.*, to obtain similar *GMD* between HM-M and RM-M, and between HM-C and RM-C (Table 1). These pairs of treatments were defined (according to *GMD*) to have similar grinding intensity. However, it can be seen that PSD of RM-M grinding treatment is more similar to PSD of HM-F treatment (Figure 1a) than to HM-M (Figure 1b). Likewise, PSD of RM-C was more similar to PSD of

HM-M treatment (Figure 1c) than to HM-C (Figure 1d), especially when looking at coarser fractions (> 2500 µm), while PSD of HM-C treatment was similar to RM--VC (Figure 1e).

Table 1. Geometric mean diameters (GMD) and geometric standard deviations (GSD) obtained with different mill type (hammer mill (HM) or roller mill (RM)) and different grinding intensity (fine (F), medium (M), coarse (C) and very coarse (VC))

Grinding treatment	GMD / µm	GSD / µm
HM-F	671	2.66
HM-M	1144	2.82
RM-M	1119	2.17
HM-C	1581	2.69
RM-C	1542	2.27
RM-VC	2108	2.09

Noticeably higher specific energy consumption for grinding was obtained for HM-F treatment comparing to other treatments (Figure 2). When comparing pairs of treatments with similar *GMD* obtained with hammer mill and roller mill (HM-M *vs*. RM-M and HM-C *vs*. RM--C), it can be seen that specific energy consumption was significantly higher ($p < 0.001$) when hammer mill was used. This suggests that significant energy savings in grinding process could be achieved by using roller mill instead of hammer mill in order to obtain similar *GMD*; specific energy consumption would be 39% lower with RM-M grinding treatment comparing to

HM-M treatment and 46% lower if HM-C treatment is substituted by RM-C treatment. Possibilities for saving the energy with roller mill are even more pronounced if grinding with hammer mill is substituted by roller mill grinding that produce similar PSD. In this way if HM-F grinding treatment is substituted by RM-M, specific energy consumption would be 82% lower. If HM-M grinding treatment is substituted by RM-C specific energy consumption would be 66% lower, and by substituting HM-C with RM-VC, 54% of energy necessary for grinding would be saved.

Expected decrease of pellet quality (expressed as *PDI*) with coarser grinding was observed for corn ground using hammer mill (Figure 3). Surprisingly, this was not observed with roller mill where obtained *PDI* values for different grinding intensities were not significantly different between each other (even for very coarsely ground corn (RM-VC)). Generally, pellet quality was better (higher *PDI*) when roller mill was used compared to hammer mill. Only for the treatment HM-F, obtained pellet quality was not significantly different from RM treatments, yet it was slightly lower.

Possible reason for lower *PDI* values of pellets produced with corn ground on hammer mill could be wider distribution of particle size which results in more inhomogeneities in pellet structure, especially presence of higher quantity of coarse particles in pellet structure. Pellets are particularly sensitive near the points of inhomogeneities in their structure due to local stresses and strains are the highest near such imperfections [20].
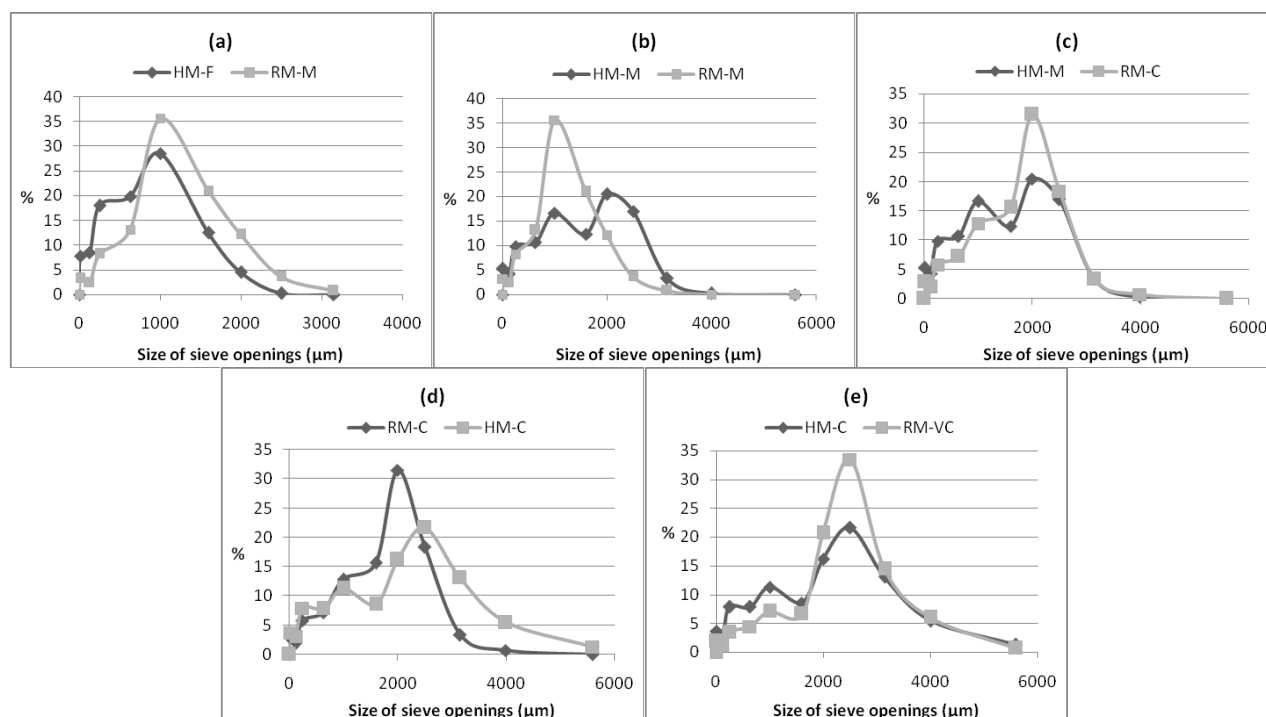

Figure 1. Comparison of particle size distributions for different grinding treatments (different mill type (hammer mill (HM) or roller mill (RM)) and different grinding intensity (fine (F), medium (M), coarse (C) and very coarse (VC)).
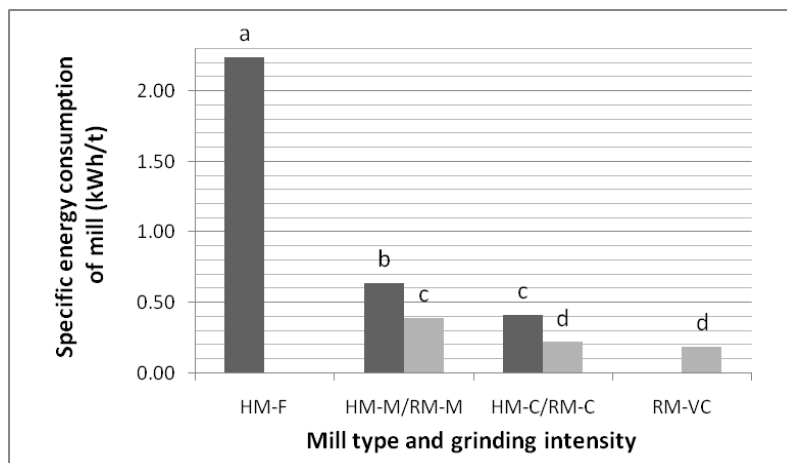
Figure 2. Influence of mill type (hammer mill (HM) or roller mill (RM)) and grinding intensity (fine (F), medium (M), coarse (C) and very coarse (VC)) on specific energy consumption of mill. Values with different letters are significantly different (p < 0.05).
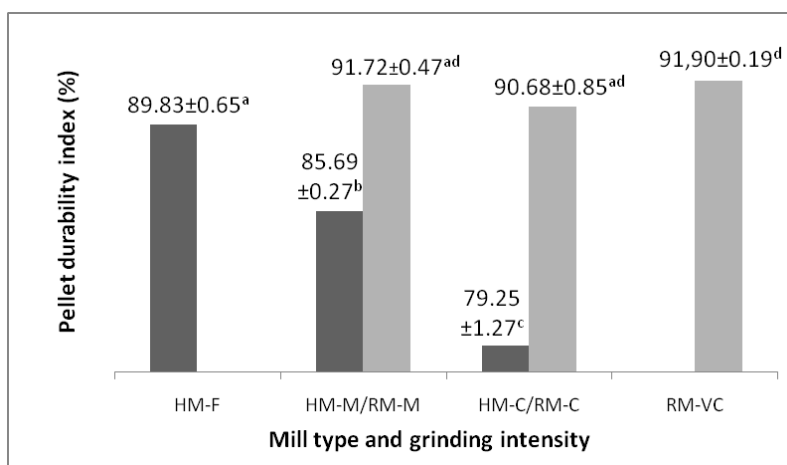

Figure 3. Influence of mill type (hammer mill (HM) or roller mill (RM)) and grinding intensity (fine (F), medium (M), coarse (C) and very coarse (VC)) on pellet durability index. Values with different letters are significantly different (p < 0.05).

Corn ground on roller mill had more uniform PSD and it can be assumed that this resulted in more uniform PSD in pellets, compared to pellets made of hammer milled corn. More uniform PSD of particles that made up the pellets contributed to better quality of pellets produced from material ground on roller mill.

CONCLUSIONS

From the obtained results it can be concluded that high energy savings could be achieved by coarser grinding of corn before pelleting. However, if coarser grinding is applied, it is better to use roller mill than hammer mill. Besides lower energy consumption for achieving the same *GMD* and especially for achieving similar PSD, quality of pellets will also be better when using roller mill instead of hammer mill. This is probably because more uniform PSD after roller mill results in more uniform PSD in pellets and this provides better pellet quality. In further research it is necessary to determine PSD in pelleted material and the amount of gelatinized starch in order to determine the reason for better quality of pellets produced with roller milled corn.

REFERENCES

[1] B. Svihus, The gizzard: function, influence of diet structure and effects on nutrient availability, World Poultry Sci. J. **67** (2001) 207–223.

[2] R.M. Engberg, M.S. Hedemann, B.B. Jensen, The influence of grinding and pelleting of feed on the microbial composition and activity in the digestive tract of broiler chickens, Brit. Poultry Sci. **43** (2002) 569–579.

[3] L.S. Jensen, Influence of pelleting on the nutritional needs of poultry, Asian-Australian J. Anim. Sci. **13** (2000) 35–46.

[4] M.R. Abdollahi, V. Ravindran, B.Svihus, Pelleting of broiler diets: An overview with emphasis on pellet quality and nutritional value, Anim. Feed Sci. Tech. **179** (2013) 1–23.

[5] M.W. Greenwood, R.S. Beyer, Effect of feed manufacturing practices on nutrient availability and feed quality, Proceedings of the 30th Annual Carolina Poultry Nutrition Conference, Raleigh, NC, USA, 2003, pp. 7–16.

[6] I. Nir, J.P. Melcion, M. Picard, Effect of particle size of sorghum grains on feed intake and performance of young broilers. Poultry Sci. **69** (1990) 2177–2184.

[7] M. Heimann, The "bottom line" of grinding. Feed Int. **23**(5) (2002) 32–34.

[8] K. Koch, in: MF-2048 Feed Manufacturing, Hammer mills and roller mills, Kansas State University, Manhattan, KS, USA, 1996, pp. 1–4.

[9] B. Svihus, K.H. Kløvstad, V. Perez, O. Zimonja, S. Sahlström, R.B. Schüller, W.K. Jeksrud, E. Prestløkken, Physical and nutritional effects of pelleting of broiler chicken diets made from wheat ground to different coarsenesses by the use of roller mill and hammer mill, Anim. Feed Sci. Tech. **117** (2004) 281–293.

[10] B. Carre, Effects de la taille des particules alimentaires sur les processus digestifs chez les oiseaux ìélevage, INRA Productions Animales **13** (2000) 131–136.

[11] G.E. Duke, Recent studies on regulation of gastric motility in turkeys, Poultry Sci. **71** (1992) 1–8.

[12] R.B. Cumming, Opportunities for whole grain feeding. Proceedings of the 9th European Poultry Conference, Glasgow, Vol. 2, 1994, pp. 219–222.

[13] E.R. Skoch, S.F. Binder, C.W. Deyoe, G.L. Allee, K.C. Behnke, Effects of pelleting conditions on performance of pigs fed a corn-soybean meal diet, J. Anim. Sci. **57**(4) (1983) 922–928.

[14] C.A. Stevens, Starch gelatinization and the influence of particle size, steam pressure and die speed on the pelleting process, Ph.D. Thesis, Kansas State University, USA, 1987, p. 86.

[15] J.P. Koopmans, P.M. Scholten, P.C. Roeleveld, Y.W.M. Velthuizen, A.C. Beynen, Hardness of diet pellets and its influence on growth of pre-weaned and weaned mice, Z. Versuchstierkd. **32** (1989) 71–75.

[16] A.M. Amerah, V. Ravindran, R.G. Lentle, D.G. Thomas, Influence of feed particle size and feed form on the performance, energy utilisation, digestive tract development, and digesta parameters of broiler starters, Poultry Sci. **86** (2007) 2615–2623.

[17] F.N. Reece, B.D. Lott, J.W. Deaton, The effects of hammer mill screen size on ground corn particle size, pellet durability, and broiler performance, Poultry Sci. **65** (1986) 1257–1261.

[18] J. Payne, W. Rattink, T. Smith, T. Winowiski, Objectives in pelleting, In: J. Payne, W. Rattink, T. Smith, T. Winowiski (Eds), The Pelleting Handbook, Borregaard Lignotech, Norway, 1994, pp. 11–12.

[19] American Society of Agricultural and Biological Engineers (A.S.A.E.), Methods of Determining and Expressing Fineness of Feed Materials by Sieving. Standard No. S319.3, 2003, pp. 202–205.

[20] M. Thomas, A.F.B. van der Poel, Physical quality of pelleted animal feed: 1.Criteria for pellet quality, Anim. Feed Sci. Tech. **61** (1996) 89–112.

IZVOD

UTICAJ NAČINA I INTENZITETA MLEVENJA KUKURUZA NA POTROŠNJU ENERGIJE MLINA I KVALITET DOBIJENIH PELETA

Đuro M. Vukmirović[1], Jovanka D. Lević[1], Aleksandar Z. Fišteš[2], Radmilo R. Čolović[1], Tea I. Brlek[1], Dušica S. Čolović[1], Olivera M. Đuragić[1]

[1]Univerzitet u Novom Sadu, Nučni institut za prehrambene tehnologije u Novom Sadu, Novi Sad
[2]Univerzitet u Novom Sadu, Tehnološki fakultet, Novi Sad

(Naučni rad)

Kod uzgoja živine se uglavnom primenjuje peletirana hrana, a prvi korak u proizvodnji peletirane hrane je mlevenje pojedinačnih sastojaka smeše. Za mlevenje su najviše u upotrebi mlinovi čekićari dok su mlinovi na valjke znatno manje zastupljeni. Iako je dugo smatrano da je sitno mlevenje ključno za proizvodnju kvalitetnih peleta i dobro iskorišćenje hrane u probavnom sistemu životinja, krupnije mlevenje žitarica, kao osnovnih komponenata hrane za živinu, postaje sve zastupljenije. Razlog za ovo je što mnoga istraživanja ukazuju da krupnije mlevenje ne dovodi do značajnijeg narušavanja kvaliteta proizvedenih peleta kao i da prisustvo krupnih čestica pozitivno deluje na probavni sistem živine. Cilj ovog istraživanja bio je da se ispita uticaj načina mlevenja (mlin čekićar ili mlin na valjke, tj. široka ili uska raspodela veličine čestica) i intenziteta usitnjavanja kukuruza na specifičnu potrošnju energije mlina i kvalitet dobijenih peleta. Sa smanjivanjem intenziteta usitnjavanja (krupnije mlevenje), došlo je do značajnog ($p < 0.05$) smanjenja specifične potrošnje energije kako mlina čekićara tako i mlina na valjke. Kada se porede slični intenziteti usitanjavanja na mlinu čekićaru i mlinu na valjke (sličan geometrijski srednji prečnik, a naročito slična raspodela veličine čestica), specifična potrošnja energije je bila veća na mlinu čekićaru. Kvalitet peleta se pogoršavao sa krupnijim mlevenjem na čekićaru, ali ne i kod mlina na valjke gde krupnoća mlevenja nije uticala na kvalitet peleta. Generalno, kvalitet peleta je bio bolji pri peletiranju kukuruza samlevenog na mlinu na valjke, bez obzira na krupnoću mlevenja. Može se zaključiti da se značajne uštede energije mogu postići krupnijim mlevenjem kukuruza pre peletiranja, a takođe i upotrebom mlina na valjke umesto mlina čekićara. Međutim, u pogledu kvaliteta peleta, ukoliko se primenjuje krupnije mlevenje, bolje je koristiti mlin na valjke s obzirom na to da ujednačenija veličina čestica koja se dobija nakon mlevenja najverovatnije dovodi i do ujednačenije veličine čestica u proizvedenim peletama što doprinosi boljem kvalitetu peleta.

Ključne reči: Mlevenje • Potrošnja energije • Kvalitet peleta • Živina • Kukuruz

Hydrophobic silica nanoparticles as reinforcing filler for poly (lactic acid) polymer matrix

Branka M. Pilić[1], Tanja I. Radusin[2], Ivan S. Ristić[1], Clara Silvestre[3], Vera L. Lazić[1], Sebastian S. Baloš[4], Donatella Duraccio[3]

[1]Faculty of Technology, University of Novi Sad, Novi Sad, Serbia
[2]Institute of Food Technology, University of Novi Sad, Novi Sad, Serbia
[3]Institute of Chemistry and Technology of Polymers (ICTP), National Research Council (CNR), Pozzuoli Naples, Italy
[4]Department of Production Engineering, Faculty of Technical Science, University of Novi Sad, Novi Sad, Serbia

Abstract

Properties of poly (lactic acid) (PLA) and its nanocomposites, with silica nanoparticles (SiO$_2$) as filler, were investigated. Neat PLA films and PLA films with different percentage of hydrophobic fumed silica nanoparticles (0.2, 0.5, 1, 2, 3 and 5 wt.%) were prepared by solution casting method. Several tools were used to characterize the influence of different silica content on crystalline behavior, and thermal, mechanical and barrier properties of PLA//SiO$_2$ nanocomposites. Results from scanning electron microscope (SEM) showed that the nanocomposite preparation and selection of specific hydrophobic spherical nano filler provide a good dispersion of the silica nanoparticles in the PLA matrix. Addition of silica nanoparticles improved mechanical properties, the most significant improvement being observed for the lowest silica content (0.2 wt.%). Barrier properties were improved for all measured gases at all loadings of silica nanoparticles. The degree of crystallinity for PLA is slightly increased by adding 0.2 and 0.5 wt.% of nanofiller.

Keywords: polylactic acid, silica nanoparticles, nanocomposite, food packaging.

Available online at the Journal website: http://www.ache.org.rs/HI/

The interest in biopolymers has increasing trend due to their positive environmental impact; they are produced from renewable sources and are biodegradable, and consequently their utilization has less negative effect compared to conventional petroleum based polymers [1–9]. Biopolymers are used in variety of applications, like therapeutic aids, medicines, coatings, food products and packaging materials [10]. Poly (lactic acid), PLA, is biodegradable aliphatic polyester derived from 100% renewable resources (corn starch or sugar beet). Approximately 25–55% less energy is required to produce PLA than petroleum-based polymers [11,12]. Popularity of PLA has significantly increased due to the ease of its processing by conventional methods (such as injection molding, film extrusion, blow molding, thermoforming, fiber spinning and film forming), which enable its utilization in diverse applications, including food packaging [13,14]. However, due to its poor barrier and mechanical properties, the utilization of PLA for food packaging is currently limited to cups, containers and films for short shelf-life products [6,7,15]. PLA properties can be improved by incorporation of nanoparticles into polymer matrix. Inorganic nanoparticles are added often to polymer matrix, especially for

improvement of mechanical and barrier properties [6,7,12,16]. Nano fillers are creating very large interfaces with polymer matrix due to their small particle size and extremely high surface area. A potential use of nanotechnology has been already identified in every segment of the food industry including food packaging [17]. Majority of the studies concerning PLA nanocomposites are related to PLA/layered nanoparticles [10,15,18]. Nevertheless, spherical silica nanoparticles are, due to their natural abundance, low cost, high thermal resistance and surface functionality, very suitable for various applications [2]. The influence of different types of hydrophilic silica nanoparticles on PLA properties has been reported [2,9,13]. It was stated that direct mixing of hydrophilic silica nanoparticles results in their aggregation [16]. The functionalization of hydrophilic silica nano particles is carried out in order to block reactive silanol end-groups. Surface modification results in hydrophobic product, less reactive than hydrophilic one, with better dispersion in polymer matrices. Hydrophobic fumed silica is produced by chemical treatment of hydrophilic grades with silanes or siloxanes. In the final product the treatment agent is chemically bonded to the oxide that was previously hydrophilic. These particles are characterized by a low moisture adsorption, excellent dispersion in polymer matrices (including PLA), and ability to adjust rheological behavior [13,16]. Large surface area and smooth nonporous surface of silica nanoparticles

can intensify the effect of particle-particle and/or polymer particle interaction, which could promote strong physical contact between the silica and polymer matrix causing the improvement in material properties [19]. Hydrophobic silica nanoparticles present new potential filer for enhancement of PLA polymer matrix properties. The goal of this research was to investigate the influence of different loadings of hydrophobic silica nanoparticles on thermal, mechanical and barrier properties of PLA polymer matrix.

MATERIAL AND METHODS

Material

The PLA used in this study was provided from Esun, China. Parameters of the neat PLA are: number-average molecular weight M_n = 60520 g mol^{-1}; weight-average molecular weight M_w = 160780 g mol^{-1} and polydispersity Q = 2.6 (from GPC).

The hydrophobic nano silica (Aerosil®R812) was kindly supplied by Evonik (Hanau, Germany) with specific area of 260±30 m^2 g^{-1} and average particle size 7 nm. They were used as received without any pre-treatment.

Sample preparation

Pure PLA film and PLA films with 0.2, 0.5, 1, 2, 3 and 5 wt.% of nanosilica were prepared by solution casting method. Appropriate amounts of nanosilica were added in chloroform and stirred in an ultrasonic bath for 10 min. PLA was added to nano silica dispersion and stirring continued with magnetic bar for 4 h at room temperature. After completely PLA dissolution, samples were poured into glass Petri dishes (10 cm diameter) and vacuum dried at room temperature. Film thickness was measured by using a micrometer (Digico 1, Tesa technology, Renens, Switzerland) with sensitivity of 0.0001 mm in eight replicates for each film, from which an average value was obtained.

Scanning electron microscopy (SEM) analysis

Morphology of fractured surface of PLA and PLA/ /silica nanocomposite films were investigated by using a Philips model XL20 apparatus. The samples were frozen in liquid nitrogen and quickly broken off to obtain a random brittle-fractured surface. Before the observation, samples were coated with Au/Pd alloy using E5 150SEM coating unit.

Wide angle X-ray diffraction (WAXD) analysis

Wide angle X-ray diffraction measurements were conducted by using a Philips XPW diffractometer with Cu Kα radiation (1.542 Å) filtered by nickel. The scanning rate was 0.02° min^{-1}, and the scanning angle was from 5 to 45°. The ratio of the area under the crys-

talline peaks and the total area multiplies by 100 was taken as the degree of crystallinity.

Differential scanning calorimetry (DSC)

Thermal properties of the samples were determined by using a DSC model Q20 (TA Instruments, USA). Aluminium pans containing 3–5 mg of nanocomposite films were hermetically sealed. The first heating scan (up to 170 °C) was performed in order to remove all thermal history and after cooling (with cooling rate 20 °C min^{-1}) samples were heated from 20 to 180 °C. The heating rate was 10 °C min^{-1}.

Mechanical properties

Tensile strength (*TS*) and elongation at break (*EB*) of prepared films were measured on Toyoseiki AT-L-118A dynamometer in accordance with ASTM D638 standard. Rectangular strips were cut from prepared films. For each data point, five samples were tested, and the average value was calculated.

Permeability tests

Determination of the gas permeability (CO_2, N_2 and O_2) was conducted according to the Lyssy method. This procedure is an isostatic gas-chromatographic method (DIN 53380, 1969), with the use of the Lyssy GPM-200 apparatus with the belonging Gasukuro Kogyo GC-320 gas chromatograph and the HP 3396A integrator attached. A standard Gow-Mac series 5 52 thermal conductivity detector gas chromatograph has been used as a basis for quantitative analysis. In the gas chromatograph oven a dual column system containing a 3 m Porapack QS and a 4.5 m molecular sieve column 60–80 mesh has been inserted in series, and the ratio of the beam splitting can be regulated with a restrictor valve incorporated before the Porapack column. This makes it possible to split all known permanent gases, especially oxygen and nitrogen, from air. The investigations were performed at 23 °C and 1 bar pressure difference, with the volume of sample (gas) injected of 0.8 ml. The film sample was fixed and placed in the investigation chamber. Permeability of gases was determined on the base of isostatical conditions in a chamber divided by the film. The pressure at both sides of the film was equal (0.2 bar). Helium was gradually enriched due to the permeation of gases from the gaseous mixture through the film, and gas concentration in helium was recorded by the gas chromatograph and integrator. The peak area (height) of the obtained chromatogram changes in function of time and represents the permeability of gases from the mixture. Air permeability was calculated on the basis of gases ratio in the air. The results of permeability determination are expressed in 10^{-18} m^2 Pa^{-1} s^{-1}.

RESULTS AND DISCUSSION

Figure 1a shows the SEM image of neat PLA fracture surface. Figure 1b–g show the SEM images of PLA filled with 0.2, 0.5, 1, 2, 3 and 5 wt.% of silica nanoparticles, respectively. In the SEM micrographs presented in Figure 1 nanoparticles are detected as white and spherical dots. PLA fracture surface (Fig. 1a) is smooth as expected for a neat polymer. Very good and uniform dispersion of nanoparticles for samples up to 1 wt.% of silica content was noticed. The very good dispersion and distribution of nanoparticles in polymer matrix, that are key factors for improved materials, can be attributed to the specific nature of hydrophobic silica nanoparticle which causes lower inter particle interaction. With the increase of silica content (from 1 up to 3 wt.%) nanoparticles start to aggregate forming cluster, and the silica homogeneity in the matrix (distribution) drastically decreases with respect to higher sil-

ica contents. Moreover more surface irregularities and voids appear. For 5 wt.% of silica content (Fig. 1g), material exhibits non-uniform distribution and dispersion of silica nanoparticles with a significant number of agglomerates. This result was expected as the consequence of the higher load of filler, causing higher volume ratio in polymer matrix as well as higher inter particle interaction. Similar results were reported for both hydrophilic [2,9] and hydrophobic silica nano fillers [16] in PLA polymer matrix.

X-ray diffraction (WAXD) was used to investigate the influence of nanosilica addition on the crystal structure and degree of crystallinity of PLA nanocomposite films. The X-ray diffraction profiles of the neat PLA and PLA/silica nanocomposites films are shown in Figure 2. For comparison purposes the WAXD profile of PLA as received (pellet) is reported.

PLA can crystallise in several polymorphic forms (α, β and γ forms), depending on the preparation con-

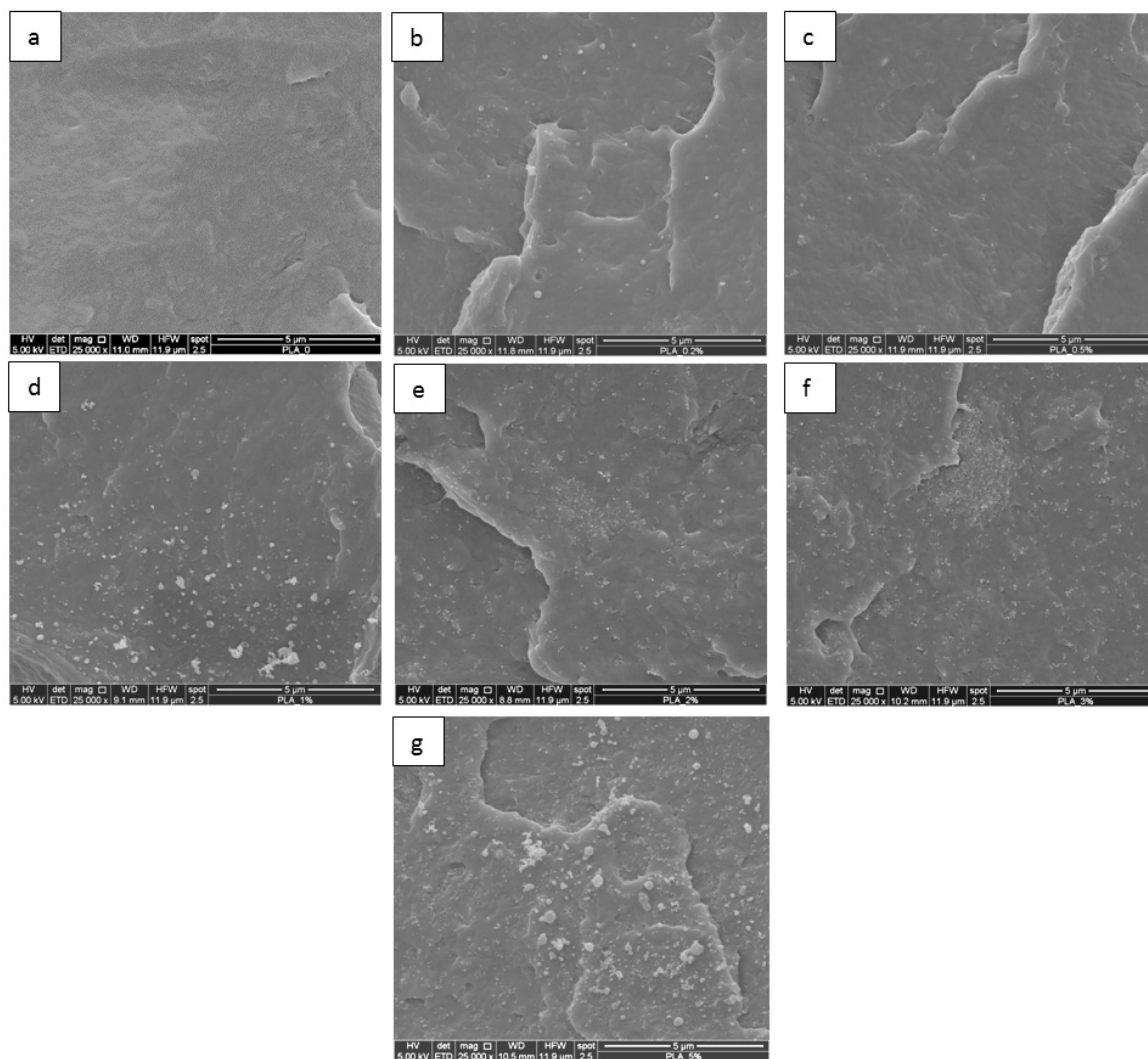

Figure 1. SEM micrographs of the fractured surface of the PLA and PLA nanocomposites: a) pure PLA ,b) PLA+0.2 wt.% silica, c) PLA+0.5 wt.% silica ,d) PLA+1 wt.% silica, e) PLA+2 wt.% silica, f) PLA+3 wt.% silica and g) PLA+5 wt.% silica.
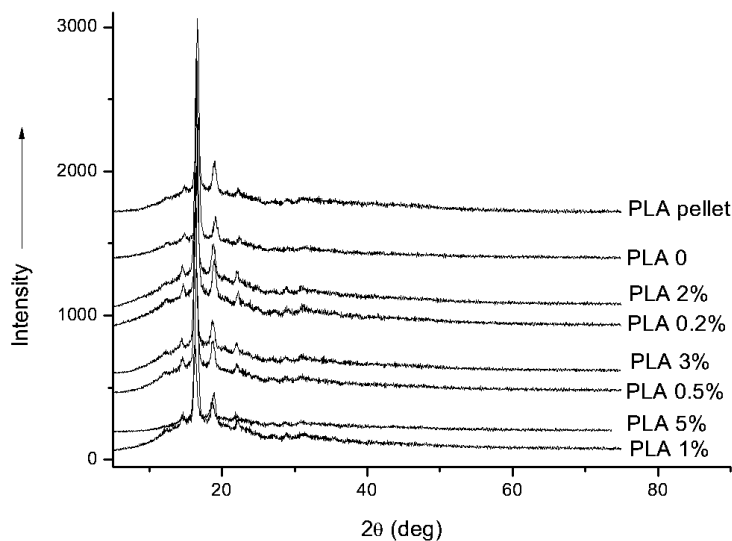
Figure 2. WAXD patterns of the PLA and PLA nanocomposites: PLA pellets, pure PLA film and PLA film with (0.2, 0.5, 1, 2, 3 and 5 wt.%) of silica.

ditions [20]. In neat PLA, strong diffraction picks appearing at 16.7 and 19.1°, which represent (200)/ /(110)$_\alpha$ and (203)$_\alpha$ reflections of stable α-crystals, together with some weak diffraction peaks at 14.8 and 22.3° indicative of (010)$_\alpha$ and (015)$_\alpha$ reflections of the stable α-form of PLA, are observed. The presence of silica nanoparticles does not modify the crystal structure of PLA for all the compositions studied. The degree of crystallinity by WAXD (*C* in %) of pure PLA and PLA/ /silica nanocomposites films is reported in Table 1. These results are showing a slight increase of crystalline content of PLA for small addition of silica nanoparticles (0.2 and 0.5 wt.%). This behavior can be attributed to the well dispersed nanoparticles that act as nucleating agents, as already reported in the literature [21,22].

Table 1. Degree of crystallinity, C, for pure PLA film and PLA film with different amount of silica

Sample	*C* / %
Pure PLA	25.1
PLA+0.2 wt.% silica	27.1
PLA+0.5 wt.% silica	27.1
PLA+1 wt.% silica	24.2
PLA+2 wt.% silica	22.0
PLA+3 wt.% silica	21.7
PLA+5 wt.% silica	24.5

DSC analysis was used to determine the glass transition temperature (T_g) of pure PLA and PLA/SiO$_2$ nanocomposite films. The effect of silica content on the T_g is shown in Figure 3. It can be seen that T_g increases from 47.6 °C for pure PLA matrix to 48.9 and 50.6 °C for the samples filled with 0.2 and 0.5 wt.% silica, respectively. With further increase of silica content (1, 2, 3 and 5 wt.%) T_g decreases with respect to neat PLA.

It is well known that polymer nanocomposite characteristics are strongly dependent on dispersion, distribution and interaction of nanoparticles and polymer matrix (adhesion between organic polymer and inorganic filler). The good dispersion and distribution of nanoparticles may be related to: 1) sample preparation method and 2) the use of hydrophobic silica nanoparticles, preventing the agglomerate formations. Good dispersion is expected when there is a good adhesion between the polymer chains and nanoparticles [23]. Increase in T_g for PLA/SiO$_2$ nanocomposites with 0.2 and 0.5% in weight with respect to neat polymer can be ascribed to the chain mobility decreasing throughout the polymer matrix volume, in presence of nanoparticle filler. Many experiments show that the reduction in the mobility chain is going through the whole volume of the polymeric matrix, but affects the chains within a few nm from the surface of filler due to the strong interaction between the fillers and polymeric matrix [23]. For the samples with 1, 2, 3 and 5 wt.% silica content, T_g decreases in respect to the neat polymer with the increase of the silica content. The agglomerate formation and the reduction of homogeneity in the polymer matrix is affecting the chain mobility and causing a decrease in the T_g in respect that of neat polymer [23].

From the thermograms in Figure 3, it is evident that in the melting process endothermic shoulder peak prior to the dominant melting peak is present for all samples. Double peak melting endotherms are commonly present in PLA samples [24]. The multiple melting behaviour of PLA was suggested to be generated due to the melt-recrystallization mechanism, when the less perfect crystals have enough time to melt and reorganise into crystals with higher structural perfection, and re-melt at higher temperature [24]. The two crystal types that
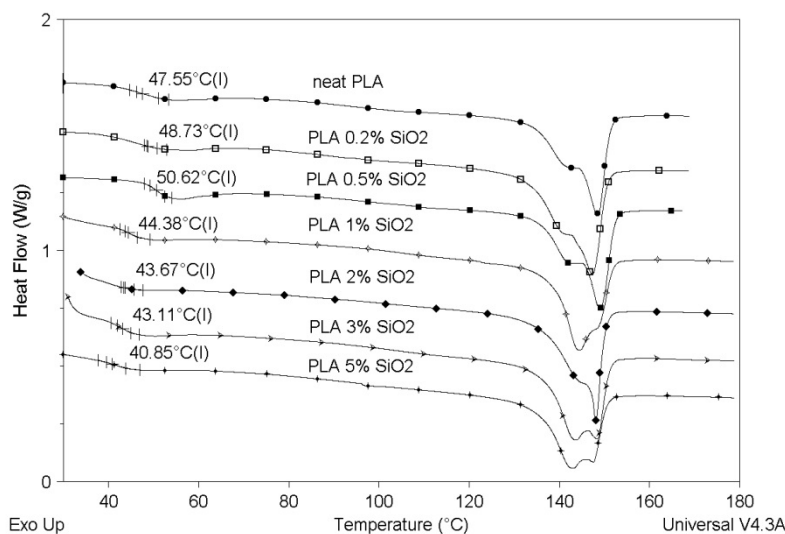
Figure 3. DSC curves of pure PLA film and PLA film with (0.2, 0.5, 1, 2, 3 and 5 wt.%) of silica, respectively.

could grow upon melt crystallisation were the α-form, which predominated at high crystallisation temperatures, and the α′-form that grew at low crystallisation temperatures [24]. In Figure 3, the shoulder peak of α′-form in PLA nanocomposites increases in the presence of silica, suggesting that the filler influences the polymorphic phase transition mechanism of PLA. Effect of silica on generation of the multiple melting temperatures of PLA is outside the scope of this article and thus it will not be discussed in more details.

The mechanical properties are measured in order to investigate the effect of silica nanoparticles filler on PLA films. The values of the tensile strength (*TS*) of PLA and PLA nanocomposite films are given in Figure 4. Significant improvement of tensile strength compared to neat PLA film is recorded for the samples with silica content of 0.2, 0.5 and 1 wt.% (from 52 to 64, 63 and 60.6 MPa, respectively). The decrease of tensile strength starts with further increase of the silica contents. For

the sample with 5 wt.% silica content, the value of tensile strength is below neat PLA. As the filler concentration increased, a worse dispersion and distribution of nanoparticles, higher surface irregularities and presence of voids were observed by SEM. Such defects may act as crack nucleating agents thus explaining the decrease in tensile behavior of the nanocomposite [16].

Gas permeability

Determination of the gas permeability (CO_2, N_2 and O_2) is conducted in accordance with the Lyssy method. Gas permeability is significantly affected by hindered diffusion of gas molecules through the polymer film due to addition of silica nanoparticles. For example, addition of 0.2% SiO_2 reduces permeability of all measured gasses (CO_2, N_2 and O_2) for almost 50% compared to neat PLA (Figure 5). For example, permeability of CO_2 was reduced from 8.16×10^{-18} to 5.45×10^{-18} m^2 Pa^{-1} s^{-1} for 0.2 wt.% of silica, and to 4.45×10^{-18}, 4.14×10^{-18} and
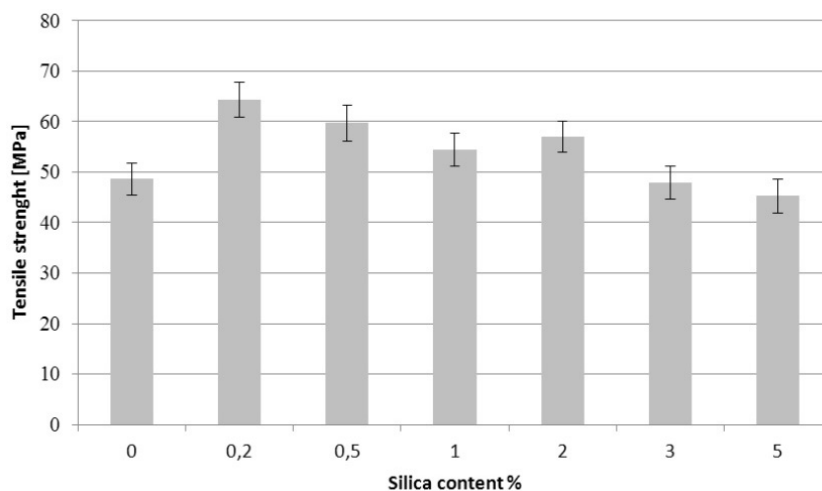

Figure 4. Tensile strength for pure PLA film and PLA film with (0.2, 0.5, 1, 2, 3 and 5 wt.%) of silica.

4.78×10^{-18} m^2 Pa^{-1} s^{-1}, for 0.5, 1 and 2 wt. % silica, respectively. For higher loadings (3 and 5 wt.%) permeability of CO_2 was a little bit higher (6.1×10^{-18} and 6.25×10^{-18} m^2 Pa^{-1} s^{-1}, respectively) but still lower than for neat PLA. Similar trend was observed for all measured gases. This behavior can be assigned to good dispersion of filler. Silica nanoparticles with small primary particle size are evenly distributed through the polymer matrix volume even for lowest loadings, causing permeability reduction. Besides, degree of crystallinity can also influence permeability reduction. Gas transport behavior of semicrystaline polymers refers to two phase model-impermeable crystalline phase, dispersed in permeable amorphous phase [25]. Lower gas permeability values could also be assigned to increase in degree of crystallinity for 0.2 and 0.5 wt.%.

ting worse with respect to those of neat polymer by increasing the silica content.

Acknowledgments

Figure 5. Gas permeability (CO_2, N_2, O_2 and air) for pure PLA film and PLA film with (0.2, 0.5, 1, 2, 3 and 5 wt.%) of silica.

CONCLUSIONS

In this article, the properties of poly (lactic acid) (PLA)/SiO_2 nanocomposites were investigated.

Neat PLA films and PLA films with different percentage of hydrophobic fumed silica nanoparticles (0.2, 0.5, 1, 2, 3 and 5 wt.%) were prepared by solution casting method. The results of conducted investigations have shown that the addition of the lowest silica content (0.2 and 0.5 wt.%) has a significant influence on polymer material behavior. In particular, PLA with 0.2 wt.% of silica nanoparticles showed an increase in degree of crystallinity, improvement in mechanical (the highest improvement in tensile strength respect to other compositions) and barrier properties of PLA, which were the drawbacks of neat polymer. The mechanical properties of the investigated nanocomposites were get-

REFERENCES

[1] M. Jamshidian, E.A. Tehrany, M. Imran, M. Jacquot, S. Desobry, Poly-Lactic Acid: Production, Applications, Nanocomposites, and Release Studies, Compr. Rev. Food. Sci. F. **9** (2010) 552–571.

[2] X. Wen, Y. Lin, C. Han, K. Zhang, X. Ran, Y. Li, L. Dong, Thermomechanical and optical properties of biodegradable poly(L-lactide)/silica nanocomposites by melt compounding, J. Appl. Polym. Sci. **114** (2009) 3379––3388.

[3] J.W. Huang, Y. Chang Hung, Y.L. Wen, C.C. Kang, M.Y. Yeh, Polylactide/nano and microscale silica composite films. I. Preparation and characterization, J. Appl. Polym. Sci. **112** (2009) 1688–1694.

[4] C.C. Chen, J.Y. Chueh, H. Tseng, H.-M. Huang, S.Y. Lee, Preparation and characterization of biodegradable PLA polymeric blends, Biomaterials **24** (2003) 1167–1173.

[5]   Y. Li, C. Han, J. Bian, L. Han, L. Dong, G. Gao, Rheology and biodegradation of polylactide/silica nanocomposites, Polym. Compos. **33** (2012) 1719–1727.

[6]   C. Silvestre, D. Duraccio, S. Cimmino, Food packaging based on polymer nanomaterials, Prog. Polym. Sci. **36** (2011) 1766–1782.

[7]   M.D. Sanchez-Garcia, A. Lopez-Rubio, J.M. Lagaron, Natural micro and nanobiocomposites with enhanced barrier properties and novel functionalities for food bio-packaging applications, Trends Food. Sci. Tech. **21** (2010) 528–536.

[8]   J.M. Lagaron, A. Lopez-Rubio, Nanotechnology for bio-plastics: opportunities, challenges and strategies, Trends Food. Sci. Tech. **22** (2011) 611–617.

[9]   X. Wen, K. Zhang, Y. Wang, L. Han, C. Han, H. Zhang, S. Chen, L. Dong, Study of the thermal stabilization mechanism of biodegradable poly(L-lactide)/silica nanocomposites, Polym. Int. **60** (2011) 202–210.

[10] L. Petersson, K. Oksman, Biopolymer based nanocomposites: Comparing layered silicates and microcrystalline cellulose as nanoreinforcement, Compos. Sci. Technol. **66** (2006) 2187–2196.

[11] R.M. Rasal, A.V. Janorkar, D.E. Hirt, Poly(lactic acid) modifications, Prog. Polym. Sci. **35** (2010) 338–356.

[12] J. Li, D. Chen, B. Gui, M. Gu, J. Ren, Crystallization morphology and crystallization kinetics of poly(lactic acid): effect of *N*-aminophthalimide as nucleating agent, Polym. Bull. **67** (2011) 775–791.

[13] J. Zhang, J. Lou, S. Ilias, P. Krishnamachari, J. Yan, Thermal properties of poly(lactic acid) fumed silica nanocomposites: Experiments and molecular dynamics simulations, Polymer **49** (2008) 2381–2386.

[14] J.W. Rhim, Effect of PLA lamination on performance characteristics of agar/*κ*-carrageenan/clay bio-nanocomposite film, Food. Res. Int. **51** (2013) 714–722.

[15] K. Nuñez, C. Rosales, R. Perera, N. Villarreal, J.M. Pastor, Nanocomposites of PLA/PP blends based on sepiolite, Polym. Bull. **67** (2011) 1991–2016.

[16] A. Dorigato, M. Sebastiani, A. Pegoretti, L. Fambri, Effect of Silica Nanoparticles on the Mechanical Performances of Poly(lactic Acid), J. Polym. Environ. **20** (2012) 713––725.

[17] T.V. Duncan, Applications of nanotechnology in food packaging and food safety: Barrier materials, antimicrobials and sensors, J. Colloid. Interface. Sci. **363** (2011) 1–24.

[18] M. Pluta, Morphology and properties of polylactide modified by thermal treatment, filling with layered silicates and plasticization, Polymer **45** (2004) 8239–8251.

[19] O. Bera, B. Pilić, J. Pavličević, M. Jovičić, B. Holló, K.M. Szécsényi, M. Špirkova, Preparation and thermal properties of polystyrene/silica nanocomposites, Thermochim. Acta. **515** (2011) 1–5.

[20] M.L. Di Lorenzo, Calorimetric analysis of the multiple melting behavior of poly(L-lactic acid), J. Appl. Polym. Sci. **100** (2006) 3145–3151.

[21] G.Z. Papageorgiou, D.S. Achilias, S. Nanaki, T. Beslikas, D. Bikiaris, PLA nanocomposites: Effect of filler type on non-isothermal crystallization, Thermochim. Acta. **511** (2010) 129–139.

[22] H. Li, M.A. Huneault, Effect of nucleation and plasticization on the crystallization of poly(lactic acid), Polymer **48** (2007) 6855–6866.

[23] D. Fragiadakis, P. Pissis, L. Bokobza, Glass transition and molecular dynamics in poly(dimethylsiloxane)/silica nanocomposites, Polymer **46** (2005) 6001–6008.

[24] P. Pan, Y. Inoue, Polymorphism and isomorphism in biodegradable polyesters, Prog. Polym. Sci. **34** (2009) 605–640.

[25] M. Drieskens, R. Peeters, J. Mullens, D. Franco, P.J. Lemstra, D.G. Hristova-Bogaerds, J. Polym. Sci., B: Polym. Phys. **47** (2009) 2247–2258.

IZVOD

UTICAJ DODATKA HIDROFOBNIH NANOČESTICA SILICIJUM(IV)-OKSIDA NA SVOJSTVA POLI(MLEČNE KISELINE)

Branka M. Pilić[1], Tanja I. Radusin[2], Ivan S. Ristić[1], Clara Silvestre[3], Vera L. Lazić[1], Sebastian S. Baloš[4], Donatella Duraccio[3]

[1]*Tehnološki fakultet, Univerzitet u Novom Sadu, Novi Sad, Srbija*
[2]*Institut za prehrambene tehnologije, Univerzitet u Novom Sadu, Novi Sad, Srbija*
[3]*Institute of Chemistry and Technology of Polymers (ICTP), National Research Council (CNR), Pozzuoli Naples, Italy*
[4]*Departman za proizvodno mašinstvo, Fakultet tehničkih nauka, Univerzitet u Novom Sadu, Novi Sad, Srbija*

(Naučni rad)

Poli(mlečna kiselina) (PLA) predstavlja jedan od najpopularnijih komercijalnih biorazgradivih materijala. Iako može da zameni neke od najčešće korišćenih sintetskih polimera, neke njegove osobine još uvek predstavljaju prepreku u široj primeni, posebno u pakovanju hrane. Poboljšanje osobina PLA može se postići primenom nanotehnologija. U ovom radu ispitan je uticaj dodatka različitih koncentracija hidrofobnih nanočestica silicijum(IV)-oksida (od 0,2 do 5 mas.%) na toplotna, mehanička, i barijerna svojstva čiste PLA. Morfološke karakteristike uzoraka nanokompozita snimljene su pomoću skenirajuće elektronske mikroskopije (SEM). Toplotna svojstva poli(mlečne kiseline) i pripremljenih nanokompozita proučavana su primenom diferencijalnog skenirajućeg kalorimetra (DSC), dok je stepen kristaliničnosti određen pomoću širokougaone difrakcije X-zracima (WAXD). Mehanička svojstva su ispitivana da bi se odredio uticaj dodatka nanočestica SiO_2 na PLA polimernu matricu. Disperzija nanočestica je izuzetno dobra za koncentracije silicijum(IV)-oksida do 1%, nakon čega dolazi do stvaranja manjih aglomerata. Dalje uvećanje udela SiO_2 (do 5 mas.%) uzrokuje stvaranje većih aglomerata i površinskih nepravilnosti unutar polimerne matrice. Uočeno je da se dodatkom male koncentracije SiO_2 postižu značajna poboljšanja mehaničkih i barijernih svojstava. Do povećanja stepena kristaliničnosti i temperature prelaska u staklasto stanje T_g dolazi samo za koncentracije od 0,2 i 0,5 mas.% SiO_2 dok za ostale koncentracije dolazi do pada ovih vrednosti. Ovakvo ponašanje veovatno je uzrokovano stvaranjem aglomerata za veće udele SiO_2.

Fe–Mo alloy coatings as cathodes in chlorate production process

Ljiljana M. Gajić-Krstajić[1], Nevenka R. Elezović[2], Borka M. Jović[2], Gian N. Martelli[3], Vladimir D. Jović[2], Nedeljko V. Krstajić[4]

[1]Institute of Technical Sciences SASA, Belgrade, Serbia
[2]Institute for Multidisciplinary Research, University of Belgrade, Belgrade, Serbia
[3]Industrie De Nora S.p.A., Milan, Italy
[4]Faculty of Technology and Metallurgy, University of Belgrade, Belgrade, Serbia

Abstract

The aim of this study was to gain a better understanding of the feasibility of partial replacement of dichromate, Cr(VI), with phosphate buffer, focusing on the cathode reaction selectivity for hydrogen evolution on mild steel and Fe–Mo cathodes in undivided cell for chlorate production. To evaluate the ability of phosphate and Cr(VI) additions to hinder hypochlorite and chlorate reduction, overall current efficiency (CE) measurements in laboratory cell for chlorate production on stationary electrodes were performed. The concentration of hypochlorite was determined by a conventional potentiometric titration method using 0.01 mol dm^{-3} As_2O_3 solution as a titrant. The chlorate concentration was determined by excess of 1.0 mol dm^{-3} As_2O_3 solution and excess of arsenic oxide was titrated with 0.1 mol dm^{-3} $KBrO_3$ solution in a strong acidic solution. Cathodic hypochlorite and chlorate reduction were suppressed efficiently by addition of 3 g dm^{-3} dichromate at both cathodes, except that Fe–Mo cathode exhibited higher catalytic activity for hydrogen evolution reaction (HER). The overvoltage for the HER was around 0.17 V lower on Fe–Mo cathode than on mild steel at the current density of 3 kA m^{-2}. It was found that a dichromate content as low as 0.1 g dm^{-3} is sufficient for complete suppression of cathodic hypochlorite and chlorate reduction onto Fe-Mo catalyst in phosphate buffering system (3 g dm^{-3} Na_2HPO_4 + NaH_2PO_4). The overall current efficiency was practically the same as in the case of the presence of 3 g dm^{-3} dichromate buffer (98%). However, for the mild steel cathode, the overall current efficiency for the chlorate production was somewhat lower in the above mentioned mixed phosphate + dichromate buffering system (95%) than in the pure dichromate buffering solution (97.5%).

Keywords: chlorate production, current efficiency, Fe–Mo cathode catalyst, phosphate buffer.

Available online at the Journal website: http://www.ache.org.rs/HI/

Sodium chlorate, $NaClO_3$, is mainly used for the production of chlorine dioxide, ClO_2, a bleaching agent in the pulp and paper industry. In the electrolytic sodium chlorate production, the main electrode reactions are hydrogen and chlorine formation (reactions (1) and (2)) similar to those in the chlor-alkali process. As chlorate cells are undivided, chlorine undergoes hydrolysis and disproportionates to form hypochlorous acid and hypochlorite (reactions (3) and (4)). Maximal current yield in chlorate production is obtained when the conversion of the hypochlorous species into chlorate occurs only directly by the Foerster reaction of chemical chlorate formation [1] (reaction (5)). The optimum rate of reaction (5) takes place at pH of 6–7 and, accordingly, the electrolyte should be set in that pH range.

$$2H_2O + 2e^- \rightarrow H_2 + 2OH^- \tag{1}$$

$$2Cl^- \rightarrow Cl_2 + 2e^- \tag{2}$$

$$Cl_2 + H_2O \rightarrow HClO + H^+ + Cl^- \tag{3}$$

$$HClO \rightleftarrows H^+ + ClO^- \tag{4}$$

$$2HClO + ClO^- \rightarrow ClO_3^- + 2H^+ + 2Cl^- \tag{5}$$
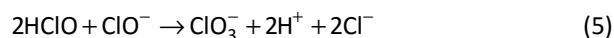
The second and almost unavoidable path represents another Foerster reaction of further anodic oxidation of hypochlorite to the final state:

$$6ClO^- + 2H_2O \rightarrow 2ClO_3^- + 4H^+ + 4Cl^- + O_2 + 6e^- \tag{6}$$
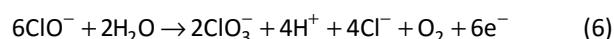
This is also known as the reaction of electrochemical chlorate formation [2] and represents the corresponding current losses.

In addition to the hydrogen evolution reaction, two other reduction processes could theoretically take place at the cathode and would lead to further current losses:

$$ClO^- + H_2O + 2e^- \rightarrow Cl^- + 2OH^- \tag{7}$$

$$ClO_3^- + 3H_2O + 6e^- \rightarrow Cl^- + 6OH^- \qquad (8)$$
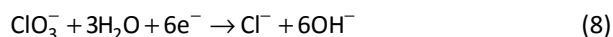
DSA$^\circledR$ anode or platinum–iridium-coated titanium are currently used as anodes and their high electro-catalytic activity for chloride oxidation ensures that, apart from the Foerster reaction of electrochemical chlorate formation (Eq. (6)), the current losses due to anodic water oxidation can be completely neglected because of the much more positive potential for this reaction.

Cathodic current losses have so far been efficiently suppressed by addition of small amounts of dichromate (about 2–4 g dm^{-3}), after Müller [3], which also acts as a pH buffer providing and maintaining the optimal pH range for the chemical conversion of available chlorine to chlorate, and alters the potential of the DSA$^\circledR$ anode [4]. In addition, the chromate may have a retarding effect on the corrosion of steel cathodes [5]. During cathodic polarization Cr(VI) becomes reduced to Cr(III) and forms a thin film of chromium(III) hydroxide on the cathode [6]. This film hinders the unwanted side reactions (7) and (8), while hydrogen evolution can still take place, though with changed kinetics [7]. The thickness and growth rate of the chromium(III) hydroxide film depends on factors such as: the cathode material, the electrode potential and the chromate concentration [8]. Although low chromate concentration as 0.1 g dm^{-3} Cr$_2$O$_7^{2-}$ has been shown to efficiently hinder reduction of Fe(CN)$_6^{3-}$ on smooth platinum electrode [9], in the chlorate production the concentration of dichromate should be much higher (3–8 g dm^{-3}) [10]. However, a higher overpotential for hydrogen evolution reaction (HER) was obtained for iron and platinum in the presence of Cr(VI) [11]. The overpotential of the HER on mild steel is quite high (about 500 mV) in the presence of dichromate, which directly affects the specific power consumption. It is estimated that power consumption can be lowered by 10–15%, if the overpotential of the HER is reduced by 100 mV [12]. The presence of dichromate in addition to the chlorate crystals appears to be undesirable in the chlorine dioxide generation process, since both salts (chlorate and dichromate) are highly soluble and it is difficult to separate them by crystallization. Dichromate in the chlorate liquor must be less than 0.5 wt.% during sodium chlorate crystallization [13], otherwise the crystal product will exhibit a characteristic yellowish color.

Many attempts have been made so far to replace, or at least to reduce, the dichromate content in the electrolyte of chlorate cells. The aim of the present paper is to present some achievements in this respect.

EXPERIMENTAL PROCEDURE AND APPARATUS

Determination of the hypochlorite and chlorate concentrations using an improved potentiometric titration method

In our experiments the following procedure was found to give sufficiently accurate results: the sum of the concentrations of available chlorine (hypochlorite, hypochlorous acid, and dissolved molecular chlorine) and the concentration of chlorate were determined using an improved potentiometric titration method, based on a procedure given by Norkus and Prokopchik [14].

Solution for determination of the hypochlorite concentration

The concentration of hypochlorite was determined by a conventional potentiometric titration method using 0.01 mol dm^{-3} As$_2$O$_3$ solution as a titrant. Reaction between As$_2$O$_3$ and active chlorine can be presented by the following equation:

$$As_2O_3 + 2ClO^- \rightarrow As_2O_5 + 2Cl^- \qquad (9)$$
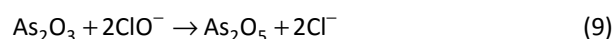
Solution for determination of the chlorate concentration

The chlorate concentration was determined by excess of 1.0 mol dm^{-3} As$_2$O$_3$ solution and excess of arsenic oxide was titrated with 0.1 mol dm^{-3} KBrO$_3$ solution in a strong acidic solution.

For potentiometric determination of chlorate it is necessary to prepare the following solutions: 1.0 mol dm^{-3} As$_2$O$_3$; 0.1 mol dm^{-3} KBrO$_3$; 37 wt.% HCl; 30 g dm^{-3} NaBr.

The reactions between arsenic oxide and chlorate and bromate are given as:

$$3As_2O_3 + 2ClO_3^- \rightarrow 3As_2O_5 + 2Cl^- \qquad (10)$$

$$3As_2O_3 + 2BrO_3^- \rightarrow 3As_2O_5 + 2Br^- \qquad (11)$$
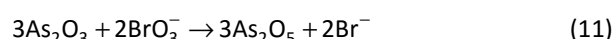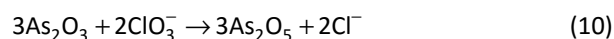
The unknown concentration of chlorate can be calculated by the following equation:

$$c(ClO_3^-) = \frac{c(As_2O_3)V(As_2O_3)}{1.5} - c(BrO_3^-)V(BrO_3^-) \qquad (12)$$

where: $c(As_2O_3)$ – the concentration of arsenic oxide solution added in excess, after reaching the hypochlorite endpoint (1.0 mol dm^{-3}); $V(As_2O_3)$ – the volume of arsenic oxide solution added in excess, after reaching the hypochlorite endpoint (2 cm^3); $c(BrO_3^-)$ – the concentration of bromate solution for potentiometric titration of arsenic oxide excess (0.1 mol dm^{-3}); $V(BrO_3^-)$ – the volume of bromate solution for potentiometric titration of arsenic oxide excess.

Analytical

The sample of 1 cm^3 was taken from the electrolyte solution at suitable intervals during the electrolysis. The analytical procedure was carried on at room temperature. After addition of some saturated solution of sodium bicarbonate to the sample, available chlorine was titrated potentiometrically with a solution of 0.01 mol dm^{-3} As$_2$O$_3$ in a 100 cm^3 beaker containing a platinum ring electrode and a calomel reference electrode (SCE). Before each run the platinum electrode was shortly immersed in a mixture of concentrated sulfuric and nitric acids and thoroughly washed with distilled water. After reaching the hypochlorite endpoint excess arsenic oxide solution was added (2 cm^3 of 1.0 mol dm^{-3} As$_2$O$_3$), some sodium bromide solution (about 30 mg, or 1 cm^3 of 30 g dm^{-3} NaBr solution) and a volume of chemically pure concentrated hydrochloric acid approximately equal to the solution volume already present in the beaker. The solution which contained now at least 20 wt.% HCl was then allowed to stand for 5–7 min. After that time the excess As$_2$O$_3$ was titrated potentiometrically with 0.1 mol dm^{-3} KBrO$_3$ solution. The relative potential change was followed using a potentiometer. The shape of the potentiometric titration curves is illustrated in Fig. 1. The accuracy of the chlorate concentration values determined by the described method was better than ±2%, for chlorate concentrations not smaller than 0.001 mol dm^{-3}.
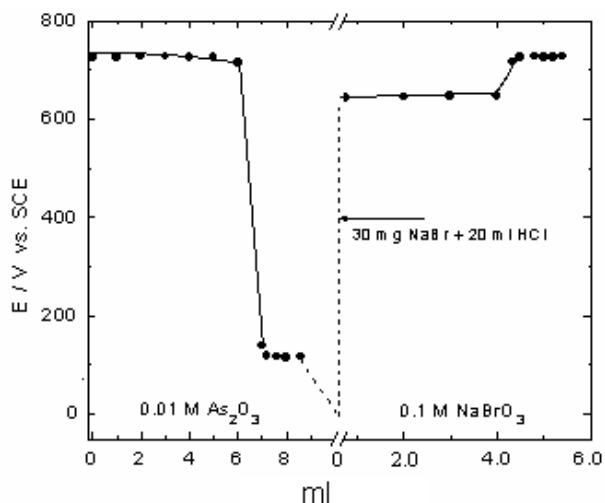
Fig.1. Potentiometric titration curves for hypochlorite and chlorate with As$_2$O$_3$.

Apparatus for simulation of chlorate production process

The experimental set-up is shown schematically in Fig. 2. The temperature throughout the whole volume was maintained constant by circulating the thermostatic liquid through a glass cooling coil situated in back-mix flow reactor. The desired pH value within the

entire volume was controlled by adding 37 wt.% hydrochloric acid from an automatic titrator. The electrical set-up consisted of a constant d.c. supply, a multirange Amper–Volt-meter with a high internal impedance. Two types of cathodes (mild steel and Fe–Mo alloy coated mild steel) and activated titanium DSA® anode were used in the experiments. The electrodes had a rectangular shape (4 cm×5 cm) with a projected surface area of 20 cm^2, and were placed face to face in a vertical position with an interelectrode gap of 3 mm to form the main part of the cell. Intensive electrolyte flow within the cell was provided by the gas-lifting effect of cathodically generated hydrogen. The high recirculation rate led to a negligible difference in the available chlorine and chlorate contents in the cell and in the total volume of electrolyte.
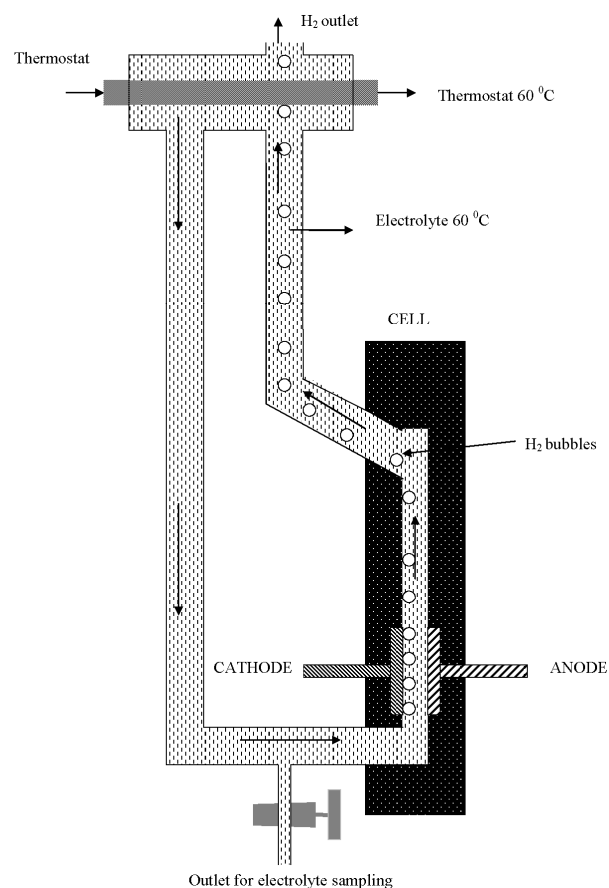
Fig. 2. The experimental set-up for continuous flow chlorate cell process.

Working conditions

Starting solutions: A) 300 g dm^{-3} NaCl + 3 g dm^{-3} K$_2$Cr$_2$O$_7$; B) 300 g dm^{-3} NaCl + 3 g dm^{-3} (NaH$_2$PO$_4$ + Na$_2$HPO$_4$) + 0.1 g dm^{-3} K$_2$Cr$_2$O$_7$; temperature 60±2 °C; pH 6.3–6.6; total volume of electrolyte, 0.3 dm^3; current density, 2.5 kA m^{-2} (active surface area = 20 cm^2, and total current *I* = 5 A); anode: activated titanium

anode (35 mol.% RuO_2 + 65 mol.% TiO_2 with 10 g m^{-2} RuO_2, home-made); cathode: 1) mild steel; 2) mild steel coated with Fe–Mo alloy catalyst.

Preparation of Fe–Mo alloy coatings onto mild steel

The mild steel substrates were first degreased in NaOH-saturated ethanol solution for 5 min. and then etched by immersion in 25 wt.% HCl for 2 min. After this procedure sample was washed with distilled water, dried and weighted and then immersed in the solution for Fe–Mo alloy deposition. After deposition samples were washed, dried and weighted again to determine the mass of the alloy. All solutions were made using distilled water and analytical grade chemicals.

Fe–Mo alloys were deposited at a constant current density of –100 mA cm^{-2} from the plating bath with the following composition: 9 g dm^{-3} $FeCl_3$, 40 g dm^{-3} Na_2MoO_4, 75 g dm^{-3} $NaHCO_3$ and 45 g dm^{-3} $Na_4P_2O_7$ at 60 °C. A Pt mesh, placed parallel to the cathode, was used as a counter electrode during the alloy deposition and electrolyte was moderately stirred with the magnetic stirrer. Fe–Mo coating thickness was approximately 20 μm consisting of 47 mass% Mo and 53 mass% Fe (energy dispersive X-ray spectroscopy (EDS) analysis was used to determine alloy composition). Certain amount of oxygen was also detected, but the content was calculated neglecting detected amount of oxygen.

Polarization curve measurements

Polarization curve measurements for mild steel and Fe–Mo alloy coatings were performed with the potentiostat Reference 600 and software DC 105 in a standard electrochemical cell. Potential was changed with a rate of 1 mV s^{-1} and was corrected for the IR_Ω drop by current interrupt technique. Silver/silver chloride electrode (Ag/AgCl) was used as a reference electrode, while Pt mesh was used as a counter electrode. Before recording polarization diagrams electrodes were exposed to hydrogen evolution in the same solution at $j =$ = –0.1 A cm^{-2} for 10 min.

RESULTS AND DISCUSSION

Polarization measurements in the absence and presence of phosphate and dichromate

Polarization diagrams for mild steel and Fe–Mo alloy coatings, recorded in the solution containing 300 g dm^{-3} NaCl + 150 g dm^{-3} $NaClO_3$ at 60 °C are presented in Fig. 3a, while those recorded in the phosphate buffering system (solution B) with addition of different amounts of $K_2Cr_2O_7$ are shown in Fig. 3b. As can be seen the addition of dichromate influences polarization curves for both electrodes, changing (increasing) their slopes at lower current densities. More pronounced influence of the addition of phosphate buffer and

(a)   (b)
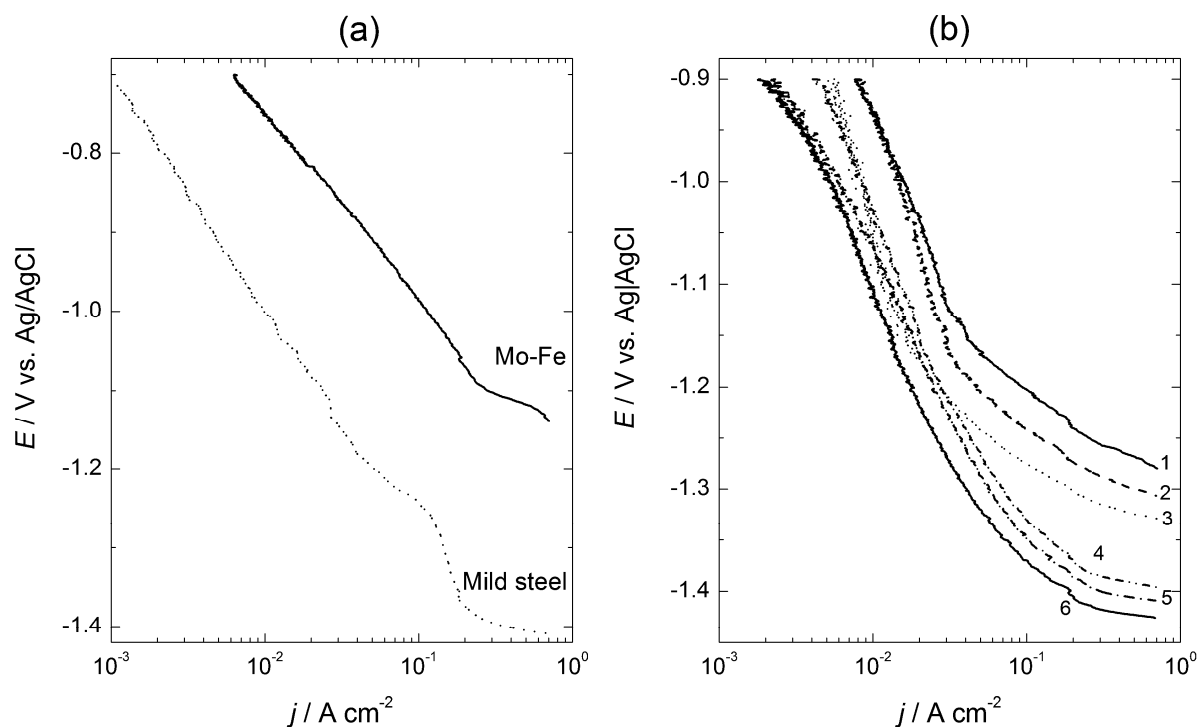
Fig. 3. a) Polarization diagrams for mild steel and Fe–Mo alloy coatings recorded in the solution containing 300 g dm^{-3} NaCl + 150 g dm^{-3} NaClO$_3$ at 60 °C. b) Polarization diagrams for mild steel (4–6) and Fe–Mo (1–3) alloy coatings recorded in the solution containing 300 g dm^{-3} NaCl + 150 g dm^{-3} NaClO$_3$ at 60 °C in the phosphate buffering system (3 g dm^{-3} (NaH$_2$PO$_4$ + Na$_2$HPO$_4$)) with addition of dichromate: 1 and 4–0.05 g dm^{-3} K$_2$Cr$_2$O$_7$; 2 and 5 – 0.10 g dm^{-3} K$_2$Cr$_2$O$_7$; 3 and 6 – 1.00 g dm^{-3} K$_2$Cr$_2$O$_7$.

dichromate on the potential has been detected for the Fe–Mo cathode (increasing overvoltage for about 0.1 V). It is interesting to note that with increasing amount of dichromate catalytic activity of both electrodes decreases, indicating that the addition of very small amount of dichromate (0.05 g dm^{-3}) would be satisfactory for preventing hypochlorite and chlorate reduction on the cathode surface in the investigated system.

Chlorate cell process with dichromate buffer (commercial electrolyte)

The values of the hypochlorite and chlorate concentrations during the electrolysis of solution A with the mild steel and with Fe–Mo cathodes, obtained in the apparatus schematically presented in Fig. 2, are given in Tables 1 and 2, respectively.

As can be seen from Tables 1 and 2, significant difference is recorded for the cell voltage, being for about 0.15 V lower for the Fe–Mo cathode, while other parameters are very similar.

The corresponding faradaic yields for chlorate cell process are presented in Fig. 4a. Slightly better faradaic

yields have been achieved with Fe–Mo cathode. The results presented in Tables 1 and 2 (cell voltage) and in Fig. 4a (faradaic yield, η_j) clearly indicate higher catalytic activity for the hydrogen evolution reaction on the Fe–Mo alloy coating (lower amount of the ClO$^-$ could be reduced at the cathode surface) in comparison with that on mild steel cathode in the presence of dichromate buffer.

The voltage *vs*. current characteristics for the cell with the mild steel and the Fe–Mo alloy coating as cathodes are presented in Fig. 4b. As can be seen the difference between the cell voltage with mild steel and Fe–Mo alloy coating becomes more pronounced at higher current densities, reaching the value of about 0.17 V at the current density of 3 kA m^{-2}.

Chlorate cell process with phosphate buffer

As already mentioned cathodic current losses during chlorate production have so far been efficiently suppressed by small addition of dichromate (3–5 g dm^{-3}) [2]. In fact, dichromate provides several benefits for the electrochemical process of chlorate production: a)

Table 1. Hypochlorite and chlorate concentrations, pH, temperature and cell voltage during chlorate cell process: starting solution 300 g dm^{-3} NaCl + 3 g dm^{-3} K$_2$Cr$_2$O$_7$; I = 5 A; mild steel cathode

τ / h	pH	t / °C	Cell voltage, V	c(ClO$^-$) / mol dm^{-3}	c(ClO$_3^-$) / mol dm^{-3}
0.0	6.41	61.0	3.17	–	–
1.0	6.48	61.5	3.15	0.070	0.098
1.5	6.46	61.0	3.16	0.06	0.148
2.0	6.58	61.3	3.16	0.06	0.200
3.0	6.50	62.0	3.14	0.06	0.299
3.5	6.59	62.0	3.14	0.06	0.350
4.0	6.6	61.8	3.15	0.06	0.400
5.0	6.59	61.4	3.16	0.06	0.491
6.0	6.48	60.8	3.15	0.06	0.600
6.5	6.6	61.0	3.15	0.06	0.650
7.0	6.52	61.2	3.16	0.06	0.700
8.0	6.47	61.4	3.16	0.065	0.798

Table 2. Hypochlorite and chlorate concentrations, pH, temperature and cell voltage during chlorate cell process: starting solution 300 g dm^{-3} NaCl + 3 g dm^{-3} K$_2$Cr$_2$O$_7$; I = 5 A; Fe–Mo coating cathode

τ / h	pH	t / °C	Cell voltage, V	c(ClO$^-$) / mol dm^{-3}	c(ClO$_3^-$) / mol dm^{-3}
0.0	6.42	61.0	3.01	–	–
0.25	6.48	61.5	3.02	0.055	0.024
0.67	6.18	61.0	3.02	0.06	0.067
1.0	6.42	61.3	3.01	0.06	0.100
2.0	6.36	62.0	3.01	0.06	0.202
3.0	6.37	62.0	3.02	0.06	0.304
4.0	6.58	61.8	3.01	0.06	0.405
5.3	6.52	61.4	3.02	0.06	0.537
6.0	6.58	60.8	3.01	0.06	0.607
7.0	6.24	61.0	3.01	0.055	0.709
8.0	6.39	61.2	3.02	0.06	0.810

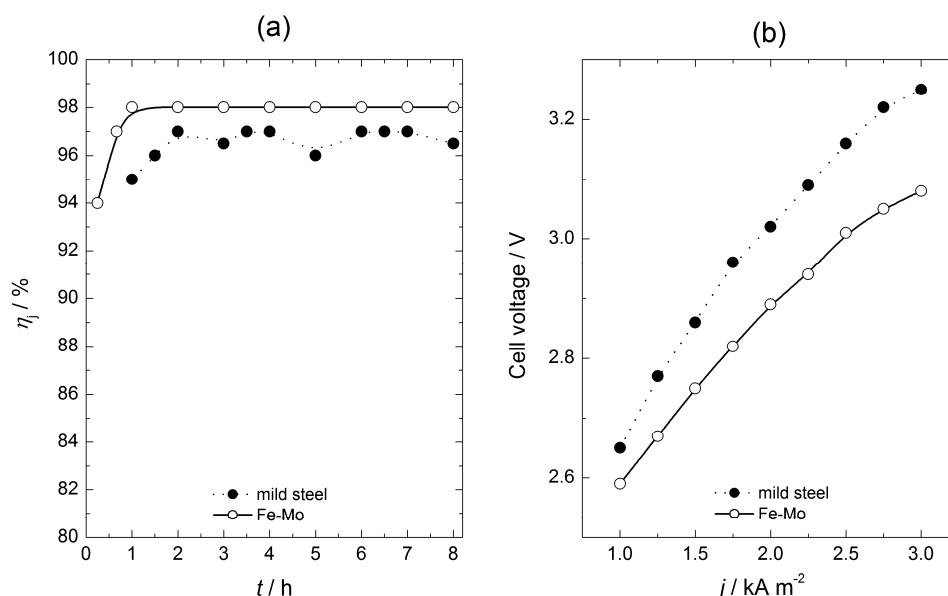*Fig. 4. a) Faradaic yields for chlorate cell process with dichromate buffer (3 g dm^{-3} K$_2$Cr$_2$O$_7$) for different cathode materials. b) Cell voltage vs. current density for chlorate cell process with dichromate buffer (3 g dm^{-3} K$_2$Cr$_2$O$_7$) for different cathode materials.*

completely suppresses the hypochlorite reduction at the cathode; b) provides and maintains the optimal pH region for the chemical conversion of available hypochlorite to chlorate; c) prevents the corrosion of the steel cathode. However, the presence of dichromate in addition to chlorate crystals appears to be undesirable in the chlorine dioxide generation process, and since both salts (chlorate and chromate) are highly soluble it is difficult to separate them by crystallization. Thus, many attempts have been made to replace, or at least to reduce, the dichromate content in the electrolyte of chlorate cells. The aim of the present investigations is to present the experimental results for chlorate production for two types of cathode materials for the following buffering system: a proper mixture of primary and secondary phosphate buffer (3 g dm^{-3} in total) + 0.1 g dm^{-3} dichromate. For above maintained buffering system dichromate is in an almost negligible amount, for 12–15 times lower than the content in normal industrial practice.

The values of the hypochlorite and chlorate concentrations during the electrolysis of solution B with the mild steel and the Fe–Mo alloy coating cathodes are presented in Tables 3 and 4, respectively.

Considering the results presented in Tables 3 and 4 the same conclusion, as in the case of the commercial electrolyte (Tables 1 and 2), can be made. The obtained results can be explained by different competitive phosphate and dichromate ions adsorption onto mild steel and Fe–Mo electrodes.

Figure 5 shows the experimentally achieved dependence of the faradaic yields of chlorate production during the electrolysis for both cathodes in phosphate buffering system. It was found in the present investigation that a dichromate content as low as 0.1 g dm^{-3} is adequate for complete protection against cathodic hypochlorite reduction onto Fe–Mo catalyst and faradaic yields are practically the same as in the case of the presence of 3 g dm^{-3} dichromate buffer. However, for the mild steel cathode, the faradic yields for the chlor-

Table 3. Hypochlorite and chlorate concentrations, pH, temperature and cell voltage during chlorate cell process: starting solution 300 g dm^{-3} NaCl + 3 g dm^{-3} (Na$_2$HPO$_4$ + NaH$_2$PO$_4$) + 0.1 g dm^{-3} K$_2$Cr$_2$O$_7$; I = 5 A; mild steel cathode

τ / h	pH	t / °C	Cell voltage, V	$c(ClO^-)$ / mol dm^{-3}	$c(ClO_3^-)$ / mol dm^{-3}
0.0	6.42	60.0	3.17	–	–
1.0	6.35	61.2	3.09	0.075	0.088
2.0	6.46	61.5	3.09	0.065	0.184
3.0	6.52	61.4	3.11	0.07	0.282
4.0	6.43	60.8	3.12	0.07	0.380
5.0	6.57	61.0	3.12	0.06	0.481
6.0	6.60	61.2	3.13	0.075	0.589
7.0	6.53	61.1	3.12	0.07	0.687
8.0	6.48	61.4	3.13	0.07	0.777

Table 4. Hypochlorite and chlorate concentrations, pH, temperature and cell voltage during chlorate cell process: starting solution 300 g dm^{-3} NaCl + 3 g dm^{-3} (Na$_2$HPO$_4$ + NaH$_2$PO$_4$) + 0.1 g dm^{-3} K$_2$Cr$_2$O$_7$; I = 5 A; Fe–Mo coating cathode

τ / h	pH	t / $^{\circ}$C	Cell voltage, V	c(ClO$^-$) / mol dm^{-3}	c(ClO$_3^-$) / mol dm^{-3}
0.0	6.40	60.0	3.00	–	–
1.0	6.44	61.3	2.97	0.060	0.100
2.0	6.70	61.5	2.97	0.065	0.202
3.0	6.77	62.0	2.97	0.060	0.304
4.0	6.45	61.4	2.96	0.060	0.405
5.0	6.65	61.5	2.96	0.060	0.506
6.0	6.60	61.0	2.97	0.060	0.607
7.0	6.62	61.2	2.97	0.060	0.672
8.0	6.52	61.1	2.97	0.055	0.810

ate production are somewhat lower in the phosphate buffering system (3 g dm^{-3} (NaH$_2$PO$_4$ + Na$_2$HPO$_4$)) with addition of 0.1 g dm^{-3} K$_2$Cr$_2$O$_7$ than in the dichromate buffering solution (commercial electrolyte, Fig. 4a).

It is interesting to note that the cell voltages are also somewhat lower (40–50 mV) in the phosphate buffering electrolyte with both types of cathode materials (Fig. 6), which could be of practical importance for industrial chlorate practice. The lower cell voltage could be explained by different influence of adsorbed phosphate or dichromate ions on the kinetics of the hydrogen evolution reaction at the investigated cathode materials. Some of the results presented in this paper are included in the recent international patent [15].
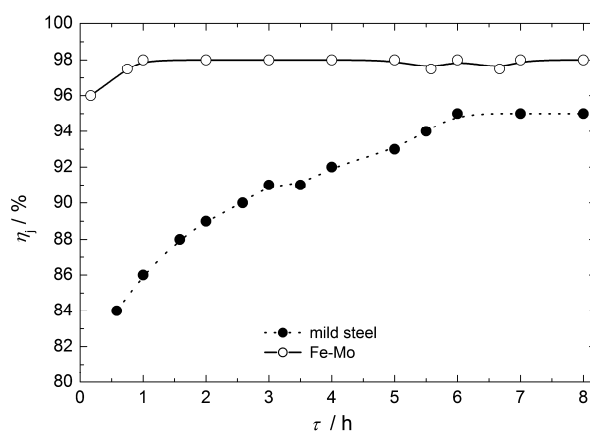
Fig. 5. The variation of faradaic yields in the chlorate cell process during electrolysis in phosphate buffering electrolyte (3 g dm^{-3} (Na$_2$HPO$_4$ + NaH$_2$PO$_4$)) with addition of 0.1 g dm^{-3} K$_2$Cr$_2$O$_7$ for mild steel and Fe–Mo cathode materials.
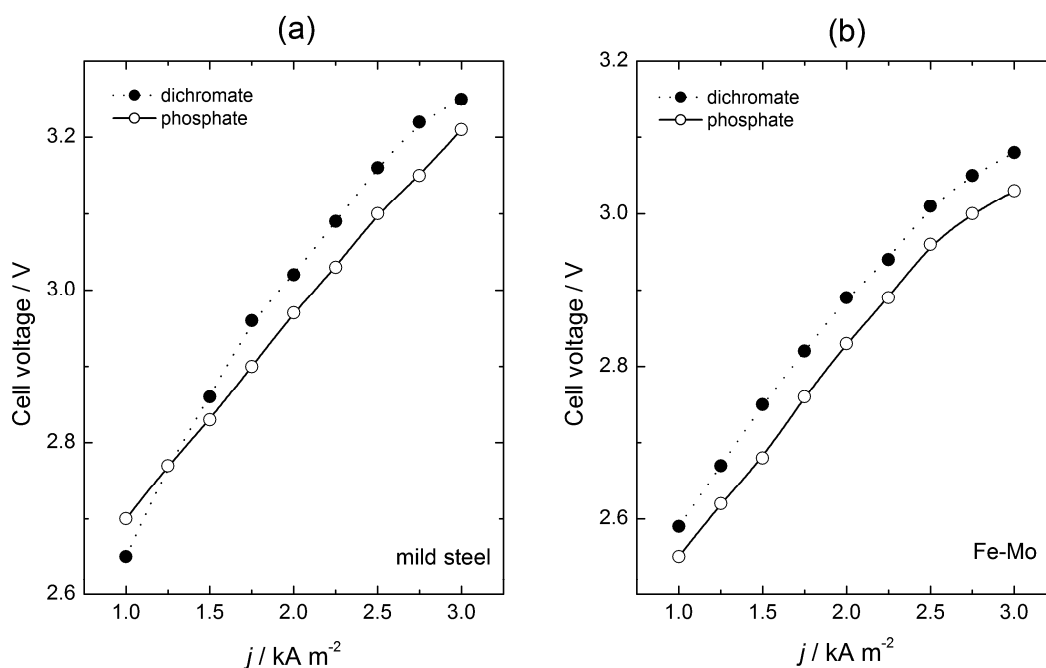
Fig. 6. Cell voltage vs. current density for chlorate cell process with dichromate (3 g dm^{-3} K$_2$Cr$_2$O$_7$) and phosphate buffers (3 g dm^{-3} (Na$_2$HPO$_4$ + NaH$_2$PO$_4$) + 0.1 g dm^{-3} K$_2$Cr$_2$O$_7$) for different cathode materials.

CONCLUSIONS

– Current efficiency experiments in pure dichromate buffering solution for chlorate production showed that high overall current efficiencies have been achieved at both mild steel and Fe-Mo cathodes.

– When starting the electrolysis, the current efficiency was initially low, but increased with time of electrolysis with the both cathode materials.

– Fe–Mo cathode exhibited the higher catalytic activity for the HER than the mild steel cathode**.** The difference between the cell voltage with mild steel and Fe––Mo alloy coating becomes more pronounced at higher current densities, reaching the value of about 0.17 V at the current density of 3 kA m^{-2}.

– It was found that a dichromate content as low as 0.1 g dm^{-3} is adequate for complete suppression of cathodic hypochlorite and chlorate reduction onto Fe––Mo catalyst in phosphate buffering system (3 g dm^{-3} Na_2HPO_4 + NaH_2PO_4). The overall current efficiency was practically the same as in the case of the presence of 3 g dm^{-3} dichromate buffer (98%).

– The overall current efficiency for the chlorate production with mild steel cathode was somewhat lower in the mixed phosphate + dichromate buffering system (95%) than in the pure dichromate buffering solution (97.5%).

– From the results obtained with stationary polarization measurements and the results of testing the process of chlorate production in the test cell (simulation of the industrial process) it could be concluded that the application of phosphate and dichromate buffering system with Fe–Mo alloy as a cathode might be promising technology for chlorate production.

REFERENCES

[1]   M.M. Jakšić, Mutual Effect of Current Density, pH, Temperature, and Hydrodynamic Factors on Current Efficiency in the Chlorate Cell Process, J. Electrochem. Soc. **121** (1974) 70–79.

[2]   F. Foerster, The Electrolysis of Hypochlorite Solutions, Trans. Am. Electrochem. Soc. **46** (1924) 23–50.

[3]   F. Müller, Über ein Elektrolytisches Verfahren zur Gewinnung der Chlor-, Brom- und Jodsauren Salze der Alkalien, Z. Elektrochem. **6** (1899) 469–476.

[4]   A. Cornell, B. Hakansson and G Lindbergh, Ruthenium-Based Dimensionally Stable Anode in Chlorate electrolysis. Effects of Electrolyte Composition on the Anode potential, J. Electrochem. Soc. **150** (2003) D6–D12.

[5]   K. Viswanathan, B.V. Tilak, Chemical, Electrochemical, and Technological Aspects of Sodium Chlorate Manufacture, J. Electrochem. Soc. **131** (1984) 1551–1559.

[6]   G. Lindbergh, D. Simonsson, The Effect of Chromate Addition on Cathodic Reduction of Hypochlorite in Hydroxide and Chlorate Solutions, J. Electrochem. Soc. **137** (1990) 3094–3099.

[7]   A.A. Tidblad, G. Lindbergh, Surface analysis with ESCA and GD-OES of the film formed by cathodic reduction of chromate, Electrochim. Acta **36** (1991) 1605–1610.

[8]   A.A. Tidblad, J. Martensson, *In situ* ellipsometric characterization of films formed by cathodic reduction of chromate, Electrochim. Acta **42** (1997) 389–398.

[9]   B.V. Tilak, K. Viswanathan, C. Rader, On the Mechanism of Sodium Chlorate Formation, J. Electrochem Soc. **128** (1981) 1228–1232.

[10] B.V. Tilak, K. Tari, C.L. Hoover, Metal Anodes and Hydrogen Cathodes: Their Activity Towards O_2 Evolution and ClO_3^- Reduction Reactions, J. Electrochem. Soc. **135** (1988) 1386–1392.

[11] Yu. V. Dobrov, L. M. Elina, Cathodic protection of Steel against Corrosion in Chlorate Solutions, Zashchita Metallov **3** (1967) 618–621.

[12] A. Cornell, D. Simonsson, In: T.C. Jeffery, J. Fenton, K. Ota, H. Kawamoto (Eds.), Proceedings of the Symposium on Chlor-Alkali and Chlorate Production and New Mathematical and Computational Methods in Electrochemical Engineering, PV 94–20. The Electrochemical Society, Pennington, 1993, pp. 191–200.

[13] A. Cornell, G. Lindbergh, D. Simonsson, The effect of addition of chromate on the hydrogen evolution reaction and on iron oxidation in hydroxide and chlorate solutions, Electrochim. Acta **37** (1992) 1873.

[14] P.K. Norkus, A.Yu. Prokopchik, Simultaneous Determination of Hypochlorites, Chlorites and Cheorates by Means of Arsenite, using OsO_4 as Catalyst, Zhur. Anal. Khim. **16** (1961) 336–339.

[15] N.V. Krstajić, V.D. Jović, G.N. Martelli, System for the electrolytic production of sodium chlorate, International Patent, WO 2007/063081 A2.

IZVOD

PREVLAKE OD Fe–Mo LEGURA KAO KATODE U PROIZVODNJI HLORATA

Ljiljana M. Gajić-Krstajić[1], Nevenka R. Elezović[2], Borka M. Jović[2], Gian N. Martelli[3], Vladimir D. Jović[2], Nedeljko V. Krstajić[4]

[1]*Institut tehničkih nauka, SANU, Knez Mihajlova 35, 11000 Beograd, Srbija*
[2]*Institut za multidisciplinarna istraživanja Univerziteta u Beogradu, Kneza Višeslava 1, 11030 Beograd, Srbija*
[3]*Industrie De Nora S.p.A., 20134 Milan, via Bistolfi 35, Italy*
[4]*Tehnološko–metalurški fakultet Univerziteta u Beogradu, Karnegijeva 4, 11000, Beograd, Srbija*

(Naučni rad)

Cilj ovih istraživanja je bio da se ispita mogućnost delimične zamene dihromata sa fosfatnim puferom u proizvodnji hlorata, razmatranjem pre svega njihovog uticaja na selektivne osobine mekog čelika i Fe–Mo katoda za izdvajanje vodonika. Da bi se ispitala sposobnost fosfata i dihromata u sprečavanju redukcije hipohlorita i hlorata kao sporednih reakcija, odredjivano je ukupno iskorišćenje struje u laboratorisjkoj ćeliji za proizvodnju hlorata sa stacionarnim elektrodama. Koncentracija hipohlorita je odredjivana standardnom potenciometrijskom titracijom korišćenjem rastvora 0,01 mol dm^{-3} As$_2$O$_3$, kao titranta. Koncentracija hlorata je odredjivana pri višku 1,0 mol dm^{-3} As$_2$O$_3$ rastvora, a neizreagovana koncentracija oksida arsena je titrisana sa 0,1 mol dm^{-3} KBrO$_3$ rastvorom u koncentrovanom kiselom rastvoru. Pokazano je da se katodna redukcija hipohlorita i hlorata može uspešno sprečiti dodatkom 3 g dm^{-3} dihromata na navedenim katodnim materijalima, s tim što je Fe–Mo katoda pokazala bolju katalitičku aktivnost za reakciju izdvajanja vodonika. Prenapetost izdvajanja vodnika je bila oko 0.17 V manja na Fe–Mo katodi nego na mekom čeliku, pri gustini struje od 3 kA m^{-2}. Ispitivanja su pokazala da je veoma niska koncentracija dihromata od svega 0,1 g dm^{-3} dovoljna za potpuno suzbijanje nepoželjnih katodni reakcija redukcije hipohlorita i hlorata na Fe–Mo katalizatoru u rastvoru sa fosfatnim puferom (3 g dm^{-3} Na$_2$HPO$_4$ + NaH$_2$PO$_4$). Postignuto je praktično isto iskorišćenje struje kao i u prisustvu 3 g dm^{-3} dihromata kao pufera (98%). Medjutim, iskorišćenje struje korišćenjem mekog čelika kao katodnog materijala je niže u prisustvu pomenutog mešovitog fosfatno-dihromatnog pufera (95%) nego u rastvoru sa dihromatnim puferom (97,5%).

Kvalitet fermentisanog napitka od surutke i mleka

Marica B. Rakin[1], Maja Lj. Bulatović[1], Danica B. Zarić[2], Marijana M. Stamenković Đoković[3], Tanja Ž. Krunić[4], Milka M. Borić[1], Maja S.Vukašinović Sekulić[1]

[1]*Tehnološko–metalurški fakultet, Univerzitet u Beogradu, Beograd, Srbija*
[2]*IHIS Tehnoexperts d.o.o, Beograd, Srbija*
[3]*IHIS Naučno–tehnološki park Zemun, Beograd, Srbija*
[4]*Inovacioni Centar Tehnološko–metalurškog fakulteta, Univerzitet u Beogradu, Beograd, Srbija*

Izvod

Jedan od najekonomičnijih načina prerade surutke predstavlja proizvodnja napitaka kojom se u okviru samo jednog procesa iskorišćavaju svi potencijali surutke kao sirovine. Funkcionalne i senzorne karakteristike napitaka na bazi surutke su kriterijum koji je od presudnog značaja za plasiranje proizvoda na tržište i pridobijanje potrošača. Cilj ovog rada je bio određivanje nutritivnih i funkcionalnih karakteristika fermentisanog napitka od surutke i mleka dobijenog primenom komercijalne ABY-6 kulture. Rezultati su pokazali da se primenjena starter kultura može koristiti za proizvodnju fermentisanog napitka od surutke i mleka sa zadovoljavajućim nutritivnim svojstvima. Dodatak mleka bio je bitan ne samo za nutritivni kvalitet nastalog proizvoda, nego je poboljšao i njegov ukus, homogenost i stabilnost. Analiza hemijskog sastava fermentisanog napitka od surutke i mleka i nutritivna informacija o njemu je pokazala da proizvod predstavlja dobar izvor proteina i kalcijuma. Proizvedeni napitak je sadržao 8,07 log (CFU/mL) starter bakterija, pokazao antioksidativnu aktivnost od najmanje 38,1% i titracijsku kiselost od 28,2 °SH koja odgovara kiselosti proizvoda iz ove kategorije.

Ključne reči: fermentisani napitak na bazi surutke, probiotici, nutritivna vrednost.

Dostupno na Internetu sa adrese časopisa: http://www.ache.org.rs/HI/

Surutka je tečni sporedni proizvod koji u velikim količinama zaostaje nakon proizvodnje sira i kazeina. U zavisnosti od vrste sira koji se proizvodi, zapremina surutke može da se kreće i do 90 L na 100 L korišćenog mleka, što je količina koja omogućava proizvodnju 10 kg sira [1].

Svetska proizvodnja surutke procenjuje se na 180––190 miliona tona godišnje, a samo 50% proizvedene surutke se dalje obrađuje i primenjuje u industriji. U Srbiji je surutka i dalje jedan od nedovoljno iskorišćenih sporednih proizvoda prehrambene industrije. Usled neiskorišćavanja, surutka postaje i veoma veliki zagađivač, što je u potpunom neskladu sa potencijalima koje poseduje [2].

Surutka sadrži više od 55% sastojaka koji su prisutni u mleku, uključujući proteine surutke (20% od ukupnih proteina), laktozu, vitamine rastvorljive u vodi i minerale. Proteini i peptidi surutke imaju važna biološka svojstva u organizmu, tj. imaju uticaj na imuni, kardiovaskularni, nervni i gastrointestinalni sistem, kao i osećaj sitosti. Shodno tome, surutka se može smatrati vrednim nusproizvodom mlekarske industrije sa širokom primenom u prehrambenoj i farmaceutskoj industriji [3–5].

Poslednjih pedeset godina u svetu su razvijani biotehnološki postupci u kojima je surutka bila polazna sirovina za dobijanje biogasa, etanola, jednoćelijskih proteina, β-galaktozidaze i mnogih drugih proizvoda. Takođe, jedan deo surutke koristi se za dobijanje biološki vrednih proteina (koncentrat i izolat proteina surutke) ili laktoze, a deo surutke može da se koristi za dobijanje funkcionalnih napitaka. Pri proizvodnji funkcionalnih napitaka na bazi surutke neophodno je ispunjavanje nekoliko važnih kriterijuma: ekonomičnost proizvodnje, funkcionalnost (broj ćelija, sadržaj mlečne kiseline i proteina), zadovoljavajuća senzorna svojstva i stabilnost tokom dužeg perioda čuvanja. Novija istraživanja pokazuju da funkcionalni napici na bazi surutke mogu prema svojim nutritivnim i biološkim svojstvima u potpunosti da zamene tradicionalne proizvode od mleka, koje će jednog dana postati i deficitarna sirovina [6–11].

Cilj ovog rada usmeren je na iskorišćenje surutke, koja bi se uz dodatak mleka putem mlečno-kisele fermentacije prevela u nutritivno vredan fermentisani napitak zadovoljavajućih senzornih karakteristika, veoma sličnih jogurtu, i sa jedinstvenim funkcionalnim karakteristikama. U cilju primene fermentisanog napitka na bazi surutke u ishrani izvršiće se njegovo deklarisanje i označavanje.

EKSPERIMENTALNI DEO

Materijali

Surutka i mleko (sa 0,5% m.m.) iz mlekare AD Imlek (Beograd, Srbija) u odnosu 70:30 (*V/V*) korišćeni su kao materijal za mlečno-kiselu fermentaciju.

Hemijski sastav 100 ml surutke: suva materija 9,8%; belančevine 2,6%; masti 1,1% i laktoza 5,6%.

Hemijski sastav 100 ml mleka: suva materija 9,7%; belančevine 2,9%; masti 0,5% i laktoza 5,6% .

Proizvodni mikroorganizam

Za proizvodnju fermentisanog napitka od surutke i mleka korišćena je komercijalna starter kultura ABY-6 pod nazivom Lactoferm (proizvođač Biochem, Italija). Primenom ove starter kulture dobija se viskozan, blago kiseo i umereno aromatičan fermentisani napitak.

Kultura ABY-6 je mešana starter kultura u čiji sastav ulaze četiri vrste bakterija u sledećem odnosu:

- *Streptococcus salivarius* subsp. *thermophilus* 80%,
- *Lactobacillus acidophilus* 13%,
- *Bifidobacterium bifidum* 6% i
- *Lactobacillus delbrueckii subsp.bulgaricus* 1%,

i koristi se u proizvodnji fermentisanih mleka i jogurta sa probiotskim karakterom. Kultura ABY-6 je u liofiliziranom obliku čuvana na −20 °C do izvođenja eksperimenata. 1 g liofilizirane starter kulture ABY-6 sadrži preko 10^{10} živih ćelija bakterija. Pre primene u procesu fermentacije kultura je aktivirana pripremom 1% (*w/V*) rastvora u mleku i inkubiranjem u trajanju od 30 min na temperaturi 42 °C.

Metode rada

Postupak fermentacije

Surutka i mleko su pre izvođenja mlečno-kisele fermentacije pasterizovani (60 °C, 60 min), pomešani u odnosu 70:30 (*V/V*) i zasejavani kulturom ABY-6.

Mlečno-kisela fermentacija sa kulturom ABY-6 trajala je 4 sata. Vreme fermentacije (4 h), temperatura (42 °C) i količina inokuluma (6%) su izabrani na osnovu naših prethodnih istraživanja [11].

Određivanje pH vrednosti

pH vrednost uzorka tokom fermentacije određivana je pomoću pH metra (Inolab, WTW 82362, Wellheim, Nemačka). Merenje je izvedeno pod apsolutno sterilnim uslovima koji su obezbeđeni sterilnim uzorkovanjem fermentacionog medijuma.

Određivanje sadržaja mlečne kiseline

Sadržaj mlečne kiseline je određivan metodom po Soxhlet–Henkel i izražavan u °SH [12].

Određivanje ukupnog broja bakterija

Ukupan broj bakterija u fermentisanom napitku od surutke određivan je metodom razblaženja [13]. Uzorci su razblaživani u fiziološkom rastvoru do reda veličine 10^{-8}, nakon čega je po 1 mL odgovarajućeg razblaženja prenošen u Petri šolje koje su prelivane sa oko 20 mL rastopljenog M17 agara pri određivanju broja ćelija *S. thermophilus*, odnosno MRS agara pri određivanju broja ćelija *L. delbrueckii* ssp. *bulgaricus*, *L. acidophilus* i *B. bifidum*. Temperatura korišćenog agara bila je oko 55 °C. Petri šolje su inkubirane anaerobno 72 h, na temperaturi od 37 °C, nakon čega su brojane izrasle kolonije. Rezultat je predstavljen kao ukupan broj živih ćelija na obe korišćene podloge i izražen je kao log (CFU/mL).

Određivanje antioksidativne aktivnosti (%DPPH inhibicije)

Za određivanja antioksidativne aktivnosti kao slobodan radikal korišćen je 0.1 mM rastvor 2,2-difenil-1--pikrilhidrazil (DPPH) u 95% metanolu, po metodi Lee i saradnika [14].

Uzorci su centrifugirani na 12000 o/min u trajanju od 30 min. Nakon centrifugiranja 500 μL supernatanta je u epruveti mešano sa 1,5 mL metanola i 1,0 mL rastvora DPPH. Sadržaj epruvete je snažno promućkan i ostavljen na sobnoj temperaturi, u mraku 30 min, nakon toga je merena apsorbanca na 517 nm. Kao kontrolni uzorak pripreman je rastvor 1,5 mL DPPH i 1,5 mL metanola.

Rezultati su izraženi kao procenat inhibicije, odnosno, neutralizacije slobodnih DPPH radikala u odnosu na kontrolu i računati su prema sledećoj jednačini:

$$\text{Inhibicija DPPH radikala (\%)} = 100(A_k - A_a)/A_k$$

gde su A_k – apsorbancija kontrole i A_a – apsorbancija uzorka.

Određivanje redukcione snage

Određivanje redukcione snage izvedeno je po metodi Oyaizi [15].

1 ml uzorka pomešan je sa 2,5 ml fosfatnog pufera i 2,5 ml kalijum-fericijanida i smeša je inkubirana na 50 °C 30 min. Smeši je zatim dodato 2,5 ml 10% trihlorsirćetne kiseline i izvršeno je centifugiranje na 10000 o/min. Nakon centrifugiranja supernatant je pomešan sa 2,5 ml vode i 0,5 ml gvožđe (III)-hlorida i izmerena je apsorbancija uzorka na 700 nm.

Određivanje hemijskog sastava surutke

Analiza hemijskog sastava fermentisanog proizvoda vršena je standardnim hemijskim metodama [16]. Analiza hemijskog sastava obuhvatila je analizu suve materije, proteina, rastvornih šećera, masti, minerala (ukupan P, Ca, Mg, K, Na, Cu, Fe, Zn i Mn). Na osnovu analize hemijskog sastava, fermentisani napitak je deklarisan u skladu sa srpskim [17,18] i evropskim pravilnicima [19] o deklarisanju, dok su nutritivne i zdravstvene izjave izabrane na osnovu evropskih regulativa i direktiva [20,21], jer je u Srbiji pripremljen samo Nacrt

pravilnika o nutritivnim i zdravstvenim izjavama za prehrambene proizvode. Nutritivni sastav fermentisanog napitka dobijen je na osnovu analize hemijskog sastava uz korišćenje faktora za preračunavanje energetskih vrednosti za osnovne komponente u proizvodu. Faktori za preračunavanje pojedinih komponenti hrane (sadržaj soli u uzorku na osnovu sadržaja natrijuma) nalaze se u pravilnicima o deklarisanju [17,19]. Određivanje sadržaja masnih kiselina vršeno je gasnom hromatografijom, a razdvajanje metilovanih masnih kiselina uzorka izvodi se i na kapilarnoj koloni gasnog hromatografa [22].

Senzorna analiza

Ukus i konzistencija su najvažnije senzorne karakteristike fermentisanih mlečnih napitaka. Ove karakteristike analizirala je panel grupa sastavljena od 5 degustatora dajući ocene od 1–5 [23]. Za ukus je korišćena skala: 1 – neprijatan, 2 – nakiseo kupus, 3 – na surutku, 4 – na blagi jogurt i 5 – na jogurt. Za konzistenciju je korišćena sledeća skala: 1– vodenasta, 3– kremasto-vodenasta koja se raslojava i 5 – kremasta.

Radi poređenja senzornih karakteristika, izvedena je i fermentacija surutke, kao i mleka, pri istim uslovima fermentacije, čija senzorna ocena je takođe navedena.

Statistička analiza

Experimenti su izvedeni u triplikatu i rezultati predstavljeni kao srednja vrednost ± standardna devijacija. Statistička analiza je izvedena u programu Origin Pro 8 (Origin Lab Co., Northampton, USA). Podaci su analizirani pomoću analize varijanse (One-Way ANOVA), a

Tukey test je primenjen kao test za poredjenje srednjih vrednosti sa nivoom značajnosti od 0,05.

REZULTATI I DISKUSIJA

Osnovni parametri kvaliteta napitka na bazi surutke

Pri čuvanju fermentisanih proizvoda osnovni problem koji se može javiti jeste post-acidifikacija koja dovodi do odumiranja bakterija čime proizvod može izgubiti svoj probiotski karakter [24]. Proces fermentacije surutke uglavnom se vodi do postizanja pH vrednosti približno 4,6. Ova vrednost je kritična tačka fermentacije, jer vrednosti pH ispod 4,6 utiču negativno na stabilnost fermentisanih mlečnih proizvoda. Vođenjem fermentacije do pH ~4,6 ispunjavaju se kriterijumi vezani za postizanje i zadržavanje stabilnosti, funkcionalnosti i optimalnih senzornih svojstava tokom dužeg perioda čuvanja [2].

Na slici 1 prikazana je promena osnovnih parametara kvaliteta (pH, titracijska kiselost i ukupan broj živih ćelija) napitka na bazi surutke nakon fermentacije i tokom 28 dana čuvanja.

Neposredno pre početka izvođenja procesa fermentacije pH vrednost mešavine surutke i mleka je iznosila 6,23, dok je titracijska kiselost u istom trenutku iznosila 3,9 °SH (slika 1).

Nakon inokulacije početni broj ćelija u uzorku surutke i mleka je iznosio 6,81 log (CFU/mL). Kao što je prikazano na slici 1, tokom procesa fermentacije dolazi do pada pH vrednosti koji je praćen porastom vrednosti titracijske kiselosti. Nakon fermentacije (nulti dan) pH
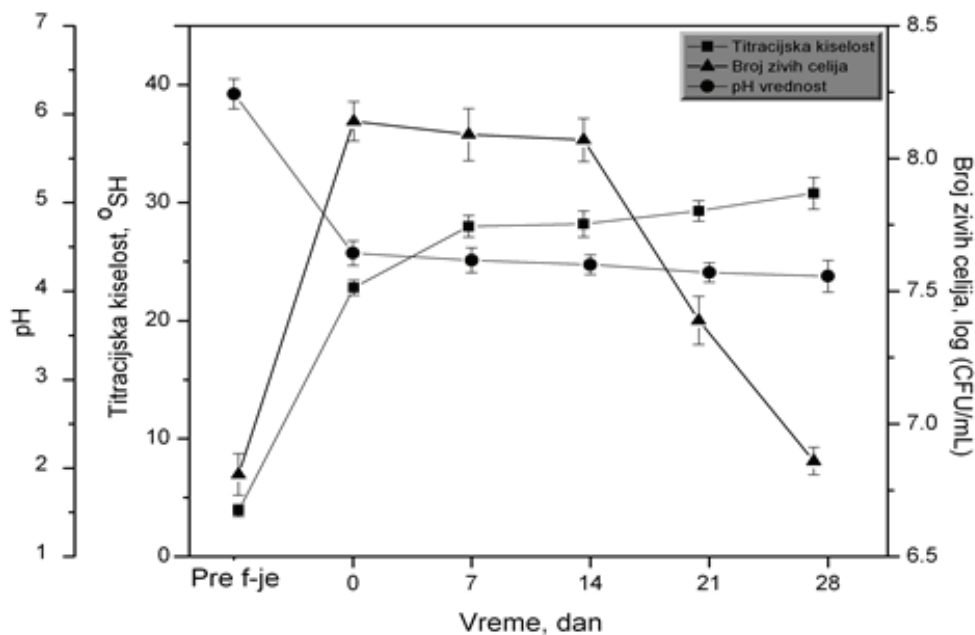
Slika 1. pH vrednost, titracijska kiselost i ukupan broj ćelija nakon fermentacije i tokom 28 dana čuvanja fermentisanog napitka na bazi surutke. Vertikalni barovi predstavljaju standardnu devijaciju tri uzastopna merenja (n = 3) za svaku tačku.
Fig. 1. pH value, titratable acidity and total number of cells after fermentation and during 28 days of storage of fermented whey-based beverage. Vertical bars represent the standard deviation (n = 3) for each data point.

vrednost uzorka je iznosila 4,43, dok je shodno tome vrednost titracijske kiselosti iznosila 22,8 °SH. Dobijeni rezultat je nešto veći od rezultata navedenih u literaturi [25] dobijenih pri fermentaciji rekonstituisane surutke sojevima *Lactobacillus acidophilus* La-5 i *Bifidobacterium lactis* BB-12. Razlika u vrednostima titracijske kiselosti se može objasniti prisustvom dodatnih sojeva (*S. thermophilus* i *L. delbrueckii* ssp. *bulgaricus*) u ABY-6 kulturi.

Tokom procesa fermentacije broj ćelija u uzorku raste za oko 1,3 log jedinice, tako da nakon 4h broj živih ćelija u fermentisanom uzorku iznosi oko 8,14 log (CFU/mL). Porast broja živih ćelija od 1.3 log jedinice tokom 4h može se smatrati visokim obzirom da se radi o relativno kratkom vremenu trajanja fermentacije i činjenici da surutka u svom sastavu ima veoma mali sadržaj nutrijenata neophodnih za rast BMK [26,27]. Postignuta vrednost broja ćelija je u skladu sa prethodnim istraživanjima [10,11] koja se odnose na rast bakterija u surutki.

Tokom 28 dana skladištenja pH vrednost uzorka ravnomerno opada da bi 28. dana ta vrednost iznosila 4,17. Istovremeno sa padom pH vrednosti dolazi do porasta kiselosti, tako da nakon 28 dana čuvanja titracijska kiselost uzorka iznosi 30,8 °SH. U prvih 7 dana dolazi do blagog pada broja živih ćelija koji se nastavlja do 28. dana kada je broj živih ćelija iznosio 6,86 log (CFU/mL). Poredeći rezultat sa navodima u literaturi, prema kojim nakon 14. dana dolazi do značajnog pada broja bakterija (≤ 6,0 log (CFU/mL) u napitku koji je proizveden fermentacijom rekonstituisane surutke [25],

može se reći da je rezultat ovog rada značajno unapređen proizvod. Zaključno sa 14. danom broj živih ćelija u fermentisanom napitku na bazi surutke i mleka iznosi 8,07 log (CFU/mL). Na osnovu svega navedenog, može se zaključiti da u periodu od dve nedelje napitak poseduje probiotski karakter, što je prihvaćeno kao zadovoljavajući rok trajanja proizvoda ove vrste.

Antioksidativna aktivnost napitka na bazi surutke

Slobodni radikali su glavni uzrok nastanka mnogih degenerativnih bolesti čoveka: ateroskleroze, raka, kardiovaskularnih bolesti, zapaljenja creva, starenja kože i artritisa. Brojna istraživanja i epidemiološki podaci ukazuju na važnost antioksidanasa kada je reč o prevenciji nastanka raka ili kardiovaskularnih bolesti. Za razliku od prehrambenih antioksidanasa koji samo sprečavaju oksidativne procese u masnim materijama tokom proizvodnje i čuvanja hrane, prirodni antioksidansi se svrstavaju u „bioaktivne materije" i imaju važnu ulogu u metabolizmu ćelija [28].

Kao što je prikazano na slici 2, tokom procesa fermentacije procenat inhibicije DPPH radikala raste sa početne vrednosti 15,0% na vrednost 46,0% koja je zabeležena nakon završetka fermentacije. Porast procenta inhibicije DPPH radikala praćen je porastom vrednosti redukcione snage koja je nakon 4 h fermentacije iznosila 0,356. Tokom procesa skladištenja, u prve dve nedelje, dolazi do pada vrednosti procenta inhibicije DPPH radikala, nakon čega antioksidativna aktivnost napitka raste verovatno kao posledica lize ćelija [29]. Dobijeni rezultati o porastu antioksidativne aktivnosti
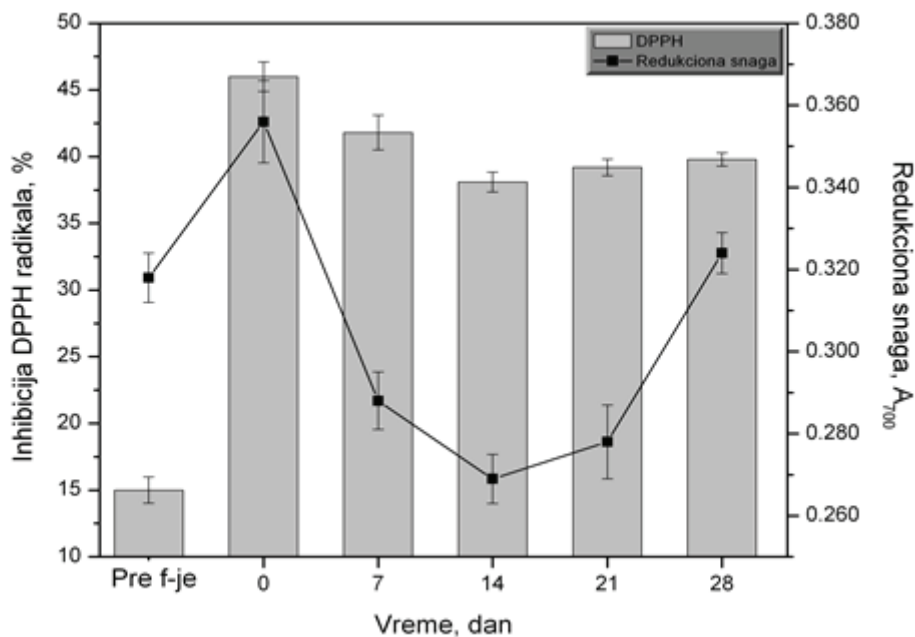
Slika 2. % Inhibicije DPPH radikala i redukciona snaga nakon fermentacije i tokom 28 dana čuvanja fermentisanog napitka na bazi surutke. Vertikalni barovi predstavljaju standardnu devijaciju tri uzastopna merenja (n = 3) za svaku tačku.
Fig. 2. DPPH scavenging activity and reducing power after fermentation and during 28 days of storage of fermented whey-based beverage. Vertical bars represent the standard deviation (n = 3) for each data point.

nakon 14 dana skladištenja su u saglasnosti sa opadanjem broja živih ćelija tokom procesa skladištenja (slika 1). Na osnovu dobijenih rezultata se može zaključiti da lizom ćelija dolazi do oslobađanja intracelularnih metabolita i enzima sposobnih da doprinesu stvaranju produkata proteolitičke razgradnje koji ispoljavaju određenu antioksidativnu aktivnost. Porast antioksidativne aktivnosti napitka praćen je istovremenim porastom vrednosti redukcione snage. Dobijeni rezultati su u saglasnosti sa rezultatima ranijih istraživanja [30] koja se odnose na antioksidativnu aktivnost jogurta a prema kojima antioksidativna aktivnost nakon 14 dana skladištenja raste i dostiže slične vrednosti.

Najviše vrednosti antioksidativne aktivnosti i redukcione snage su zabeležene neposredno nakon fermentacije kada su iznosile 46,0% i 0,356, redom. Sa druge strane, najniže vrednosti antioksidativne aktivnosti i redukcione snage su zabeležene 14. dana skladištenja i iznosile 38,1% i 0,269, redom, uz naglašavanje činjenice da su čak i u tom trenutku obe vrednosti statistički značajno ($P < 0.05$) više od vrednosti zabeleženih u nefermentisanom uzorku.

Senzorna svojstva napitka na bazi surutke

Na tržištu mlečnih proizvoda u Srbiji ne postoji veliki broj napitaka na bazi surutke, a naročito nisu prisutni proizvodi dobijeni mlečno-kiselom fermentacijom surutke, za razliku od tržišta Nemačke, Austrije i Švajcarske, gde postoji duga tradicija u konzumiranju ove vrste napitaka. Usled toga, senzorna analiza je bila usmerena na karakteristike na koje su domaći potrošači već naviknuti.

Kao što se može uočiti na slici 3, dodatak mleka utiče na ocenu senzornih karakteristika napitka na bazi surutke. Ukus napitka koji u svom sastavu osim surutke sadrži i mleko je bio, tokom čitavog procesa skladiš-

tenja, značajno ($P < 0.05$) prihvatljiviji u odnosu na ukus napitaka koji je sadržao samo surutku. U prvih 14 dana ovaj napitak je po ukusu bio veoma sličan jogurtu. Nakon 14. dana ukus fermentisanog napitka od surutke i mleka je ocenjen nešto nižom ocenom (ocena 4) u odnosu na fermentisano mleko (ocena 5), da bi se 21. dana skladištenja senzorne ocene oba napitka izjednačile (ocena 5). Bez obzira na uočeno variranje, napitak dobijen fermentacijom surutke uz dodatak mleka do kraja procesa skladištenja zadržava značajno ($P < 0.05$) veću ocenu ukusa u odnosu na napitak dobijen fermentacijom surutke. Konzistencija fermentisanog napitka na bazi surutke i mleka je u prvih 7 dana skladištenja potpuno ista kao konzistencija fermentisanog mleka. (ocena 5). Tokom čitavog procesa skladištenja konzistencija napitka od surutke i mleka je nešto lošija (ocena 4) nego konzistencija fermentisanog mleka (ocena 5) ali sa druge strane značajno bolja od konzistencije napitka proizvedenog fermentacijom surutke (ocene 3, 2 i 1). Na osnovu svega gore navedenog, može se zaključiti da dodatak mleka u surutku dovodi do poboljšanja kako ukusa tako i konzistencije fermentisanog napitka.

Hemijski sastav napitka na bazi surutke

Sastav i svojstva surutke zavise od kvaliteta mleka i tehnologije proizvodnje sira tj. načina koagulacije mleka. Proteini surutke u celosti prelaze u surutku jer su neosetljivi na dejstvo kiselina i primenjenih enzima u proizvodnji sira, dok su značajna variranja moguća u sadržaju minerala, naročito kalcijuma i fosfora.

Analiza hemijskog sastav dobijenog fermentisanog proizvoda od surutke i mleka prikazana je u tabeli 1.

Sadržaj suve materije u fermentisanom napitku je iznosio oko 9,8%, što je u skladu sa sadržajem suve materije polaznih sirovina. Zanimljivo je napomenuti da

a) ukus   b) konzistencija
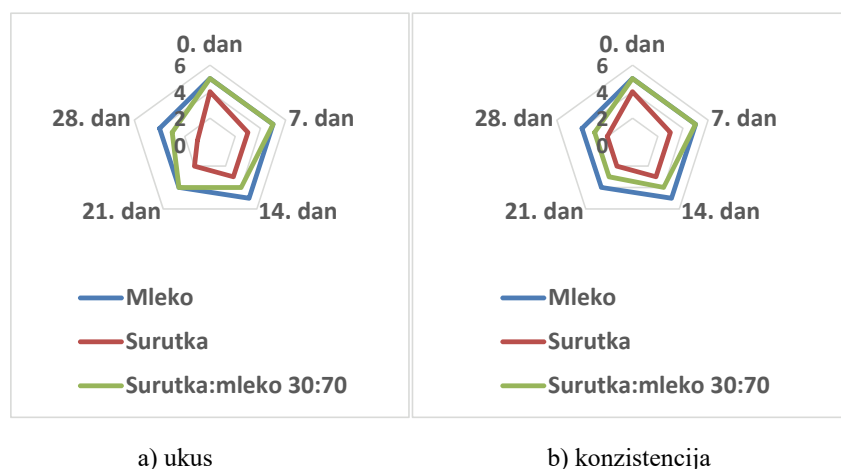
Slika 3. Poređenje senzornih karakteristika napitaka proizvedenih fermentacijom surutke, mleka i mešavine surutke i mleka tokom 28 dana čuvanja.
Fig. 3. Comparison of sensory characteristics of beverages produced by fermentation of whey, milk and mixtures of whey and milk during 28 days of storage; a) taste, b) consistency.

je polazna sirovina imala nešto veći sadržaj suve materije od uobičajenih vrednosti za surutku navedenih u literaturi koje se kreću u intervalu 6–8%. Povećan sadržaj suve materije uslovljen je sadržajem proteina u surutki, koji je oko 2,5 puta veći od uobičajenih vrednosti u literaturi [4] koje iznose oko 1%. Ovako visok sadržaj proteina ukazuje da su tokom procesa prerade mleka i nastanka surutke primenjeni tehnološki postupci koji nisu značajno uticali na smanjenje sadržaja proteina. Visok sadržaj suve materije surutke rezultirao i visokim sadržajem minerala, pre svega kalcijuma, u proizvedenom fermentisanom napitku od surutke i mleka.

Tabela 1. Hemijski sastav fermentisanog napitka na bazi surutke
Table 1. The chemical composition of fermented whey-based beverage

Parametar	Vrednost
pH vrednost	4,6±0,1
Suva materija, %	9,8± 0,1
Proteini, %	2,3±0,03
Masti, %	1,05±0,04
Šećeri, %	3,3±0,04
Natrijum, mg/l	450,0±0,3
Kalijum, mg/l	1400,0±0,3
Kalcijum, mg/l	1945±0,2
Magnezijum, mg/l	53,75±0,01
Ukupan fosfor, mg/l	710,0±0,02
Gvožđe, mg/l	0,50±0,2
Cink, mg/l	0,18±0,5
Mangan, mg/l	<0,02±0,01
Bakar, mg/l	<0,05±0,01

Deklarisanje proizvedenog napitka na bazi surutke

Zbog kvalitetnog hemijskog sastava, deklaracija napitka na bazi surutke može da sadrži veliki broj nutritivnih i zdravstvenih izjava. Uslov za navođenje nutritivnih i zdravstvenih izjava je da se na ambalaži proizvoda nalazi nutritivni sastav. Na osnovu rezultata prikazanih u tabeli 1 i na slici 1 može se predstaviti nutritivna informacija o fermentisanom proizvodu, koja je data u tabeli 2. Energetska vrednost u tabeli 2 izračunata je na osnovu konverzionih faktora datih u Prilogu 8 Pravilnika o deklarisanju [17].

Sadržaj proteina u 100 ml fermentisanog napitka iznosio je 2,3 g. Prema važećim pravilnicima o hrani i evropskim regulativama [20], proizvod koji ima najmanje 20% energetske vrednosti koja potiče od proteina, može da ima nutritivnu izjavu „Bogat proteinima“.

U 100 ml proizvoda se nalazi 194 mg kalcijuma, što zadovoljava 24,2% dnevnih potreba za ovim mineralom. Prema važećim standardima za hranu [20], proizvod koji ima više od 15% dnevnih potreba na 100 ml može poneti nutritivne i zdravstvene izjave [21]. Od nutritivnih izjava za kalcijum biramo izjavu „Prirodan izvor kalcijuma“, a od zdravstvenih izjava „Kalcijum je potreban za održavanje normalnih kostiju“.

Zbog količine proteina, ovaj proizvod može da ima i zdravstvenu izjavu koja se odnosi na proteine: „Proteini doprinose normalnom održavanju kostiju“. Prema EU Direktivi [21] uslov za ovu izjavu je da fermentisani napitak ima više od 12% energije koja potiče od proteina. Napitak ima čak 29% energije koja potiče od proteina.

Ukoliko proizvod sadrži najmanje 10^8 (CFU/g ili CFU/ml) živih mikroorganizama (*Lactobacillus delbrueckii ssp. bulgaricus* i *Streptococcus thermophilus*), a fermentisani napitak ispunjava ovaj zahtev nakon fermentacije i do 14 dana čuvanja – proizvod može na deklaraciji da ima i zdravstvenu izjavu „Žive kulture u jogurtu ili fermentisanom mleku poboljšavaju probavu laktoze kod osoba koje imaju problem sa probavom laktoze“ [21].

Takođe, ukoliko na proizvodu postoji bar jedna zdravstvena izjava, mora se navesti i izjava „Proizvod treba koristiti kao deo uravnotežene ishrane i zdravog načina života“ [20].

Tabela 2. Nutritivni sastav fermentisanog napitka na bazi surutke
Table 2. Nutritional composition of fermented whey-based beverage

Hranljiva vrednost	100 ml	Porcija, 250 ml[a]	PDU[b] po porciji, %
Energetska vrednost	100 kJ / 32 kcal	335 kJ / 80 kcal	4.00
Masti,	1.05g	2.62 g	3.70
od toga zasićene masne kiseline	0.79 g	1.97 g	9.80
Ugljeni hidrati,	3.30 g	8.25 g	3.10
od toga šećeri	3.30 g	8.25 g	9.20
Proteini	2.30 g	5.75 g	11.5
So	0.11 g	0.27 g	4.50
Minerali			
Kalcijum	194 mg	485 mg	60.0

[a]Porcija: 250 ml; broj porcija u pakovanju: 1; [b]PDU – preporučeni dnevni unos za prosečnu odraslu osobu (8400 kJ/2000 kcal)

ZAKLJUČAK

Fermentacijom surutke uz dodatak mleka sa komercijalnom jogurtnom kulturom značajno se utiče na kvalitet fermentisanog proizvoda. Dodatak mleka je bitan ne samo za nutritivni kvalitet nastalog proizvoda, nego je poboljšao i njegov ukus, homogenost fermentisanog proizvoda i njegovu stabilnost.

Postignuti rezultati su pokazali da se primenjena starter kultura može koristiti za proizvodnju i razvoj funkcionalnog fermentisanog napitka od surutke i mleka sa zadovoljavajućim nutritivnim svojstvima. Analiza hemijskog sastava fermentisanog napitka od surutke i mleka i nuritivna informacija o njemu je pokazala da proizvod predstavlja izvor proteina, izvor kalcijuma, a sadrži i žive ćelije probiotske kulture u broju koji može pozitivno delovati na probavu laktoze u organizmu.

Kao rezultat ovog rada proizveden je napitak koji do 14. dana ima zadovoljavajuć ukus, konzistenciju i broj živih bakterija. Proizvedeni napitak sadrži 8,07 log (CFU/mL) čime je ispunjen kriterijum funkcionalnosti i omogućeno da napitak bude deklarisan zdravstvenom izjavom „Žive kulture u jogurtu ili fermentisanom mleku poboljšavaju probavu laktoze kod osoba koje imaju problem sa probavom laktoze". Dobijeni napitak ispoljava antioksidativnu aktivnost od najmanje 38,1% i kiselost od 28,2 °SH koja odgovara kiselosti proizvoda iz ove kategorije.

Rezultati istraživanja ukazuju da bi prerada surutke u fermentisani napitak uz dodatak mleka otvorila prostor za razvoj novih nekonvencionalnih mlečnih proizvoda u Srbiji, koji danas u svetu predstavljaju kategoriju proizvoda koja je u ekspanziji.

Zahvalnica

LITERATURA

[1] M. Harju, H. Kallioinen, O. Tossavainen, Lactose hydrolzsis and other conversions in dairy products: Technological aspects, Int. Dairy J. **22** (2012) 104–109.

[2] M. Bulatović, M. Rakin, Lj. Mojović, S. Nikolić, M. Vukašinović Sekulić, A. Djukić Vuković, Surutka kao sirovina za proizvodnju funkcionalnih napitaka, Hem. Ind. **66** (2012) 567–579.

[3] M. Bulatović, M. Rakin, Lj. Mojović, S. Nikolić, M. Vukašinović-Sekulić, A. Đukić-Vuković, Improvement of production performance of functional fermented whey-based beverage, Chem. Ind. Chem. Eng. **20** (2014) 1–8.

[4] V. Legarova, L. Kourimska, Sensory quality evaluation of whey-based beverages, Mljekarstvo **60** (2010) 280–287.

[5] M. Pescuma, H.E. Maria, F. Mozzi, G. Font de Valdez, Functional fermented whey-based beverage using lactic acid bacteria, Int. J. Food Microbiology **141** (2010) 73––81.

[6] L. Ebringer, M. Ferenčik, J. Krajčović, Beneficial Health Effects of Milk and Fermented Dairy Products-Review, Folia Microbiol. **53** (2008) 378–394.

[7] M. Rakin, M. Vukašinović Sekulić, Lj. Mojović, Health Benefits of Fermented Vegetable Juices in Handbook of Plant-based Fermented Food and Beverage Technology (Y.H.Hui Ed), 2012, Vol. 2, CRC Press of Florida, ISBN 9781439849040, 385-407.

[8] A. Foegending, J. Davis, D. Doucet, M. McGuffey, Advances in modifying and understanding whey protein functionality, Trends Food Sci. Technol **13** (2002) 151–159.

[9] S. Akalin, Dairy-derived antimicrobial peptides: Action mechanisms, pharmaceutical uses and production proposal, Trends Food Sci. Technol **36** (2014) 79–95.

[10] M. Bulatović, M. Rakin, M. Vukašinović-Sekulić, Lj. Mojović, T. Krunić, Effect of nutrient supplements on growth and viability of Lactobacillus johnsonii NRRL B-2178 in whey, Int. Dairy J. **34** (2014) 109–115.

[11] M.Lj. Bulatovic, T.Ž. Krunić, M.S. Vukašinović, D.B. Zaric, M.B. Rakin, Quality attributes of fermented whey-based beverage enriched with milk and probiotic strain, RSC Adv. **4** (2014) 55503–55510.

[12] L. Varga, Effect of acacia (*Robinia pseudo-acacia* L.) honey on the characteristic microflora on yogurt during refrigerated storage., Int. J. Food Microbiol. **108** (2006) 272–275.

[13] Lj. Vrbaški, S. Markov, Praktikum iz mikrobiologije, prvo izdanje, Prometej, Novi Sad, 1993.

[14] S.K. Lee, Z.H. Mbwambo, H.Chung, L. Luyengi, E.J. Gamez, R.G.Mehta, A.D. Kinghorn, J.M. Pezzuto, Evaluation of the antioxidant potential of natural products, Comb. Chem. High Throughput Screen. **1** (1998) 35–46.

[15] M. Oyaizi, Studies on product of browning reaction prepared from glucose amine, Jpn. J. Nutr. **44** (1986) 307–315.

[16] AOAC, Official methods of analysis, 15th ed., Association of Official Analytical Chemists, Arlington, VA, 1990, p. 1298.

[17] Pravilnik o deklarisanju, označavanju i reklamiranju hrane, Sl. glasnik RS, 85/2013 i 101/2013.

[18] Pravilniku o deklarisanju i označavanju upakovanih namirnica, Sl. list SCG 4/2004, 12/2004 i 48/2004.

[19] Regulation (EC) No 1169/2011 of the European Parliament and of the Council of 25 October 2011, OJ L 304, 22.11.2012, pp. 18–59.

[20] Regulation (EC) No 1924/2006 of the European Parliament and of the Council of 20 December 2006 on nutrition and health claims made on foods, OJ L 404, 30.12.2006, pp. 9–25.

[21] Commission Regulation (EU) No. 432/2012 of the European Parliament and of the Council of 16 May 2012, OJ L 136, 25.05.2012, pp. 1–40.

[22] SRPS EN ISO 15304, Ulja i masti biljnog i životinjskog porekla – Metode gasne hromatografije, 2008.

[23] J. Hemsworth, S. Hekmat, G. Reid, The development of micronutrient supplemented probiotic yogurt for people

living with HIV: Laboratory testing and sensory evaluation. Innov. Food Sci. Emerg. **12** (2011) 79–84.

[24] R.R. Ravula, N.P. Shah, Effect of acid casein hydrolysate and cysteine on the viability of yogurt and probiotic bacteria in fermented frozen dairy desserts, Aust. J. Dairy Technol. **53** (1998) 175–179.

[25] B. Matijević, R. Božanić, Lj. Tratnik, The influence of lactulose on growth and survival of probiotic bacteria *Lactobacillus acidophilus* La-5 and Bifidobacterium animalis subsp. *lactis* BB-12 in reconstituted sweet whey, Mljekarstvo **59** (2009) 20–27.

[26] M. Pescuma, E.M. Hébert, E. Bru, G. Font de Valdez, F. Mozzi, Diversity in growth and protein degradation by dairy relevant lactic acid bacteria species in reconstituted whey. J. Dairy Res. **79** (2012) 201–208.

[27] M. Elli, R. Zink, R. Reniero, L. Morelli, Growth requirements of Lactobacillus johnsonii in skim and UHT milk, Int. Dairy J. **9** (1999) 507–513.

[28] W. Grajek, A. Olejnik, A. Sip, Probiotics, prebiotics and antioxidants as functional foods, Acta Biochim. Pol. **52** (2005) 665–671.

[29] R.D. Cagnoa, M. Quintob, A. Corsettic, F. Minervinia, M. Gobbettia, Assessing the proteolytic and lipolytic activities of single strains of mesophilic lactobacilli as adjunct cultures using a Caciotta cheese model system, Int. Dairy J. **16** (2006) 119–130.

[30] V. Illupapalayam, S.C. Smith, S. Gamlath, Consumer acceptability and antioxidant potential of probiotic-yogurt with spices, LWT – Food Sci. Technol. **55** (2014) 255–262.

SUMMARY

QUALITY OF FERMENTED WHEY BEVERAGE WITH MILK

Marica B. Rakin[1], Maja Lj. Bulatović[1], Danica B. Zarić[2], Marijana M. Stamenković Đoković[3], Tanja Ž. Krunić[4], Milka M. Borić[1], Maja S.Vukašinović Sekulić[1]

[1]*Faculty of Technology and Metallurgy, University of Belgrade, Karnegijeva 4, 11000 Belgrade, Serbia*
[2]*IHIS Tehno Experts Ltd., Batajnički put 23, 11000 Belgrade, Serbia*
[3]*IHIS Science and Technology Park Zemun, Batajnički put 23, 11000 Belgrade, Serbia*
[4]*Innovation center, Faculty of Technology and Metallurgy, University of Belgrade, Karnegijeva 4, 11000 Belgrade, Serbia*

(Scientific paper)

One of the most economical ways of whey processing is the production of beverages, which represents a single process that exploits all the potential of whey as a raw material. Functional and sensory characteristics of whey-based beverages are a criterion that is crucial to the marketing of products and win over consumers. The aim of this study was to determine nutritional and functional characteristics of fermented whey beverage with milk and commercial ABY-6 culture. The results showed that the applied starter culture can be used for the production of fermented whey based beverage with satisfactory nutritional properties. Addition of milk was important not only in the nutritional quality of the resulting product, but also improved the taste, the homogeneity and stability. Analysis of the chemical composition of fermented whey based beverage and nutritional information about it indicates that the product is a good source of protein and calcium. Fermented beverage contained 8.07 log (CFU/mL), showed antioxidant activity of at least 38.1% and the titratable acidity of 28.2 °SH corresponding to the acidity of the product in this category.

Keywords: Fermented whey-based beverage • Probiotics • Nutritive value

Antioxidant activity of *Ruscus* species from Serbia: Potential new sources of natural antioxidants

Violeta D. Jakovljević[1], Jasmina M. Milićević[1], Gorica T. Đelić[1], Miroslav M. Vrvić[2]

[1]*Institute for Biology and Ecology, Faculty of Science, University of Kragujevac, Kragujevac, Serbia*
[2]*Department of Biochemistry, Faculty of Chemistry, University of Belgrade, Belgrade, Serbia*

Abstract

The antioxidant activity and total phenolic and flavonoid content of ethanolic, acetone and ethyl acetate extracts of *Ruscus hypoglossum* L. and *Ruscus aculeatus* L. (aerial parts) from Serbia were investigated in this paper. The best total antioxidant capacity (23.329 µg AA g^{-1}) and the highest DPPH scavenging activity (IC_{50} = 182.54 µg mL^{-1}) were found in acetone and ethyl acetate extract of *R. aculeatus* L. Ethanolic extract of *R. hypoglossum* L. showed the highest ABTS radical cation scavenging activity (IC_{50} = 3.04 µg mL^{-1}), as well as reducing power (IC_{50} = 143 µg mL^{-1}). The best inhibitory activity against lipid peroxidation (IC_{50} = 651 µg mL^{-1}) and the best ferrous ion chelating ability (IC_{50} = 110 µg mL^{-1}) were found in acetone and ethyl acetate extract of *R. hypoglossum* L. The highest total phenolic (8.569 mg GAE g^{-1}) and flavonoid contents (0.136 mg RU g^{-1}) were found in ethanolic and acetone extract of *R. hypoglossum* L. and *R. aculeatus* L, respectively.

Keywords: free radical scavenging, reducing power, chelating ability, lipid peroxidation, total phenolic and flavonoid contents.

Available online at the Journal website: http://www.ache.org.rs/HI/

Different plant species are the subject of numerous studies throughout the world in order to obtain natural products with their potential application in medicine, pharmacy and food industry in recent two decades. From ancient times, the plants have been using as rich source of effective and safe medicines. About 80% of world population is still dependent on traditional medicines. Bioactive compounds and antioxidant activity are important parameters that regulate the therapeutic effects of a plant [1]. The most important bioactive phytochemical constituents are alkaloids, essential oils, flavonoids, tannins, saponins, lactones and terpenoids [2]. Phenolics are widely distributed in medicinal plants and they have multiple biological effects, including antioxidant, anti-inflammatory, anti-cancer, anti-viral, anti-bacterial and cardio-protective activity [3]. An antioxidant is any substance that, when present at low concentrations, significantly delays or prevents oxidation of cell content like proteins, lipids, carbohydrates and DNA [4]. It can interfere with the oxidation process by scavenging reactive oxygen species (SOD removing O_2^-), by binding transition metal ions and preventing formation OH and/or decomposition of lipid hydroperoxides, by repairing damages (*e.g.*, α-tocopherol repairing peroxyl radicals and so terminating the chain reaction of lipid peroxidation) or

by any combination of the above [5–7]. According to these abilities, numerous methods are applied for testing antioxidative activity of plants, such as the oxygen radical absorption capacity (ORAC), ferric reducing anti-oxidant power (FRAP), 2,2-diphenyl-1-picryl-hydrazil (DPPH) radical scavenging and inhibition of the formation of thiobarbituric acid reactive substances (TBARS) [8]. Thus, antioxidant and phytochemical screening of different plants are essential to provide valuable information in the search of new pharmaceuticals.

Ruscus hypoglossum L. and *R. aculeatus* L. are two of the three species from genus *Ruscus* (fam. Liliaceae, order Asparagales) which grow in Serbia. The native range of *Ruscus hypoglossum* L. extends from Western Europe to Iran. Common names include Mouse Thorn, Spineless Butcher's Broom and Horse Tongue Lily. *Ruscus aculeatus* L. (Butcher's Broom) is originally from Mediterranean Europe and Africa [9]. The rhizomes of European species of *Ruscus* are used in herbal medicines due to their anti-inflammatory and vasoconstriction properties. Flavonoids from *Ruscus* species strengthen blood vessels, reduce capillary fragility and support healthy circulation. Many chemical constituents have been isolated from these plants. Species from *Ruscus* genus are recognizing for ruscogenin and flavonoids, especially *R. aculeatus* L. The aerial parts of these two *Ruscus* species contain several flavonoid glycosides and phenolic acids [10]. However, *R. aculeatus* L. rhizome contains *p*-coumaric acid and amides of hydroxycinnamic acids, but it has no flavonoids. Recently, Hadzifejzovic *et al.* [11] have found that ethyl acetate and butanol fraction of methanolic extract of

herb and rhizome of *R. aculeatus* L. and herb of *R. hypoglossum* L. have antimicrobial and antioxidant activity. The authors showed, in mentioned results, that there is a relatively strong correlation between the total phenolic content and the antioxidant capacity of plants' extracts.

In literature there is no data related to the study of antioxidant activity of *Ruscus* species from the territory of Serbia. Therefore, the aim of this study was designed for the evaluation of antioxidant activity of aerial parts of two *Ruscus* species from Serbia in order to investigate the relationship between antioxidant properties and total phenolic and flavonoid content. These data will provide some useful information for healthier living, as well as the further screening of plants as potential sources of new natural antioxidants.

EXPERIMENTAL

Chemicals

2,2-Diphenyl-1-picrylhydrazyl (DPPH), gallic acid, ascorbic acid, quercetin, butylated hydroxytoluene, ammonium molybdate, sodium phosphate, sulphuric acid, ferrous sulfate heptahydrate, Folin–Ciocalteu reagent, aluminum chloride, potassium ferricyanide, trichloroacetic acid, ferric chloride, linoleic acid, sodium acetate, Tween-20, ammonium thiocyanate, hydrochloric acid, 3-(2-pyridyl)-5,6-diphenyl-1,2,4-triazine--*p,p*'-disulfonic acid monosodium salt hydrate, 2,2--azino-bis(3-ethylbenzothiazoline6-sulfonic acid) (ABTS), sodium carbonate, potassium sodium tartrate tetrahydrate, rutine, were obtained from Sigma-Aldrich, St. Louis, MO, USA; ethanol, methanol, acetone and ethyl acetate were obtained from Fluka Chemie AG Buchs, St. Louis, MO, USA.

Plant materials

Aerial parts of *Ruscus hypoglossum* L. were collected from mountain Žeželj, near Kragujevac (Serbia), whereas aerial parts of *Ruscus aculeatus* L. were collected from Ovčar–Kablar gorge, near Čačak (Serbia), in late September, 2012. The species were identified according to Systematic key at the Institute for biology and ecology, Faculty of Science, University of Kragujevac, Serbia. Voucher specimens of *R. aculeatus* L. (17074 BEOU) and *R. hypoglossum* L. (17075 BEOU) were deposited in the Herbarium of Institute of Botany and Botanical Garden "Jevremovac", University of Belgrade, Serbia.

Solvent extraction

The air-dried aerial parts of plant (30 g) were broken into small pieces (2–6 mm) and extracted with ethanol (96%), acetone and ethyl acetate (150 mL) using a Soxhlet apparatus. The extracts were filtered through a filter paper (Whatman No. 1) followed by

evaporated on rotary vacuum evaporator at 40 °C. The resulting extracts were dried at room temperature to constant dry weight mass. The dark greenish residues were stored in a dark glass bottle at 4 °C to prevent oxidative damage until the further analysis.

Antioxidative methods

Total phenolic content

The total phenolic compounds in the extract were determined according to the Folin–Ciocalteu method by Singleton and Rossi [12] with some modifications. To 1 mL of each extract dissolved in methanol, 2 mL of 7.5% (*w/V*) sodium carbonate solution was added and vortexed vigorously. After 5 min, 1 mL of 1:10 diluted Folin–Ciocalteu's phenol reagent was added and vortexed again. Same procedure was repeated for the standard solution of gallic acid. All the tubes were incubated at room temperature for 30 min and then the absorbance was measured at 765 nm. The total phenolic content in the extracts was calculated from the standard curve and values are expressed as gallic acid equivalent (GAE) in mg g^{-1} of dry weight (DW) extract.

Total flavonoid content

The aluminum chloride method was used for the determination of the total flavonoids content of the sample extracts [13]. Aliquots of extract solutions were taken and made up to volume 3 mL with methanol. Then 0.1 mL $AlCl_3$ (10%), 0.1 mL potassium sodium tartrate and 2.8 mL distilled water were added sequentially. The test solution was vigorously shaken. Absorbance at 415 nm was measured after 30 min of incubation. A standard calibration plot was generated at 415 nm using known concentrations of rutine. The concentration of flavonoids in the test samples was calculated from the standard curve and values are expressed as rutine (RU) equivalent in mg g^{-1} of DW extract.

Total antioxidant capacity

The total antioxidant capacity was determined by phosphomolybdenum method according to Prieto *et al.* [14]. To 1 mL of samples or standard at different concentration performed from stock solutions (1 mg mL^{-1}), 2 mL reagent solution (ammonium molybdate 4 mM, sodium phosphate 28 mM and sulphuric acid 0.6 M) was mixed vigorously. All the reaction tubes were incubated at 95 °C for 90 min. The absorbance was measured at 695 nm against blank (methanol) after cooling at room temperature. Ascorbic acid (AA) was used as standard and total antioxidant capacity of extracts is expressed as mg AA g^{-1} of DW extract.

DPPH radical scavenging assay

DPPH radical scavenging activity was done according to the method by Takao *et al.* [15] with slight modi-

fication. Working solution of extracts was carried out by dilution stock solution (2 mg mL^{-1}) of extracts. DPPH was dissolved in methanol to obtain a concentration at 8 μg mL^{-1}. To 1 mL of DPPH solution, 1 mL of various concentrations of the extracts or the standard solution was added separately. The reaction mixtures were incubated at 37 °C for 30 min, following by absorbance measured at 517 nm using methanol as blank reference. The DPPH scavenging activity (%) of extracts and standards AA, gallic acid, butylated hydroxytoluene (BHT), *α*-tocopherol, quercetin were determined using the following equation:

% Inhibition = 100(Ac–As)/Ac (1)

where Ac was absorbance of control reaction and As the absorbance in presence of the sample.

2,2'-Azino-di(3-ethylbenzthiazoline-6-sulfonic acid) (ABTS) decolorization assay

The ABTS$^{•+}$ decolorization assay is spectrophotometric method widely use for determination of the antioxidative activity of substances. The ABTS$^{•+}$ scavenging activity was measured according to the method of Re *et al.* [16]. In brief, ABTS$^{•+}$ was first produced by reacting ABTS stock solution (7 mM) with potassium persulfate (2.45 mM). The mixture was then placed in the dark at room temperature for 12 to16 h before using. Under this condition, ABTS$^{•+}$ can be stable in this form for more than 2 days. The ABTS$^{•+}$ solution was diluted with double-distilled water to obtain an absorbance of 0.70±0.02 at 734 nm. Aliquots of 30 μL of the sample extracts of different concentrations (from 2 mg mL^{-1} to 3.91 μg mL^{-1}) were then added to 2.7 mL diluted ABTS$^{•+}$ solution, and mixture was incubated at room temperature for 30 min. Absorbance was determined spectrophometrically at 734 nm. For the control, 1.0 mL of methanol was used instead of extract. AA was used as a positive control. The percentage of inhibition was calculated using the Eq. (1) and results are expressed as IC_{50} value.

Determination of inhibitory activity against lipid peroxidation

Antioxidant activity was determined by the thiocyanate method of Hsu *et al.* [17]. Serial dilutions were carried out with the stock solution (2 mg mL^{-1}) of the extracts, and 0.5 mL of each solution was added to linoleic acid emulsion (2.5 mL, 40 mM, pH 7.0). The linoleic acid emulsion was prepared by mixing 0.2804 g linoleic acid, 0.2804 g Tween-20 as emulsifier in 50 mL 40 mM phosphate buffer and the mixture was then homogenized. The final volume was adjusted to 5 mL with 40 mM phosphate buffer, pH 7.0. After incubation at 37 °C in the dark for 48 h, 72 and 96 h, a 0.1 mL aliquot of the reaction solution was mixed with 4.7 mL of ethanol (75 %), 0.1 mL FeSO$_4$ (20 mM FeSO$_4$ was

diluted in 3.5% HCl) and 0.1 mL ammonium thiocyanate (30%). The absorbance of the mixture was measured at 500 nm and the mixture was stirred for 3 min. Ascorbic acid was used as reference compound. To eliminate the solvent effect, the control sample, which contained the same amount of solvent added to the linoleic acid emulsion in the test sample and reference compounds (AA, GA, BHT, *α*-tocopherol and quercetin) was used. Inhibition percent of linoleic acid peroxidation was also calculated using Eq. (1), and results are expressed as IC_{50} value.

Reducing power assay

The reducing power assay was determined according to the method described by Oyaizu [18]. Serial dilutions were carried out with the stock solution (1 mg mL^{-1}) of each extract. To 1 mL sample extract at different concentrations, 2.5 mL 0.2 M phosphate buffer pH 6.6, and 2.5 mL 1% potassium ferricyanide were added followed by mixed vigorously. After incubation at 50 °C for 20 min, 2.5 mL 10% trichloroacetic acid was added to mixture followed by centrifugation at 3000 rpm for 10 min. Subsequently, 2.5 mL of upper layer of mixture was added to 2.5 mL distilled water and 0.5 mL 0.1% ferric chloride, and absorbance of resulting solution was read at 700 nm against a blank. AA was used as standard. The reducing capacity of extracts was calculated using Eq. (1), and results are expressed as IC_{50} value.

Measurement of ferrous ion chelating ability

The ferrous ion chelating activity extracts was measured by the decrease in absorbance at 562 nm of the iron (II)–ferrozine complex according to Carter [19] and Yan *et al.* [20]. One mL of 0.125 mM FeSO$_4$ was added to 1 mL sample extract at different concentrations (from 2 mg mL^{-1} to 3.91 μg mL^{-1}), followed by 1 mL 0.3125 mM ferrozine. The test tubes were allowed to equilibrate at room temperature for 10 min. The absorbance was measured at 562 nm against blank. AA, BHT, *α*-tocopherol and quercetin were used as positive control. The ability of the extract to chelate ferrous ion was calculated using Eq. (1), and results are expressed as IC_{50} value.

Statistical analysis

All the results are expressed as means (MS) ± standard deviation (SD) of three independent measurements. For tested the normality of distribution, means and standard deviation, Student *t*-test at the level of significance 0.05 and 0.01 was used. Correlation coefficient was analyzed through Pearson's and Spearman's correlation coefficient. The IC_{50} values were calculated by nonlinear regression analysis from the sigmoidal dose-response inhibition curve. For statistical analysis, the SPSS 13.0 software program was used.

RESULTS AND DISSCUSION

According to traditional usage of these plants in herb medicine, the antioxidant capacity of different extracts of *R. hypoglossum* L. and *R. aculeatus* L. (aerial parts) from Serbia was systematically investigated by different assays. In addition, the total content of phenols and flavonoids was determined in each extracts, as well as the correlation between these phytochemicals and the antioxidant activity.

Generally, the antioxidant activity of plants is mainly associated to their bioactive compounds, such as phenolics, flavonols and flavonoids [21]. Phenolics are compounds possessing one or more aromatic rings with one or more hydroxyl groups. The results of total phenolic content (TPC) determined in the different plants extracts are presented in Fig. 1. The TPC in all tested extracts of *R. hypoglossum* L. was higher than TPC in extracts of *R. aculeatus* L. The content of total phenolics in EtOH, EtOAc and AcOH extract of *R. hypoglossum* L. were 8.569, 8.175 and 8.036 mg GAE g^{-1}, respectively. However, the significant lesser TPC was found in extracts of *R. aculeatus* L. in following order: AcOH extract > EtOAc extract > EtOH extract. Statistically significant differences in TPC between AcOH and EtOH ($p < 0.05$, $R^2 = 0.612$), as well as between EtOAc and EtOH extracts ($p < 0.05$, $R^2 = 0.548$) of *R. aculeatus* L. were found. The highest TPC was determined in EtOH extract of *R. hypoglossum* L., whereas the highest TPC was found in AcOH extract of *R. aculeatus* L. Obviously, these plants contain phenolics by different polarity, which are involved in their antioxidant activity. The least polar solvents are generally considered to be suitable for extracting lipophilic phenols, and polar solvents are used for hydrophilic phenols [22].

Flavonoids are the most abundant polyphenols. The basic flavonoid structure is the flavan nucleus, containing 15 carbon atoms arranged in three rings (C6-C3-C6). The results of total flavonoid content (TFC) determined in the different plants extracts are also given in Fig. 1. The greatest quantity of TFC was found in AcOH extract of *R. aculeatus* L. (0.136 mg RU g^{-1}) whereas the lowest quantity was found in EtOH extract of same plant (0.113 mg RU g^{-1}). The *R. hypoglossum* L. extract with the greatest quantity of TFC was AcOH (0.129 mg RU g^{-1}), followed by EtOH (0.125 mg RU g^{-1}) and EtOAc (0.121 mg RU g^{-1}). Among all tested extracts, the AcOH extracts of both plants contain the highest quantity of TFC. However, the AcOH extract of *R. aculeatus* L. has higher flavonoid content than *R. hypoglossum* L. Our dates are in accordance with those

Plant extract or standard	Part of plant	IC$_{50}$ (µg mL^{-1})						
		DPPH scavenging activity	Metal chelating activity	ABTS cation scavenging activity	Reducing power	Inhibitory activity against lipid peroxidation		
						48 h	72 h	96 h
RAEtOH	Aerial	502.03 ± 1.04	150 ± 0.25	3.45 ± 0.25	209 ± 0.08	1000 ± 1.26	950 ± 0.67	790 ± 0.71
RAEtOAc	Aerial	182.54 ± 0.21	165 ± 0.33	3.43 ± 0.25	223 ± 0.10	1050 ± 1.28	968 ± 0.84	810 ± 0.85
RAAcOH	Aerial	227.17 ± 0.37	170 ± 0.55	3.42 ± 0.12	239 ± 0.12	1200 ± 1.41	970 ± 0.91	840 ± 0.96
RHEtOH	Aerial	1632.33 ± 1.21	130 ± 0.17	3.04 ± 0.12	143 ± 0.05	960 ± 0.97	890 ± 0.82	765 ± 0.53
RHEtOAc	Aerial	278.37 ± 0.35	110 ± 0.09	3.09 ± 0.08	160 ± 0.10	1020 ± 0.99	1010 ± 0.95	989 ± 1.12
RHAcOH	Aerial	538.78 ± 1.18	230 ± 0.68	3.14 ± 0.10	162 ± 0.10	870 ± 0.74	742 ± 0.66	651 ± 0.81
GA	-	3.97 ± 0.10	nd	nd	nd	nd	nd	255.43 ± 1.21
AA	-	6.05 ± 0.12	352.9 ± 1.25	2.85 ± 0.05	881 ± 0.15	400 ± 0.63	350 ± 0.45	250 ± 1.05
BHT	-	362 ± 0.84	>1500	nd	nd	nd	nd	1 ± 0.49
α-tocopherol	-	12 ± 0.33	>1000	nd	nd	nd	nd	3.92 ± 0.74
Quercetin	-	1.48 ± 0.29	550 ± 1.18	nd	nd	nd	nd	2.90 ± 0.25

RA-*Ruscus aculeatus* L., RH-*Ruscus hypoglossum* L, EtOH-ethanolic extract, AcOH-acetone extract, EtOAc-ethyl acetate extract, BHT-butylated hydroxytoluene, GA-gallic acid, AA-ascorbic acid, nd-not determined. Reasults are mean values ± SD from three experiments.

Fig. 1. Total antioxidant activity, total phenolic and flavonoid content of plants extracts.

reported in the literature, which revealed that acetone is the best solvent for the extraction of phenols and flavonoids [23–25].

The total antioxidant potential (TAP) of extracts from both plant species and standard (AA) was investigated (Fig. 1). The AcOH extract of *R. aculeatus* L. showed the highest antioxidant potential (23.329 µg AA g^{-1}), two fold higher than the same extract of *R. hypoglossum* L. (14.976 µg AA g^{-1}). The EtOAc extracts of *R. aculeatus* L. and *R. hypoglossum* L. showed some lesser TAP with 21.330 and 13.491 µg AA g^{-1}, whereas the EtOH extracts of *R. aculeatus* L. and *R. hypoglossum* L. were the least active extracts with 20.027 and 13.092 µg AA g^{-1}, respectively. Obviously, the aerial parts of *R. aculeatus* L. possess much stronger antioxidant potential than *R. hypoglossum* L. Results of this study showed that AcOH extract of both plants has the highest antioxidant potential followed by EtOAc and EtOH extracts. The significant differences in total antioxidant capacity between these two plants can be explained by differences in morph-physiological characteristics of plants, their natural habitat and ecological factors [26].

The results of DPPH scavenging activity of different plants extracts, as well as some synthetics antioxidants, are shown in Fig. 2. The best anti-DPPH activity was found in EtOAc extract of *R. aculeatus* L. This extract produced 50% of DPPH scavenging activity in concentrations of 182.54 µg mL^{-1}. However, slightly lower scavenger activity of *R. aculeatus* L. was found in AcOH (IC_{50} = 227.17 µg mL^{-1}), but about three times lower activity was found in EtOH extract (IC_{50} = 502.03 µg mL^{-1}). All examined extracts of *R. hypoglossum* L. showed significantly lower free radical scavenging activity, compared to *R. aculeatus* L. The extract of *R. hypoglossum* L. with the best anti-DPPH activity was also EtOAc with IC_{50} = 278.37 µg mL^{-1}, followed by AcOH and EtOH with IC_{50} = 538.78 µg mL^{-1} and IC_{50} = 1632.33 µg mL^{-1}, respectively. All tested extracts of *R. aculeatus* L. have

significantly higher free radical scavenging activity, compared to *R. hypoglossum* L. The EtOAc extracts of both plants possess the best DPPH scavenging activity. This result is in accordance with report by Hadzifejzovic *et al.* [11] who found that EtOAc extract of *R. aculeatus* L. shows the best DPPH scavenging activity, with IC_{50} = 157.83 µg mL^{-1}. However, same authors investigated only DPPH activity of *R. hypoglossum* L. methanolic extract. The authors determined IC_{50} value as 518.19 µg mL^{-1}. The results of this study confirmed that this plant contains double higher free radical scavenging activity in EtOAc than in methanolic extract.

ABTS$^{•+}$ scavenging capacities of extracts and reference compound (AA) were also determined in this study (Fig. 2). All examined extracts showed significant ABTS$^{•+}$ scavenging activity. The EtOH extract of *R. hypoglossum L.* showed the greatest ABTS$^{•+}$ scavenging activity, with IC_{50} = 3.04 µg mL^{-1}, followed by AcOH (IC_{50} = 3.09 µg mL^{-1}) and EtOAH (IC_{50} = 3.14 µg mL^{-1}). Slightly lesser ABTS$^{•+}$ scavenging activity showed the extracts of *R. aculeatus L.* The extract of *R. aculeatus L.* with the greatest ABTS$^{•+}$ scavenging activity was AcOH, with IC_{50} = 3.32 µg mL^{-1}, followed by EtOAc (IC_{50} = 3.43 µg mL^{-1}) and EtOH (IC_{50} = 3.45 µg mL^{-1}). This study shows that the aerial part of *R. hypoglossum* L. has better ABTS$^{•+}$ scavenging activity than *R. aculeatus* L. The EtOH and AcOH are the solvents with best properties for the extraction of antioxidants, which are responsible for the best ABTS$^{•+}$ scavenging activity of *R. hypoglossum* L. and *R. aculeatus* L, respectively. In literature, the influence type of alcohol used for extraction on the estimation of antioxidant activity of phenolic compounds in ABTS assay is well discussed. According to Oszmianski *et al.* [27], the antioxidant activity of plants against ABTS is correlated with the concentration, chemical structures, and polymerization degrees of organ antioxidants.

Plant extract	Part of plant	Total antioxidant activity µg AA g^{-1}	Total phenolic content mg GAE g^{-1}	Total flavonoid content mg RU g^{-1}
RAEtOH	Aerial	20.027 ± 1.48	5.800 ± 0.65	0.113 ± 0.02
RAEtOAc	Aerial	21.330 ± 1.39	6.275 ± 0.82	0.127 ± 0.11
RAAcOH	Aerial	23.329 ± 1.85	6.510 ± 0.53	0.136 ± 0.14
RHEtOH	Aerial	13.092 ± 1.22	8.569 ± 0.94	0.125 ± 0.18
RHEtOAc	Aerial	13.491 ± 1.35	8.175 ± 0.91	0.121 ± 0.15
RHAcOH	Aerial	14.976 ± 1.86	8.036 ± 1.03	0.129 ± 0.10

RA-*R. aculeatus* L, RH-*R. hypoglossum* L, EtOH-ethanolic extract, AcOH-acetone extract, EtOAc-ethyl acetate extract. Reasults are mean values ± SD from three experiments.

Fig. 2. The values of IC_{50} of the plants extracts and some synthetics antioxidants.

Many researchers reported that phenolic and flavonoid compounds have play an important role in stabilizing lipid oxidation in biological systems [28]. The inhibiting activity of each plant extracts against lipid peroxidation was determined at different incubation times (Fig. 2). The extract of *R. hypoglossum* L. with the greatest inhibiting activity was AcOH, with IC_{50} =651 µg mL^{-1}, followed by EtOH (IC_{50} = 765 µg mL^{-1}) and EtOAc (IC_{50} = 989 µg mL^{-1}). However, the EtOH extract of *R. aculeatus* L. showed the greatest activity in inhibiting oxidation of linoleic acid (IC_{50} = 790 µg mL^{-1}), followed by EtOAc (IC_{50} = 810 µg mL^{-1}) and AcOH (IC_{50} = 849 µg mL^{-1}). Obviously, the aerial part of *R. hypoglossum* L. exhibits better inhibitory activity than *R. aculeatus* L. The AcOH of *R. hypoglossum* L. and EtOH of *R. aculeatus* L. are the extracts with greatest activity in inhibiting oxidation of linoleic acid.

Results of reducing power of tested plants extracts and standard (AA) are presented in Fig. 2. All tested plants' extracts showed very significant reducing power with IC_{50} values in the range from 143 to 239 µg mL^{-1}. These values were more powerful than the synthetic antioxidant AA (IC_{50} = 881 µg mL^{-1}). The EtOH extract of *R. hypoglossum L.* showed the highest reducing power, with IC_{50} = 143 µg mL^{-1}, followed by EtAOc (IC_{50} = 160 µg mL^{-1}) and AcOH (IC_{50} = 162 µg mL^{-1}). The reductive potential of *R. aculeatus* L. was as follow: EtOH (IC_{50} = 209 µg mL^{-1}), EtOAc (IC_{50} = 223 µg mL^{-1}) and AcOH (IC_{50} = 239 µg mL^{-1}). The results of this study showed that *R. hypoglossum* L. has the better reductive potential than *R. aculeatus* L. The EtOH is the best solvent for the extraction of antioxidants with the best reductive potential of both plants.

Ferrous ion chelating ability of each plant extracts was determined and results are given in Fig. 2. Among all tested extracts of *R. hypoglossum* L., the EtOAc extract showed the greatest ferrous ion chelating capacity, with the lowest IC_{50} = 110 µg mL^{-1}, followed by EtOH with IC_{50} = 130 µg mL^{-1} and AcOH with the greatest IC_{50} = 230 µg mL^{-1}. Ferrous ion chelating ability of *R. aculeatus* L. was the greatest in EtOH, with IC_{50} = 150 µg mL^{-1}, followed by EtOAc and AcOH extracts with IC_{50} = 165 µg mL^{-1} and IC_{50} = 170 µg mL^{-1}, respectively. All tested extracts of both plants demonstrated high ferrous ion chelating capacity and much better compare to synthetic compounds (Fig. 2). Presented results showed that *R. hypoglossum* L. has better ferrous ion chelating capacity than *R. aculeatus* L.

The correlation between total phenolic and flavonoid content and antioxidant activity of plants was also evaluated, and results are given in Fig. 3. The results show very strong correlation between TPC and TOA (R^2 = 1.000), as well as between TFC and TOA (R^2 = 1.000) in aerial parts of *R. aculeatus* L. Very strong positive correlation was also found between TPC (or TFC) and antioxidant activity by using the ABTS cation scavenging capacity (R^2 = 1.000) and reducing power (R^2 = 1.000). However, very strong negative correlation was found between TPC (or TFC) and metal chelating activity (R^2 = −1.000) of *R. aculeatus* L. These results show the importance of TPC and TFC in the antioxidant activity when measured through the methods mentioned above. For DPPH scavenging activity and inhibitory activity toward lipid peroxidation, no correlation between their IC_{50} and TPC (or TFC) was found. This finding is consistent with results of other authors [29],

	Total antioxidant activity	DPPH scavenging activity	Metal chelating activity	ABTS cation scavenging activity	Reducing power	Inhibitory activity against lipid peroxidation
R. hypoglossum L.						
TPC	-1.000[a]	-	-	-	1.000[a]	-
TFC	-	-	-1.000[a]	-	-	1.000[a]
R. aculeatus L.						
TPC	1.000[a]	-	-1.000[a]	1.000[a]	1.000[a]	-
TFC	1.000[a]	-	-1.000[a]	1.000[a]	1.000[a]	-

[a]Corelation is significant at the 0.01 level

Fig. 3. The correlation coefficient (R^2) between antioxidant activities, total phenolic and flavonoid content of plants.

and suggests on the possible presence of non-ionic compounds in extracts.

In the extracts of *R. hypoglossum* L., very strong negative correlation was found between TPC and TOA ($R^2 = -1.000$), but no correlation between TFC and TOA was found. These results suggest that the antioxidant activity of *R. hypoglossum* L. might be attributed to the presence of some non-phenolic compounds or some individual phenolic, which act in synergism with flavonoids. Very strong positive correlation was also found between TPC and reducing power ($R^2 = 1.000$) of *R. hypoglossum* L. From this result, it was clear that phenols play an important role in reducing power. This result is in accordance with results of Boulanour *et al.* [30]. For inhibitory activity toward lipid peroxidation and metal chelating activity, very strong positive ($R^2 = 1.000$) and very strong negative correlation ($R^2 = -1.000$) between their IC_{50} and TFC was found, respectively. Obviously, flavonoids are correlated with antioxidant activity when measured through the inhibitory activity toward lipid peroxidation. The mentioned authors [30] have also reported that flavonoids are correlated well in the protection of biological membranes. However, for DPPH scavenging activity, ABTS cation scavenging activity and reducing power, no correlation between their IC_{50} and TFC was found.

CONCLUSIONS

This is the first report about the antioxidant activity of *Ruscus hypoglossum* L. and *R. aculeatus* L. from Serbia. Acetone extract of *R. aculeatus* L. showed the best total antioxidant capacity whereas the highest DPPH scavenging activity was found in ethyl acetate extract. Ethanolic extract of *R. hypoglossum* L. showed the highest ABTS radical cation scavenging activity as well as reducing power. Acetone extract of this plant showed the best inhibitory activity against lipid peroxidation whereas the best ferrous ion chelating ability was found in ethyl acetate extract. The highest total phenolic content was found in ethanolic extract of *R. hypoglossum* L.*,* but the highest total flavonoids content was found in acetone extract of *R. aculeatus* L. Both plant species had significant higher total phenolic than flavonoid content. Probably, some non-phenolic compounds are also involved in antioxidant activity of plants. This preliminary study provides data for supporting the use of these plant species as natural antioxidant agents, and confirms that these extracts represent a significant source of phenolic compounds. The further investigation will be focused on the chemical composition and biological activity of selected plants in order to apply them in pharmaceutical and food industry.

REFERENCES

[1] U. Chandur, S. Shashidhar, S.B. Chandrasekar, M. Bhanumathy, T. Midhun, Phytochemical evaluation and anti-arthritic activity of root of *Saussure alappa*, Pharmacologia **2** (2011) 265–267.

[2] D. Krishnaiah, R. Sarbatly, A. Bono, Phytochemical antioxidants for health and medicine-A move towards nature, Biotechnol. Mol. Biol. Rev. **1** (2007) 97–104.

[3] R.L. Prior, X. Wu, K. Schaich, Standardized methods for the determination of antioxidant capacity and phenolics in foods and dietary supplements, J. Agric. Food Chem. **53** (2005) 4290–4302.

[4] C.G. Nagendrappa, An appreciation of free radical chemistry-3, free radicals in diseases and health, Resonance **10** (2005) 65–73.

[5] R.S. Daniel, B.C. Mathew, D.S. Devi, K.T. Augusti, Antioxidant effect of two flavonoids from the bark of *Ficus bengalensis* Linn. in hyperlipidemic rats, Indian. J. Exp. Biol. **36** (1998) 902–906.

[6] T. Niwa, U. Doi, Y. Kato, T. Osawa, Antioxidative properties of phenolic antioxidants isolated from corn steep liquor, J. Agric. Food Chem. **49** (2001) 177–182.

[7] B. Halliwell, J.M.C. Gutteridge, Free radical in biology and medicine, 4th ed., Oxford University Press, London, 2007.

[8] T.G. Taruscio, D.L. Barney, J. Exon, Content and profile of flavonoids and phenolic acid compounds in conjunction with antioxidant capacity for a variety of Northwest *Vaccinium berries*, J. Agric. Food Chem. **52** (2004) 3169–3176.

[9] P.F. Yeo, in: T.G. Tutin, V.H. Heywood, N.A. Burges, D.M. Moore, D.H. Valentine, S.M. Walters, D.A. Webb (Eds.), Flora Europaea, Vol. 5, Cambridge University Press, Cambridge, 1980, pp. 71–73.

[10] N. Hadžifejzović, Flavonoide und hydroxyzimtsäureamide in *Ruscus aculeatus* L. und in anderen verwandten Arten. Strukturaufklärung, verteilung und physiologische bedeutung. PhD, University of Münster, 2006.

[11] N. Hadžifejzović, J. Kukić-Marković, S. Petrović, M. Soković, J. Glamočlija, D. Stojković, A. Nahrstedt, Bioactivity of the extracts and compounds of *Ruscus aculeatus* L. and *Ruscus hypoglossum* L, Ind. Crop. Prod. **49** (2013) 407–411.

[12] V.L. Singleton, J.A. Rossi, Colorimetry of total phenolics with phosphomolybdic-phosphotungstic acid reagents, Am. J. Enol. Vitic. **16** (1965) 144–158.

[13] I.M.C. Brighente, M. Dias, L.G, Verdi, M.G. Pizzolatti, Antioxidant activity and total phenolic content of some Brazilian species, Pharm. Biol. **45** (2007) 156–161.

[14] P. Prieto, M. Pineda, M. Aguilar, Spectrophotometric quantization of antioxidant capacity through the form-

ation of a phosphomolybdenum complex: specific application to the determination of vitamin E, Anal. Biochem. **269** (1999) 337–341.

[15] T. Takao, F. Kitatani, N. Watanabe, A. Yagi, K. Sakata, A simple screening method for antioxidants and isolation of several antioxidants produced by marine bacteria from fish and shellfish, Biosci. Biotechnol. Biochem. **58** (1994) 1780–1783.

[16] R. Re, N. Pellegrini, A. Proteggente, A. Pannala, M. Yang, C. Rice-Evans, Antioxidant activity applying an improved ABTS radical cation decolorization assay, Free Radic. Biol. Med. **26** (1999) 1231–1237.

[17] C.K. Hsu, B.H. Chiang, Y.S. Chen, J.H. Yang, C.L. Liu, Improving the antioxidant activity of buckwheat (*Fagopyrum tataricm* Gaertn) sprout with trace element water, Food Chem. **108** (2008) 633–641.

[18] M. Oyaizu, Studies on product of browning reaction prepared from glucose amine, Jap. J. Nut. **44** (1986) 307–315.

[19] P. Carter, Spectrophotometric determination of serum iron at the submicrogram level with a new reagent (ferrozine), Anal. Biochem. **40** (1971) 450–458.

[20] L.Y. Yan, L.T. Teng, T.J. Jhi, Antioxidant properties of Guava fruits: comparison with some local fruits, SAJ **3** (2006) 9–20.

[21] A. Kumar, P. Chaudhary, N.K. Verma, P. Kumar, TLC based phytochemical and antioxidant analysis of *Oxalis corniculata* Linn., Int. Res. J. Pharm. App. Sci. **3** (2013) 6––12.

[22] F. Medini, H. Fellah, R. Ksouri, C. Abdelly, Total phenolic, flavonoid and tannin contents and antioxidant and anti–microbial activities of organic extracts of shoots of the plant *Limonium delicatulum*, JTUSCI **8** (2014) 216–224.

[23] M. Alothman, R. Bhat, A.A. Karim, Antioxidant capacity and phenolic content of selected tropical fruits from Malaysia, extracted with different solvents, Food Chem. **115** (2009) 785–788.

[24] C.P. Anokwuru, E. Ijeoma, A. Olusola, O.A. Ayobami, Polyphenolic Content and Antioxidant Activity of *Hibiscus sabdariffa* Calyx, Research Journal of Medicinal Plant **5** (2011) 557–566.

[25] P.Z. Mašković, J.D. Mladenović, M.S. Cvijović, G. Aćamović-Đoković, S.R. Solijić, M.M. Radojković, Phenolic content, antioxidant and antifungal activities of acetonic, ethanolic and petroleum ether extracts of *Hypericum perforatum* L., Hem. Ind. **65** (2011) 159–164.

[26] J. Moor, J.G. Liu, K. Zhou, L. Yu, Effects of genotype and environment on the antioxidant properties of hard winter wheat bran, J. Agric. Food Chem. **54** (2006) 5313–5322.

[27] J. Oszmianski, A. Wojdylo, E. Lamer-Zarawska, K. Swiader, Antioxidant tannins from *Rosaceae* plant roots, Food Chem. **100** (2007) 579–583.

[28] S.J. Wu, L.T. Ng, Antioxidant and free radical scavenging activities of wild bitter melon (*Momordica charantia* Linn. var. *abbreviate* Ser.) in Taiwan, LWT-Food Sci. Technol. **41** (2008) 323–330.

[29] N. Nićiforivić, V. Mihailović, P. Mašković, S. Solujić, D. Pavlović Muratspahić, Antioxidant activity of selected plant species; potential new sources of natural antioxidants, Food Chem. Toxicol. **48** (2010) 3125–3130.

[30] B. Boulanouar, G. Abdelaziz, S. Aazza, C. Gago, M. Graca Miguel, Antioxidant activities of eight Algerian plant extracts and two essential oils, Ind. Crop Prod. **46** (2013) 85–96.

IZVOD

ANTIOKSIDATIVNA AKTIVNOST VRSTA *Ruscus* IZ SRBIJE: POTENCIJALNI IZVORI NOVIH PRIRODNIH ANTIOKSIDANATA

Violeta D. Jakovljević[1], Jasmina M. Milićević[1], Gorica T. Đelić[1], Miroslav M. Vrvić[2]

[1]*Institut za biologiju i ekologiju, Prirodno–matematički fakultet, Univerzitet u Kragujevcu, Radoja Domanovića 12, 34000 Kragujevac, Srbija*
[2]*Departman za Biohemiju, Hemijski fakultet, Univerzitet u Beogradu, Studentski trg 12–16, 11000 Beograd, Srbija*

(Naučni rad)

Antioksidativna aktivnost etanolnog, acetonskog i etil-acetatnog ekstrakta nadzemnih delova biljaka *Ruscus hypoglossum* L. i *Ruscus aculeatus* L. poreklom iz Srbije, kao i ukupan sadržaj fenola i flavonoida u ekstraktima, ispitivani su u ovom radu. Acetonski ekstrakt *R. aculeatus* L. pokazao je najveći ukupni antioksidativni kapacitet (23.329 µg AA g^{-1}), a etil-acetatni ekstrakt najbolju sposobnost neutralizacije slobodnih DPPH radikala (IC_{50} = 182,54 µg mL^{-1}). Etanolni ekstrakt *R. hypoglossum* L. pokazao je najbolju sposobnost neutralizacije ABTS$^{•+}$ (IC_{50} = 3,04 µg mL^{-1}) i Fe^{3+}-redukujući kapacitet (IC_{50} = 143 µg mL^{-1}). Acetonski ekstrakt biljke pokazao je najbolju sposobnost inhibicije pri lipidnoj peroksidaciji (IC_{50} =651 µg mL^{-1}), a etil-acetatni ekstrakt najbolju Fe^{2+}-helatacionu aktivnost (IC_{50} = 110 µg mL^{-1}). Najveća količina ukupnih fenola (8,569 mg GAE g^{-1}) izmerena je u etanolnom ekstraktu *R. hypoglossum* L., dok je najveća količina ukupnih flavonoida (0,136 mg RU g^{-1}) izmerena u acetonskom ekstraktu *R. aculeatus* L. Na osnovu prikazanih rezultata, obe vrste *Ruscus* koje žive na teritoriji Srbije predstavljaju značajne izvore novih prirodnih antioksidanata sa mogućom primenom u farmaceutskoj i prehrambenoj industriji.

Ključne reči: Hvatanje slobodnih radikala • Redukujući kapacitet • Helataciona sposobnost • Lipidna peroksidacija • Ukupan sadržaj fenola i flavonoida

DOKTORSKE DISERTACIJE I MAGISTARSKE TEZE HEMIJSKO–TEHNOLOŠKE STRUKE ODBRANJENE NA UNIVERZITETIMA U SRBIJI U 2015. GODINI

TEHNOLOŠKO–METALURŠKI FAKULTET, UNIVERZITET U BEOGRADU

Ime i prezime	Tema	Mentori
Doktorske disertacije		
1. RAMADAN AL-MUKHTAR DUKALI	SINTEZA I KARAKTERIZACIJA SCINTILACIONIH KOMPOZITNIH MATERIJALA SA POLIMERNOM MATRICOM	Dr Vesna Radojević
2. IMHIMAD ALSADIK ALI ABOOD	KOMPONENTE NA BAZI SILICIJUM-KARBIDA U ELEKTRONSKIM KOLIMA VELIKE SNAGE	Dr Rajko Šašić
3. SANjA (Radomir) MARINOVIĆ	PRIMENA NOVIH POLIMERNIH NANOKOMPOZITNIH MATERIJALA SA GLINOM U PREČIŠĆAVANjU OTPADNIH VODA KOJE SADRŽE DERIVATE FENOLA	Dr Dušan Antonović
4. ZVEZDANA (Dimitrije) BAŠČAREVIĆ	UTICAJ RASTVORA AMONIJUM-NITRATA I NATRIJUM-SULFATA NA MEHANIČKA SVOJSTVA I STRUKTURU GEOPOLIMERA NA BAZI ELEKTROFILTERSKOG PEPELA TERMOELEKTRANA	Dr Rada Petrović Dr Miroslav Komljenović
5. MIROSLAV (Miomir) PAVLOVIĆ	SINTEZA I KARAKTERIZACIJA ELEKTROPROVODNIH KOMPOZITNIH MATERIJALA NA BAZI BIORAZGRADIVIH POLIMERA I METALNIH PRAHOVA	Dr Vesna Radojević
6. AJAJ ABDALRHMAN ISMAIL	SINTEZA, STRUKTURA I SVOJSTVA 2(6)-HIDROKSI-6(2)-OKSO-N(1),4-DISUPSTITUISANIH-1,2(1,6)-DIHIDROPIRIDINA-3-KARBONITRILA I NjIHOVIH AZO DERIVATA	Dr Aleksandar Marinković
7. HALAP ARIEBI M. AKRAM	STRUKTURA I ZAVARLjIVOST Al-Mg LEGURA VISOKE ČVRSTOĆE ZA BRODOGRADNjU	Dr Endre Romhanji
8. STOJA (Lazo) MILOVANOVIĆ	IMPREGNACIJA TIMOLA NA ČVRSTE NOSAČE NATKRITIČNIM UGLjENIK(IV)-OKSIDOM	Dr Irena Žižović
9. IVANA (Ljiljana) JEVREMOVIĆ	PRIMENA ORGANSKIH INHIBITORA ZA SPREČAVANjE POJAVE KOROZIJE NISKOUGLjENIČNOG ČELIKA U PRISUSTVU CO_2	Dr Vesna Mišković-Stanković
10. MARIJA (Sretko) ĐOŠIĆ	BIOKERAMIČKE PREVLAKE NA BAZI KALCIJUM-FOSFATNIH JEDINjENjA DOBIJENE NA TITANU ELEKTROHEMIJSKIM METODAMA	Dr Vesna Mišković-Stanković
11. IVANA (Tomislav) KOSTIĆ	PROCESNO OČUVANE MEMBRANE ERITROCITA DOBIJENE IZ KLANIČNE KRVI KAO SISTEMI ZA PRODUŽENO OSLOBAĐANjE AKTIVNIH SUPSTANCI	Dr Branko Bugarski Dr Vesna Ilić
12. VESNA (Dragić) NIKOLIĆ	KATALITIČKI MATERIJALI NA BAZI SISTEMA Ni-Pd/Al_2O_3	Dr Željko Kamberović
13. MAJA (Ljubomir) BULATOVIĆ	PROIZVODNjA I KARAKTERISTIKE FUNKCIONALNIH FERMENTISANIH NAPITAKA NA BAZI SURUTKE	Dr Marica Rakin
14. IVANA (Zoran) LUKIĆ	KINETIKA HETEROGENE METANOLIZE SVEŽEG I KORIŠĆENOG BILjNOG ULjA	Dr Dejan Skala Dr Irena Žižović
15. MILOŠ (Tomislav) NENADOVIĆ	MORFOLOŠKA I STRUKTURNA SVOJSTVA NANOČESTICA SREBRA I ZLATA DOBIJENIH JONSKOM IMPLANTACIJOM U POLIETILEN VELIKE GUSTINE	Dr Đorđe Janaćković Dr Zlatko Rakočević

Ime i prezime	Tema	Mentori

<div align="center">

Doktorske disertacije

</div>

Ime i prezime	Tema	Mentori
16. BRANISLAV (Srbo) TODIĆ	MODELOVANjE HEMIJSKE KINETIKE I OPTIMIZACIJA REAKTORA SA PAKOVANIM SLOJEM ZA *Fischer-Tropsch* SINTEZU	Dr Nikola Nikačević Dr Dragomir Bukur
17.ŽELjKA (Saša) ĐURĐEVIĆ	NANOKOMPOZITI SREBRO/POLI(*N*-VINIL-2-PIROLIDON) I SREBRO/ALGINAT DOBIJENI ELEKTROHEMIJSKIM POSTUPCIMA	Dr Vesna Mišković-Stanković
18. SONjA (Zoran) MILIĆEVIĆ	ADSORPCIJA JONA BAKRA IZ RUDNIČKIH OTPADNIH VODA NA RAZLIČITIM MINERALNIM ADSORBENTIMA	Dr Dragan Povrenović
19. SANjA (Ostoja) JEVTIĆ	SINTEZA I KARAKTERIZACIJA MATERIJALA NASTALIH MODIFIKACIJOM PRIRODNOG ZEOLITA (KLINOPTILOLITA) I MIKROPOROZNIH FOSFATA SA STRUKTUROM ZEOLITA	Dr Nevenka Rajić
20. JELENA (Vojislav) MILOJKOVIĆ	BIOSORPCIJA ODABRANIH TEŠKIH METALA KOMPOSTOM *Myriophyllum spicatum*	Dr Mirjana Ristić
21. JELENA (Miroslav) MIRKOVIĆ	STRUKTURNE I SOLVATOHROMNE KARAKTERISTIKE 5-ARILAZO-3-CIJANO-6-HIDROKSI-4-METIL-1-SUPSTITUISANIH-2-PIRIDONA: EKSPERIMENTALNA I KVANTNO-HEMIJSKA PROUČAVANjA	Dr Dušan Mijin
22. MARIJA (Radomir) RANIĆ	ANTIOKSIDATIVNA AKTIVNOST EKSTRAKATA KAFE I OTPADNE KAFE I NjIHOV UTICAJ NA AKTIVACIJU TROMBOCITA	Suzana Dimitrijević Branković
23. DANIJELA (Vitomir) BRKOVIĆ	UTICAJ RAZLIČITIH POSTUPAKA MODIFIKACIJE POVRŠINE UGLjENIČNIH NANOMATERIJALA NA NjIHOVA SVOJSTVA I MOGUĆNOSTI PRIMENE	Dr Aleksandar Marinković
24. NATAŠA (Miroslav) MARJANOVIĆ	SINTEZA I KARAKTERIZACIJA VEZIVNIH MATERIJALA NA BAZI ALKALNO AKTIVIRANOG ELEKTROFILTERSKOG PEPELA TERMOELEKTRANA I ZGURE VISOKE PEĆI	Dr Rada Petrović Dr Miroslav Komljenović
25. ANA (Dragan) KRAMAR	MODIFIKOVANjE POVRŠINE CELULOZNIH VLAKANA PRIMENOM DIELEKTRIČNOG BARIJERNOG PRAŽNjENjA	Dr Mirjana Kostić
26. IVANA (Dragiša) SREDOVIĆ IGNjATOVIĆ	RAZVOJ METODA ZA ANALIZU HALOGENIH ELEMENATA U ČVRSTIM UZORCIMA U ATMOSFERI KISEONIKA	Dr Ljubinka Rajaković
27. ALEKSANDAR (Radule) MLADENOVIĆ	PROUČAVANjE STABILNOSTI DONEPEZIL-HIDROHLORIDA RAZLIČITIM ANALITIČKIM METODAMA	Dr Slobodan Petrović
28.JASMINA (Jovan) STOJKOVSKA	DOBIJANjE I KARAKTERISANjE NANOKOMPOZITNIH HIDROGELOVA NA BAZI ALGINATA I NANOČESTICA SREBRA ZA PRIMENU U BIOMEDICINI	Dr Bojana Obradović
29. MILUTIN (LJubodrag) SMILjANIĆ	ELEKTROHEMIJSKA KATALIZA REAKCIJE IZDVAJANjA VODONIKA NA MODIFIKOVANIM POVRŠINAMA ZLATA, PLATINE I PALADIJUMA	Dr Branimir Grgur
30. NIKOLA (Vidan) ŽIVKOVIĆ	REGENERATIVNI POSTUPCI UKLANjANjA SUMPOR-DIOKSIDA IZ DIMNIH GASOVA–IZBOR I ODREĐIVANjE TERMOFIZIČKIH SVOJSTAVA NOVIH RASTVARAČA I NjIHOVIH SMEŠA I MODELOVANjE PROCESA	Dr Slobodan Šerbanović
31. MILENA (Milorad) KNEŽEVIĆ	UKLANjANjE AZOTNIH JEDINjENjA IZ OTPADNIH VODA U DISPERZNIM SISTEMIMA	Dr Dragan Povrenović
32. MARINA (Aleksandar) MIHAJLOVIĆ	SMANjENjE EMISIJA LAKOISPARLjIVIH ORGANSKIH JEDINjENjA U INDUSTRIJI PRERADE NAFTE PRIMENOM ČISTIJE PROIZVODNjE	Dr Mića Jovanović
33. SANjA (Borislav) ĆULUBRK	SINTEZA, OPTIČKA I TERMOMETRIJSKA SVOJSTVA NANOČESTICA GADOLINIJUM-TITANATA I LUTECIJUM-TITANATA DOPIRANIH JONIMA RETKIH ZEMALjA	Dr Đorđe Janaćković Dr Miroslav Dramićanin

Ime i prezime	Tema	Mentori

Doktorske disertacije

34. MINA (Milan) MEDIĆ	MULTIFUNKCIONALNE NANOČESTICE MAGNEZIJUM-ORTOTITANATA DOPIRANOG JONIMA RETKIH ZEMALjA I PRELAZNIH METALA	Dr Đorđe Janaćković Dr Miroslav Dramićanin
35. MARIJA (Dragan) PAVLOVIĆ	IZOLOVANjE BIOAKTIVNIH JEDINjENjA IZ OTPADNE KAFE I NjENO POTPUNO ISKORIŠĆENjE KAO ADSORBENTA	Dr Slavica Šiler-Marinković
36. OLIVERA (Stanoje) GLAVAŠKI	PROUČAVANjE DEGRADACIJE DIMETENAMIDA-P U VODENOJ SREDINI PRIMENOM RAZLIČITIH FIZIČKO-HEMIJSKIH METODA	Dr Slobodan Petrović
37. NIKOLA (Dušan) GROZDANIĆ	EKSPERIMENTALNO ODREĐIVANjE I MODELOVANjE RAVNOTEŽE TEČNOST–TEČNOST VIŠEKOMPONENTNIH SISTEMA ZELENIH RASTVARAČA	Dr Slobodan Šerbanović

Magistarske teze

1. MARIJA (Slobodan) STEVANOVIĆ	ANTIOKSIDATIVNA I ANTIINFLAMATORNA AKTIVNOST EKSTRAKATA NEVENA	Dr Slavica Šiler-Marinković

TEHNOLOŠKI FAKULTET, UNIVERZITET U NOVOM SADU

Doktorske disertacije

1. ROBERT REKECKI	ISTRAŽIVANjE DOBIJANjA I KARAKTERIZACIJA BIORAZGRADIVIH KOMPOZITNIH FILMOVA NA BAZI BILJNIH PROTEINA	prof. dr Jonjaua Ranogajec
2. JOVANA KOS	AFLATOKSINI: ANALIZA POJAVE, PROCENA RIZIKA I OPTIMIZACIJA METODOLOGIJE ODREĐIVANjA U KUKURUZU I MLEKU	prof. dr Marija Škrinjar dr Jasna Mastilović
3. DAMJAN VUČUROVIĆ	MODEL BIOPROCESA PROIZVODNjE ETANOLA IZ MEĐU- I NUSPROIZVODA PRERADE ŠEĆERNE REPE	prof. dr Siniša Dodić
4. JELENA PRODANOVIĆ	PRIRODNI KOAGULANTI IZ ZRNA PASULJA (*Phaseolus vulgaris*) U OBRADI VODE	prof. dr Marina Šćiban
5. ELIZABET JANIĆ HAJNAL	MOGUĆNOSTI REDUKCIJE SADRŽAJA ALTERNARIA TOKSINA U PŠENICI PRIMENOM ODABRANIH TEHNOLOŠKIH POSTUPAKA	prof. dr Marija Škrinjar dr Jasna Mastilović
6. UROŠ MILJIĆ	PROIZVODNJA I OCENA KVALITETA VOĆNOG VINA OD SORTI DOMAĆE ŠLJIVE (*Prunus domestica L.*)	prof. dr Vladimir Puškaš
7. BILJANA LONČAR	HEMOMETRIJSKI PRISTUP ANALIZI OSMOTSKE DEHIDRACIJE SREBRNOG KARAŠA (*Carassius gibelio*)	prof. dr Ljubinko Lević
8. IVANA ČABARKAPA	SPOSOBNOST FORMIRANJA BIOFILMA RAZLIČITIH SOJEVA *Salmonella enteritidis* I INHIBITORNI EFEKAT ETARSKIH ULJA NA INICIJALNU ADHEZIJU I FORMIRANI BIOFILM	prof. dr Marija Škrinjar
9. STRAHINJA KOVAČEVIĆ	HEMOMETRIJSKO MODELOVANJE HROMATOGRAFSKOG PONAŠANJA I BIOLOŠKE AKTIVNOSTI SERIJE ANDROSTANSKIH DERIVATA	prof. dr Sanja Podunavac Kuzmanović
10. TANJA RADUSIN	PRIPREMA I KARAKTERIZACIJA NANOKOMPOZITA POLIMLEČNE KISELINE I SILICIJUM(IV)-OKSIDA NAMENJENOG ZA PAKOVANJE HRANE	prof. dr Branka Pilić
11. NEVENA HROMIŠ	RAZVOJ BIORAZGRADIVOG AKTIVNOG AMBALAŽNOG MATERIJALA NA BAZI HITOZANA: SINTEZA, OPTIMIZACIJA SVOJSTAVA, KARAKTERIZACIJA I PRIMENA	prof. dr Vera Lazić
12. DAJANA HRNJEZ	BIOLOŠKA AKTIVNOST FERMENTISANIH MLEČNIH NAPITAKA DOBIJENIH PRIMENOM KOMBUHE I KONVENCIONALNIH STARTER KULTURA	prof. dr Spasenija Milanović

Ime i prezime	Tema	Mentori
Doktorske disertacije		
13. ACA JOVANOVIĆ	SIMULACIJA PROCESA KRETANJA ČESTICA PRI TRANSPORTU U STATIČKIM MEŠALICAMA I MODIFIKOVANIM PUŽNIM TRANSPORTERIMA PRIMENOM METODE DISKRETNIH ELEMENATA	prof. dr Ljubinko Lević
14. ĐURO VUKMIROVIĆ	UTICAJ PARAMETARA MLEVENJA I PELETIRANJA NA GRANULACIJU I FIZIČKE KARAKTERISTIKE PELETIRANE HRANE ZA ŽIVOTINJE	prof. dr Aleksandar Fišteš dr Jovanka Lević
15. IVANA NIKOLIĆ	FIZIČKE I SENZORSKE KARAKTERISTIKE FUNKCIONALNIH PREHRAMBENIH NAMAZA NA BAZI CELULOZNIH HIDROKOLOIDA I BRAŠNA POGAČE ULJANE TIKVE	prof. dr Ljubica Dokić
16. LJUBIŠA ŠARIĆ	ANTIBAKTERIJSKA AKTIVNOST MLEKA MAGARICE BALKANSKE RASE	prof. dr Dragoljub Cvetković
17. SANJA OSTOJIĆ	TERMALNA SVOJSTVA PROTEINA MESA U PROCESU OSMOTSKE DEHIDRACIJE U MELASI ŠEĆERNE REPE	prof. dr Ljubinko Lević dr Branislav Simonović
18. DRAGANA ILIĆ-UDOVIČIĆ	OPTIMIZACIJA TEHNOLOŠKOG PROCESA PROIZVODNJE NAPITAKA OD ENZIMSKI HIDROLIZOVANOG PERMEATA MLEKA	prof. dr Spasenija Milanović
19. RANKO ROMANIĆ	HEMOMETRIJSKI PRISTUP OPTIMIZACIJI TEHNOLOŠKIH PARAMETARA PROIZVODNJE HLADNO PRESOVANOG ULJA SEMENA VISOKOOLEINSKOG SUNCOKRETA	prof. dr Spasenija Milanović prof. dr Sanja Podunavac Kuzmanović

TEHNOLOŠKI FAKULTET U LESKOVCU, UNIVERZITET U NIŠU

Doktorske disertacije		
1. VESNA SAVIĆ	„HEMIJSKI SASTAV I FARMAKOLOŠKE AKTIVNOSTI VODENOG EKSTRAKTA KORENA GAVEZA (*Symphytum officinale* L.)"	Vesna Nikolić
2. NENAD ĆIRKOVIĆ	ANALIZA DEFORMACIONIH KARAKTERISTIKA ŠAVOVA U ZAVISNOSTI OD STRUKTURNIH PARAMETARA PRIMENJENIH KONACA I TKANINA	Jovan Stepanović
3. NEBOJŠA MILOSAVLjEVIĆ	BAKTERIJE MLEČNE KISELINE PIROTSKOG KAČKAVALjA	Dragiša Savić
4. SAŠA SAVIĆ	ENZIMSKA MODIFIKACIJA KVERCETINA SA CISTEINOM POMOĆU PEROKSIDAZE IZ RENA	Živomir Petronijević

TEHNIČKI FAKULTET U BORU, UNIVERZITET U BEOGRADU

Ime i prezime	Tema	Mentor
Doktorske disertacije		
1. MILOŠ PAPIĆ	VIŠEKRITERIJUMSKA ANALIZA KVALITETA ZEMLjIŠTA ČAČANSKE KOTLINE	dr Milovan Vuković, red. profesor
2. IVAN MIHAJLOVIĆ	RAZVOJ ALGORITMA ZA SELEKCIJU ADEKVATNOG MODELA PROCESA NA OSNOVU STRUKTURE ULAZNIH PODATAKA	dr Živan Živković, red. profesor
3. ALEKSANDRA MITOVSKI	KARAKTERIZACIJA NESTANDARDNIH KONCENTRATA BAKRA I MOGUĆNOSTI NjIHOVE PRERADE	dr Nada Štrbac, red. profesor
4. MILENA PREMOVIĆ	EKSPERIMENTALNO ODREĐIVANjE I TERMODINAMIČKO MODELOVANjE RAVNOTEŽNIH DIJAGRAMA STANjA TROJNIH SISTEMA GE-SB-AG I GE-SB-IN	dr Dragan Manasijević, van. profesor
5. VESNA CONIĆ	BIOTEHNOLOGIJA ZA TRETMAN KOMPLEKSNIH SULFIDNIH KONCENTRATA	dr Mirjana Rajčić-Vujasinović, red. profesor
6. NENAD MILIJIĆ	MODELOVANjE UTICAJNIH FAKTORA RADNOG MESTA NA BEZBEDNOST RADA U PROIZVODNIM KOMPANIJAMA	dr Ivan Mihajlović, van. profesor

Ime i prezime	Tema	Mentor
	Doktorske disertacije	
7. MILAN GORGIEVSKI	ADSORPCIJA JONA TEŠKIH METALA IZ VODENIH RASTVORA KORIŠĆENjEM PŠENIČNE SLAME KAO ADSORBENSA	dr Nada Štrbac, red. profesor
8. MARIJA SAVIĆ	VIŠEKRITERIJUMSKA OPTIMIZACIJA SASTAVA ŠARŽE ZA HIDROMETALURŠKI PROCES DOBIJANjA CINKA	dr Živan Živković, red. profesor
9. MAJA TRUMIĆ	MODEL KINETIKE IZDVAJANjA ČESTICA TONERA IZ VODENE SUSPENZIJE PAPIRA	dr Milan Antonijević, red. profesor
10. STEVAN DIMITRIJEVIĆ	ELEKTROHEMIJSKA I POVRŠINSKA KARAKTERIZACIJA TROKOMPONENTNIH LEGURA SISTEMA AG–CU–ZN U BLISKO NEUTRALNIM HLORIDNIM RASTVORIMA	dr Mirjana Rajčić-Vujasinović, red. profesor
11. MLADEN MIRIĆ	UTICAJ REŽIMA PRERADE LEGURA ZLATA NA SVOJSTVA POLUFABRIKATA ZA IZRADU NAKITA	dr Dragoslav Gusković, red. profesor
	Magistarske teze	
1. LjILjANA AVRAMOVIĆ	ELEKTROHEMIJSKO PONAŠANjE PALADIJUMA, ZLATA I SREBRA U RASTVORU SREBRO NITRATA	dr Snežana Urošević, van. profesor
2. SANjA ĐORĐEVIĆ	UTICAJ SVETSKE EKONOMSKE KRIZE NA TREND POTRAŽNjE BAKRA NA SVETSKOM TRŽIŠTU	dr Ivan Mihajlović, van. profesor